Faculty of Science and Engineering

Department of Chemistry

Novel Approaches to Forensic Explosives Recovery, Storage and Analysis

Holly April Yu

This thesis is presented for the Degree of

Doctor of Philosophy

of

Curtin University

April 2017

Declaration

To the best of my knowledge and belief, this thesis contains no material previously published by any other person except where due acknowledgement has been made.

This thesis contains no material which has been accepted for the award of any other degree or diploma in any university.

Signature:

Date: **27/04/2017**

Abstract

In a forensic explosives investigation, it is crucial to obtain rapid information on the type of explosive involved in an incident. A forensic explosives investigation comprises several stages: collection of items of post-blast debris and transportation to a laboratory, frequently storage of the items in the laboratory, recovery of the explosive residues from the sample, and finally analysis of the recovered explosive residues. This thesis describes a series of studies aiming to understand aspects of the retention, recovery, storage and analysis of a series of explosives in association with common substrates (textiles and soil).

Atomic force microscopy (AFM) was used to investigate the surface roughness of ten textile and five non-textile surfaces. Subsequently, the adhesion (and therefore retention) of crystals of TNT, PETN and RDX to the 15 surfaces was measured using AFM. The results showed that the explosives had a tendency of higher adhesion to the smoother surfaces examined (the non-textile surfaces), particularly glass. This knowledge may be of use when trying to prioritise debris for analysis after a large-scale incident which has generated numerous types of debris, formed of different materials, in order to maximise the likelihood of an analysis yielding information on the type of explosive involved.

In conjunction with this AFM data, a novel device, a contact heater, was used to explore how the variability of TNT, PETN and RDX recovery differed from the ten textile surfaces previously examined using AFM, to determine whether trends exist between an explosive's adhesion to a surface and its recovery from a surface. The contact heater works by heating a surface at the same time as drawing vacuum from it, with any volatilised explosive vapours caught in a sampling cartridge. This work found that for TNT in particular, higher recoveries (of up to approximately 17 %) were obtained from those textiles to which TNT had demonstrated the lowest adhesion via AFM, supporting an inverse correlation between TNT adhesion to a textile surface and its recovery. The contact heater was also compared to a vacuum sampling technique in common use by the UK Forensic Explosives Laboratory and was found to be superior for those explosives with higher vapour pressures (for example, average TNT recoveries of 14.7 % were obtained from wool using the contact heater, compared with average TNT recoveries of 7.1 % using vacuum sampling).

Another common substrate recovered from explosion sites is soil and as such the recovery of explosive residues from soil is of importance. A number of storage conditions for soil samples containing explosives were examined. Three different soils were spiked using solutions of TNT, PETN and RDX, with the samples stored at room temperature, refrigerated or frozen.

Additional samples were prepared with a nitrogen, rather than air, headspace, with further samples gamma-irradiated prior to storage at room temperature. The rate of explosive residue attenuation was shown to have a dependence on the type of soil involved, with sandier soils giving faster rates of attenuation. For example, no TNT was recovered from an explosives-spiked sandy soil stored at room temperature after just 4 days, whereas TNT was still recovered from two other non-sandy soils after 42 days. In all cases, storage in a freezer proved the most effective method of mitigating degradation, with TNT recoveries on the order of 90 % after 42 days. Storage under a nitrogen headspace was of slight benefit in mitigating degradation, though gamma-irradiation of the explosives-spiked soils was shown, in some cases, to destroy a proportion of the spiked explosive. The magnitude of this loss also had a soil-related dependence, with RDX recoveries from spiked and gamma irradiated Spearwood soil approximately 5 % at each sampling time point, compared to approximately 30 % from spiked and gamma irradiated native soil.

Further work in this area examined the fate of explosives deposited into the same three soils following actual detonation events, to assess whether solution-spiking of soils is representative of samples which would be generated following actual vehicle bombings or landmine detonations. SEM analyses of post-detonation soils revealed that fracturing of the soil particles had occurred, regardless of whether an explosive charge was detonated in contact with (simulating a landmine detonation) or 50 cm above (simulating a vehicle bombing) a soil sample. A comparison of explosives attenuation rates in these post-detonation soils against the previously-described solution-spiked soils revealed similar patterns of loss, though the rate was markedly faster in the detonation-spiked soils. Micro computed tomography (μCT) analyses of the pre- and post-detonation soils revealed an increased porosity in the post-detonation soils (for native soil, average porosity increased from approximately 8 % to approximately 13 %), hypothesised to facilitate bacterial transport through the soils to increase the rate of explosive residue degradation.

Finally, electrochemical experiments were performed with the aim of developing a novel method for the detection of TNT in aqueous samples. A room temperature ionic liquid (RTIL) was combined with a polymer, poly(hexyl methacrylate), and coated onto the surface of a gold thin-film electrode. Conditions were then optimised for the use of this functionalised electrode for TNT pre-concentration from aqueous samples. The technique was able to detect TNT at levels typical of those present in groundwater around TNT manufacturing sites (1-10 μg/mL), with a limit of detection of 0.37 μg/mL, and may thus be of use for those tasked with TNT bioremediation.

Acknowledgements

This PhD has been an immense collaborative effort and there are many people I would like to thank for their support and encouragement over the last three years.

First and foremost, huge thanks are due to Professor Simon Lewis - I have been incredibly lucky to have had such a supportive, flexible and good-natured principal supervisor. Huge thanks are also due to my three fantastic co-supervisors. I have learnt a wealth of information from Dr David DeTata and I feel very privileged to have had the chance to work with him. As always, it has been a pleasure to work with Professor Niamh Nic Daéid and I am very grateful to her and her group at the University of Dundee for hosting me on exchange for two semesters. Many thanks also to Dr Debbie Silvester – I have had an exciting semester in her electrochemistry lab and I am grateful to her for really driving this phase of my research forward with her enthusiasm and interest.

Thank you to the very welcoming Forensic and Analytical Chemistry Research Group at Curtin. Any apprehension I felt about moving halfway around the world for this PhD was quickly quashed when I met them all! Particular thanks to Buddhika Dorakumbura, my PhD buddy (and the other half of the unforgettable Team Jacaranda..!), and to Jaime Cesar, the third member of our tea break group – it has been great to share this experience with you both and I'm delighted that we will all be finishing our PhDs this year. Thanks also to the now-Dr Georgina Sauzier, who was always happy to answer any questions I had.

As an AFM novice, I would like to thank the very patient Dr Tom Becker for expertly teaching me how to use his AFM instruments, as well as for his advice in writing up this aspect of my research. Thank you to the UK Forensic Explosives Laboratory for lending me the contact heater used during this thesis, and for hosting me in their lab for a week to see a world-leading forensic explosives laboratory in action.

For my soils work, huge thanks to all of the staff at ChemCentre WA for welcoming me into their workplace and answering any questions I had. In particular, thank you to Jeremy Brown for helping with my soil characterisations, and Dr Kari Pitts for her help with the initial SEM analyses. Thank you also to the staff at the James Hutton Institute in Aberdeen, where I performed some additional soil analyses – in particular, thank you to Professor Lorna Dawson for hosting me for a week, Jasmine Ross for showing me how to use all of the equipment in the lab, and Evelyne Delbos for help with later SEM analyses.

The soils work would have been much less fun without the chance to perform some detonations, so I would like to thank Chris, Scottie, Seamus, Rick and Dean from the Western Australia Police Tactical Response Group – Bomb Response Unit for their collaboration, expertise and professionalism during this work's detonation trials – definitely two of the best days of my PhD!

Enormous thanks are also due to Dr Juni Lee, electrochemist extraordinaire, for transforming me from an electrochemistry novice to a proficient electrochemist in four short months. Thanks too to Ghulam Hussain for his additional help in the electrochemistry lab. Similarly, thank you to the inimitable Peter Chapman for his technical help with assorted aspects of my work over the last three years.

Huge thanks go to Curtin University, not only for providing me with my PhD scholarship, but also for the provision of so many invaluable seminars and workshops to aid PhD students. These certainly saved me a few grey hairs and have enabled me to submit my PhD within three years. Similarly, many thanks to Lana Dewar and her housing team at Curtin's Guild House housing complex – it has been challenging to spend alternating semesters of my PhD in Australia and Scotland, but Lana and her team helped to make my Scotland-Australia transitions very smooth and always had a comfortable room on hand upon my return to Perth. In addition, many thanks for the support of the friends I left behind when I came to Australia, with whom I'm looking forward to a long-overdue catch up.

I am very lucky to have a fantastic family who have supported me throughout this PhD, as well as throughout my previous university studies. Many thanks to my sisters, for always taking an interest in my work. Thanks also to my Dad, for always being proud of my achievements, and particular thanks to my Mum, for always having time to hear how my work was going (or not going!). Last, but definitely not least, thank you to the wonderful Dr Tahsin Tezdoğan, without whose wholehearted support commencing this PhD would not have been possible.

Publications

This thesis contains work which has been submitted for publication in the following peer reviewed journals:

H.A. Yu, J. Lee, S.W. Lewis and D.S. Silvester. *Detection of 2,4,6-trinitrotoluene using a miniaturized, disposable electrochemical sensor with an ionic liquid gel-polymer electrolyte film.* Analytical Chemistry, 2017. **89**(8): p. 4729-4736.

H.A. Yu, T. Becker, N. Nic Daeid and S.W. Lewis. *Fundamental studies of the adhesion of explosives to textile and non-textile surfaces.* Forensic Science International, 2017. **273**: p. 88-95.

H.A. Yu, D.A. DeTata, S.W. Lewis, and N. Nic Daeid. *The stability of TNT, RDX and PETN in simulated post-explosion soils: Implications of sample preparation for analysis.* Talanta, 2017. **164**: p. 716-726.

N. Nic Daeid, **H.A. Yu**, L.A. Dawson, D.A. DeTata and S.W. Lewis. *Explosive detonation causes an increase in soil porosity leading to increased TNT transformation.* Submitted to PLOS One, under review.

In addition, the following peer reviewed articles were published during the course of this thesis:

N. Nic Daeid, **H.A. Yu** and M.S. Beardah. *Investigating TNT loss between sample collection and analysis.* Science and Justice, 2017. **57**(2): p. 95-100.

H.A. Yu, S.W. Lewis, M.S. Beardah, and N. Nic Daeid. *Assessing a novel contact heater as a new method of recovering explosives traces from porous surfaces.* Talanta, 2016. **148**: p. 721-728.

Conference Presentations

Selected aspects of the work contained within this thesis have been presented at the following conferences:

Oral Presentations

A comparison of TNT degradation patterns in simulated and actual post-blast soils, presented at Flinders University's Centre of Expertise in Energetic Materials' 5th Australian Energetic Materials Symposium, 26th – 28th September 2016, Adelaide, Australia.

- Winner of best student presentation.

Investigations into the fate of explosives in soil, presented at the 23rd International Symposium on the Forensic Sciences of the Australian and New Zealand Forensic Science Society (ANZFSS 2016), 18th – 22nd September 2016, Auckland, New Zealand.

- Winner of best oral presentation (Fire Investigation and Explosives stream).

Investigations into the fate of explosives in soil, presented at the 3rd Scottish Student Forensic Research Symposium, 1st April 2016, Glasgow, UK.

- Winner of 2nd prize for best oral presentation.

Investigating the adhesion of explosives to different surfaces, presented at the Inaugural Curtin University CUPSA Conference, 3rd September 2015, Perth, Australia.

Investigating the adhesion of explosives to different surfaces, presented at the 2nd Scottish Student Forensic Research Symposium, 27th March 2015, Dundee, UK.

- Winner of best oral presentation.

Investigating the fundamental interactions of explosives with textile fibres to improve the recovery of explosives residues from fabrics, presented at the 22nd Annual Royal Australian Chemical Institute's Research and Development Topics Conference, 13th – 15th December 2014, Adelaide, Australia.

The recovery of explosives residues from porous surfaces: Emerging techniques, presented at Flinders University's Centre of Expertise in Energetic Materials' 4th Australian Energetic Materials Symposium, 27th – 28th November 2014, Adelaide, Australia.

- Invited talk.

Poster Presentations

Investigating the adhesion of explosives to different surfaces, presented at the 23rd International Symposium on the Forensic Sciences of the Australian and New Zealand Forensic Science Society (ANZFSS 2016), 18th – 22nd September 2016, Auckland, New Zealand.

- Highly commended poster (Fire Investigation and Explosives stream).

Investigations into the fate of explosives in soil, presented at the 23rd Annual Royal Australian Chemical Institute's Research and Development Topics Conference, 6th – 9th December 2015, Melbourne, Australia.

- Winner of best poster.

Investigating the adhesion of explosives to different surfaces, presented in absentia at the 11th Annual Forensic International Network for Explosives Investigation Conference (FINEX 2015), 18th – 20th May 2015, Budenheim, Germany.

Table of Contents

List of Figures

List of Tables

List of Abbreviations

$[C_2mim][NTf_2]$	1-Ethyl-3-methylimidazolium bis(trifluoromethylsulfonyl)imide
$[C_4mim][NTf_2]$	1-Butyl-3-methylimidazolium bis(trifluoromethylsulfonyl)imide
$[P_{14,6,6,6}][NTf_2]$	Tris(n-hexyl)tetradecylphosphonium bis(trifluoromethylsulfonyl)imide
µCT	Micro computed tomography
1,2-DNB	1,2-Dinitrobenzene
2,4-DNT	2,4-Dinitrotoluene
2-ADNT	2-Amino-4,6-dinitrotoluene
2-NT	2-Nitrotoluene
4-ADNT	4-Amino-2,6-dinitrotoluene
ADNT	Aminodinitrotoluene
AFM	Atomic force microscopy
AFP	Australian Federal Police
ANFO	Ammonium nitrate-fuel oil
APCI	Atmospheric pressure chemical ionisation
Au-TFE	Gold thin-film electrode
BEI	Backscattered electron imaging
CE	Capillary electrophoresis (Chapter 1) or Counter electrode (Chapter 6)
CT	Computed tomography
CV	Cyclic voltammetry
DAD	Diode array detector
DART-MS	Direct analysis in real-time mass spectrometry
DESI-MS	Desorption electrospray ionisation mass spectrometry
DMDNB	Dimethyl dinitrobutane
DNX	Hexahydro-1,3-dinitroso-5-nitro-1,3,5-triazine
EDX	Energy Dispersive X-Ray
EGDN	Ethylene glycol dinitrate
EPA	Environmental Protection Agency (US)
ESI	Electrospray ionisation

ETN	Erythritol tetranitrate
FBI	Federal Bureau of Investigation (US)
Fc	Ferrocene
Fc^+	Ferrocenium
FEL	Forensic Explosives Laboratory (UK)
FTIR	Fourier transform infrared
GC	Gas chromatography
GC-MS	Gas chromatography-mass spectrometry
GC-TEA	Gas chromatography-thermal energy analysis
GPE	Gel polymer electrolyte
HDPE	High density polyethylene
HMTD	Hexamethylene triperoxide diamine
HMX	High melting explosive (Cyclotetramethylene tetranitramine)
HPLC	High performance liquid chromatography
HPOM	Hydrogen peroxide organic mixture
IC(-MS)	Ion chromatography(-mass spectrometry)
IED	Improvised explosive device
IMS	Ion mobility spectrometry
i_p	Observed peak current
IR	Infrared
IST	Ignition susceptibility test
K_d	Adsorption coefficient
LC	Liquid chromatography
LC-MS(/MS)	Liquid chromatography-mass spectrometry(/mass spectrometry)
LC-TEA	Liquid chromatography-thermal energy analyser
LED	Light-emitting diode
MNX	Hexahydro-1-nitroso-3,5-dinitro-1,3,5-triazine
MT	Musk Tibetene
NAD(P)H	Nicotinamide adenine dinucleotide phosphate (reduced form)
NG	Nitroglycerin

PETN	Pentaerythritol tetranitrate
PHMA	Poly(hexyl methacrylate)
PLM	Polarising light microscopy
PMMA	Poly(methyl methacrylate)
ppb	Parts-per-billion
PTFE	Polytetrafluoroethylene
RDX	Research Department Explosive (Cyclotrimethylene trinitramine)
RE	Reference electrode
R_f	Retention factor
ROI	Region of interest
rpm	Rotations per minute
RSD	Relative standard deviation (%)
RTIL	Room temperature ionic liquid
SAM	Self-assembled monolayer
SCCM	Standard cubic centimetres per minute
SEI	Secondary electron imaging
SEM(-EDX)	Scanning electron microscopy(-energy dispersive X-ray)
SFM	Scanning force microscopy
SLM	Stereo light microscopy
SPE	Screen-printed electrode
SPME	Solid phase microextraction
SWG	Scientific Working Group
SWV	Square wave voltammetry
TATP	Triacetone triperoxide
TFE	Thin-film electrode
TLC	Thin-layer chromatography
TNT	2,4,6-Trinitrotoluene
TNX	Hexahydro-1,3,5-trinitroso-1,3,5-triazine
TWG	Technical Working Group
TWGFEX	Technical Working Group for Fire and Explosions Analysis

UV	Ultraviolet
UV-Vis	Ultraviolet-Visible
WA	Western Australia
WE	Working electrode
XRF	X-ray fluorescence
XRPD	X-ray powder diffraction

Chapter 1 Introduction

The analysis and characterisation of explosive residues is a complex area of forensic chemistry, given the unknown nature of the explosive residue in question [1-4] and the complex matrix often associated with the residue [5, 6]. For this reason, a number of investigative and analytical challenges exist in forensic explosives chemistry. These challenges occur during the immediate aftermath of an explosion [3, 7-10] and are present throughout the subsequent examination of various forms of evidence submitted to the laboratory for analysis [11-17]. This thesis aims to address specific challenges present in three aspects of the forensic explosives evidence process: recovery, storage and analysis.

Information resulting from the analysis of forensic explosives samples can be of great significance in an investigation. This may include linking a suspect to an explosive device, or to determine whether an explosion was part of a terrorist attack; the findings may ultimately be used as evidence in court [18, 19]. A notable case involving forensic explosives evidence is the 2002 Bali bombings, during which three bombs were detonated, killing 202 people. Royds *et al.* [8] provided a detailed overview of the forensic chemistry techniques employed during the investigation, including the establishment of a mobile laboratory, the sampling strategy used and the types of sample analysed. Other examples include the Oklahoma City bomber, upon whose clothing traces of PETN were found, and the foiled 'Millennium bomber', who also bore traces of explosives on his clothing [6]. Forensic explosives techniques were also instrumental in the investigation of the 2005 London transport bombings. This is an unusual example in that a class of explosives previously not used before for terror attacks was used (so-called 'HPOM' explosives (hydrogen peroxide organic mixtures)) [12, 20]. Unlike more conventional peroxide explosives, such as TATP and HMTD, which consist of monomolecular compounds, HPOMs consist of mixtures of fuels (typically carbohydrates, such as flour or sugar) and concentrated hydrogen peroxide. They began to emerge sometime after 2002 [20].

1.1 Explosives

Explosives are defined as chemicals which can instantaneously release energy from a small volume of material [21]. This explosion process involves the release of chemical energy caused by changes in the chemical composition of the explosive substance. Explosives are classified as either 'high' or 'low' explosives, with high explosives producing a supersonic shockwave when detonated, with the shockwave's velocity progressing through the material faster than the speed of sound, whereas low explosives involve burning (deflagration) and a

subsonic shockwave, with the reaction speed slower than the speed of sound [22]. Figure 1.1 illustrates a typical shockwave and overpressure profile of an explosion.

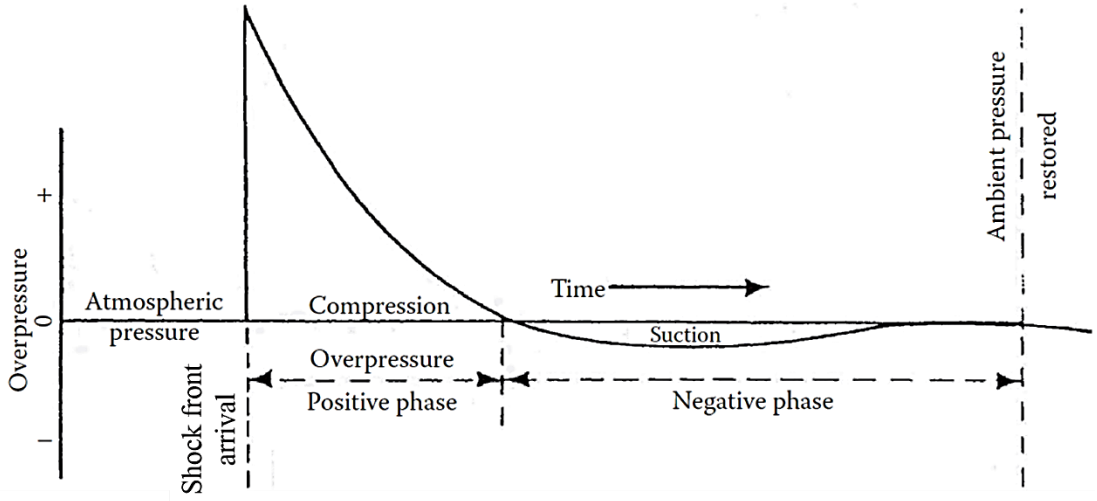

Figure 1.1: Shockwave and overpressure profile of a free-air explosion, sourced from Mohanty [21]

A wide variety of explosives exist. These include commercial explosives, such as 2,4,6-trinitrotoluene (TNT), nitroglycerin (NG), pentaerythritol tetranitrate (PETN), cyclotrimethylene trinitramine (RDX) and ammonium nitrate-based compositions such as ammonium nitrate-fuel oil (ANFO), and homemade or improvised explosives, which are typically used in improvised explosive devices (IEDs). Homemade explosives may be peroxide-based, such as triacetone triperoxide (TATP) and hexamethylene triperoxide diamine (HMTD), or the result of combining nitric acid with a readily available precursor, such as urea, to form species such as urea nitrate [23]. Table 1.1 provides information regarding the structures, applications and examples of incidences of use of a range of explosives.

Table 1.1: Explosives structures, applications and incidences of use

Explosive	Structure	Applications	Incidences of use
TNT (2,4,6-trinitrotoluene)	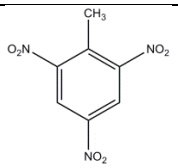	Commercial; also used by the military [22].	Often used as a booster for ANFO explosives.
NG (nitroglycerin)	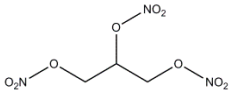	Used in early blasting caps. Used in dynamite for historical mining applications, though now mostly superseded by ANFO [22].	Dynamite was used in the bombing of the New Tokyo International Airport, Narita, Japan, 1985 [18] and in the 2004 Madrid train bombings.
PETN (pentaerythritol tetranitrate)	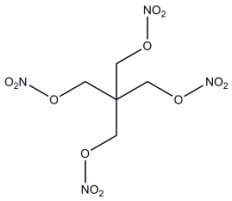	Military explosive, often used in combination with TNT, known as pentolite, or with RDX, to form Semtex. A common filler for detonating cord and blasting caps [22].	Used in Lockerbie bombing, 1988 [24].
RDX (1,3,5-trinitro-1,3,5-triazacyclohexane; cyclotrimethylene trinitramine)	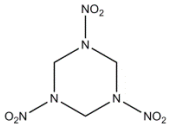	Also known as 'Research Department Explosive'. Widely used military explosive. Major component (91 %) of military explosive known as Composition C-4. Also a key component of Semtex, along with PETN [22].	RDX (as part of Semtex) used in Lockerbie bombing, 1988 [24].
HMX (cyclotetramethylene tetranitramine)	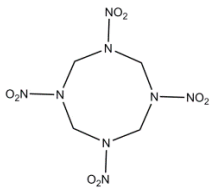	Also known as 'High Melting Explosive' [22]. By-product of RDX manufacture.	

TATP (triacetone triperoxide)	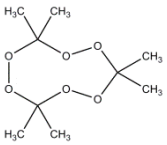	An improvised explosive; no commercial applications as shock sensitivity is too high. Commonly utilised by terrorists worldwide [22]. Typically used as a detonator in an IED.	First emerged as an explosive in Israel in the 1980s. Appeared in the US in the subsequent decade [25]. Used by failed 'shoe bomber' in 2001 [26], and by the Brussels airport bomber in 2016 [27].
HMTD (hexamethylene triperoxide diamine)	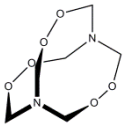	An improvised explosive; less common than TATP. No commercial uses [22].	Emerged as an improvised explosive in the 1980s [25].
EGDN (ethylene glycol dinitrate)	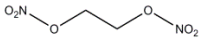	Used in some later dynamite formulations with NG to lower the freezing point and make it safer to handle [22].	
2,4-DNT (2,4-dinitrotoluene)	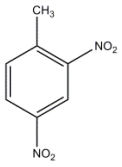	By-product in TNT synthesis. Also sometimes used as an explosive in its own right. A common additive to propellant formulations.	Used as a propellant in pipe bombs.
ETN (erythritol tetranitrate)	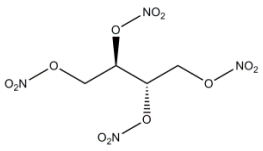	An improvised explosive formed by the nitration of erythritol, a common sweetener [28, 29].	
DMDNB (dimethyl dinitrobutane)		A taggant for explosives, used by several manufacturers to aid identification and detection of explosives.	
ANFO (ammonium nitrate-fuel oil)		Widely used by the mining industry for blasting purposes; thought to be the most common explosive in current use today [22].	Used in Oklahoma bombing, 1995, and Oslo bombings, 2011 [9, 30].

Black powder (charcoal, sulfur, potassium nitrate - often 15:10:75 by mass [22])	First military explosive and the first propellant. Occasionally still used as a firearms propellant, though has been superseded by smokeless powder [22].	Often used in pipe bombs [31, 32].
Potassium chlorate, sulfur, aluminium	A physical mixture of chemicals used in improvised explosive devices.	Used in Bali bombings, 2002 [8].
HPOM (hydrogen peroxide organic mixture)	An improvised explosive mixture. Fuels can include flour, sugar etc.	Used in London bombings, 2005 [2, 20]

1.2 Forensic chemical analysis of explosives and explosive residues

The chemical analysis of samples suspected of containing explosive residues is important to confirm whether explosives are definitely present, in addition to the determination of the exact type of explosive present. This knowledge may then aid investigators and may help to introduce or eliminate specific lines of enquiry based on previous intelligence [8, 33]. A wide variety of techniques is required for the analysis of forensic explosives samples, given their unknown nature. In some cases, initial analyses may be performed at an explosion scene itself to provide preliminary intelligence about the type of explosive used at a scene [8, 33, 34]. For example, presumptive, or spot, testing may be performed at a post-blast scene [35, 36] - this is a rapid method to obtain a tentative identification of the class of explosive present. Portable explosive detection instruments can also be used on-site to provide provisional identities of any explosive species involved in a blast [3, 20, 33, 37-39]. Any preliminary intelligence gathered can be useful in guiding subsequent investigative decisions [33], such as in prioritising samples for further, confirmatory, analyses back in the laboratory [3].

As the nature of many explosives samples received into a laboratory will be unknown, it must be ensured that an analytical sequence is performed which will allow the detection of whatever species is present. There is no single analytical protocol which can be applied for the analysis of all explosives [34], though there are widely accepted flowcharts available [3, 40]. Explosives can have vastly different properties, and they may thus require a broad range of instrumentation for analysis. The FBI and US Department of Justice's National Institute of Justice have established around 30 Scientific Working Groups (SWGs) and Technical

Working Groups (TWGs) aiming to establish standards and guidelines for a number of forensic science disciplines [41]. TWGFEX (the Technical Working Group for Fire and Explosions Analysis) have prepared a comprehensive set of recommended guidelines for those involved in the analysis of both intact and post-blast explosives. These guidelines have divided the most commonly-used analytical techniques for explosives into categories designated from 1-4, depending on their contribution towards the identification of an explosive [42, 43]. Category 1 techniques (e.g. GC-MS) provide significant structural/elemental identification and are sufficient on their own for an identification, Category 2 techniques (e.g. Raman) provide limited structural or elemental identification which must be verified by one more supporting technique for identification, Category 3 techniques (e.g. ion chromatography) provide some degree of selectivity and require two more supporting techniques for identification, and Category 4 techniques (e.g. spot tests) cover other useful techniques which do not fall into Categories 1-3. Table 1.2 summarises the techniques detailed in the TWGFEX guidelines:

Table 1.2: TWGFEX evidential significance categories [42, 43] for forensic explosives analysis techniques. Note that a single technique may be classified as either Category 1 or Category 2, depending on the specific explosive concerned.

Categories 1 and 2	Category 3	Category 4
Infrared Spectroscopy (IR)	Gas Chromatography (GC)	Flame Test
Gas Chromatography-Mass Spectrometry (GC-MS)	Gas Chromatography-Thermal Energy Analyzer (GC-TEA or EGIS)	Spot Test
Energy Dispersive X-Ray Analyzer (EDX)	Liquid Chromatography-Thermal Energy Analyzer (LC-TEA)	Melting Point
Raman Spectroscopy	Liquid Chromatography (LC)	
X-Ray Powder Diffraction (XRPD)	Ion Chromatography (IC)	
Liquid Chromatography-Mass Spectrometry (LC-MS)	Capillary Electrophoresis (CE)	
Ion chromatography-Mass Spectrometry (IC-MS)	Thin Layer Chromatography (TLC)	
X-Ray Fluorescence (XFR)	Ion Mobility Spectrometry (IMS)	
	Polarizing Light Microscopy (PLM)	
	Stereo Light Microscopy (SLM)	

A comprehensive examination sequence illustrating the use of these techniques is shown in Figure 1.2, adapted from Strobel [3].

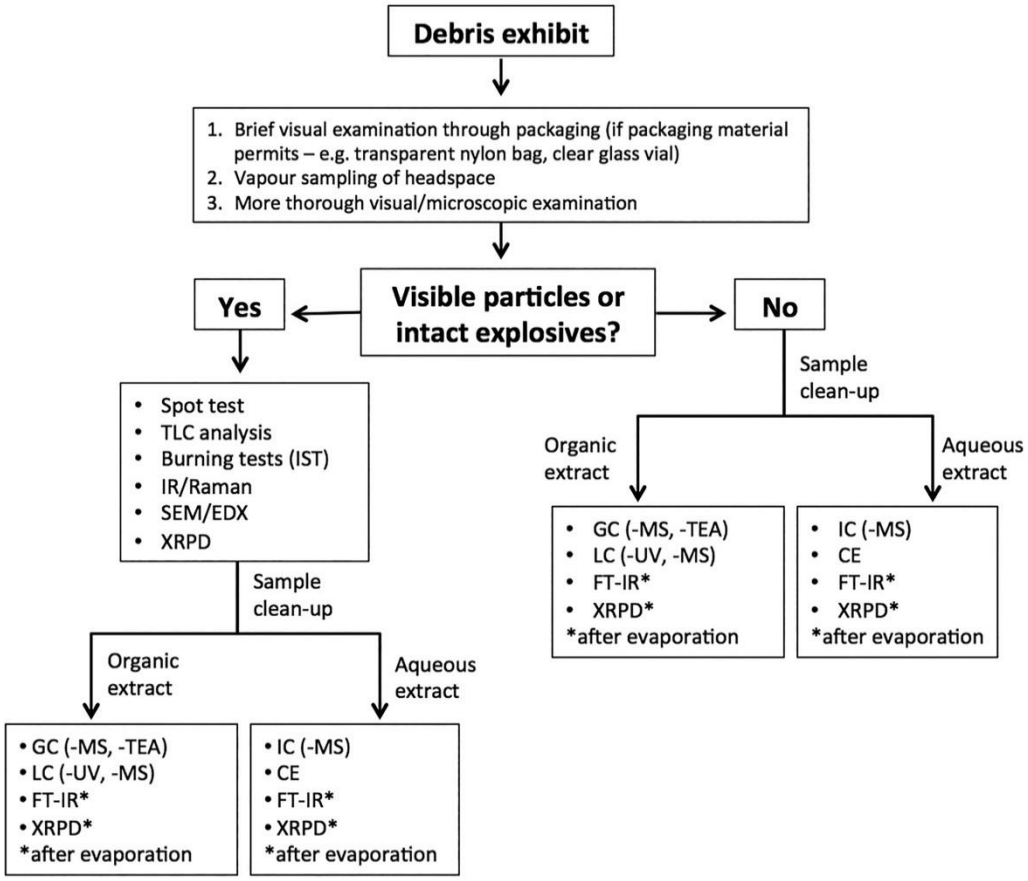

Figure 1.2: Flow-chart detailing typical analytical sequences and techniques for explosives evidence (adapted from Strobel [3])

1.2.1 Rapid screening tests for explosives

Visual and microscopic examinations can provide useful information. Depending on the sample submitted, such examinations may provide information on the method of device construction and other evidence such as circuitry, switches and wires used in a device, and whether or not a device was involved in a high or low order explosion [3, 34, 40]. Occasionally, unburned particles of explosives, such as black powder or smokeless powder particles, may be observed on a piece of debris [3]. These can help to establish the composition of explosives used within a particular device. If such particles or intact explosives are found, then they can be subjected to various analytical techniques, such as IR spectroscopy [4, 34, 44], Raman spectroscopy [34, 45-47], scanning electron microscopy (SEM)-based techniques [34, 48], X-ray powder diffraction [48], thin-layer chromatography [31, 49] and spot tests [34-36]. Each technique is briefly discussed below.

Spot tests are a valuable technique as they can give an almost instant identification of the class

of an explosive [34-36]. Although a simple and quick technique, spot tests tend to have relatively high limits of detection. In addition, as spot tests only indicate the general class of an explosive compound, further tests must be performed in order to identify the exact compound present. In addition, there is a danger of false positives from such tests [50]. The process involves placing a small quantity of recovered material (typically a few grains) onto a ceramic tile, and adding specifically designed reagents [35, 36]. The presence of the class of explosive which the reagents are designed to test for will lead to a visible colour change. Different classes of explosives can give rise to different colours. For example, the Griess test and the diphenylamine test have both been developed, with positive results seen as a deep pink colour or a blue-black colour [34, 51] (see Table 1.3).

Table 1.3: Spot test results for various explosives using diphenylamine and Griess tests. Data from Parker *et al.* [51]

	Reagent	
Substance tested	Diphenylamine	Griess
Nitrate	Blue to blue-black	Pink to red
Nitrite	Blue-black	Red to yellow
Nitrocellulose	Blue-black	Pink
Nitroglycerin	Blue to blue-black	Pink to red
PETN	Blue	Pink to red
RDX	No reaction	Pink to red
TNT	No reaction	No reaction
2,4-DNT	No reaction	No reaction

Thin-layer chromatography (TLC) is one of the oldest techniques for explosives analysis [31], and can be a useful complementary technique to spot tests. It can provide rapid information about the types of explosive present in a sample. TLC analysis of visible particles of explosives involves dissolving a small quantity of material in a small volume of solvent. This is then spotted onto a TLC plate, alongside reference explosive standards, and the plate is eluted using a suitable solvent system. Visualisation of the plate can be performed using UV light, or by the addition of visualisation reagents, such as by spraying the plate with Griess reagent to bring about a colour change. The retention factor (R_f) value of the unknown sample's spot can then be compared with the R_f values of the reference standards, to give an indication of the likely explosive compound present within the sample [31].

The use of TLC separation and visualisation techniques for explosives compounds has many advantages – it is very fast, inexpensive, easy to perform and can give a good indication of the type of explosive present within a sample. It can also be used for extract clean ups [40]. It is

also possible to analyse several samples at once, on the same plate [31]. However, TLC's main disadvantage is its low sensitivity for detection and visualisation – estimated to be in the low microgram/high nanogram range [49]. Additionally, the method is not efficient for large-scale examinations, and its utility may be limited as alternative methods with higher specificity are likely to be used.

Infrared (IR) spectroscopy can provide direct information about the molecular structure of an explosive. It is non-destructive in nature and offers rapid analysis times. IR spectroscopy has been shown to be useful for the analysis of both organic and inorganic explosives; many inorganic ions in particular have very strong absorption bands [34]. For example, IR can give good characterisation of nitrate, chlorate and ammonium ions [44]. A drawback is that bulk material is required for analysis; the technique is not suitable for trace explosive residue identification. Raman spectroscopy can be used as a complementary technique to infrared spectroscopy, being particularly useful as it can analyse a wider spectroscopic range than IR [34].

1.2.2 Scanning electron microscopy/energy dispersive X-ray spectroscopy and X-ray powder diffraction

Scanning electron microscopy/energy dispersive X-ray spectroscopy (SEM/EDX) is a non-destructive technique which can be useful for the analysis of recovered explosives particles. Many elements can be detected using this technique. It is excellent for detecting carbon and sulfur in black powder, and it offers low detection limits. Sample preparation is straightforward, and, unlike IR spectroscopy, the technique can be used to analyse and determine the identity of metal particles [34]. Metallic particles will often be found in pyrotechnic compositions, such as sparklers (hand-held fireworks), and aluminium may be added as a fuel in explosives compositions.

Another non-destructive technique which can be useful for the analysis of recovered explosives particles is X-ray powder diffraction (XRPD) [34]. This technique is well-suited to the analysis of crystalline compounds. In order to identify an explosive, the diffraction patterns generated by the crystals are compared to standard diffraction patterns held within a database. XRPD is useful for both pre- and post-blast trace and bulk sample analyses. XRPD and SEM/EDX are excellent complementary techniques for use during the analysis of explosives samples, though it should be noted that each of the techniques requires discrete identifiable solid/crystalline material for analysis.

1.2.3 Separation techniques

Gas chromatography (GC) techniques are widely used for the analysis of explosives. Gas chromatographs can be readily coupled to a variety of detection systems, giving a number of different analysis methods. In GC-based techniques, the analytes of interest first undergo volatilisation, before separation on a GC column and subsequent detection [31]. The most common detectors for explosives using GC analyses are mass spectrometers (GC-MS) and chemiluminescent/thermal energy analysers (GC-TEA).

A wide variety of explosives can be analysed using GC-MS, with reliable identifications possible by comparison with comprehensive spectral libraries. In addition to conventional organic explosives, GC-MS techniques are also suitable for the analysis of organic additives used in propellant powders [34]. Although they do show many benefits, such as high specificity, GC-MS techniques are less sensitive than GC-TEA techniques [12].

GC-TEA techniques are highly selective, and more sensitive than GC-MS systems. Following compound separation by the GC column, compounds are pyrolysed in a furnace coupled to the end of the column. Many explosives containing nitro groups will produce nitric oxide as a pyrolysis product, which reacts with ozone to yield an excited nitrogen dioxide radical. Upon relaxation, this species will chemiluminesce, and this emission is detected using a photomultiplier [12]. It is for these reasons that GC-TEA is so selective and sensitive. However, although it is suitable for many nitro-containing explosives, such as TNT, 2,4-DNT and EGDN, it cannot detect nitro-containing nitrocellulose and HMX molecules [12]. Additionally, GC-TEA is solely suitable for the detection of nitro-containing explosives – peroxide explosives, for example, which do not contain nitro-groups, cannot be detected using GC-TEA.

Other GC detectors in use for the analysis of explosives include flame ionisation detectors (GC-FID) and electron capture detectors (GC-ECD). GC-FID can be used to detect most organic compounds and is particularly useful for the detection of the fuels used in ANFO explosives [31]. GC-ECD is a highly sensitive technique, with detection limits reported to be an order of magnitude lower than with GC-MS [31]. In general, gas chromatography-based techniques are poorly-suited for the analysis of peroxides. This is due to the thermal lability of peroxides, meaning they may break down in the GC inlet port. This can make satisfactory separations difficult [16].

On the other hand, liquid chromatography (LC)-based techniques have been shown to be well-suited for the analysis of peroxide explosives and other thermally labile explosives, such as PETN and HMX. As liquid chromatographic analyses are performed at much lower

temperatures than GC-based methods, thermal lability is not an issue [12]. As is the case for GC analyses, several detectors can be coupled to liquid chromatographs. The two most common detectors for LC analyses are UV and mass spectral detectors [31]. Although much less expensive than LC-MS based techniques, LC-UV instruments show less specificity for identifications, and, in addition, analytes typically must possess chromophores in order for a more reliable provisional identification to be made. This makes LC-UV techniques less suitable for some explosives, such as TATP, which lack suitable chromophores.

For this reason, mass spectral-based LC-techniques are often employed for explosives analysis, with tandem MS/MS instruments particularly useful. The degree of identification and confirmation offered by LC-MS/MS instruments is of huge benefit during the forensic analysis of explosives. LC-MS/MS instruments typically employ either electrospray ionisation (ESI) or atmospheric pressure chemical ionisation (APCI) techniques, each of which can be performed in either positive or negative ionisation mode, giving highly reproducible results [31, 52-54].

Ion chromatography (IC) is widely used for the analysis of inorganic species found in post-blast debris [31, 34]. Ion chromatographic separations rely on differential interactions between ions and a stationary phase [34]. Ion chromatography is a very sensitive technique, with detection levels in the parts per million range. However, it does show a weakness in that it can be affected by matrix effects and high sample concentrations. For this reason, it is often necessary to use an orthogonal technique such as CE, XRPD, TLC or Fourier Transform Infrared (FTIR) to confirm results. More recently, IC-MS instruments have been developed, coupling ion chromatographs with mass spectral detectors, to allow an orthogonal analysis to be performed using a single instrument [31].

Capillary electrophoresis (CE) can be employed as an orthogonal technique to ion chromatography. It relies on a different separation mechanism to ion chromatography – separations occur based on an ion's mass/charge ratio [34]. Capillary electrophoresis can provide excellent separations of all ions of interest present within a sample. Additionally, it is more efficient than ion chromatography, with higher numbers of theoretical plates. In addition, poisoning of the contained stationary phase is not as likely to occur, compared to ion chromatography [31]. However, as with ion chromatography, problems can occur due to sample concentration effects, with relatively 'clean' extracts also required for analysis [31]. Additionally, matrix effects can also be problematic [55].

1.3 The recovery of explosives from textile surfaces

As outlined above, it is clear that a wide range of techniques have been established for the analysis of forensic explosives samples. However, although much effort has been devoted towards the development and validation of methods for the *analysis* of trace explosives samples, less work has been performed with regards to the *recovery* of explosives traces from submitted exhibits. This is arguably the most important stage in an examination sequence, as if no explosives are recovered from an exhibit, then it follows that no explosives will be detected during the analysis of these samples. As only nanogram quantities of undetonated explosive typically remain at a post-explosion scene [1, 23], it is vital that these traces are recovered and detected. It is therefore of paramount importance that suitable recovery methods are used, taking into account the nature of the surface to be sampled.

Vapour or headspace sampling can provide a useful starting point to provide an indication of the type of explosive present in a sample, particularly when volatile explosives, such as TATP, are present. Several techniques have been developed to perform headspace examinations [31, 56-59]. One such technique involves taking a direct sample of the headspace above a piece of debris using a syringe, the contents of which can then be injected into a gas chromatography system for analysis. Other techniques include the use of activated charcoal, Tenax strips, cartridges containing adsorbent polymers such as XAD-7, and the use of solid phase microextraction (SPME) fibres [31, 56-58]. SPME has been shown to be effective in the detection of peroxide explosives, including TATP, giving rise to chromatograms relatively free from contamination [31]. Additionally, SPME fibres can be re-used multiple times, making them an economical option.

Swabbing is a widely used technique for explosive residue recovery from different surfaces. The process involves passing a swab over a surface of interest, after which the swab is subjected to a clean-up process, and the extract analysed as shown in Figure 1.2. Different laboratories have different swab/solvent preferences. For example, in the US, the FBI employs dry cotton swabs to collect explosive residues [20]. In the UK, the Forensic Explosives Laboratory (FEL) uses 1:1 *v/v* ethanol:water wetted cotton swabs [6]. The Australian Federal Police (AFP) have recently developed a procedure using polyester-based alcohol wipes wetted with 7:3 *v/v* isopropanol:water [60]. These different methods appear to be dependent on jurisdictional preferences, and to date no comprehensive studies have been performed to compare the wide variety of swabbing techniques available.

Recovering explosive residues by swabbing may be an effective technique for smooth, non-

porous surfaces such as glass, metal and plastics, where explosive residues are not absorbed [61, 62]. However, although the technique is also used for porous surfaces such as clothing and carpets [31, 63], solvent-swabbing is less successful from these porous surfaces compared to non-porous surfaces [64]. There are several explanations for this: The use of solvents on fabrics may cause damage to the fabric in question. Additionally, when solvent-swabbing a piece of clothing, often only a general swab of the garment is taken, meaning that any sections containing high concentrations of explosive residues may be inadvertently passed over and not sampled [23]. The technique is not a targeted approach as explosive residues are typically not visible on textiles.

Alternative methods in current use for explosive residue recovery from textiles include vacuum sampling and solvent extraction [12, 24, 63]. Figure 1.3 illustrates the vacuum sampling apparatus employed by the UK Forensic Explosives Laboratory [65] (note that the bung is removed in use).

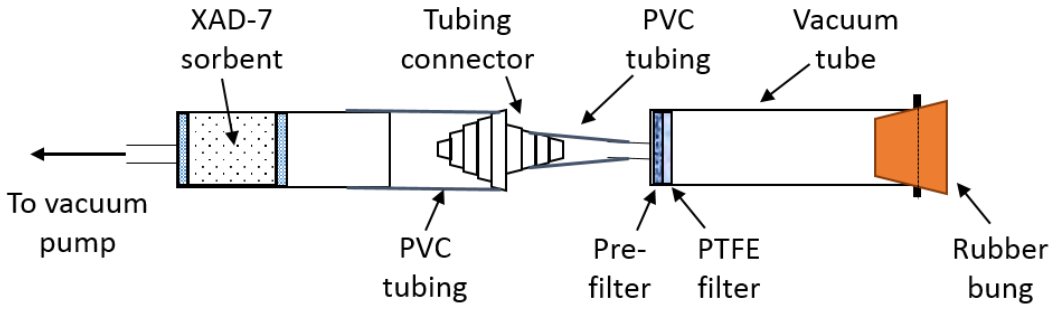

Figure 1.3: Vacuum sampling apparatus used by the UK's Forensic Explosives Laboratory, adapted from reference [65]

With vacuum sampling, explosive crystals are caught and collected onto a fine filter [12, 24, 61]. This method relies on the presence of relatively large explosive particles, which may not always be present. Solvent extraction, on the other hand, involves cutting a swatch from the garment in question, followed by solvent extraction [63, 66, 67]. However, this technique also carries limitations in that it is destructive to the item in question, as well as being time-consuming and labour-intensive, with the resulting extract relatively dilute and requiring pre-concentration prior to analysis.

Although there are limitations to explosives recovery methods for porous surfaces, such surfaces have been useful sources of explosives evidence in investigations [3, 64, 66, 68]. For example, traces of PETN were found on the clothing of the Oklahoma City bomber, and traces of explosives were found on the clothing of the foiled 'Millennium bomber' [6]. Brust *et al.* [66] describe the detection of PETN from the clothing of a suspect in a series of safe-crackings. Other literature also highlights the fact that textiles are a good matrix for trapping explosive

residues [3, 6]. These cases illustrate the potential importance that explosive residues on fabrics can have during an investigation.

Recently, new methods for explosive residue sampling from clothing and textiles have been reported, with several researchers employing Raman-based sampling techniques [45-47]. Although these analyses are fast and non-destructive, with high sensitivity, they typically require focusing of the Raman laser beam (with a 5 μm diameter) onto explosive particles [45, 46], which may be challenging due to the small size of explosive particles. A further drawback of Raman-based techniques is that the technique does not permit the removal of the explosive from a surface, to enable further analyses to be performed. Ionisation-based techniques are also emerging as alternatives for sampling from textiles, allowing *in situ* detection with suitable detection limits [64, 69, 70]. However, these ionisation-based techniques also do not permit the isolation of the bulk explosives present on a surface, to enable further analyses.

Textile fabrics are ubiquitous and thus are likely to be present at many post-blast scenes. It is therefore clear that they present good potential as sources for trace explosive residue evidence, by acting as a good collection medium both at scenes or sites where explosive materials may have been constructed or transported. Further work must be performed to try to improve current techniques used for explosive residue recoveries from textile surfaces.

Atomic force microscopy enables information to be obtained regarding the adhesion of a substance to a surface of interest. Atomic force microscopy may therefore be an ideal technique to determine the types of textile surfaces explosive crystals are most likely to adhere to. This ability has previously been used to assess the adhesion of explosive crystals to painted aluminium surfaces and monolayers [71, 72]. By extending this concept and investigating the adhesion of explosives to a wide variety of textile surfaces, this information may help to improve current sampling methods for recovering explosive residues from textile surfaces. A detailed overview of atomic force microscopy is provided in Chapter 2, and experiments are detailed to investigate the adhesion of explosives to a variety of surfaces.

In addition, it may also be useful to compare the adhesion of explosives to different textile surfaces with their recoveries from the same surfaces, to determine whether a relationship exists between the two. The contact heater is a heated recovery apparatus specifically designed for the recovery of explosive residues from textile surfaces, and its use should enable the relationship between explosives' adhesion and recovery from a surface to be investigated. A detailed background of the contact heater is provided in Chapter 3, followed by experiments exploring the recovery of explosive residues from a variety of textile surfaces. In addition, a small-scale comparison using the vacuum sampling approach used by the UK's Forensic

Explosives Laboratory [65] is trialled, to compare the utility of the contact heater against a more commonly-used recovery technique.

1.4 Soil as a source of forensic explosives evidence

Soils also pose a challenging potential source of explosives evidence. Explosives are a common soil contaminant at a range of sites, including military training and firing ranges and areas associated with landmine detonations [73-77]. Soil samples are routinely taken from the vicinities of outdoor explosions such as car bombs and landmines [8]. Soil close to the blast seat is likely to capture explosive residues meaning it is potentially a good source of evidence. However, when collecting soil samples in this manner, the persistence of explosive residues in soil within the vicinity of an explosion scene also needs to be considered, as explosive residues in soils can undergo a variety of attenuation processes (discussed in more detail in Chapter 4).

Explosive residues are particularly susceptible to undergo microbial-mediated degradation in soils [75, 78-85]. The degradation of explosive residues in soils may occur within timeframes as short as two or three days [10], with this time period typical of those found in any forensic investigation [8]. This is therefore a major challenge for the forensic explosives analyst, and investigations into the fate of explosive residues in soils immediately after their deposition would be of benefit from a forensic analysis perspective.

From a bioremediation perspective, a considerable body of work has been performed to investigate the fate of explosive residues in soils [10, 74-78, 83, 85-108]. This research has revealed that a number of processes may affect the stability or attenuation of explosive residues in soil. Biodegradation of explosive residues by soil-borne microbes and bacteria is one of the major pathways for the attenuation of explosive residues in soil. RDX can biodegrade under both aerobic and anaerobic conditions [73, 109], with less known about the biodegradation of PETN [109]. TNT is highly susceptible to reduction by bacteria, and has been shown to rapidly biodegrade under both aerobic and anaerobic conditions [109]. The initial transformation products are aminodinitrotoluenes (ADNTs; either 2-ADNT or 4-ADNT), with 4-ADNT reported to form in greater quantity than 2-ADNT [92] due to steric effects [109, 110].

By storing soil samples at low temperatures, the rate of microbial degradation of explosive residues may be reduced. However, although a large proportion of research investigating the degradation of explosive residues in soil has stored soil samples at room temperature [77, 83, 88, 89, 92, 96, 99-101, 103, 104, 108], comparatively little research [10, 95, 98] exists in the

literature where researchers have studied different storage temperatures to assess the effect of temperature on the stability of explosive residues in soil samples. One recent example investigated the fate of a variety of explosive residues in three different soils [10]. The majority of the soil samples were stored at room temperature, though one soil type was also spiked and stored refrigerated or frozen, with the explosive residues displaying a higher stability in the samples stored at lower temperatures. The authors concluded it would be useful to assess the stability of explosive residues under different storage conditions in a wider variety of soils.

Although research has been performed to investigate the fate of explosive residues in soils from a bioremediation point of view, very little research has investigated the degradation of 'freshly-deposited' explosive residues from bombing incidents, despite soil from the vicinity of vehicle bombings being likely to be a good source of such residues [8]. Though recent research has been directed towards the development of at-the-scene detection techniques for explosive residues in soil [111-113], it is likely that for the foreseeable future, soil samples will continue to be transported back to laboratories for analysis. It would therefore be of use to assess a variety of storage conditions with the aim to maximise the stability of explosive residues in such soil samples, prior to their analysis. This idea is explored in Chapter 4 of this thesis. In addition, it would be of benefit to assess whether previous work investigating the degradation of explosive residues in pristine soils spiked with solutions of explosives (the most common approach taken for explosives-degradation studies in soils) is representative of the degradation rates observed in post-blast soils exposed to an actual detonation process. Micro computed tomography (μCT) has previously been used to analyse soils to determine internal pore structures and connectivity [114-116]. It may also be a useful technique for the analysis and comparison of pristine and detonated soils to provide information regarding the effects of a detonation on a soil's structure, and how this may influence explosive residue degradation rates. Work towards this goal is detailed more fully in Chapter 5.

1.5 Portable detection instruments for at-the-scene analysis

As described above, the vast majority of forensic explosives samples will be transported to a laboratory for analysis. On the other hand, the ability to detect explosive residues at or near an explosion scene itself would offer a number of advantages. These advantages include faster investigative intelligence and a potentially higher likelihood of encountering explosives. As only nanograms of undetonated explosive residues are expected at a post-explosion site [1, 23], a longer duration between the detonation and sampling may reduce the quantity of detected explosive if it has a low persistence on the surface it is deposited on. In addition, as sampling at a scene would remove the need for exhibit packaging, transportation to a

laboratory and then unpackaging, it has the potential to reduce the risk of cross-contamination [23].

For these reasons, the development of field-deployable portable analytical instruments to characterise explosive residues 'at-the-scene' is an active area of research. Portable explosives detection instruments can be used on-site or at nearby portable laboratories to provide provisional identities of any explosives species involved in a blast. Portable explosives detection equipment can offer many benefits, the main one being that of very rapid screening. This is particularly useful for large explosion scenes. A number of different portable explosives detectors have been developed [3, 20, 33]. Typically, these are smaller, lighter versions of standard laboratory-based analytical instruments. Examples include field-portable Raman and IR instruments, gas chromatographs with chemiluminescent detection, ion mobility spectrometers, ion chromatographs, capillary electrophoresis instruments, gas chromatography-mass spectrometers and gas chromatography-surface acoustic wave instruments [3, 20, 33].

Typically, analyses can be performed on the second- or minute-timescale, with analyses usually completed within around 10 minutes. This allows the rapid screening of multiple samples on site, to provide preliminary intelligence about the type of explosive used at a scene, which can be useful in guiding investigations [33]. For remote explosion scenes, it may take some time for explosives samples to be transported and received into a suitable laboratory for analysis. For example, the Australian Federal Police have used portable analytical equipment in a mobile laboratory to aid investigations where the transportation of samples to a suitable laboratory would have taken over eight hours by plane [8, 33]. The results generated by such portable analytical equipment can also be useful in prioritising samples for further, confirmatory, analyses back in the laboratory [3].

Innovative portable equipment has been developed for the ultra-rapid detection of explosive residues following an explosion. Hutchinson *et al.* have developed a portable capillary electrophoresis instrument containing a light-emitting diode (LED) detector for photometric detection [37]. Related work by Hutchinson *et al.* has developed a portable CE method which can separate 10 anions within 45 seconds, which offers the potential of giving very rapid indications of any possible explosive residues present [38]. Taudte *et al.* have also recently developed an interesting portable explosives detector, using wax-printed paper, treated with a fluorescent pyrene solution. In the presence of 10 separate organic explosives, fluorescence quenching of the pyrene was observed, with limits of detection for the explosives as low as 100 ppm [39]. In addition to their use at post-blast scenes, such systems show the potential for use in airport security screening, due to their fast analysis times and low limits of detection.

Recently, new developments in portable detection instrumentation have begun to emerge. For example, Contreras *et al*. [117] reported the development of a portable GC-MS bearing a toroidal ion trap mass analyser, using a solid-phase microextraction fibre for sample collection and transfer into the GC inlet port. Sample analysis can be performed within 5 minutes, and the battery life can support up to 50 analyses. This technique has so far been trialled for environmental samples [117, 118], though it shows good potential for use with regards to explosives detection. A recent review by Syms and Wright [119] describes a number of other portable detection instruments with likely applications as portable explosives detectors.

However, portable explosives detection instruments do have some drawbacks. For example, portable GCs tend to contain shorter columns than conventional GCs, in order to reduce the overall size and thus increase the portability of the instrument. This means that they tend to give poorer chromatographic resolution than conventional GCs [120]. A further challenge of such portable detection equipment is that the devices involved can be expensive, and difficult to operate. It should also be noted that such devices do not provide information of the evidentiary value required for court; rather, they are used to guide sampling and ensure contamination is minimised.

The use of electrochemical sensors for at-the-scene detection presents a viable alternative. Electrochemical sensors are very small, lightweight and relatively inexpensive, yet they can detect explosive residues with high specificity and sensitivity, and with reproducible results [121], meaning they show good potential for trace residue indication. Additionally, the necessary instrumentation is simple and user-friendly. Low-cost, disposable electrodes have been developed, minimising the potential for any contamination [122, 123]. Many studies have been performed to investigate the electrochemical detection of nitroaromatic explosives, nitrate esters and nitramine-based explosives, which give rise to characteristic redox peaks [122-135]. In each case, 'conventional' electrochemical systems were used, using aqueous solutions of electrolyte to submerge the necessary electrodes. However, such solutions are prone to evaporation, meaning that solvent levels must often be replenished to ensure the electrodes do not dry out.

Room temperature ionic liquids (RTILs) are emerging as a promising alternative electrolyte medium. These are non-volatile, show good thermal stability, excellent conductivities and wide electrochemical potential windows [136, 137]. These therefore have good potential for use in portable electrochemical detection instruments for at-the-scene explosive residue detection, particularly as TNT has previously been shown to have a high solubility in RTILs [138]. Chapter 6 provides an introduction to electrochemical techniques, before outlining work towards the development of a novel electrochemical sensor for the detection of TNT in

aqueous samples.

1.6 Summary and aims

Although established forensic explosives investigation techniques exist, it is clear that a number of challenging areas remain in the field of forensic explosives analysis. This thesis therefore describes a series of studies aiming to improve current practices associated with forensic explosives recovery, storage and analysis. A variety of novel techniques are utilised, including the use of atomic force microscopy (AFM), a novel contact heater instrument, micro computed tomography (μCT) analyses and electrochemical analysis techniques.

Chapter 2 describes the use of atomic force microscopy to investigate the surface roughness of ten textile and five non-textile surfaces. Following this, the adhesion of crystals of TNT, PETN and RDX to the 15 surfaces are measured using AFM, and conclusions drawn with regards to the type of surface explosive crystals are most likely to adhere to.

Following this, in Chapter 3, the recoveries of TNT, PETN and RDX from the ten textile surfaces examined in Chapter 2 are investigated using a contact heater. A variety of storage conditions and sample ageing times are trialled, to assess the stability and persistence of these explosives on the different surfaces. An assessment is made with regards to the relationship between the adhesion of an explosive to a surface, and its recovery from a surface. In addition, a small-scale study is performed in which spiked surfaces are vacuum sampled, to enable a comparison to be made between the recoveries of TNT, PETN and RDX obtained using the contact heater and vacuum sampling.

In Chapter 4, a number of storage conditions for soil samples containing explosives are examined. Three different soils are spiked using solutions of TNT, PETN and RDX, with the samples stored at room temperature, refrigerated or frozen. Additional samples are purged with nitrogen or are subjected to gamma-irradiation prior to storage, in order to assess the effect of different sample treatment and storage conditions on explosives recovery.

Chapter 5 continues the work performed in Chapter 4, but examines the fate of explosive residues deposited into the same three soils following actual detonation events, to assess whether solution-spiking of soils is representative of samples which would be generated following actual vehicle bombings or landmine detonations. SEM analyses are performed to assess the effect of a detonation on a soil's external structure, and micro computed tomography analyses are utilised to assess the effect of a detonation on a soil's internal structure.

In Chapter 6, electrochemical experiments are performed with the aim of developing a novel

method for the detection of TNT in aqueous samples. A room temperature ionic liquid (RTIL) is combined with a polymer and coated onto the surface of a gold thin-film electrode. This is used as a pre-concentration medium for the TNT. Conditions are then optimised for the use of this functionalised electrode for at-the-scene explosive residue detection.

Finally, in Chapter 7, conclusions are drawn regarding the work presented in this thesis, and suggestions are made for future avenues of research.

Chapter 2 Investigating the adhesion of explosives to textile and non-textile surfaces

2.1 Introduction

Textiles, such as clothing and furnishings, are ubiquitous in our daily lives, and textile trace evidence is often encountered during criminal investigations [139]. Cotton, acrylic and polyester are three of the most commonly-encountered textiles in forensic casework [66], though other textiles reported include wool, silk, denim, fleece, rayon and linen [46, 47, 64, 69]. There are two major classes of textiles: natural and man-made. A typical hierarchy of textile fibres is shown in Figure 2.1.

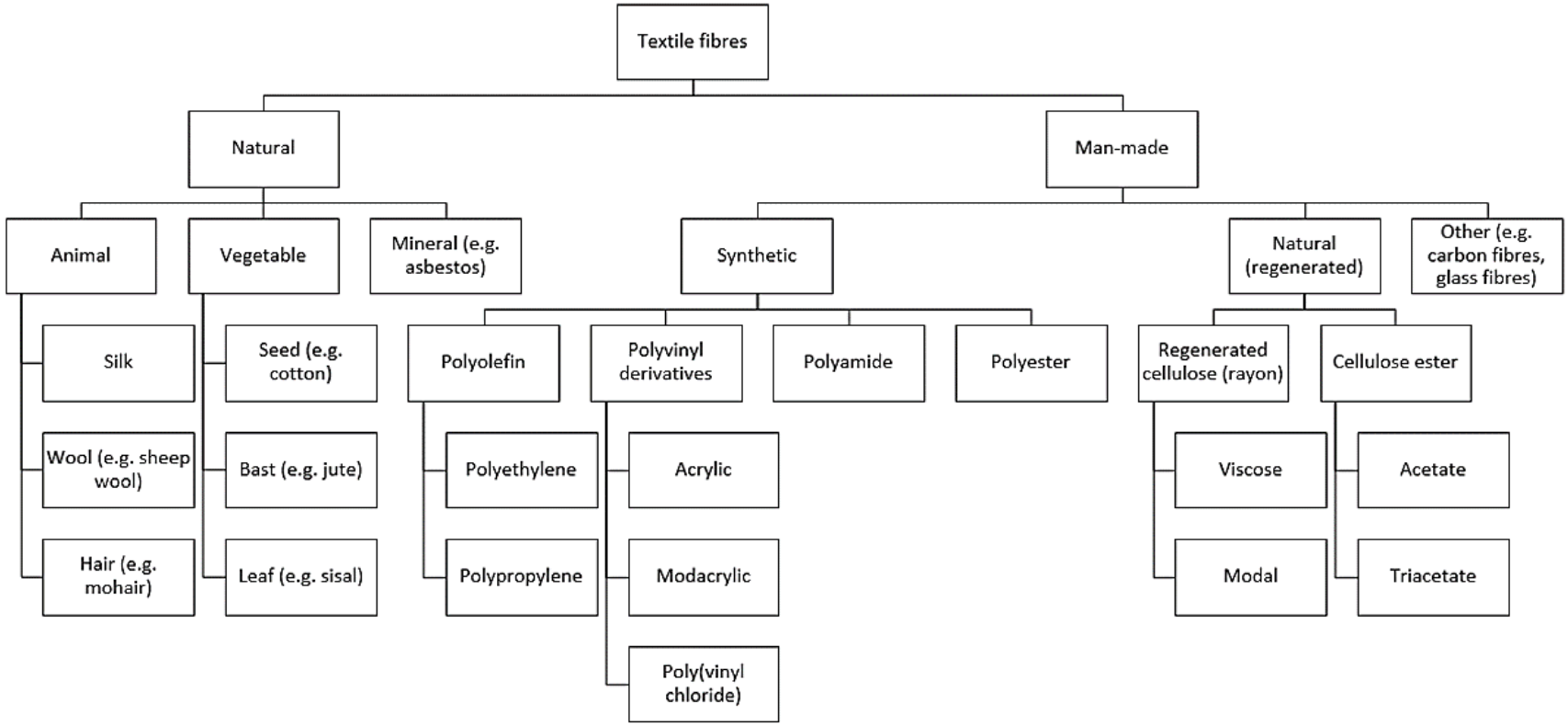

Figure 2.1: Hierarchy of textile fibre classes (adapted from reference [140])

The recovery of explosives evidence from textile surfaces can be vital during a forensic investigation. For example, during the construction of an explosive device, it is likely that traces of explosives will be transferred to the bomb-maker's clothing [6, 63]. Other textile surfaces such as carpets have also been demonstrated to be a good matrix for retaining explosives, with nitrate ester explosives reported to have a particularly high affinity for such substrates [3]. Given the ubiquitous nature of textile fabrics, they represent an excellent collection media for trace explosives, which may be deposited at the time of device manufacture, transportation or at the scene of the detonation. For example, textiles may be present at the scene of an explosion from car seats in the case of a vehicle-borne improvised explosive device, or from the textiles forming part of a suicide vest. However, as discussed in Chapter 1, current methods for the recovery of explosives traces from textiles are inadequate.

In order to improve the recovery of explosives from porous surfaces, a greater understanding is required of the fundamental interactions between explosives and these surfaces. Although techniques are available with which to recover explosive residues from porous surfaces, there is little fundamental research published within the available research literature detailing the nature of the interaction of explosives with porous surfaces. This knowledge will contribute to the establishment and development of new methods to recover explosives from such surfaces, such as the preferred porous surfaces to target for explosives recovery. Atomic force microscopy (AFM) provides an ideal means of assessing the interaction of explosives with different surfaces [71, 72].

2.1.1 Introduction to Atomic Force Microscopy

Atomic force microscopes are a type of scanning force microscope (SFM). The atomic force microscope was first proposed in 1985 by Binnig, Quate and Gerber [141]. It was constructed by combining a scanning tunnelling microscope with a stylus tip, enabling the profiling of a surface under investigation. Atomic force microscopes have a wide range of applications. For example, high resolution images of the surface morphology of a sample can be obtained [142], in addition to the measurement of forces between an AFM probe and a surface (AFM force spectroscopy) down to pico Newton levels of sensitivity. Other novel applications include nano-manipulation of surfaces using an AFM probe [142]. Analysis using AFM involves a cantilever, which is scanned across a surface of interest. A number of different imaging modes are available, which all use different quantities as their feedback parameter. In the current chapter, contact mode AFM was utilised. The key feedback parameter in AFM is the deflection of the cantilever [142]. In contact mode AFM analyses, the interaction force between the AFM cantilever tip and the sample is held at a constant value during the scanning process. The deflection of the cantilever tip is monitored by the use of a laser beam directed onto the tip of

the cantilever, which is reflected back to a position-sensitive four-segment photodiode [143]. A schematic of an AFM is shown in Figure 2.2.

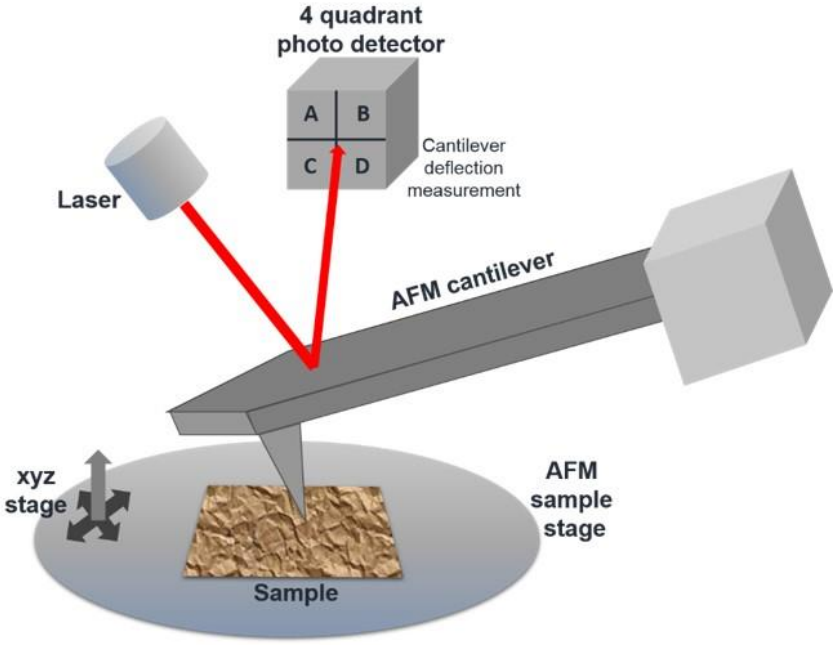

Figure 2.2: Schematic of an atomic force microscope

2.1.2 AFM for adhesion measurements

As well as being useful for measuring the topography of a sample of interest, AFM can also be used to measure forces, such as molecular and surface adhesion forces, between the cantilever tip and a sample of interest with pico Newton sensitivity, which can help to provide an understanding of the surface-level interactions at play between two materials [144]. The flexible cantilever can be treated like a spring and the force can be calculated from the deflection of the cantilever by applying Hooke's law, $F = k\Delta x$, where k is the cantilever spring constant and Δx is the cantilever deflection. The AFM adhesion force comprises four main components, which can be summarised as follows (eq. 1) [72]:

$$F_{ad} = F_{el} + F_{vdW} + F_{cap} + F_{chem} \quad \textbf{(1)}$$

Here, F_{ad} represents adhesion forces, F_{el} electrostatic forces, F_{vdW} van der Waals forces, F_{cap} capillary forces and F_{chem} chemical interactions [72]. Short-range attractive forces are formed from van der Waals forces, and longer-range repulsive forces are Coulombic forces [142]. The van der Waals component of adhesion forces is dependent on a particle's composition, the nature of the substrate of interest, and the medium through which sample analysis occurs (such as air or water). Additionally, surface and particle roughness and their geometries are also believed to have an effect on any van der Waals forces occurring [71].

At large distances between the tip and the sample, the magnitude of any of these forces is negligible, meaning the cantilever undergoes no deflection. However, at much shorter distances between the tip and the sample, the adhesion between a cantilever tip and a sample of interest can be determined by measuring force-distance curves. This sequence is illustrated in Figure 2.3, below.

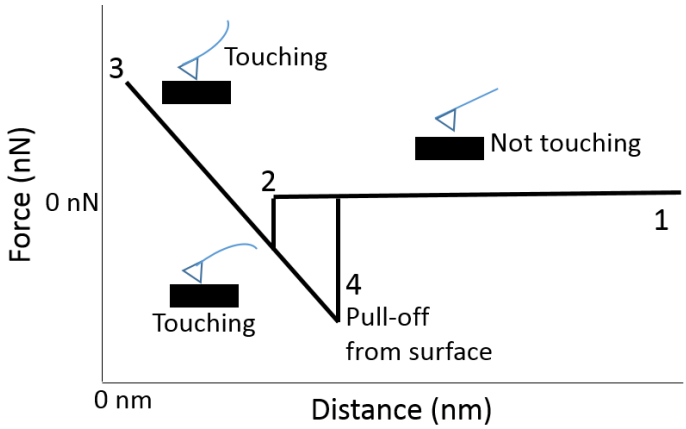

Figure 2.3: Force distance curve, adapted from Birdi [142]. At position 1, the cantilever is a large distance from the sample; the tip is not touching. The tip and sample are in contact (touching) at positions 2 and 3, with the tip retracted from the surface at position 4

At position 1, at larger distances, there is no interaction between the cantilever tip and the sample. This is termed the 'noncontact region' [142]. As the sample is raised in the z-direction by the piezoelectric scanner towards the AFM tip, the cantilever will begin to undergo deflection, owing to a combination of attractive and repulsive forces. With decreasing distance between the tip and the sample, the cantilever undergoes deflection due to interaction between the tip and the sample [144], shown in position 2. When the tip makes contact with the surface, the cantilever deflects upwards, as shown in position 3. This causes the contact force to linearly increase [144]. Here, repulsive forces are dominant, due to the overlap between molecular orbitals. Finally, as the tip begins to retract from the surface (position 4), adhesive forces are present between the cantilever tip and the substrate [142], and the tip may adhere to the surface. Eventually, the pulling force will exceed the adhesive force, and the cantilever will snap away from the surface to return to its equilibrium position [144]. This 'negative' force which is necessary to pull the tip away from the surface is designated the adhesion force [144]. Its value can be extracted mathematically from measured force-distance curves. For example, the adhesion between the cantilever tip and the substrate can be calculated by multiplying the cantilever's spring constant by the deflection of the cantilever [142]. Figure 2.4 illustrates a typical force curve generated throughout this chapter's work, showing the adhesion of a TNT crystal to polyester.

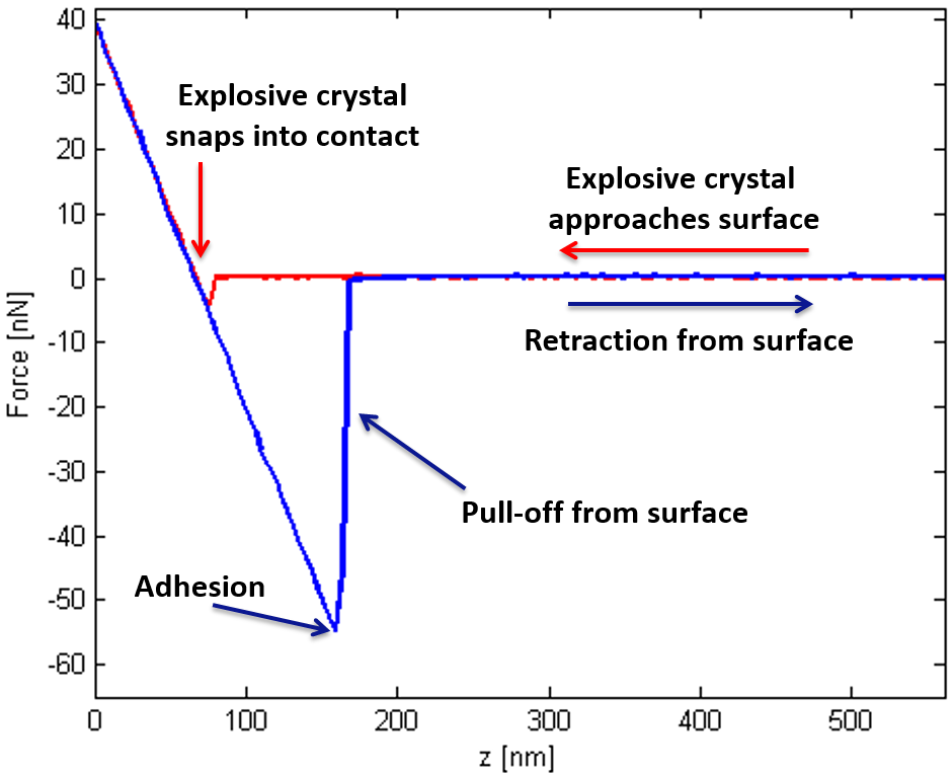

Figure 2.4: Force curve generated throughout this chapter's work illustrating the adhesion of a TNT crystal to polyester

2.1.3 Previous AFM research involving explosives

In order to measure the force between a cantilever and a sample of interest, tipless cantilevers are often modified by attaching a specific particle of interest onto the end of the cantilever. This approach enables the adhesion force between this modified tip and a substrate to be measured [142]. The use of AFM using such modified cantilevers is termed colloidal probe microscopy [71]. Using this approach, some work has recently been performed to determine the fundamental interactions between explosives and military-grade paints, and explosives and various self-assembled monolayers. Zakon *et al.* studied the adhesion of explosive crystals to various self-assembled monolayers [72] by mounting a self-assembled monolayer (SAM) or an explosive crystal onto the end of a tipless AFM cantilever, then measuring the adhesion between the mounted SAM and an explosive particle secured on a glass slide, or between the mounted explosive particle and a SAM secured on a glass slide. The monolayers contained a variety of end groups (-OH, $-CH_3$, $-NH_2$, $-CF_3$, -COOH, $-C_6H_5$, $-C_3H_4SN$), and they examined four explosives (TNT, RDX, HMX and PETN). The results of their study showed that the SAMs with –OH and $–C_6H_5$ end groups showed the strongest adhesion towards the explosives analysed [72]. With this work, one point to note is that the authors examined uncoated PETN crystals. These PETN crystals may therefore be thought to represent the free-flowing PETN crystals found within detonating cord, but cannot be thought to represent the polymer-coated crystals of PETN found in many plastic explosives [145].

Chaffee-Cipich *et al.* [71] used AFM to investigate the adhesion between TNT, RDX and PETN and three coated aluminium surfaces, bearing an acrylic melamine clear coat, a polyester acrylic melamine white coat or a green military-grade finish, of differing roughness. The authors found that the roughness of a substrate had a strong effect on the adhesion of an explosive crystal, with rougher surfaces tending to give lower adhesion than smoother surfaces. From this, it was concluded that the roughness of a surface has a much stronger contribution to any observed adhesion than the inherent chemical composition of such a surface [71]. Canetta *et al.* used AFM to periodically analyse fibres exposed to different environmental conditions, to see how the surface texture changed over time [143]. Their experiments focused on cotton, wool and viscose fibres exposed to various environmental conditions.

However, although previous work has been performed using AFM to investigate the adhesion of explosives to non-textile surfaces, or the morphology of textile fibres, no research has examined the adhesion of explosive crystals to a wider variety of surfaces, including textiles. Currently, investigative judgement is used when deciding which post-explosion scene surfaces should be sampled, with preference given to surfaces thought most likely to yield explosive residues [1]. There is little fundamental research detailing the nature of the interaction of explosives with a variety of different surfaces. Such research will enable the development of additional methods with which to recover explosives from surfaces and will allow for an increased understanding of the optimal method to be used. This chapter aims to add to current knowledge surrounding the molecular-level interactions of explosives with a large variety of surfaces, including textile fibres.

2.2 Experimental

2.2.1 Fabrics

All fabrics analysed in this work were obtained from Spotlight Fabrics, Perth, Western Australia. The following fabrics were investigated in this work: rayon, silk, polyester stretch fabric, acetate, cotton jersey, wool, denim, calico natural cotton, mercerised cotton and polyester fleece.

2.2.2 Non-textiles

Aluminium foil was Confoil heavy duty catering foil brand; topography and adhesion measurements were performed on the matte side of the foil. A glass microscope slide (Biolab plain microscope slides, pre-cleaned) was used for topography and adhesion measurements with glass. A Multix plastic lid was used as a source of polypropylene plastic for

measurements. White and metallic orange car paint were obtained from car panels donated by Prestige Sunroofs WA sunroof fitters.

2.2.3 AFM instruments

AFM analyses were performed at the Scanning Probe Microscopy facility of the Department of Chemistry at Curtin University. Topography and adhesion measurements were performed on a WITec alpha300 SAR (WITec GmbH, Ulm, Germany). A 20x (NA = 0.4) objective (Zeiss, Germany) was used. Data were collected using WITec ControlFOUR software. Cantilever functionalisation using explosive crystals was performed using a custom Nanoscope program using a Dimension 3100 Atomic Force Microscope (Digital Instruments, Santa Barbara, USA).

2.2.4 AFM analysis: Topographic measurements

2.2.4.1 Sample preparation

Textile fibre samples were prepared by laying a fibre across a piece of black double-sided adhesive tape (Stylus tapes brand) adhered to a clean glass microscope slide. The fibre was then taped at each end using a piece of adhesive tape, ensuring the fibres were not stretched during their preparation. Sample preparation for the non-textile surfaces was performed by cleaning the surfaces using ethanol then ultrapure water, drying with a lint-free tissue and attaching to a glass slide using double-sided tape. A photomicrograph was taken of each surface prior to topographic measurements. This was performed using a 20x (NA = 0.4) objective and the WITec alpha300 SAR.

2.2.4.2 Topography measurements

The topographies of all surfaces (with the exception of wool) were measured using WiTec AFM arrow cantilevers, reflex-coated, contact mode, nominal spring constant 0.2 N/m, resonant frequency 14 kHz. The topography of wool was obtained using a WiTec AFM arrow cantilever, reflex-coated, NC (AC) intermittent contact mode, spring constant 42 N/m, resonant frequency 285 kHz. For each textile fibre, the topography was measured at three separate regions along the length of the fibre. For the non-textile surfaces, the topography was measured at three distinct regions of the surface. An area measuring 16 × 10 μm was selected on each sample to be analysed. A total of 256 points per line were used within this area, and 160 lines per image, to maintain a square pixel size.

2.2.4.3 Surface roughness calculations

Surface roughness values of all 15 surfaces analysed were calculated using Project FOUR

software, Version 4.0.14.11. All topography data were background corrected before extracting the root mean square roughness. This process involved opening the saved Topography file for a sample, and performing a background subtraction. For this, a 2nd order surface subtraction was performed to flatten the images and a 3D image saved, before performing a roughness calculation. For the roughness calculations, Project FOUR's Image Statistics mode was used, with the roughness of the area calculated as the SQ roughness (the root mean square roughness) in nm. Roughness values were calculated and averaged for each of the three topographies recorded for a given surface.

2.2.5 AFM analysis: Adhesion measurements

2.2.5.1 AFM probe preparation for adhesion measurements

Two sets of AFM probes were used in this work. One set of explosive crystals was mounted onto the F cantilever of Bruker MLCT-O10 tipless silicon nitride cantilevers (spring constant 0.6 N/m). Unnecessary cantilevers were removed from the probes using a scalpel blade. A second set of explosive crystals was mounted onto the A cantilever of Veeco NP-O cantilevers (spring constant 0.58 N/m). In order to collect measurements, the probes containing the cantilevers were mounted onto Zenith 1/4" Zinc Plated Flat Washers using Selleys Araldite Five Minute Epoxy Adhesive (both purchased from Bunnings, Perth, WA).

2.2.5.2 Explosive crystal generation

The explosives used were supplied as standard solutions from Accustandard: TNT (1000 µg/mL in methanol:acetonitrile (1:1)); RDX (1000 µg/mL in methanol:acetonitrile (1:1)) and PETN (1000 µg/mL in methanol). A polytetrafluoroethylene (PTFE) sheet, 0.81 mm / 0.031" thick, on which evaporation of explosive solutions was performed, was obtained from Alfa Aesar, MA, USA.

Explosive crystals were generated by evaporating standard solutions of the explosives, adapting the method employed by Chaffee-Cipich *et al.* [71]. For this, evaporation was performed on a piece of PTFE sheet (pre-cleaned using acetone and ultrapure water, then dried with a lint-free tissue). 20 µL of explosive solution was spiked onto the PTFE, and the solvent allowed to evaporate at ambient temperature. This process required approximately one hour for PETN and RDX. In order to generate TNT crystals, a slightly different procedure was employed following the procedure outlined by Chaffee-Cipich *et al.* [71]. A 20 µL aliquot of TNT solution (in 1:1 acetonitrile:methanol) was spiked onto a pre-cleaned and dried piece of PTFE and the solvent allowed to evaporate at ambient temperature forming a white emulsion surface. To this emulsion, a 20 µL drop of ultra-pure water was added as a co-solvent. This

facilitated the evaporation of the residual acetonitrile and methanol, removing the emulsion-like structure. Upon evaporation of the remaining water, TNT crystals were obtained. A minimum explosive crystal size of 10 µm was used for mounting onto the tipless cantilevers. This size takes precedence from the work of Chaffee-Cipich *et al.* [71], who discovered that TNT crystals below this size were too fragile to work with. In each case, the crystal diameter was below that of the explosive's respective critical diameters (the particle size above which shock or friction may cause the material to detonate). Literature values for these critical diameters are 2 mm for TNT [146], 0.5-1.5 mm for RDX [146, 147] and 1-1.5 mm for PETN [147].

Following generation of the crystals of explosives, their sizes were measured under an optical microscope. The size of each crystal was approximately 100 µm which was too large to mount on a cantilever. The crystals were milled between two clean glass slides while periodically checking the crystal size using an optical microscope, until crystals of around 10 µm width were obtained for each explosive. Images of the explosive crystals before and after milling are provided in Figure 2.5.

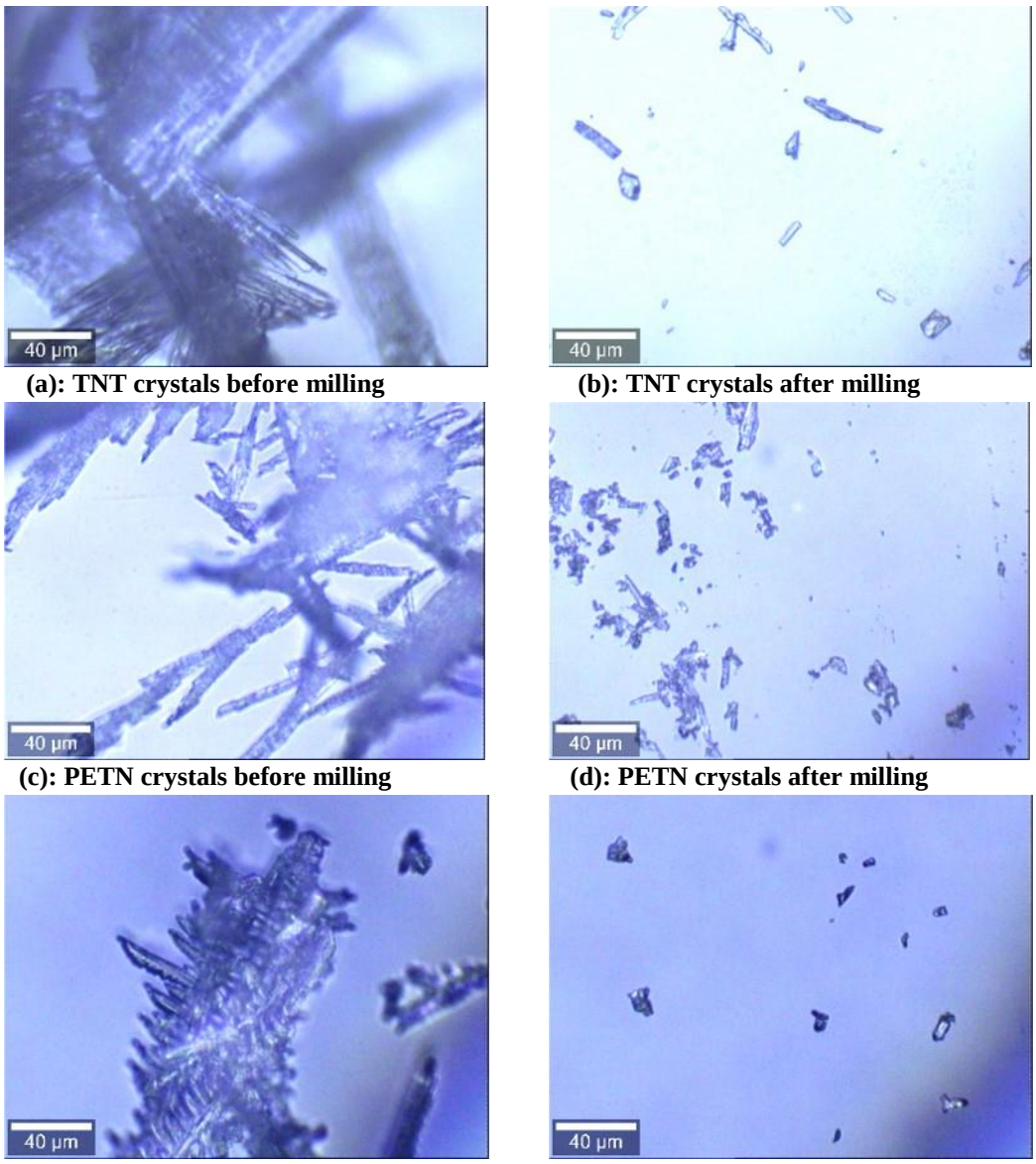

(a): TNT crystals before milling **(b): TNT crystals after milling**

(c): PETN crystals before milling **(d): PETN crystals after milling**

(e): RDX crystals before milling **(f): RDX crystals after milling**

Figure 2.5: Photomicrographs of explosive crystals (a) – (f) before and after milling ready for mounting onto AFM cantilevers

2.2.5.3 Explosive crystal mounting onto tipless cantilevers

A Bruker Dimension 3100 Atomic Force Microscope instrument and Nanoscope software was used to mount the explosive crystals onto the tipless cantilevers. A custom tip modification workspace was used for particle mounting. This required the explosive crystals to be placed on a glass slide on the sample stage of the instrument. On a separate glass slide, a small amount of epoxy resin was smeared. The tip of the cantilever was dipped into a very small glue droplet and then immediately moved to a previously selected crystal, on which the cantilever engaged and was held for 10 seconds before the scanner was withdrawn. The modified cantilever was left overnight to allow the glue to set, before being used for adhesion measurements. Optical microscope images of each explosive crystal at the end of a cantilever were taken prior to their

use, and the cantilevers were checked periodically between adhesion measurements to ensure the explosive crystal was still present. Examples of TNT, PETN and RDX crystals mounted onto cantilevers and used during this work are shown in Figure 2.6, Figure 2.7 and Figure 2.8, respectively.

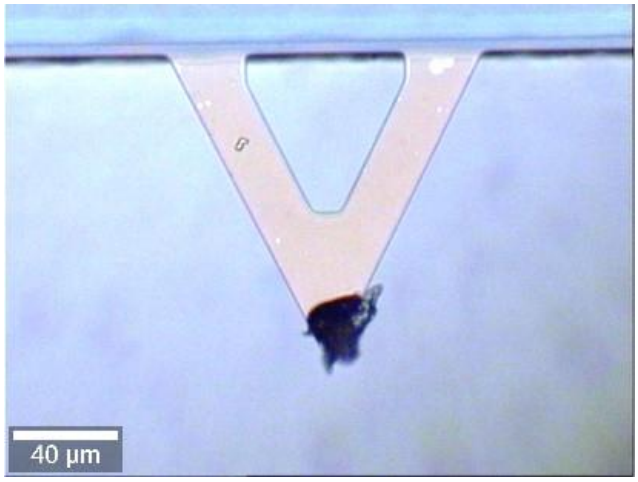

Figure 2.6: TNT crystal mounted onto cantilever. Crystal size is approximately 20 µm

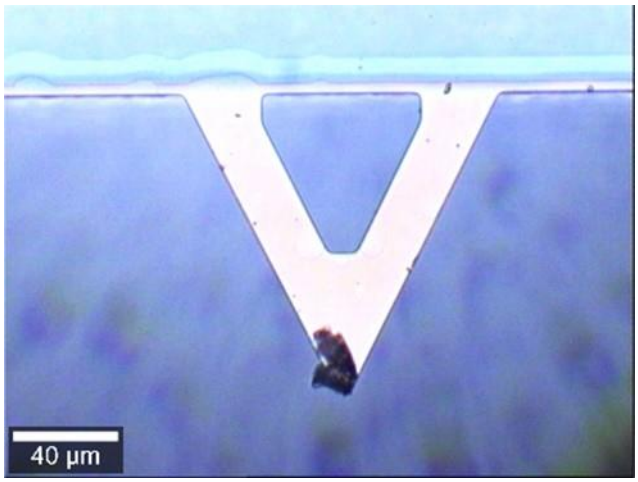

Figure 2.7: PETN crystal mounted onto cantilever. Crystal size is approximately 14 µm

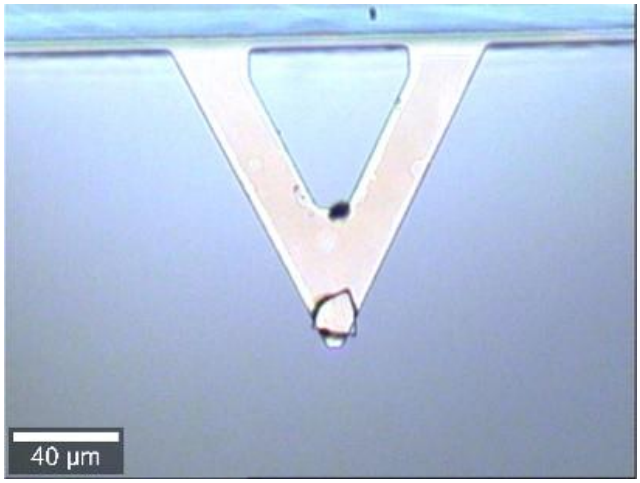

Figure 2.8: RDX crystal mounted onto cantilever. Crystal size is approximately 14 µm

Six explosive-functionalised cantilevers were prepared for this work: two each for TNT, PETN and RDX, with the adhesion measurements for a given explosive split between these two cantilevers.

2.2.5.4 Adhesion data collection

Adhesion measurements were performed using AFM contact configuration taking individual force-distance curves across sixteen regions of each different surface. At each of the 16 regions, an average of seven measurements was taken at the same position, with a total of 118 measurements obtained for each surface. The adhesion data collection process involved repeatedly bringing the explosive particle mounted on the cantilever into contact with the surface of interest, before pulling the two apart and measuring the force required to separate the two. For each force-distance curve, 1000 data points were recorded. Each set of adhesion measurements was performed under ambient conditions. For the force curves, a small 'push' distance of 0.05 µm was used, to avoid damage to the explosive crystals. A pull of 2-3 µm was used in each case at a speed of 1 µm/s. Measurements were performed in a laboratory environment with the temperature held between 16-24 °C, and humidity levels between 37 and 73 %.

2.2.5.5 Adhesion force data extraction

The adhesion force between the explosive crystal and the surface was calculated based on Hooke's law ($F = -kX$), where F represents force, k the spring constant of the cantilever and X the deflection distance. Initially this involved selecting the file for a given force curve and performing a background subtraction, to ensure the baseline setpoint value had a value of 0 V. This background subtraction was performed using a polynomial order of zero to subtract an offset. For this background subtraction, two fit masks were employed at the left and right edges of the force curve, with each fit mask spanning a distance of approximately 100 nm. Following background subtraction of all data files, the files were post-processed using a custom MatLab program written by Dr Thomas Becker (Curtin University). This custom-written Matlab code (provided in Appendix A) was used to convert the raw data into force vs distance data and extract the magnitude of the adhesion force between the explosive crystal and a given surface.

To compare the adhesion forces between different explosives and surfaces, the adhesion force values were extracted from the raw data generated from taking the force curves. For this, the raw data from the AFM (provided as a voltage value from the photodetector) was converted into a value representing the cantilever deflection (in nm) using the custom MatLab program. In conjunction with Hooke's Law, this program then calculated the adhesion force present between the explosive and a given surface. This process is a standard AFM routine for force-

distance curves.

2.3 Results and discussion

2.3.1 Preliminary considerations

A variety of textiles were chosen for analysis which aimed to represent the most-commonly encountered textiles in forensic casework [66], as well as those examined by other researchers in the context of forensic explosives analysis [46, 47, 64, 69]. Although the main focus of this work was to investigate the adhesion of explosives to textiles, several non-textile surfaces were also investigated. These non-textile surfaces were chosen to represent surfaces which may also be associated with an explosive event, such as glass, aluminium, polypropylene plastic, metallic orange car paint and non-metallic white car paint.

Three explosives were used during this work: TNT, PETN and RDX. These represent three of the most commonly studied organic explosives: nitroaromatics, nitrate esters and nitramines, respectively.

PTFE was employed for the evaporation of the explosive crystals, rather than a glass microscope slide, as the PTFE surface prevents spreading of the droplet of solution. This enabled a slower rate of solvent evaporation to occur, and ultimately the formation of a large crystal of explosive, rather than the metastable glass which may form with more rapid evaporation if spreading and wetting occurs.

2.3.2 Adhesion measurements

It has been reported that the glue present for mounting particles has a negligible effect on a particle's surface properties [71]. This assertion holds true when the glue is restricted to the region between the explosive crystal and cantilever, to ensure that the glue does not interact with the surface under analysis, and when a very small droplet of glue is used, to ensure it is not absorbed by the explosive crystal which would otherwise affect its interactions. In the present work, the glue drops used were very small (with an estimated diameter of 2 μm), and are not anticipated to have affected the measurements obtained. The glue drops are not visible in Figure 2.6, Figure 2.7 and Figure 2.8.

It should be noted that, due to the rough nature of the explosive crystal's surfaces, it is not possible to know the exact contact area between the particle and the surface being examined. Although this may appear to be problematic, it has been proposed [72] that this situation should lead to the attainment of more realistic adhesion forces from the adhesion measurements. Larger adhesion forces are expected between a larger particle and a given surface, than a

smaller particle and the same surface [71]. This is due to a larger particle having a higher mass, and more possible points of contact with the surface. Due to this, efforts were made to mount explosive crystals of as similar sizes as possible.

2.3.3 Surface photomicrographs and AFM topographies

Figure 2.9 contains photomicrographs (left column) and AFM 3D topographies (right column) of the textile and non-textile surfaces examined in this work.

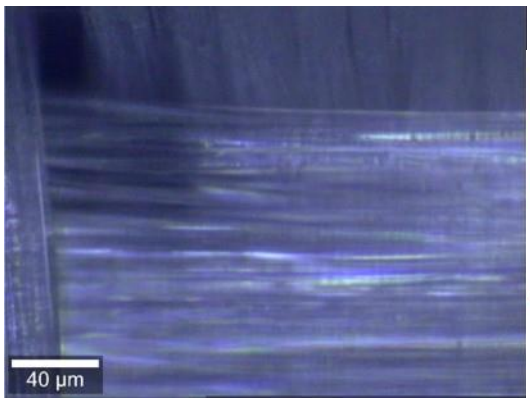

a1: Acetate

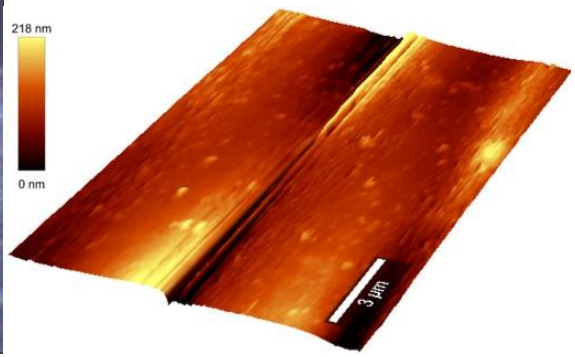

a2: 3D topography of acetate fibre

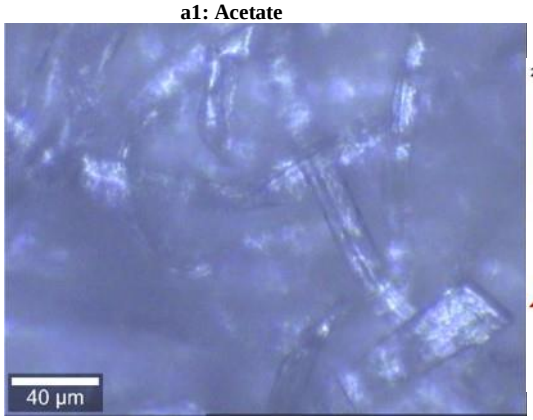

b1: Calico natural cotton

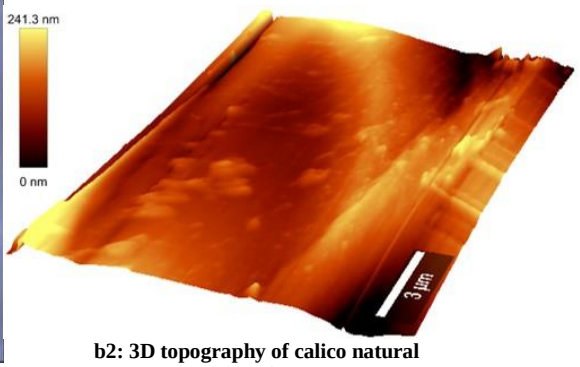

b2: 3D topography of calico natural cotton fibre

c1: Cotton jersey

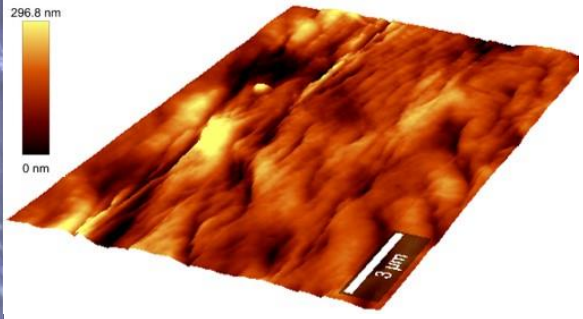

c2: 3D topography of cotton jersey fibre

d1: Denim

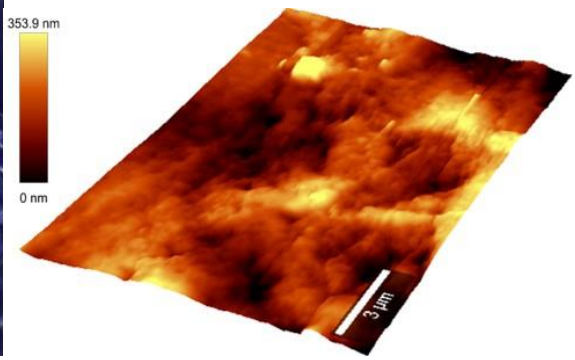

d2: 3D topography of denim fibre

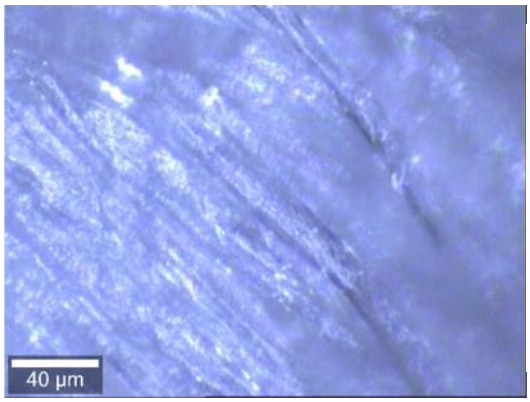

e1: Mercerised cotton

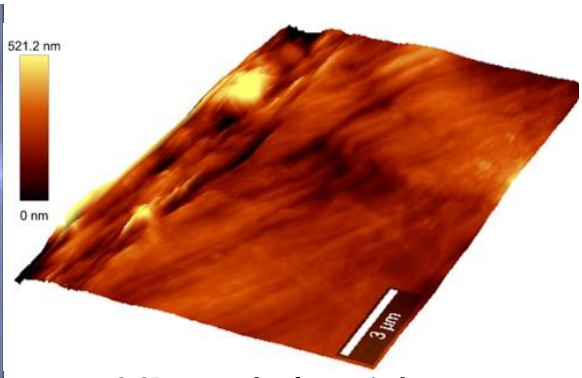

e2: 3D topography of mercerised cotton fibre

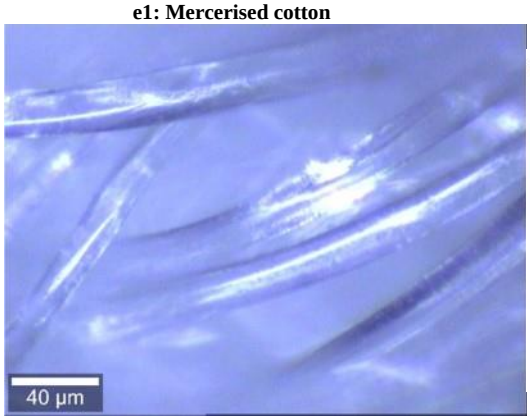

f1: 100 % polyester

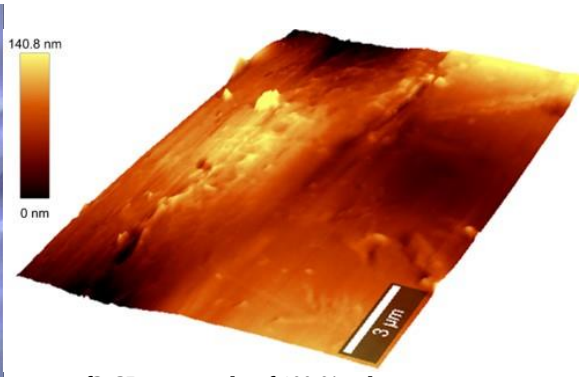

f2: 3D topography of 100 % polyester fibre

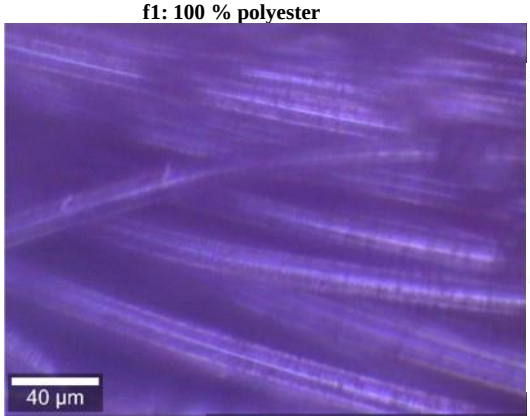

g1: Polyester fleece

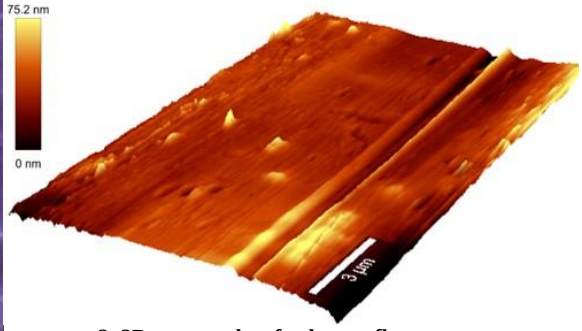

g2: 3D topography of polyester fleece fibre

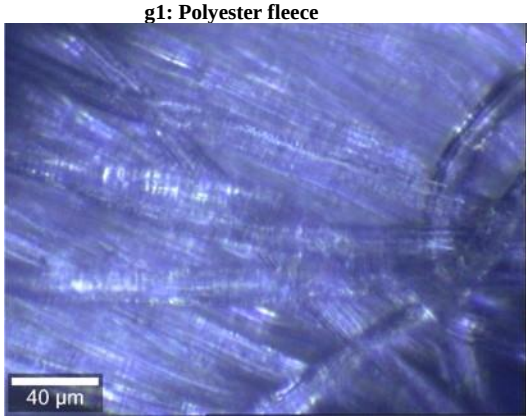

h1: Rayon

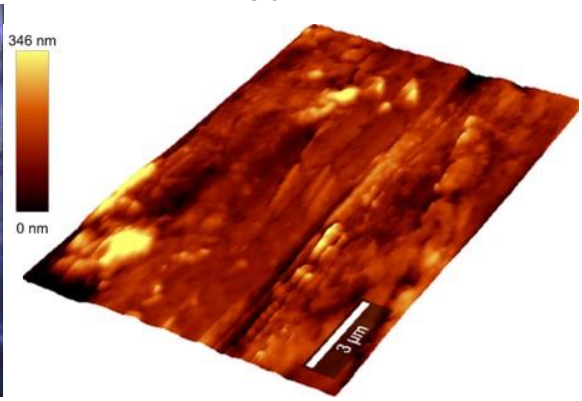

h2: 3D topography of rayon fibre

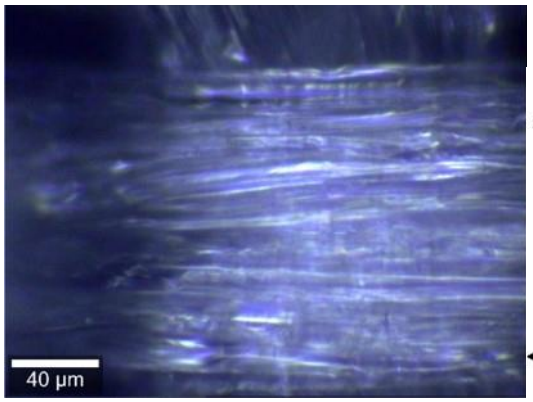

i1: Silk

i2: 3D topography of silk fibre

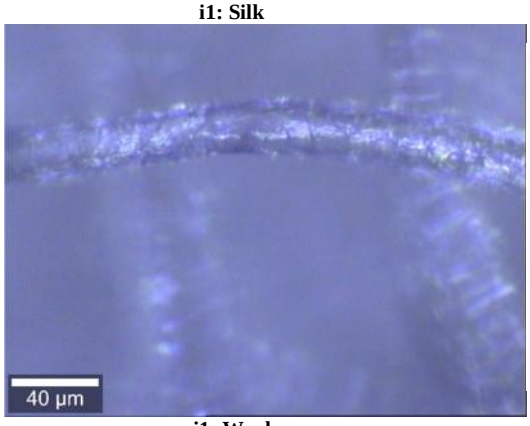

j1: Wool

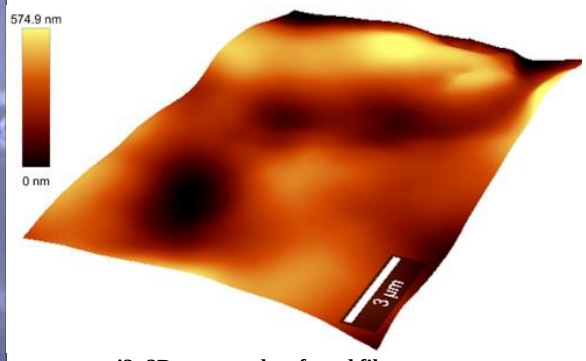

j2: 3D topography of wool fibre (tapping mode)

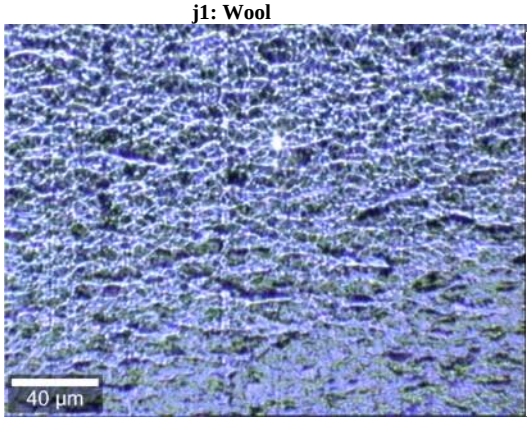

k1: Aluminium

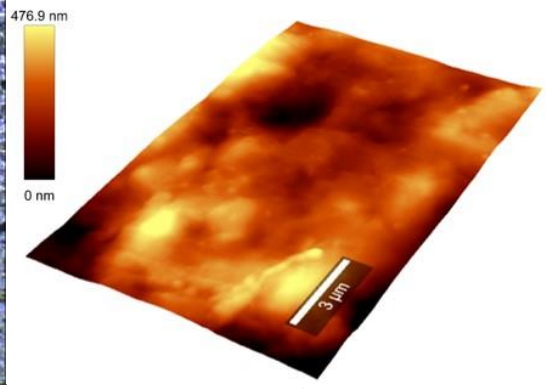

k2: 3D topography of aluminium

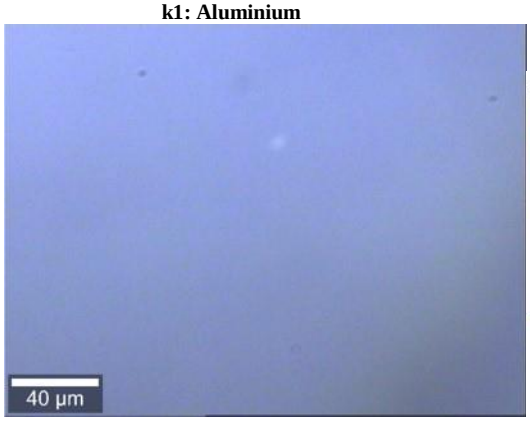

l1: Glass

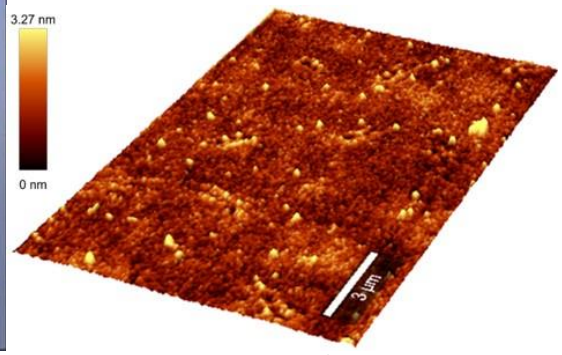

l2: 3D topography of glass

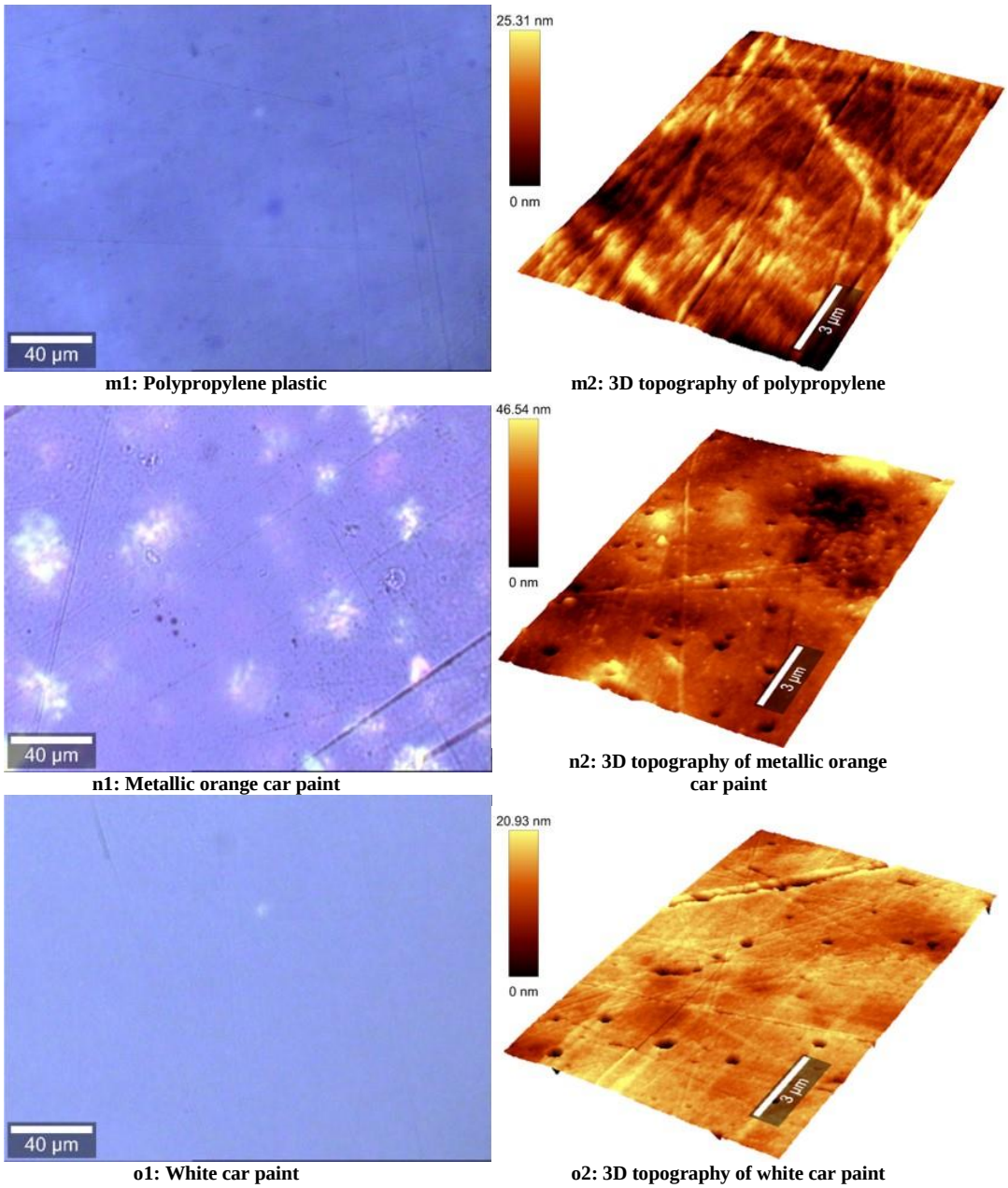

m1: Polypropylene plastic **m2: 3D topography of polypropylene**

n1: Metallic orange car paint **n2: 3D topography of metallic orange car paint**

o1: White car paint **o2: 3D topography of white car paint**

Figure 2.9: Optical photomicrographs and 3D AFM topographies of the surfaces analysed in this work

It can clearly be seen from Figure 2.9 that the various surfaces all display very different physical morphologies. A number of the textile surfaces (acetate, polyester fleece and rayon) display what appear to be 'draw' marks on their surfaces, likely originating from the extrusion process during formation of the textile fibres. Silk, as expected, displayed a very smooth surface. For the silk fibre, an area twice as long and half as wide was mapped compared to each of the other surfaces. This was due to the silk fibre sample having a much narrower diameter than any of the other fibre samples, meaning it was not possible to measure the topography of areas measuring 16 × 10 µm as the silk fibre's diameter was around 10 µm.

A number of the cotton-based surfaces (calico natural cotton, cotton jersey and denim) all

showed relatively uneven surfaces, with the wool surface also bearing large ridges, likely from the scales present on the wool's surface. Wool has previously been shown [145] to be a good material for capturing traces of explosives, and one hypothesis for this may be that explosive particles can snag onto the surface of wool fibres and be retained. In the present work, the topography of wool was measured in tapping mode, because the scales on the surface of the wool prevented the smooth measurement of topography in contact mode (the cantilever tip was snagging on the boundaries between the scales).

The photomicrograph of aluminium in Figure 2.9 (k1) displays many pits/ridges within the surface. These are also seen in the 3D topography in Figure 2.9 (k2). In comparison to aluminium, glass displays a much smoother surface, with the elevation difference between the lowest and highest points on the glass 3D topography in Figure 2.9 (l2) only around 3 nm. Glass was the smoothest surface examined in this work. The photomicrograph of polypropylene reveals some small scratches present within the surface, which are reflected well in the 3D topography of the polypropylene in Figure 2.9 (m2).

Figure 2.9 (n1) and (o1) show photomicrographs of the metallic orange and white car paint examined during this work, with their corresponding 3D topographies in Figure 2.9 (n2) and (o2). These represent the topography of the uppermost clear coat layer of each paint. For each of the clear coats, visible 'pits' are present in the surface, which indicates that these may prove to be good receptacles for capturing particles of explosives at a post-blast scene.

The photomicrographs and 3D topographic images provide an indication of the physical morphology of the different surfaces investigated during this work. The different physical morphologies may lend themselves to capturing explosives in different manners. It should be noted that several of the surfaces are expected to have similar chemical surface compositions, such as calico natural cotton, cotton jersey and denim, and the polyester fleece and 100 % polyester. However, the obtained 3D topographies have illustrated that materials with the same chemical structure can have very different physical morphologies which is a result of differing processing techniques during manufacture. This work aims to draw conclusions between the chemical composition of a fibre type and the importance of physical morphology for explosives' adhesion.

2.3.4 Surface roughness

The SQ roughness of a surface can also be defined as the Root Mean Square roughness of the different heights recorded within the area, relative to a plane representing the mean of the measured height values running parallel to the sample plane. Figure 2.10 shows the average SQ roughness values obtained for each of the 15 surfaces. Each column represents the mean

surface roughness from three separate topographic measurements on a given surface. The error bars show the standard deviation within these measurements (n=3).

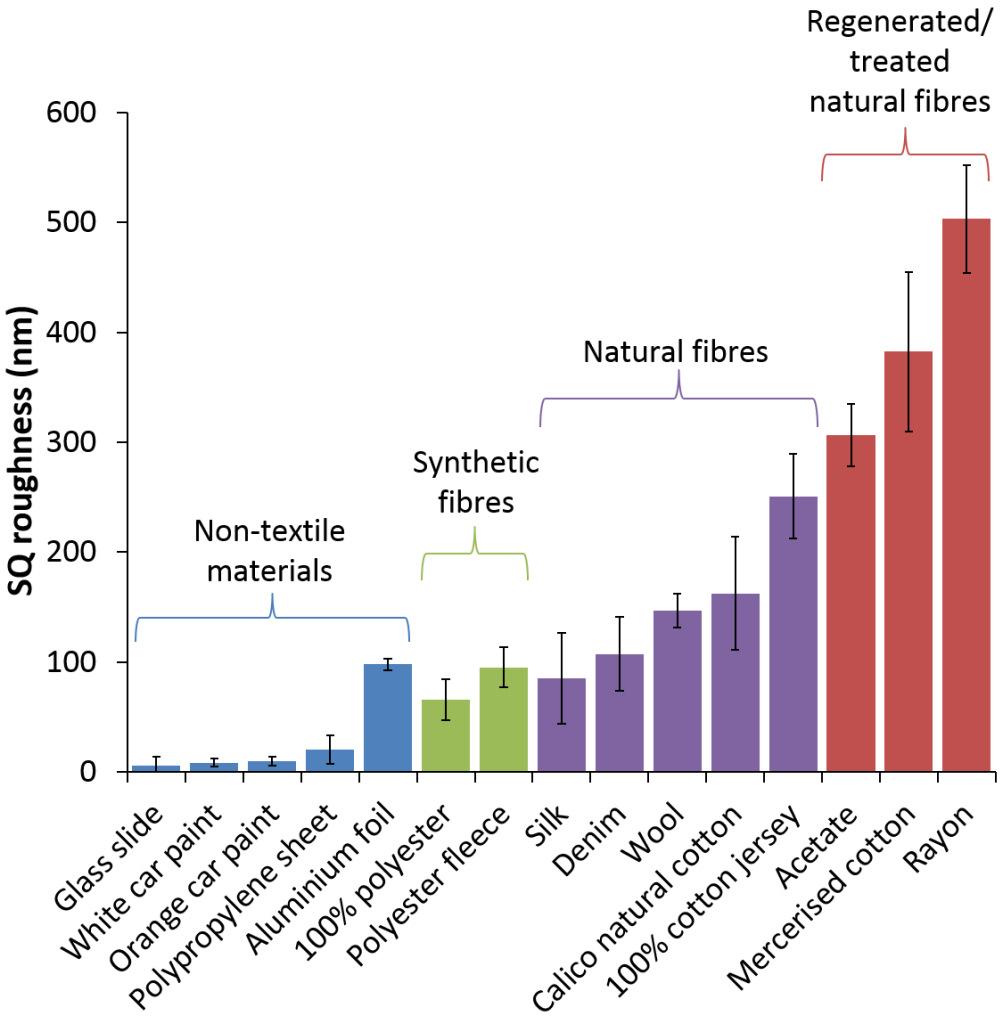

Figure 2.10: Average surface roughness values of the 15 surfaces investigated in this work, including non-textiles, synthetic fibres, natural fibres and regenerated natural fibres. Error bars show the standard deviation within a set of three measurements

The surfaces have been classified into four different groups: non-textile materials, synthetic fibres, natural fibres and regenerated/treated natural fibres based on the hierarchy of textile fibre classes displayed in Figure 2.1. Each group has been displayed in increasing order of roughness. Figure 2.10 clearly shows that the majority of the non-textile materials (with the exception of aluminium) are smoother than any of the textile surfaces examined. This was also evident from the topographic images displayed in Figure 2.9. Aluminium foil demonstrates the highest surface roughness from the non-textile materials; its roughness is comparable to that of the synthetic fibres. Generally, the natural fibres are rougher than the synthetic fibres, and the regenerated/treated natural fibres are rougher still. This was anticipated, as the additional processing steps involved in the regeneration or treating of fibres is likely to cause

some additional physical roughness.

2.3.5 Sample preparation

Initially, fibre sample preparation involved pulling a fibre taut across a glass microscope slide, and taping the ends in place, without the addition of double-sided tape beneath the fibre. This sample preparation method produced very high adhesion values. It was suspected that by only securing the fibre at its ends, some movement of the fibre in the z-direction (perpendicular to the plane of the glass slide) could occur, causing the fibre to 'bounce', and follow the movement of the AFM scanner during the retraction part of the force distance measurements. This z-direction movement was therefore thought to be contributing to difficulty in the cantilever being able to physically detach from the fibre after its initial contact. The addition of double-sided tape beneath the fibres gave much lower and more consistent adhesion values, and this approach was used for all subsequent fibre adhesion measurements. Prior to any AFM measurements being performed, the fibre was secured firmly to the double-sided tape.

2.3.6 The adhesion of explosives to 15 different surfaces

Chaffee-Cipich *et al.* [71] used AFM to measure the adhesion between three explosives and three painted aluminium surfaces of different roughness, finding that the explosives had a higher adhesion to smoother surfaces. The authors hypothesised that the major source for this difference was due to the different physical roughness of the surfaces [71]. It was therefore considered that these findings may apply to the adhesion measurements of this work. Considering Chaffee-Cipich's finding, it was expected that a higher adhesion should be recorded between the explosives used in this study and the smoothest surfaces illustrated in Figure 2.10 – the non-textile surfaces. In contrast, the lowest adhesion would therefore be expected between the explosives and the regenerated/treated natural fibres, owing to their high surface roughness.

Chaffee-Cipich's work only considers physical roughness when correlating adhesion to surfaces. Zakon *et al.* [72] instead focused on the chemical characteristics of a surface with regards to the adhesion of explosives. In their study cantilevers were functionalised with explosives and then the adhesion forces measured between four explosives and various self-assembled monolayers with different end-groups. They found the highest adhesion between explosives and the self-assembled monolayers which had hydroxyl and phenyl end groups.

The research published by Chaffee-Cipich and Zakon only considers one parameter with respect to the adhesion of explosives – physical roughness or chemical composition. The

current study aims to investigate the contribution of both physical roughness and chemical composition, to assess the significance of these parameters when considering the adhesion of explosives to a given surface. Several of the surfaces examined in this study have identical structural groups at the surface (for example, glass, denim, cotton jersey, natural cotton and rayon all have hydroxyl groups at their surface), yet they each have very different physical roughness (Figure 2.10).

If adhesion is strongly dependent on the chemical composition of a surface, similar adhesion may be expected to each of those surfaces. Alternatively, if adhesion is more dependent on a surface's physical roughness, higher adhesion should be associated with glass, and a much lower adhesion should be associated with rayon which is a much rougher surface.

It should be noted that, for the textile surfaces, the adhesion was measured between the mounted explosive crystals and single fibres extricated from each of the textile surfaces, rather than using a larger swatch of each textile. This current work is designed to act as a 'starting point' to provide an initial method which can then be further developed using larger scale systems. For this reason, in the current work, adhesion was measured to individual textile fibres. In addition, although it may be envisaged that, with a larger piece of fabric bearing a 'mesh' type structure, explosive crystals may have the potential to become embedded in the gaps of the mesh, this scenario would involve physical adhesion, which would be the case for any type of particle, rather than just explosives. The present work is therefore concerned with the chemical adhesion between explosives and a textile fibre surface.

Figure 2.11 contains the adhesion data obtained between TNT, PETN and RDX across the 15 different surfaces studied. Individual adhesion graphs for each of the three explosives are also displayed in Appendix A, Figure A.1 to Figure A.3. Each column represents the mean of 118 adhesion measurements between a given explosive crystal and a given surface. The error bars indicate the standard deviation within the set of measurements.

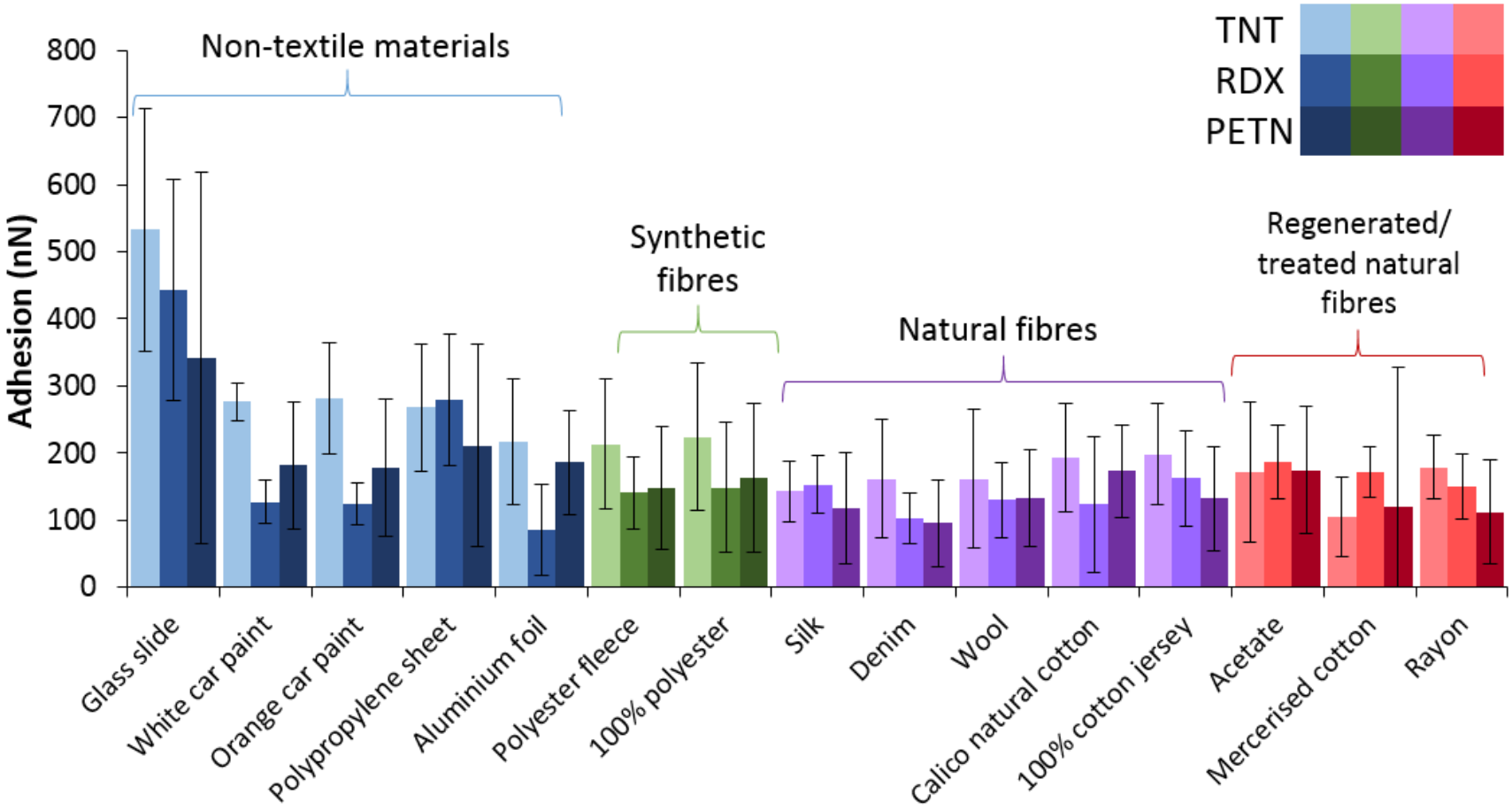

Figure 2.11: Average adhesion measurements between TNT, PETN and RDX with 15 different surfaces. Error bars show standard deviations within the 118 adhesion measurements for each surface

.

Although it may appear that the standard deviations for a given set of measurements are quite high, this effect is not thought to be due to any inherent problems resulting from the nature of the data collection. Instead, these standard deviation values are attributed to the irregular surface morphology of the mounted explosive crystals, and possible variations in surface morphology across a given surface [72, 144]. These standard deviations are not atypical of those for adhesion measurements in AFM [148].

In the optical microscope images of cantilevers functionalised with TNT, PETN and RDX crystals (Figure 2.6, Figure 2.7 and Figure 2.8, respectively), it is noted that the morphologies of the crystals are very rough. These rough surfaces may lead to multiple points of contact with a given textile fibre. It is also possible that regions of differing morphology in the crystals may give rise to varying areas of contact between the explosive and a given surface [72].

The adhesion data are not only dependent on the crystal's surface structure, but the number of points of contact which is related to the morphology of the surface at any given point, and the degree of complementarity between the crystal and a surface at a given measurement point. For example, Chaffee-Cipich *et al.* suggest that with a smoother surface, the level of interpenetration between an explosive crystal and a surface is likely to be higher than that for a rough surface [71]. Due to the unknown nature of a rough surface, the peaks and valleys on an explosive crystal and the surface it is placed in contact with may have only a low degree of complementarity [71], resulting in fewer points of contact between the explosive crystal and the surface. As a result, rather than normalising the data obtained in this work, attempts were made to use explosive crystals of approximately the same diameter for a given set of surfaces (ranging from 14 to 20 μm; see Figure 2.6, Figure 2.7 and Figure 2.8), and to take force-distance curves across a large number of different points on a given surface, to generate representative data for a given combination of explosive and surface.

Overall, it can clearly be seen from Figure 2.11 that all of the explosive crystals have a tendency to have a higher adhesion to the non-textile surfaces than to any of the textile surfaces. Figure 2.10, showing the surface roughness of the different surfaces, revealed that the non-textile surfaces are, on average, much smoother than any of the textile surfaces. Combining the data from both Figure 2.10 and Figure 2.11, a broad conclusion can be made that the explosives demonstrate higher adhesion to smoother surfaces. This finding is in agreement with the findings of Chaffee-Cipich *et al.* [71], who found a higher adhesion between explosives and smoother painted aluminium surfaces.

As shown in Figure 2.11, each of the three explosives displayed the highest adhesion to glass,

the smoothest surface examined in this work and with a surface primarily composed of hydroxyl groups. This finding is in strong agreement with both the findings of Chaffee-Cipich [71], who found the highest adhesion between explosives and smoother surfaces, and Zakon [72], who showed explosives have a strong adhesion towards hydroxyl groups. Comparatively lower adhesion values were obtained between the explosives and the cellulose-based textiles (denim, calico natural cotton, mercerised cotton and rayon), which would also bear surface hydroxyl groups. This finding suggests that the adhesion of explosives to a surface is more strongly-dependent on how rough or smooth a surface is, rather than the chemical nature of the surface itself.

It should be noted that Chaffee-Cipich's work only examined adhesion due to the presence of van der Waal's forces [71]. However, it is likely that textiles may have traces of water absorbed onto their surfaces. Canetta [143] reports high water absorption onto viscose and rayon fibres due to the presence of hydroxyl groups on the fibre surfaces. Similarly, Zakon *et al.* [72] found that explosives had the highest adhesion to hydroxyl and amine end groups and suggested that this may be due to adsorption of water molecules onto these end-groups, which could then form a water bridge to the explosive crystals. They proposed that such capillary forces may be the dominant factor contributing towards the adhesion force between an explosive crystal and a given surface. Although effects due to humidity in the present work may have influenced the recorded adhesion measurements, significant variation in humidity is highly likely in real-life situations. It should also be noted that the environment within the AFM instrument enclosure was likely to be relatively stable compared to the surrounding room.

A particularly high adhesion can be observed to the glass slide for TNT, which was the smoothest surface examined in this work. There is a tendency of TNT to display a higher adhesion to the smoother, non-textile surfaces and a lower adhesion to aluminium foil than to any of the other non-textile materials. Aluminium foil had the highest roughness of all of the non-textile materials (see Figure 2.10) which was expected based on the conclusions from Chaffee-Cipich's work [71].

The aluminium foil used in this work is formed from only a single chemical element, which limits the potential types of interactions possible with an explosive crystal. In contrast, wool is formed from a wide variety of amino acids and will have a number of different functional groups on its surface with which to interact with an explosive crystal. This factor alone seems to suggest that chemical composition plays a lesser role than other properties such as surface roughness. Compared to the smoothest non-textile surfaces (glass, car paint and polypropylene), TNT displayed a much lower adhesion to the textile surfaces.

PETN showed a higher degree of variation within the recorded average adhesions compared to the adhesion between TNT and the 15 surfaces. A very high adhesion force appears to form between PETN and glass, whereas a much lower adhesion force is present between PETN and the white and orange car paint. This is interesting, as the two both have similar surface roughness (see Figure 2.10), suggesting that the chemical nature of the surface may play a role, with the chemical composition of glass interacting more favourably with PETN than the chemical composition of the white car paint and orange car paint clear coats indicating that car paint clear coat is a poorer surface for capturing PETN compared to glass.

PETN displayed a particularly high adhesion to glass and polypropylene, with a lower adhesion to the remaining surfaces. One point to note is that in this work, the adhesion force between a bare PETN crystal was examined with the 15 different surfaces, rather than a polymer-coated PETN crystal as might be found in a plastic explosive. This is also the case for the work of Zakon and Chaffee-Cipich [71, 72]. The PETN examined in this work represents free-flowing PETN crystals found in detonating cord and some explosives boosters, rather than the polyisobutylene or styrene butadiene polymer-coated crystals found in many plastic explosives [149]. It would be of benefit in future work to also investigate coated explosive crystals originating from plastic explosives as these results would be of use with regards to pre-blast explosives detection.

Finally, RDX, like TNT and PETN, demonstrated a very high adhesion to glass. This result seems to suggest that glass is a good substrate for capturing RDX residues. It is known that glass fibre swabs are in use for some airport-based sampling which appears to be very suitable for the recovery of RDX, TNT and PETN [72]. The adhesion measured between RDX and the white and metallic orange car paints is similar; lower than that to glass. The adhesion of RDX to the 10 different textile materials examined indicated that the adhesion of RDX to the textile materials appears to follow a similar trend to TNT and PETN with the different textiles.

2.4 Conclusions and future work

This research has investigated the adhesion of explosives to a variety of textile and non-textile surfaces using AFM. Although previous AFM studies have investigated the adhesion of explosives to vehicle paints and monolayers, no previous work has been performed to investigate the adhesion of explosives to the wide variety of textiles and non-textiles explored in this work. These findings therefore expand on existing fundamental knowledge regarding the interactions of explosive crystals with a variety of surfaces.

Surface roughness measurements demonstrated that non-textile surfaces tend to be much

smoother than any textile surfaces. Following this, 118 adhesion measurements were obtained between TNT, PETN and RDX and each of the 15 different surfaces, to give a total of over 5,000 measurements. The results suggest that the explosives have a higher adhesion to smoother surfaces (in this case, the non-textile surfaces), with a particularly high adhesion observed between the three explosives and glass (the smoothest surface examined). This result is in strong agreement with previous literature [71, 72] which found the highest adhesion of these explosives to smoother surfaces, and surfaces bearing surface hydroxyl groups, respectively.

Based on the results of this work, smooth pieces of debris, such as glass, should be targeted for sampling following an explosion to attempt to maximise the quantity of explosives recovered. In addition, the results of this work are also of potential benefit towards enhancing the detection of pre-blast explosive residues (such as for aviation security). In the present work, explosive crystals were generated by evaporating solutions of explosives, and it is acknowledged that the shape of these crystals may differ from those manufactured for industrial use. This is because this work aimed to use a very simple model system to develop a method of analysis. This method may then be used in the future for more complex systems, such as those involving industrial grade explosive crystals or controlled detonations. For example, recent work by Abdul-Karim *et al.* [150] looked at the morphology of post-blast RDX particles, finding that with increasing distance from a detonation site, RDX particles tended to become spheroidal, attributed to the RDX melting during the high temperatures generated by the detonation, then coalescing into a sphere upon cooling whilst travelling through the air. The majority of the collected RDX particles ranged from 5-100 μm; in good agreement with the crystals sizes used during this work. It would therefore be of interest to perform AFM measurements with post-blast crystals of TNT, PETN and RDX, to compare their adhesion to the surfaces used throughout this work with the adhesion measured using the pre-blast crystals utilised in this work.

In addition, this work has primarily focused on the interaction of explosives with new, clean surfaces. However, it would be useful to also consider some non-ideal cases, which may be more representative of a real-life scenario. One such example would be investigating the adhesion of explosives to laundered fabrics, likely containing traces of washing powder [151] which may affect the adhesion of explosives to the fabric. Similarly, wearing or washing fabrics may also cause a change in the properties of a surface [151]. Work by Canetta *et al.* [143] has shown that fibres become rougher upon exposure to environmental conditions. Based on the conclusions from this work, this would suggest that a roughening of the fibres

would give rise to a lower adhesion of explosives. This hypothesis would therefore be interesting to investigate in the future.

Other environmental factors may also have an effect on the properties of fibres contained within a fabric, or on the surfaces of non-textiles, such as the car paints, aluminium, polypropylene and glass examined in this work. These factors include surface stains, exposure to sunlight and every day wear and tear [151]. If a localised stain is present on a surface, then it is highly likely that this would affect the adhesion of explosives to such a surface. Additionally, it is also likely that the presence of a localised stain would complicate the recovery of any explosives adhering to that region.

Another key consideration with this work is that, even if an explosive does display a high adhesion to a surface at a given time of measurement (for example, TNT, RDX and PETN all showed a higher adhesion to glass than to any of the other surfaces examined), this is no guarantee that they will also demonstrate a high persistence to complement this initial high adhesion. Chapter 3 investigates the persistence of explosive crystals on the majority of the surfaces investigated in this current chapter. This enables an assessment of whether an initial high adhesion indicates a long-term high adhesion, or whether the adhesion will change over time, depending on the nature of the surface to which the explosive adheres.

Chapter 3 Assessing the contact heater for the recovery of explosive residues from textile and non-textile surfaces

3.1 Introduction

As discussed in the previous chapter, explosive residues on clothing and other textiles can be an important source of evidence during the investigation of explosion incidents [3, 64, 66, 68]. For example, traces of PETN were recovered from the clothing of the Oklahoma City bomber, and from the trousers of the foiled Millennium Bomber Ressam Ahmed [3]. In prominent cases such as these, a suspect's clothing at the time of apprehension is typically examined for explosive residues, as well as any bags and backpacks the suspect is carrying. Even in somewhat lower profile cases, the detection of explosive residues from clothing can form a central part of an investigation. Brust *et al.* [66] describes the detection of PETN from the clothing of a suspect in a series of safe-crackings. Published literature indicates that textiles are a good matrix for trapping explosive residues [3]. These examples all serve to illustrate the potential utility of clothing and textiles as a source of evidence in forensic investigations.

Clothing and other textiles are examples of porous surfaces, compared to non-porous surfaces such as glass, metals and plastics. Whereas it is relatively easy to sample for explosive residues from non-porous surfaces by swabbing the surface with solvent-wetted cotton swabs [61], it is less straightforward to sample for explosive residues from porous surfaces. Although swabbing is sometimes applied to clothing and textiles [63], other techniques are also in use. One current method in use is vacuum sampling, with explosive crystals caught and collected onto a fine filter [61]. However, this method relies on the presence of relatively large explosive particles, which may not always be present. Another technique is through solvent extraction, where a swatch is cut from the garment in question and solvent extracted [63, 66, 67]. This technique leads to the destruction of the item, is time-consuming and labour-intensive, and the resulting extract may require pre-concentration prior to analysis.

Due to these limitations, new contenders for sampling for explosive residues on clothing and textiles are emerging, with several researchers employing Raman-based sampling techniques for the detection of a number of explosives (including PETN and TNT) from textiles (including polyester, denim, cotton, wool and silk) [45-47]. Although these analyses are rapid and non-

destructive, with high sensitivity, they typically require focusing of the Raman laser beam (with a 5 µm diameter) onto explosive particles [45, 46], which is difficult, especially on light-coloured fabrics where the explosive crystals may be difficult to visualise. A further drawback of Raman-based techniques is that the technique does not permit the removal of the explosive residues from a surface, to enable further analyses to be performed. Additionally, there may be background interference in the Raman spectra from the background substrate on which the explosive residues are located [152, 153], meaning the interpretation of the results must be approached carefully.

Ionisation-based techniques are also emerging as alternatives for sampling from textiles, allowing in situ detection with suitable detection limits [64, 69, 70]. However, as with the Raman techniques described above, these ionisation-based techniques still require the isolation of the bulk explosives present on a surface for further analyses.

A recent promising candidate for recovering explosive residues from textile surfaces is the contact heater [154], a purpose-built instrument of the UK Forensic Explosives Laboratory (FEL). The contact heater consists of a heated aluminium platen connected to a vacuum pump. The heated platen is placed in contact with an area of fabric, and air is drawn over and through the surface of the fabric. This air passes through a cartridge containing an adsorbent polymer, where any volatilised analytes of interest are captured. The cartridge can then be eluted using a solvent, with the extract then analysed for explosive residues [155, 156]. A photograph of the contact heater is provided in Figure 3.1a, with a schematic of the contact heater's workings provided in Figure 3.1b.

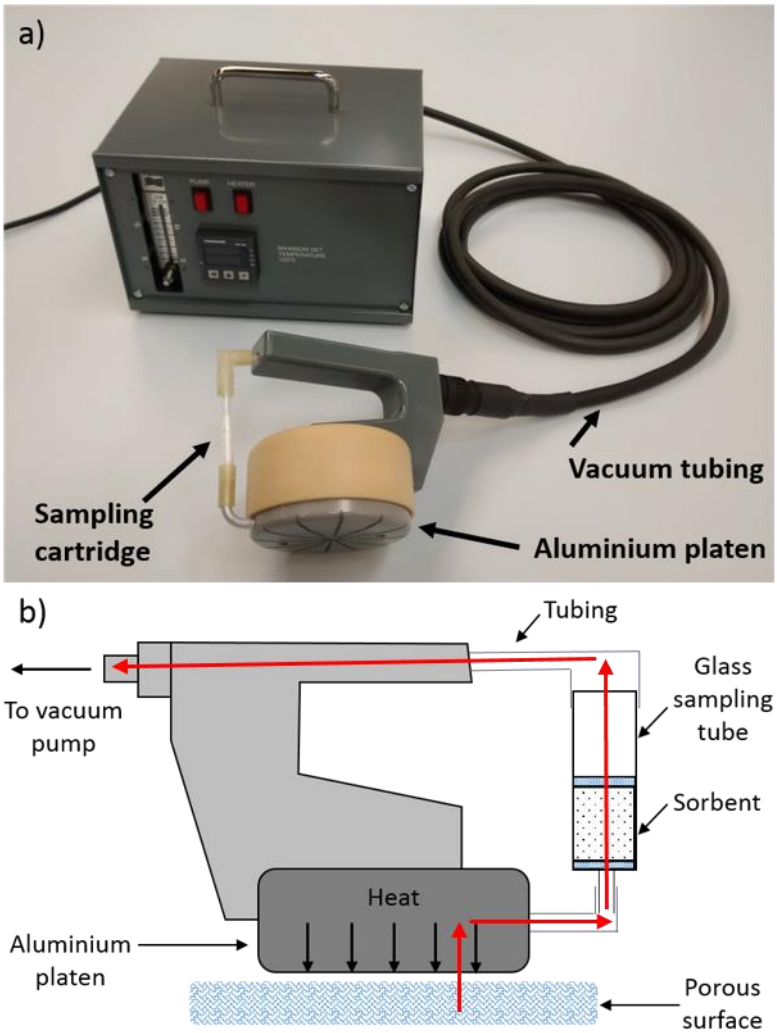

Figure 3.1: a) Labelled photograph of the contact heater and b) schematic of the contact heater sampling head's internal workings. The red arrows illustrate the air flow path through the contact heater

The contact heater has previously been shown to give encouraging recoveries of TATP and EGDN from both non-porous (ceramic tiles) and porous (denim, carpet) surfaces [154]. As discussed in Chapter 2, AFM has the potential to provide information on the *adhesion* of explosives to different textile surfaces. The contact heater can potentially provide information regarding the *recovery* of explosives from textile surfaces, enabling a link to be made between the adhesion and recovery of explosives with respect to a given surface.

In the current work, the contact heater recovery efficiency from selected surfaces was determined for TNT, PETN and RDX. As the contact heater is primarily designed for the recovery of explosive residues from textile surfaces, textile surfaces were the main focus of the present research. However, two non-textile surfaces (aluminium and polypropylene) were also included for comparison. A range of textile (porous) sampling surfaces were studied,

based on previous literature investigating sampling for explosive residues from textiles [46, 47, 64, 66, 69, 70]. The current work will also assess the stability and persistence of these explosive residues on the different surfaces. AFM work in Chapter 2 detailed the adhesion properties of TNT, PETN and RDX to a variety of surfaces. The aim of the current chapter is therefore to assess the relationship between the adhesion of an explosive to a surface, and its recovery from a surface. Further, the results of this work will also provide information on the viability of the contact heater as a sampling tool.

In addition, a small-scale study was performed where explosive residues were recovered by vacuum sampling, adapting the vacuum sampling conditions used by the UK's Forensic Explosives Laboratory [65], to enable a comparison to be made with the recoveries of TNT, PETN and RDX obtained using the contact heater.

3.2 Experimental

3.2.1 Materials to be sampled

The fabrics included in this study were rayon, silk, polyester fabric, acetate, 100 % cotton jersey, wool, denim, calico natural cotton, mercerised cotton and polyester fleece (Spotlight Fabrics, Perth, WA). Aluminium foil (Vogue brand catering aluminium foil, Vogue, Bristol, UK) and polypropylene were also investigated. Polypropylene-based contact heater samples were taken from unused, disposable polypropylene tub lids (KitchenCorner brand). These were washed with water then acetone, and dried with laboratory roll prior to use.

3.2.2 Other consumables

Aged samples were stored in nylon bags measuring 250 × 300 mm (Rilsan brand). General liquid chromatography vials (Agilent, Stockport, Cheshire, UK) were used for analyses. Low adsorption liquid chromatography vials (Supelco brand, Sigma Aldrich, Gillingham, Dorset, UK) were used to store the explosives spiking solution. 5 mL glass snap cap vials (VWR International Ltd, Lutterworth, Leicestershire, UK) measuring 40 × 20 × 18 mm were used for XAD-7 extraction. D6/9 silicone tubing (Buchi UK Ltd, Chadderton, Oldham, UK) was used for the contact heater connections.

3.2.3 Chemicals

TNT (1000 µg/mL solution in 1:1 methanol:acetonitrile), RDX (1000 µg/mL solution in 1:1 methanol:acetonitrile) and PETN (1000 µg/mL solution in methanol) (AccuStandard, New Haven, CT) were used for sample spiking. Acetonitrile (VWR International Ltd, Lutterworth,

Leicestershire, UK) was HiPerSolv Chromanorm for HPLC (Super Gradient Grade). Water (VWR International Ltd, Lutterworth, Leicestershire, UK) was HiPerSolv Chromanorm for HPLC (LC-MS grade). Musk Tibetene (1-tert-butyl-3,4,5-trimethyl-2,6-dinitrobenzene; Givaudan) was kindly donated by the Centre for Forensic Science at the University of Strathclyde, Glasgow, UK.

3.2.4 Materials for contact heater cartridges and vacuum sampling tubes

2 mL glass dropping pipettes with teats (Fisher Scientific Ltd, Loughborough, Leicestershire, UK), superfine 11 µm glass wool (Glaswarenfabrik Karl Hecht brand, VWR International Ltd, Lutterworth, Leicestershire, UK) and high purity 20-60 mesh Amberlite XAD-7 (Sigma Aldrich Ltd, Gillingham, Dorset, UK) were used for contact heater cartridge preparation. The Forensic Explosives Laboratory, Dstl, UK donated sufficient materials to prepare ten vacuum sampling tubes. These materials included 8 mL glass syringe barrel samplers with a 4 mm Luer fitting (Multilab Scientific Glass Blowers), 13 mm prefilters and 13 mm PTFE membrane filters (Millipore UK Ltd.), plastic retaining rings (Just Plastics Ltd.) and 90 mm lengths of PVC tubing (4 mm i.d., 7 mm o.d., Fisher Scientific UK). Whatman mini Uniprep syringeless filter vials (0.2 µm membrane size) were provided for filtering extracts prior to HPLC-UV analysis.

3.2.5 HPLC-UV instrument and analysis details

The HPLC-UV instrument used was an Agilent 1220 Infinity HPLC using Agilent LC OpenLAB CDS software, Version Rev.C.01.06(61). A number of analytical columns were utilised depending on availability. Details of methods developed and used in conjunction with these columns are provided in Table 3.1.

Table 3.1: Method details for HPLC-UV analyses of contact heater and vacuum samples

	Contact heater: 75 mm column	Contact heater: 50 mm column	Vacuum samples
Explosives analysed	TNT, PETN, RDX	TNT, PETN, RDX	TNT, PETN, RDX
Column details	YMC-UltraHT Pro C18 S-2 µm, 12 nm, 75 × 2.0 mm i.d.	YMC-UltraHT Pro C18 S-2 µm, 12 nm, 50 × 2.0 mm i.d.	YMC-UltraHT Pro C18 S-2 µm, 12 nm, 50 × 2.0 mm i.d.
Mobile phase	51:49 Acetonitrile:Water (isocratic)	51:49 Acetonitrile:Water (isocratic)	51:49 Acetonitrile:Water (isocratic)
Flow rate	0.4 mL/min	0.35 mL/min	0.35 mL/min
Column temperature	30 °C	30 °C	30 °C
Detection wavelengths	PETN: 212nm, TNT and RDX: 254 nm	PETN: 212 nm, TNT and RDX: 254 nm	PETN: 212 nm, TNT and RDX: 254 nm
Internal standard	Musk Tibetene	Musk Tibetene	Musk Tibetene
Run time	15 minutes	11.5 minutes	11.5 minutes
Injection volume	5 µL	5 µL	5 µL

All methods and columns generated linear calibration curves with R^2 values > 0.99. Standards ranged in concentration from 0.001 mg/mL to 0.063 mg/mL in each component. Details of these calibration curves, along with Figures of the calibration plots, are provided in Appendix B.

3.2.6 Contact heater sampling cartridge preparation

The cartridge assembly procedure was adapted from that of Salt *et al.* [156], with cartridges assembled as follows: the pipette teat was removed from the end of the dropping pipette and discarded. A small plug of glass wool (approximately 60 mg) was inserted into the wide end of the pipette and pushed into place at the tapered end of the tube using a clean microspatula. 0.36 g XAD-7 (± 0.01 g) was weighed and added into the pipette. This mass was chosen based on previous work [154] using XAD-7 cartridges, which contained an average mass of 0.36 g XAD-7. A larger plug of glass wool (approximately 200 mg) was added into the top of the pipette and pushed into place using a clean microspatula. All cartridges were rinsed through using 2 × 1 mL acetonitrile prior to use. A photograph of an assembled cartridge is provided in Figure 3.2.

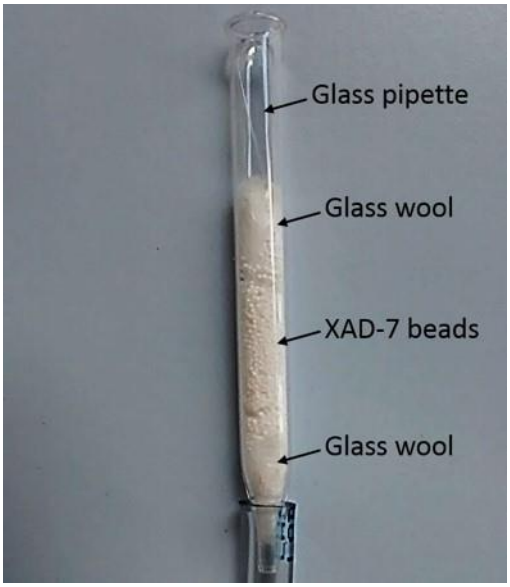

Figure 3.2: Labelled photograph of an assembled contact heater cartridge

3.2.7 Contact heater cartridge extraction

A number of cartridge extraction procedures were investigated throughout this work, discussed later in Section 3.3.2. The final method used is provided in the following sentences: After taking a contact heater sample, the glass wool was removed from the top of the cartridge and the XAD-7 beads poured into a clean 7 mL glass vial, adding 0.75 mL acetonitrile. The vial was sonicated at 40 °C for 2 minutes, before decanting the solution surrounding the XAD-7 beads into a clean vial. A further 0.75 mL acetonitrile was added to the XAD-7 beads, and the vial sonicated again at 40 °C for 2 minutes. This sonicated solution was decanted and added to the solution from the previous sonication, before drawing the solution up through a quartered piece of filter paper (Whatman Quantitative Filter Papers, 47 mm circles) held around the end of an empty 1 mL syringe's needle. This process removed any particulate matter from the solution. Filtration was performed by drawing the solution into the syringe through the filter paper, until no visible solution remained in the vial. The process of filtering by drawing the solution into a syringe enabled a concurrent manual volume measurement to be performed, before dispensing the solution into a clean LC vial and spiking in a Musk Tibetene internal standard at an overall concentration of 0.01 mg/mL prior to HPLC-UV analysis.

3.2.8 Sample preparation, spiking and storage

To avoid the possibility of sampling effects having an effect on the observed recoveries, contact heater sampling was performed following a randomised sequence for each of the six planned sets of samples. Each of these six sets of samples corresponded to a different spiking

technique/storage time combination, as shown in Table 3.2.

Table 3.2: Details of sample sets used, including spiking technique and subsequent storage conditions

Sample set number	Spike/storage combination
1	Solution spike, immediate sampling
2	Crystal spike, immediate sampling
3	Solution spike, room temperature (20 to 26 °C) dark storage for 1 week
4	Solution spike, freezer (-20 to -22 °C) storage for 1 week
5	Crystal spike, room temperature (20 to 26 °C) dark storage for 1 week
6	Crystal spike, freezer (-20 to -22 °C) storage for 1 week

The randomised sequence was generated by assigning a unique number from one to n, with n equalling the number of surfaces within the sample set. A random number generator (located at randomizer.org/form.htm) was then used to 'scramble' this list of numbers, and sampling was performed following this randomised number sequence.

3.2.8.1 Solution spiking procedure

A mixed spiking solution was prepared by combining equal volumes of the individual explosive standards: TNT (1000 µg/mL in 1:1 methanol:acetonitrile), RDX (1000 µg/mL in 1:1 methanol:acetonitrile) and PETN (1000 µg/mL in methanol). This gave a solution of 1:1:1 TNT:RDX:PETN, each at 333.3 µg/mL, in 3:2 methanol:acetonitrile.

Prior to spiking, each material was placed onto a clean piece of laboratory roll. Using a microsyringe, 70 µL of the mixed spiking solution was spiked onto each material to be sampled. Porous materials such as fabrics were held just off the laboratory roll during spiking, until all visible solvent had evaporated, to prevent any of the spiking solution from passing through and being absorbed by the laboratory roll beneath. When spiking aluminium samples, spiking was performed on the matte side of the aluminium foil, rather than the shiny side, as the matte side of aluminium foil was investigated during earlier AFM studies (Chapter 2).

3.2.8.2 Crystal spiking procedure

Crystals were generated by placing 70 µL of the spiking solution into the slightly concave base of an upturned 7 mL glass vial. The solution was allowed to evaporate at room temperature

over approximately 15 minutes, which resulted in the formation of white crystals. The resulting crystals from the base of the glass vial were then wiped onto the required surface until no visible residue remained on the glass vial (Figure 3.3).

Figure 3.3: Explosive crystals generated by evaporating 70 µL of spiking solution in the concave base of an upturned glass vial

Following this, the base of the glass vial was rinsed using 500 µL acetonitrile, capturing the washings in a clean glass vial, to recover any residual explosives adhering to the glass, enabling the exact mass of explosives transferred to each surface to be determined. This in turn enabled exact percentage recoveries to be calculated relative to the mass of explosives transferred. A manual volume measurement of these vial washings was performed, and Musk Tibetene added at a concentration of 0.01 mg/mL prior to HPLC-UV analysis.

The efficiency of the vial base rinsing step used following crystal transfer was evaluated by spiking 70 µL of the spiking solution onto the base of three glass vials, then rinsing each base using 500 µL acetonitrile (i.e. without transferring any crystals to a textile surface). The three washings were then analysed, and the percentage recoveries of TNT, RDX and PETN evaluated.

3.2.8.3 Sample storage containers and temperatures

Each contact heater sample was prepared as either a solution-spiked or crystal-spiked sample. For samples subjected to an ageing period prior to sampling, the spiked samples were placed into individual nylon bags, before swan-necking the bag and sealing with adhesive tape. Samples were placed into cardboard boxes and the boxes placed into either cupboards at room temperature (between 20 and 26 °C), or into a freezer held between -20 and -22 °C.

3.2.9 Contact heater sampling procedure

Before taking each sample, a negative control was taken from the surface to be sampled from. This ensured that the surface was free from contamination, that the platen was clean, and that the batch of XAD-7 cartridges was free from contamination. These negative controls were

taken as follows:

The surface to be sampled was placed on a clean piece of laboratory roll on the lab bench, and the contact heater platen switched on and allowed to heat to 120 °C. 0.7 mL acetonitrile was added to an XAD-7 sampling cartridge to wet the XAD-7 beads, and the cartridge was fitted into the silicone tubing of the contact heater's sampling head. The pump was turned on at a flow rate of 1000 mL/min and placed on the surface and sampling performed by moving the platen in small circles around the surface for five minutes. After five minutes, the pump and platen heater were switched off and the cartridge removed from the sampling head, with extraction of the XAD-7 beads performed as described earlier (Section 3.2.7).

Corresponding samples were taken from each surface following a negative control. These were performed in an identical manner to the negative controls, though the surface had now been spiked using either the Solution Spiking Procedure (Section 3.2.8.1) or Crystal Spiking Procedure (Section 3.2.8.2). Quantification of TNT, PETN and RDX was performed by determining their concentrations in the measured volume of solution obtained following XAD-7 cartridge processing, then comparing this to the maximum possible concentrations in the same volume of solution, based on the quantity of TNT, PETN and RDX spiked on the surface. Peak areas were used for quantification purposes. Each surface was used only twice, for a negative control and corresponding spiked sample, before being discarded.

3.2.10 Vacuum sampling procedure

Vacuum sampling tube preparation was performed by adapting the procedure of the FEL [65], see Figure 1.3. Tube preparation involved placing a prefilter and PTFE membrane filter into a glass syringe barrel sampler. Following this, a plastic retaining ring was added, pushed down to approximately 1-2 mm above the membrane filter using a clean length of tubing. A length of PVC tubing (approximately 90 mm, 4 mm diameter) was attached to the end of the vacuum tube, and into this was inserted the tapered end of a pre-prepared XAD-7 sampling cartridge. Vacuum sampling was performed on three types of fabric: cotton jersey, wool and polyester. Each fabric was analysed in triplicate. A control sample was also taken, which involved taking an air blank for five minutes and then extracting the vacuum sampling tubes in the same manner as for a spiked sample.

Due to the limited number (10) of vacuum sampling tubes available for this work, the decision was made to spike all vacuum sampling surfaces using crystals of explosives, rather than solutions. Crystal spiking of the vacuum sampled fabrics was performed in an analogous manner as for the contact heater sampled fabrics, detailed earlier (Crystal spiking procedure,

Section 3.2.8.2). Vacuum sampling was performed as follows:

A clean piece of fabric (cotton jersey, wool or polyester) was placed onto a clean piece of laboratory roll and spiked in a pre-marked area measuring 2 × 2 cm using a mixture of TNT, PETN and RDX crystals. The base of the glass vial used for explosive crystal transfer was rinsed into a clean vial using 500 µL acetonitrile, to enable quantification of the exact mass of TNT, PETN and RDX transferred onto the fabric. A manual volume measurement was performed of this vial rinse and the required volume of 1 mg/mL Musk Tibetene (MT) solution added as internal standard to give a concentration of 0.01 mg/mL, before analysing using HPLC-UV, injecting each sample in duplicate and averaging the results.

0.7 mL acetonitrile was added to an XAD-7 sampling cartridge to wet the XAD-7 beads, before fitting the wide end of the cartridge into the silicone tubing of the contact heater's sampling head, and the vacuum tube was connected to the tapered end of the XAD-7 cartridge using its attached PVC tubing. The contact heater's vacuum pump was used for the vacuum sampling to ensure that vacuum power of equivalent strength was used in order to enable a fairer comparison between the contact heater and vacuum sampling techniques. Vacuum sampling was performed for five minutes at full flow (1000 mL/minute), keeping the open end of the vacuum tube at a slight angle to the fabric to ensure satisfactory air flow and ensuring vigorous contact during the five minutes. After five minutes, the vacuum tube was inverted (to ensure no crystals were lost due to gravity when the pump was stopped) and the pump turned off. The vacuum tube was carefully disconnected from its PVC tubing and eluted into a clean vial using 2 × 0.5 mL acetonitrile, running the solvent down the internal walls of the vacuum tube and forcing the solvent through using pressure from a clean rubber bung. A manual volume measurement was made of the vacuum tube eluent and the required volume of internal standard, before analysing using HPLC-UV, injecting each sample in duplicate and averaging the results.

The XAD-7 tube was removed from the contact heater's sampling head and the glass wool from the wide end removed and discarded. The XAD-7 beads were tipped into a clean 7 mL glass vial and 0.75 mL acetonitrile added. The vial was capped and sonicated at 40 °C for two minutes, and the resulting solution decanted from the beads into a clean vial. A further 0.75 mL acetonitrile was added to the beads and the sonication stage repeated, with the solution decanted and added to the solution decanted from the first sonication step. A manual volume measurement of the solution was performed and the required volume of MT solution added as internal standard. An aliquot of approximately 400 µL of the solution was then filtered through a mini Uniprep vial and analysed using HPLC-UV, using the method detailed in Table 3.1.

Samples were analysed in duplicate and the results averaged.

Quantification of TNT, PETN and RDX was performed by determining their concentrations in the measured volume of solutions generated following vacuum sampling, then comparing this to the maximum possible concentrations in the same volume of solution, based on the quantity of TNT, PETN and RDX spiked on the surface. Peak areas were used for quantification purposes.

3.3 Results and discussion

3.3.1 HPLC-UV method development

HPLC-UV was considered a suitable technique with which to quantify explosives recoveries from this work, as previous authors have demonstrated the utility of HPLC-UV for the analysis of TNT, PETN and RDX [15, 157]. These authors used slightly different HPLC-UV conditions for their analyses, which are detailed in Table 3.3.

Table 3.3: HPLC-UV conditions used for TNT, PETN and RDX analyses by previous researchers

Author	DeTata *et al.* [15]	Song-im *et al.* [157]
Explosives analysed	TNT, PETN, RDX	TNT, PETN
Column name	Dionex Acclaim E1	Zorbax Eclipse XDB-C18
Column specifications	5 µm, 4.6 × 250 mm	5 µm, 4.6 × 150 mm
Mobile phase	43:57 Methanol:Water	60:40 Methanol:Water
Flow rate	1 mL/min	1 mL/min
Column temperature	32 °C	30 °C
Detection wavelengths	PETN: 210nm; TNT and RDX: 254 nm	212 nm
Internal standard	1,2-Dinitrobenzene (1,2-DNB)	2-Nitrotoluene (2-NT)

Although neither column from Table 3.3 was available for use in this work, an alternative C18 column (YMC-UltraHT Pro C18 S-2 µm, 12 nm, 75 × 2.0 mm i.d.) was available, so efforts were made to develop a method for use with this column.

Though DeTata [15] and Song-im [157] both used mobile phases consisting of methanol:water, a mobile phase of acetonitrile:water was used in this work, to better suit the acetonitrile used during extraction of the XAD-7 beads. A HPLC-UV method was therefore formulated, by adapting the conditions of Song-im [157] and DeTata [15]. Details of this initial

method are provided in Table 3.4.

Table 3.4: Details of initial HPLC-UV method for explosives analysis

Column details	YMC-UltraHT Pro C18 S-2 µm, 12 nm, 75 × 2.0 mm i.d.
Mobile phase	60:40 Acetonitrile:Water (isocratic)
Flow rate	0.4 mL/min
Column temperature	30 °C
Detection wavelengths	PETN: 212nm, TNT and RDX: 254 nm
Injection volume	5 µL
Retention times	RDX 0.738 min, TNT 1.122 min, PETN 1.517 min

It can be seen from Table 3.4 that RDX, TNT and PETN all eluted with similar retention times. At this stage, although separation of the three compounds had been achieved, it was hypothesised that at higher concentrations, the baseline separation between the peaks may be compromised, and that this would affect subsequent quantifications. Work was therefore performed to increase the baseline separation between each of the peaks, to prevent any possible co-elution during sample analyses. These modifications are detailed in Table 3.5.

Table 3.5: Attempts to improve baseline resolution between TNT, PETN and RDX

Modification	Acetonitrile: Water ratio	Flow rate (mL/min)	Column temp. (°C)	Comments
1	60:40	0.4	30	Initial conditions
2	55:45	0.4	30	Little difference in retention times and baseline separation
3	45:55	0.4	30	Improved baseline separation between peaks; PETN co-eluting with solvent impurity
4	50:50	0.4	30	PETN co-eluting with solvent impurity
5	51:49	0.4	30	Satisfactory baseline resolution of all solution components. Final retention times: RDX: 0.936 min, TNT: 1.722 min, PETN: 2.889 min

The conditions used in Modification 5 of Table 3.5 gave rise to excellent baseline separation between the three explosives being analysed (see Figure 3.4), with these conditions therefore

used for the preparation of suitable calibration curves, and in subsequent analyses.

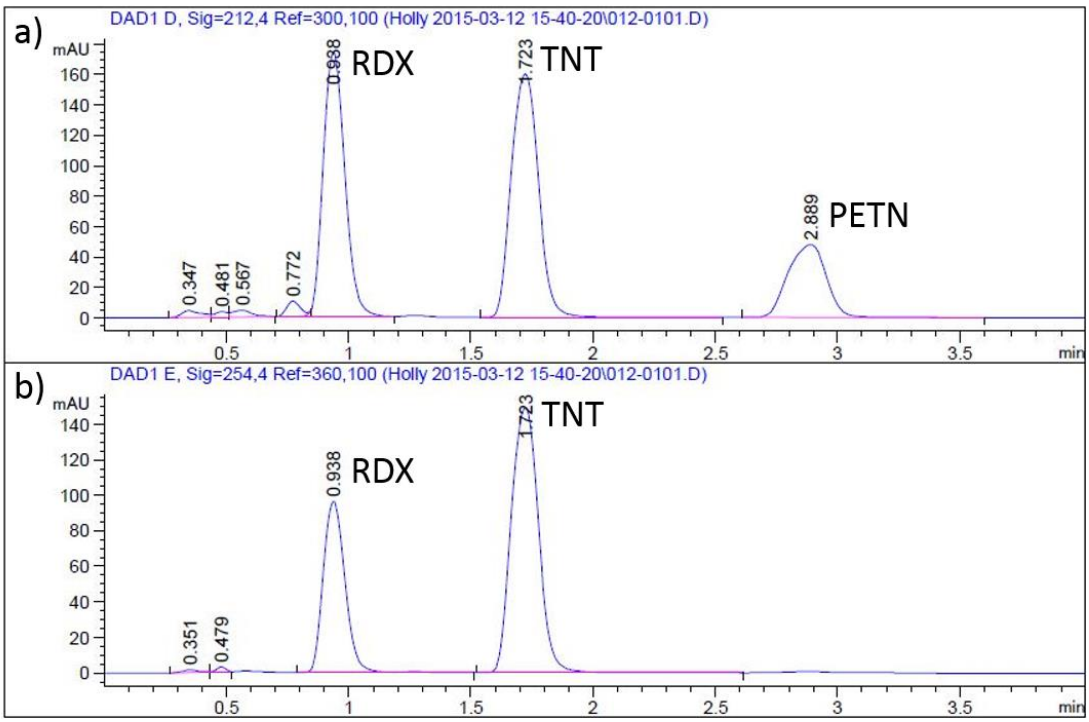

Figure 3.4: Separation of a 5 µL injection of a mixed 0.032 mg/mL RDX, TNT and PETN standard on a YMC-UltraHT Pro C18 S-2 µm, 12 nm, 75 × 2.0 mm i.d. HPLC column at 30 °C using a mobile phase of 51:49 acetonitrile:water using a) a 212 nm detector and b) a 254 nm detector

Following the development of a suitable method for the analysis of TNT, PETN and RDX, a suitable internal standard was sought. Initially 1,2-dinitrobenzene (1,2-DNB) was chosen as a suitable internal standard for this work, based on the work of DeTata *et al.* [15]. However, due to a lengthy delay regarding the supply of 1,2-DNB, an alternative internal standard was utilised in the form of 2-nitrotoluene (2-NT), based on the work of Song-im *et al.* [157].

2-NT was therefore assessed for its suitability as an internal standard in combination with the developed HPLC-UV method. A 0.01 mg/mL solution was prepared in acetonitrile and analysed via HPLC-UV, to determine its retention time. Unfortunately, the 2-NT peak eluted at 1.758 minutes; an almost identical retention time to TNT (1.703 minutes). For confirmation, a mixture of 2-NT and TNT in acetonitrile was analysed, though as expected this only gave rise to a single peak. Three options were considered feasible to attempt to separate the TNT and 2-NT: 1) adjust the flow rate, 2) adjust the mobile phase composition, and 3) adjust the column temperature.

Earlier work for this thesis using this HPLC-UV instrument had found that decreasing the flow rate gave rise to broader peaks, and it was thought that this may worsen any separation

attempts. Therefore, several attempts were instead made to separate the analytes by changing the mobile phase composition and flow rate. These attempts are outlined in Table 3.6.

Table 3.6: Attempts to overcome the co-elution of TNT and 2-NT

Modification	Acetonitrile:Water ratio	Flow rate (mL/min)	Outcome
1	51:49	0.4	Co-elution
2	47:53	0.4	Co-elution
3	47:53	0.3	Co-elution
4	42:58	0.4	Co-elution

However, it can be seen that each separation attempt resulted in co-elution of the 2-NT and TNT, likely due to their very similar chemical structures. In the interests of time, an alternative internal standard was therefore explored in the form of Musk Tibetene, which has previously been used with success as an internal standard for LC analyses [158].

A solution of Musk Tibetene in acetonitrile at 0.1 mg/mL was therefore prepared and analysed using the conditions detailed in Modification 5, Table 3.5. The Musk Tibetene gave a sharp peak, well isolated from those of TNT, PETN and RDX. Musk Tibetene was therefore chosen as a suitable internal standard for this work. A 1 mg/mL solution of Musk Tibetene was prepared in acetonitrile, with the solution added as an internal standard as 1 % of the total volume of a sample, to give an overall Musk Tibetene concentration of 0.01 mg/mL in each sample.

After running the majority of contact heater samples through the 75 mm YMCUltraHT-C18 column using the developed HPLC-UV method, the column performance began to deteriorate, and a decision was made to change the column for an alternative column. This was in the form of a nearly identical, YMC-UltraHT Pro C18 S-2 µm, 12 nm, 50 × 2.0 mm i.d., differing only in the length of the column (50 mm rather than the previous 75 mm).

The previously-developed HPLC-UV method was therefore used on this shorter column, analysing a previously-analysed contact heater sample. Unfortunately, the peak corresponding to RDX had very little baseline separation from an impurity resulting from the XAD-7 post-sampling processing stage. A new HPLC-UV method was therefore developed for this column, accounting for the difference in column length. This was achieved by decreasing the column flow rate to 0.35 mL/minute, rather than 0.4 mL/minute, to enable satisfactory baseline resolution to be achieved.

3.3.2 Contact heater cartridge extraction: Method development

Prior to performing any contact heater sampling, it was necessary to determine a suitable sampling cartridge extraction procedure. For this, simulated post-sampling contact heater cartridges were prepared by removing the glass wool from individual unused XAD-7 cartridges and tipping the beads from each cartridge into individual clean weighing boats. Three aliquots of beads were each spiked using a 70 µL spike of the spiking solution, corresponding to the intended spike quantity (70 µL) to be used for the subsequent contact heater sampling. The beads were shaken gently to distribute the explosives evenly amongst the beads, and the spiked beads were then tipped back into their respective cartridges, capping each cartridge with a fresh plug of glass wool.

As an initial extraction procedure, each spiked cartridge was eluted into a clean glass vial using 3 × 0.5 mL acetonitrile, aiding elution using a gentle stream of nitrogen. A manual volume measurement was performed and the extract analysed to quantify the recovered explosives. This was repeated three times. The averaged recoveries for each explosive, along with the average recovery between the three explosives, are provided in Table 3.7.

Table 3.7: Average RDX, TNT and PETN recoveries from triplicate cartridge extractions using 3 × 0.5 mL acetonitrile rinses

RDX recovery (%)	TNT recovery (%)	PETN recovery (%)	Average recovery
68.8	65.5	70.3	68.2

It can be seen from Table 3.7 that recoveries were relatively low using this extraction technique. Next, the inclusion of a sonication step to promote the explosives' release from the XAD-7 beads was explored. For an initial sonication experiment, XAD-7 beads were placed into a clean glass vial and spiked with 70 µL of the spiking solution. 1.5 mL acetonitrile was added, and the vial was sonicated at room temperature for 2 minutes. This gave recoveries of around 72 % (Modification 1, Table 3.8).

Table 3.8: Results from sonication experiments in an attempt to improve explosives recoveries from spiked XAD-7 beads

Modification	Acetonitrile volume used during sonication (mL)	Sonication temp. (°C)	Sonication time (min)	Recovery (%)			
				RDX	TNT	PETN	Average
1	1 × 1.5	20	2	72.9	70.8	73.6	72.4
2	1 × 1.5	30	5	68.9	67.2	70.1	68.7
3	2 × 0.75	30	2 × 2	85.2	80.7	84.5	83.4
4	2 × 0.75	40	2 × 2	89.2	83.1	86.7	86.3

This modification was repeated after heating the sonicating bath to 30 °C and allowing for a longer extraction time in an attempt to enhance explosives recoveries (Modification 2, Table 3.8), but this did not improve recoveries. Additional modifications were therefore tested. It was hypothesised that some form of equilibrium may be forming around the XAD-7 beads, which was preventing all of the explosives from desorbing during the sonication step. By adding solvent to the explosives-spiked XAD-7 beads, and sonicating them, this may induce some explosives to desorb from the beads to dissolve in the solvent. However, the presence of such explosives in solution around the XAD-7 beads may have prevented any further explosives from desorbing from the beads – the explosives' concentration may have formed an equilibrium between the beads and the solution, preventing the remaining explosives from desorbing.

An alternative approach was therefore used - rather than using a single 1.5 mL aliquot of acetonitrile during the sonication step, two individual 0.75 mL aliquots of acetonitrile were used. After sonication of the beads in the first 0.75 mL aliquot, the resulting solution was decanted into a clean vial before adding an additional 0.75 mL of acetonitrile, and repeating the sonication. This meant that any equilibrium existing between the explosives on the beads and the explosives in the solution will have been removed after decanting the initial sonication solution. Addition of the second aliquot of acetonitrile should then encourage a further quantity of explosives to desorb from the XAD-7. This approach was performed at 30 °C and 40 °C (Modifications 3 and 4, Table 3.8). It can be seen that explosives recoveries of 83.4 and 86.3 % were obtained, respectively. Although it would have been possible to further increase the temperature of the sonication bath, this was not performed due to concerns that higher temperatures would induce evaporation of the acetonitrile during sonication, with possible loss via volatilisation of the contained explosives within the solution. Explosives extraction using the conditions from Modification 4 was performed in triplicate, to enable the repeatability of

the procedure to be determined. The results are displayed in Figure 3.5.

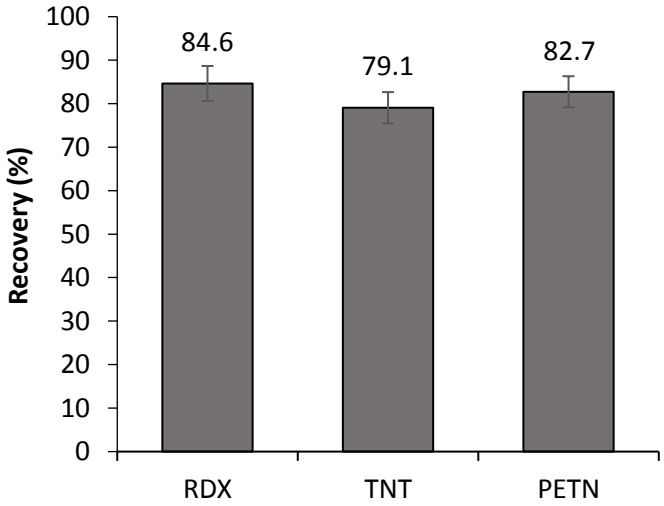

Figure 3.5: Assessing the repeatability of the double sonication method for explosives extraction. Error bars show standard deviation within a set of three measurements

From Figure 3.5 it can be seen that relatively high and reproducible explosives recoveries were obtained. The conditions of Modification 4 were therefore used for the recovery of explosives from the XAD-7 cartridges following contact heater sampling throughout this chapter.

3.3.3 Choice of fabrics for sampling

In the present work, identical fabrics were sampled as those investigated using AFM in Chapter 2. The AFM work had determined the adhesion force of TNT, PETN and RDX to the respective surfaces, and with the current contact heater and vacuum sampling work, it was envisaged that any relationships between the adhesion of an explosive to a surface and its recovery from a surface could be elucidated.

In addition, the selection of fabrics used in the current work expands on those looked at by other researchers investigating the recovery of explosives from fabrics [46, 47, 64, 66, 69, 70], involving fabrics such as wool, silk, cotton, polyester and denim. Table 3.9 illustrates the textiles under analysis in this chapter, compared to previous research investigating explosives recoveries from textiles.

Table 3.9: A comparison between the textiles under analysis in this chapter, compared to previous research investigating the recovery of TNT, PETN and RDX from the same textiles

Textiles under analysis in this chapter	Previous research investigating TNT recovery from this textile	Previous research investigating PETN recovery from this textile	Previous research investigating RDX recovery from this textile
100 % polyester	[46, 47, 64]	[46, 47, 64, 66]	[64, 69]
Acetate			
Calico natural cotton			[69]
Cotton jersey	[46, 64]	[46, 64, 66]	[64]
Denim	[46, 47, 64]	[46, 47, 64]	[64]
Mercerised cotton			
Polyester fleece	[64]	[64]	[64]
Rayon			
Silk	[46, 64]	[46, 64]	[64]
Wool	[46]	[46]	

3.3.4 Choice of spiking method

When assessing different techniques for the recovery of explosives from textiles, previous researchers have opted to spike explosives using solutions of explosives, and/or crystals of explosives. Solution-spiking and crystal-spiking both have benefits and limitations, which will be briefly discussed below, before the specific spiking procedures used throughout the current work are detailed.

Solution spiking enables 100 % transfer of the desired spike onto the surface of interest, meaning an accurate quantification of the percentage recovery of the spike can later be easily calculated. Spiking using a solution is also likely to produce a more homogeneous distribution of the explosives molecules on a surface, compared to the process of crystal spiking [66]. However, spiking using a solution is less representative of a real-life situation, compared to spiking using crystals of explosives. Explosives are typically solids during use, meaning transfer of explosives crystals is more likely during a real-life scenario. On the other hand, spiking using solutions of explosives may be representative of spillage or transfer of a solution of explosives, such as during their illicit synthesis or manufacture. Fabrics and textiles tend to be absorbent, and so the process of spiking them using a solution is likely to lead to absorption of the solution into the mesh of the fabric in question.

On the other hand, with crystal spiking, the nature of interaction between an explosive and a textile is likely to differ compared to the interactions between a solution of explosive and a textile. Unlike solutions, which can undergo deep absorption into a fabric, it is likely that explosive crystals will sit closer to the surface of a textile, so the recovery mechanism is likely to differ. In addition, spiking a textile using crystals of explosives is less likely to give a homogeneous distribution of the explosives. Although more representative of a real-life situation, such as a person handling explosives and transferring residues onto their clothing [66], the process of crystal spiking may not result in 100 % transfer of the explosives, meaning any subsequent percentage recovery calculations may potentially be skewed.

Almaviva *et al.* performed Raman measurements of explosives, and explosive precursor chemicals, on different types of fabric [47]. The authors used a special instrument to drop uniform microdroplets of explosive solutions (containing TNT and PETN) onto the different fabrics. This procedure produced a homogeneous distribution of the explosives on the surface. The authors deposited the solutions onto a 1 × 1 cm^2 area of fabric, to give final surface densities for the different explosives of 100-400 $\mu g/cm^2$. The authors estimated that this surface concentration can be approximated to the surface density of explosive residue transferred onto a fabric from a contaminated fingerprint.

Talaty *et al.* [64] also spiked different fabrics using solutions of explosives, in this case using DESI-MS to analyse the deposited explosives. Talaty *et al.* also used 1 × 1 cm^2 squares of the different fabrics, spiking 1 µL aliquots of RDX, HMX, TNT and PETN, and reported that in some cases, the spiking solution stayed close to a fabric's surface, whereas in other cases, such as polyester fleece, it was absorbed. The authors reported higher limits of detection from certain fabrics, compared to smooth, non-fabric test surfaces such as Teflon, glass and metal. This finding was attributed to the different surface geometries (i.e. texture), physical properties and composition of the different spiked surfaces.

Fletcher *et al.* [68] assessed the recoveries of polymer spheres of different diameters (1 µm to 45 µm) from cloth, using an air or nitrogen jet. The polymer spheres acted as simulated explosive particles, to mimic the situation where someone who had been handling explosives had wiped their hands on their clothing. The authors found that larger particles were more easily removed. Taking this finding into account, this suggests that it should be easier to recover crystals of explosive from textiles, compared to explosives deposited as a solution, where much smaller, individual molecules of explosive would be distributed throughout a fabric.

Brust *et al.* [66] investigated the stability and recovery of PETN from different textiles. PETN was applied either as a solution or a solid, onto cotton, acrylic and polyester fabrics. In this work, the authors either spiked 3 mg of solid PETN onto the fabrics, or an aliquot of PETN solution containing 3 mg PETN. The authors reported a higher rate of PETN degradation from the solution-spiked samples than the solid-spiked samples, attributing this to the increased contact area between the PETN deposited from a solution compared to the PETN deposited as a solid.

Finally, work by Hubert *et al.* [69] assessed the ability of Direct Analysis in Real Time Mass Spectrometry (DART-MS) and Desorption Electrospray Ionisation Mass Spectrometry (DESI-MS) to analyse explosive-contaminated fabrics. The authors also evaluated the effect of different mesh sizes for the fabrics. Looking solely at RDX, the authors spiked RDX as a solution and as crystals (generated by depositing a solution of RDX onto a glass slide, allowing evaporation of the solvent, and then wiping the glass slide using the fabrics). The authors reported that lower recoveries were obtained from the RDX deposited as crystals from glass slides, than the RDX deposited as a solution. This finding was attributed to the explosives deposited from glass slides being spread over a larger surface area of the fabric, making it more difficult to remove all of the crystals of RDX. In contrast, the explosives deposited as a solution were highly concentrated in a smaller area, making it easier to remove more of the RDX. The rationale behind this conclusion must be questioned, as it is arguably easier to recover explosives from a low-density coverage of crystals than a high-density solution spike. This argument is supported by the findings of Gillen [68], who found that larger particles are easier to remove from textiles, and Brust [66], who found that higher recoveries of PETN were obtained from fabrics spiked using crystals of PETN than fabrics spiked using solutions of PETN.

Based on the findings of the present piece of work (discussed later, Section 3.3.6.1), a likely reason for Tabet's finding of lower recoveries from the crystal-spiked fabrics is that 100 % transfer of the crystals was not achieved from the glass onto the fabrics when wiping the glass slides using the different fabrics. This is supported by both the AFM results reported in Chapter 2 (where TNT, PETN and RDX all demonstrated the highest adhesion to glass), and by a transfer efficiency evaluation performed during the present chapter. This is discussed further in the sections below.

In the present work, a mixture of TNT, PETN and RDX was spiked onto a variety of textile and non-textile surfaces using both solution spikes and crystal spikes, to compare the recoveries and persistence of the explosives using the respective spiking methods. Although

the solution spiking technique enables 100 % transfer of the desired spike onto a surface, the crystal spiking technique is unlikely to be 100 % efficient, so it was necessary to identify a suitable crystal spiking procedure before spiking and sampling could be performed.

3.3.4.1 Crystal spiking procedure

Initial plans for crystal spiking the respective surfaces had been to spike 70 µL of the spiking solution onto the matte side of a piece of aluminium foil, allowing the solvent to evaporate, before wiping the resulting crystals onto the respective sampling surfaces. Unfortunately, upon performing this procedure, the spiking mixture immediately spread across the foil's surface, with the solvent evaporating in under one minute. The procedure was repeated using the shiny side of a piece of foil, but the same phenomenon was observed. In each case, no explosive crystals were visible, suggesting the formation of very small explosive crystals. A slower rate of solvent evaporation was desired, to enable the formation of larger explosive crystals.

An alternative crystal-generation surface was therefore sought, with glass considered to have the potential to be a suitable crystal-generation surface. A flat glass slide was investigated, taking precedence from the work of Hubert *et al.* [69] (detailed earlier) but, as with the aluminium foil, this resulted in significant spreading of the spiking solution. An alternative glass surface was investigated in the form of a 7 mL glass vial, which, when upturned, had a slightly concave base. 70 µL of the spiking solution was spiked into the concave base, to assess its suitability for explosive crystal generation. Ultimately this appeared to be a very suitable surface upon which to generate explosive crystals. The concave base provided a shallow 'well' in which the solution could sit (similar to the wells within a dimple tile), preventing significant spreading, and a much slower rate of solvent evaporation was observed. Visible explosive crystals were seen once all of the solvent had evaporated. This crystal generation technique was therefore adopted for all crystal-spiked surfaces, using a new glass vial for each sample.

3.3.4.2 Crystal spiking efficiency considerations and validation

As the crystal-spiking procedure was unlikely to be 100 % efficient, an additional step was incorporated into the crystal spiking procedure, with the aim to quantify the mass of explosives remaining on the glass vial base after crystal transfer onto a material. This involved rinsing the base of each glass vial using 500 µL acetonitrile after the crystal transfer step. The acetonitrile was then transferred into a clean LC vial, performing a manual volume measurement of the solution's volume during transfer, and quantification was performed of any TNT, RDX or PETN remaining on the vial base. These residual quantities of explosives

were then subtracted from the quantity originally spiked onto the glass vial, to give accurate, 'actually transferred' values, specific to each sample.

The efficiency of this vial rinsing step was assessed by spiking three glass vial bases using 70 µL of the mixed spiking solution, allowing evaporation and thus crystal formation to occur, and then rinsing the bases of the glass vials, to act as a 'positive control' for the vial rinse step. The results from three replicates of this vial washing efficiency evaluation are displayed in Figure 3.6.

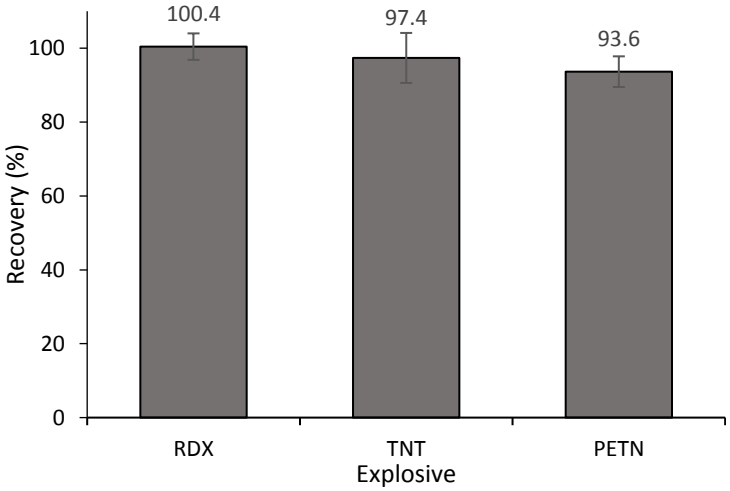

Figure 3.6: Recoveries of TNT, PETN and RDX from crystal transfer vial washing efficiency validation. Error bars show standard deviations within triplicate measurements

Figure 3.6 shows that a very high recovery was obtained from these vial washing efficiency tests, suggesting that a 0.5 mL acetonitrile wash is sufficient to recover any non-transferred explosives following the crystal transfer step. It is recognised that an alternative method to prevent the problem of explosive crystals adhering strongly to glass following generation by evaporation of solutions is to use solid explosive crystals instead. However, it was not possible to realistically obtain solid, pure explosives samples for this work.

3.3.5 Sampling surfaces and storage conditions

Details of the surfaces, spiking techniques and storage conditions employed in this work are outlined in Table 3.10.

Table 3.10: Surfaces, spiking technique and storage conditions investigated during this work. Samples stored in the dark were stored at room temperature (20 to 26 °C), whereas samples stored in the freezer were held between -20 and -22 °C

	Group number					
	1	2	3	4	5	6
Surface number	Immediate sampling		Solution spike		Crystal spike	
	Solution spike	Crystal spike	Dark (1 week)	Freezer (1 week)	Dark (1 week)	Freezer (1 week)
1	Polyester fabric	Polyester fabric	Polyester fabric	Polyester fabric	Polyester fabric	Polyester fabric
2	100 % cotton jersey	100 % cotton jersey	100 % cotton jersey	100 % cotton jersey	100 % cotton jersey	10 0% cotton jersey
3	Wool	Wool	Wool	Wool	Wool	Wool
4	Denim	Denim	Denim	Denim	Denim	Denim
5	Rayon	Rayon	Aluminium	Aluminium		
6	Silk	Silk				
7	Acetate	Acetate				
8	Calico natural cotton	Calico natural cotton				
9	Mercerised cotton	Mercerised cotton				
10	Polyester fleece	Polyester fleece				
11	Aluminium					
12	Polypropylene					

For the solution-spiked samples with immediate sampling (Table 3.10, Group 1), a four minute wait period was observed following spiking to allow any residual spiking solvent to evaporate prior to sampling. The ‘immediate sampling’ crystal spiked samples (Table 3.10, Group 2) were sampled immediately following crystal transfer onto the respective surfaces.

The aged spiked samples (Groups 3-6) were stored under two conditions: in the dark (at room temperature) and in a freezer. No samples were stored with exposure to UV light, i.e. exposure to daylight. Previous work [159] has shown that storage of TNT-spiked samples in the presence of UV light resulted in the rapid degradation of TNT stored on cotton swabs, whereas storage in the dark and in the freezer lessened this degradation. For this reason, samples in this

work were stored in the 'best' two conditions determined from this previous work - in the dark at room temperature, and frozen.

For the aged samples, a sub-selection of surfaces was used. These surfaces were denim, wool, cotton jersey and polypropylene, and, for the solution-spiked aged samples, aluminium was also investigated.

3.3.6 Sampling considerations

Prior to presenting and discussing the explosive residue recoveries obtained using the contact heater and vacuum sampling, a discussion on some sampling considerations which arose throughout this work will be provided. This may aid interpretation of the obtained explosive residue recoveries. For example, the solution-spiked acetate samples proved problematic. The spiking solution appeared to dissolve the acetate, making it very stiff in the areas where the spiking solution had been applied. This meant that when contact heater samples were taken from the acetate, substantial friction existed between the acetate and the contact heater. No recovery of any of the three explosives was observed from any of the solution-spiked acetate samples.

3.3.6.1 A comparison between crystal transfer efficiency and fabric mesh size

In addition to enabling the exact mass of each explosive transferred during each crystal spike to be calculated, the process of rinsing each vial base and quantifying the mass of explosives remaining on the vial base provided some additional, fabric-specific data. Figure 3.7 displays the average percentage of TNT, PETN and RDX remaining on the vial bases following each crystal transfer procedure.

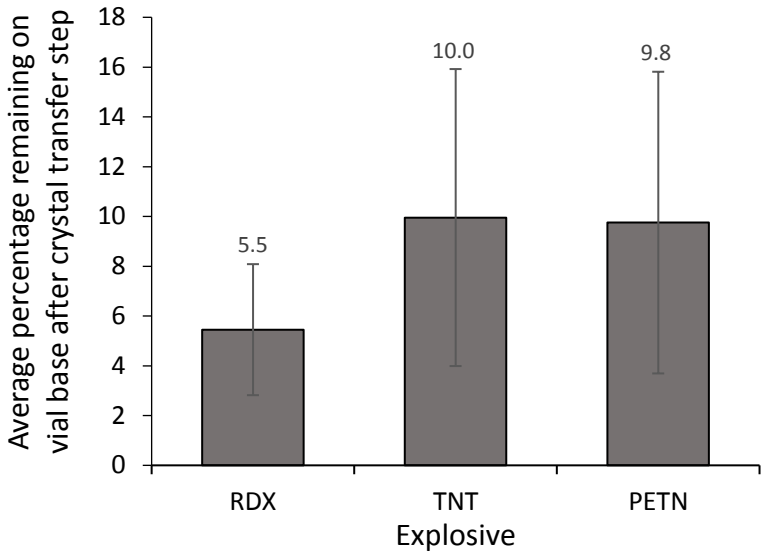

Figure 3.7: Average percentage recoveries of TNT, PETN and RDX that remained on vial bases following crystal transfer step. Error bars show standard deviations between 54 measurements

From Figure 3.7 it can be seen that for all of the ten fabrics analysed, 100 % crystal transfer efficiency was not achieved. RDX on average transferred with the highest efficiency onto the different fabrics, whereas TNT and PETN displayed similar, lower, transfer efficiencies onto each of the fabrics. As alluded to earlier, it is likely that this sub-100 % transfer efficiency phenomenon occurred in Tabet's work [69], and this may therefore account for the fact that the authors ostensibly recovered higher levels of RDX from their solution-spiked fabrics than their crystal-spiked fabrics – the authors may not have deposited 100 % of their crystalline RDX onto the surfaces. The mesh size and mass per square metre of each fabric were evaluated, with Figure 3.8 containing textures and mesh structures of the respective fabrics, and Table 3.11 containing numerical information regarding the mesh sizes and masses of the fabrics used throughout this work.

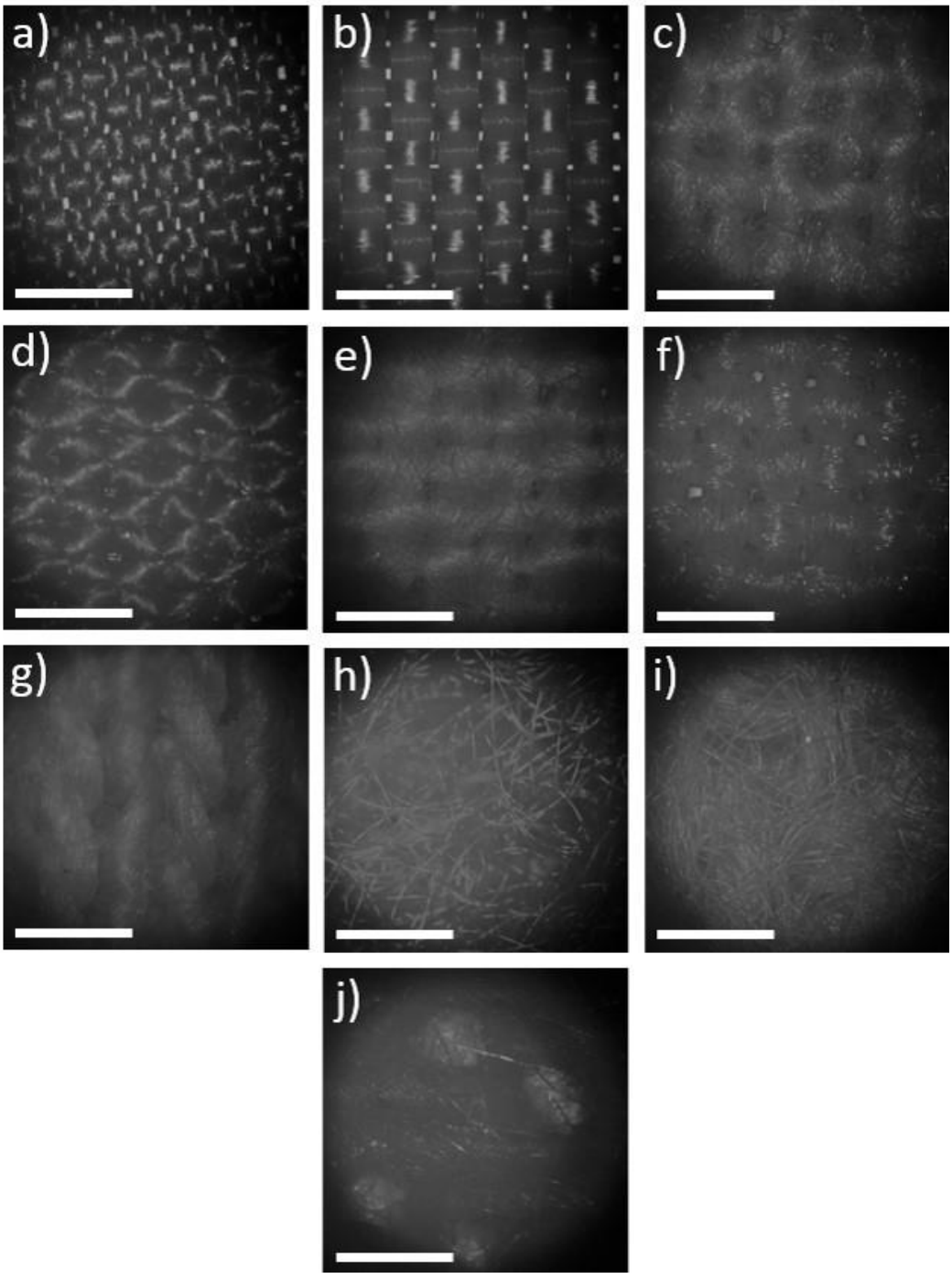

Figure 3.8: Photographs of the different fabrics analysed: a) silk, b) acetate, c) calico natural cotton, d) rayon, e) mercerised cotton, f) 100 % polyester, g) cotton jersey, h) polyester fleece, i) wool and j) denim. Scale bar on each photograph represents 1 mm

Table 3.11: Masses of fabrics used during this work

Fabric	Mass (g/m^2)	Approx. mesh size (mm)
Silk	45.0	0.25
Acetate	64.0	0.35
Calico natural cotton	139.2	0.42
Rayon	149.3	0.42
Mercerised cotton	153.6	0.65
100 % polyester	172.3	0.54
Cotton jersey	175.8	0.54
Polyester fleece	178.6	N/A
Wool	262.3	1
Denim	265.1	1.46

Plotting the percentage of non-transferred TNT, PETN and RDX for a given fabric, against a fabric's mesh size, gave the results in Figure 3.9.

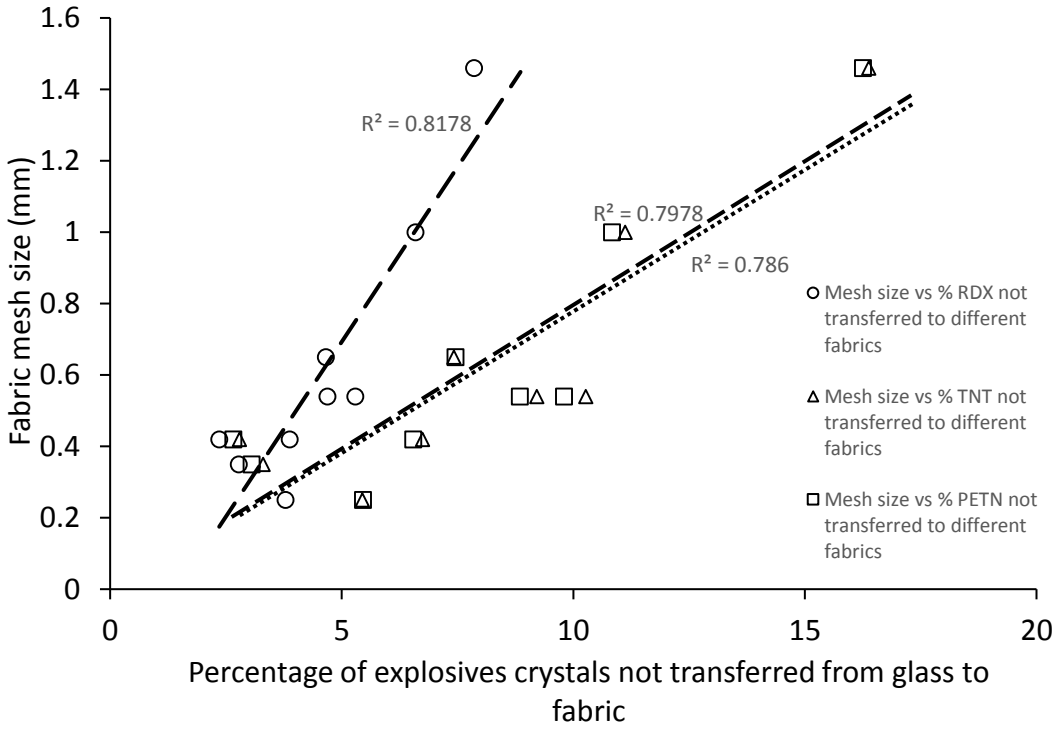

Figure 3.9: Comparing a fabric's mesh size against crystal transfer efficiency of TNT, PETN and RDX

From Figure 3.9 it is interesting to note that a strong correlation exists between the mesh size of a fabric and the degree of explosive crystal transfer from glass to the fabrics, with correlation coefficients of approximately 0.8. This suggests that a smaller mesh size results in a greater percentage of explosive crystal transfer (and thus a lower recovery from the glass vial during

the subsequent washing step), and, conversely, a larger fabric mesh size results in a lower explosive transfer efficiency.

While this work has mainly focused on assessing the utility of the contact heater with regards to the recovery of explosives spiked onto different fabrics, the data from Figure 3.9 suggests that it would be worthwhile prioritising fabrics with a finer mesh size to increase the likelihood of explosive residue recovery, as it appears that fabrics of a finer mesh size may be better recipients for explosive crystals. It is also encouraging to note that all of the ten fabrics were able to 'accept' explosive crystals from glass, despite the fact that, as seen from the AFM results in Chapter 2, all of the 3 explosives display a higher adhesion to glass than to any of the fabrics examined in this work.

3.3.6.2 Contact heater platen temperature

A platen temperature of 120 °C (the maximum operating temperature of the contact heater) was used during sampling. This temperature was used as the vapour pressure of the three explosives used is relatively low, as seen in Table 3.12.

Table 3.12: Approximate vapour pressures (Torr) of TNT, PETN and RDX at 25 °C and 120 °C. Values were obtained from Oestmark [160] by interpolating or extrapolating from the Clausius-Clapeyron fit lines contained within Oestmark's work

	25 °C	120 °C
TNT	4×10^{-6}	1.5×10^{-1}
PETN	1×10^{-8}	2×10^{-2}
RDX	1×10^{-8}	8.5×10^{-4}

Given the low vapour pressure of these explosives, the highest sampling temperature possible would result in maximum volatilisation of the explosives. It should be noted that even when contact heater sampling at this temperature, no additional peaks were observed in the HPLC chromatograms compared to the corresponding negative controls, with the exception of the peaks corresponding to TNT, PETN and RDX. This suggests that no thermal decomposition of the explosives occurred when sampling at 120 °C.

3.3.7 Contact heater recoveries

3.3.7.1 Solution-spiking: Immediate sampling

Figure 3.10 shows the recoveries of RDX, TNT and PETN from solution-spiked surfaces subjected to immediate contact heater sampling. The error bars indicate the relative standard deviations within the three replicate samples performed for each surface. From left to right,

the surfaces are displayed in increasing order of roughness, based on the surface roughness measurements from Chapter 2.

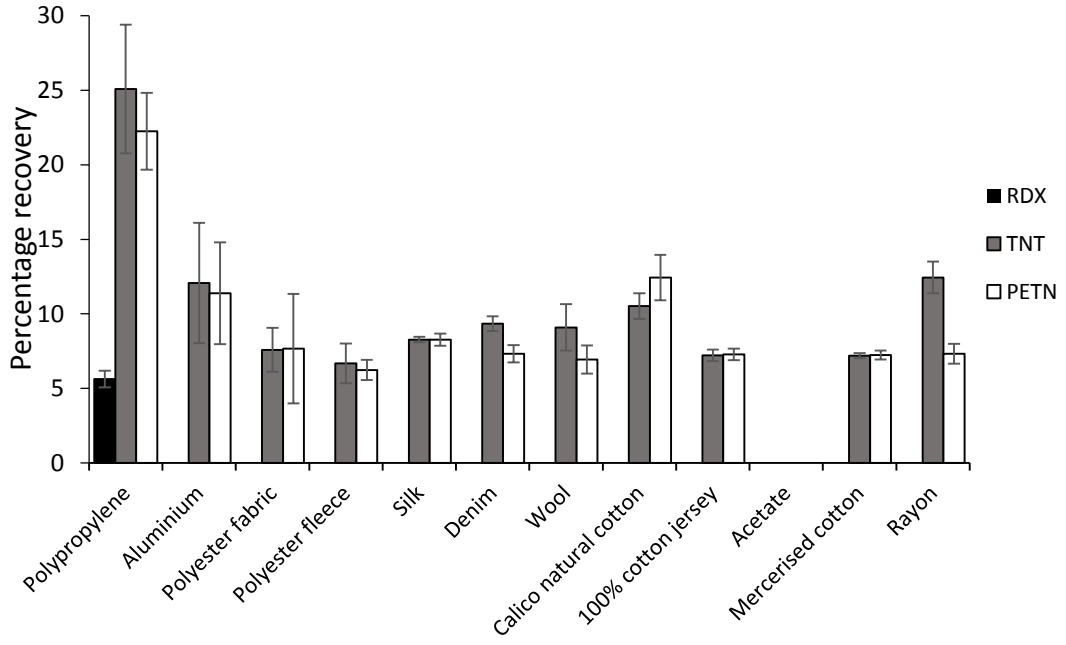

Figure 3.10: TNT, PETN and RDX recoveries from solution-spiked surfaces following immediate sampling, obtained using the contact heater. Error bars show standard deviations of 3 replicates for a given surface

The results displayed in Figure 3.10 indicate that the highest recoveries of the solution-spiked explosives were obtained from polypropylene, the smoothest surface investigated. The second highest average recoveries were obtained from aluminium, the second smoothest surface. It is interesting to note that, in addition to being the two smoothest surfaces, the polypropylene and aluminium are also non-porous surfaces, whereas the remaining ten surfaces are all porous fabrics. This suggests that the porosity of a surface plays an important role in the recovery of explosives using the contact heater, with higher recoveries from non-porous surfaces. This is in agreement with the findings of Talaty *et al.* [64], described earlier.

Figure 3.10 also shows that RDX was only recovered from one of the twelve surfaces (polypropylene), whereas TNT and PETN were recovered from all surfaces, excepting acetate. It is likely that the low RDX recoveries may be attributed to RDX's vapour pressure being much lower than that of TNT and PETN (see Table 3.12). Figure 3.10 also shows that no explosives were recovered from the acetate fabric. This is likely due to the reasons outlined earlier - the spiking solution dissolved the acetate, and upon evaporation of the residual spiking solvent it is likely that the explosives became 'fixed' within the acetate's structure.

Similar recoveries of TNT and PETN were obtained from the majority of surfaces. This is

interesting, because at the contact heater sampling temperature of 120 °C, their vapour pressures differ by almost one order of magnitude, with TNT's vapour pressure approximately 7.5 times higher than PETN's (see Table 3.12). This means that it may not purely be an explosive's vapour pressure which is contributing towards its rate of volatilisation and recovery. Instead, this suggests that the TNT is undergoing additional chemical interactions with the surfaces causing a reduced recovery. This phenomenon could be further explored by performing some thermal desorption experiments over different periods of time.

With reference to the three explosives' adhesion to different surfaces (Chapter 2), RDX had a much higher adhesion to all of the non-textile, non-porous materials than either TNT or PETN. This suggests that a combination of low vapour pressure and strong surface-level chemical interactions have contributed to the low recoveries of RDX from the different surfaces. It is possible that this is due to the nitramine moiety present in RDX, as this is not present in either TNT or PETN.

The solution spiking technique is representative of an individual spilling a solution containing explosives onto a surface. With the porous, textile surfaces used, it is likely that the explosives molecules will have been drawn down and held within the mesh of the fabric, whereas for the non-porous surfaces, the explosives will have remained on the surface of the spiked surface. This depth difference is likely to have had an effect on the observed recoveries, which may explain why higher recoveries were observed from the two non-porous surfaces (polypropylene and aluminium).

3.3.7.2 Crystal-spiking: Immediate sampling

Figure 3.11 shows the recoveries of explosives from ten different fabrics, each spiked with explosive crystals followed by immediate sampling.

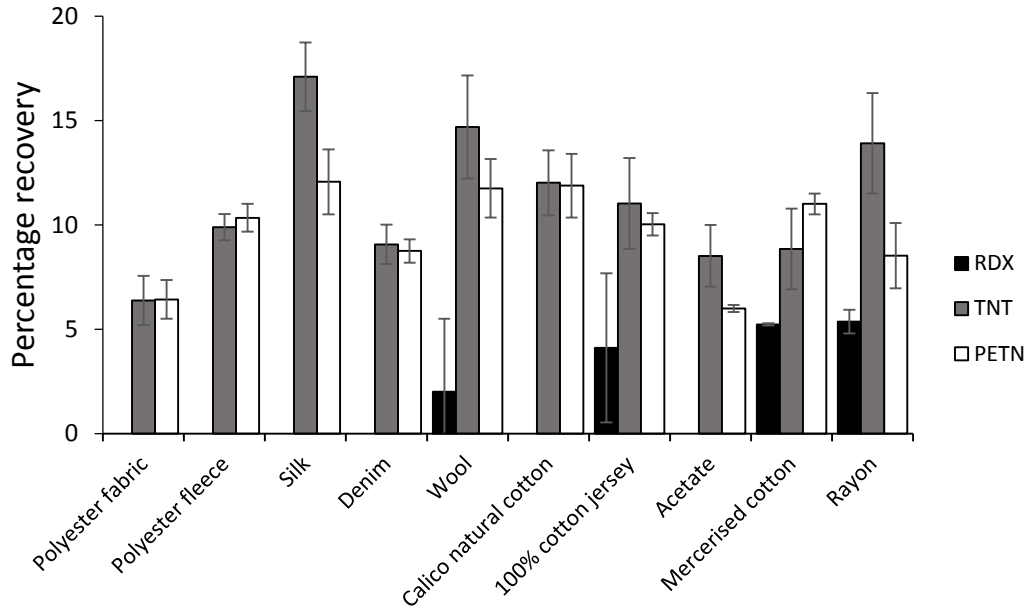

Figure 3.11: RDX, TNT and PETN recoveries from crystal-spiked surfaces, with immediate sampling, obtained using the contact heater. Error bars show standard deviations of 3 replicates for a given surface

It should be noted that 'percentage recovery' of the explosives in Figure 3.11 refers to the percentage recovery relative to the exact mass of each explosive transferred onto each sampling surface (determined using the technique specified earlier – Crystal spiking efficiency considerations and validation, Section 3.3.4.2). As for the solution-spiked surfaces (Figure 3.10), similar recoveries of TNT and PETN were recovered from all of the surfaces, with slightly higher recoveries of TNT than PETN in the majority of cases (mirroring their vapour pressures).

RDX was recovered from four of the 10 surfaces; an improvement on its recoveries from the solution-spiked surfaces displayed in Figure 3.10. This suggests that it is easier to recover crystalline RDX from surfaces than RDX deposited as a solution. Similarly, the magnitude of TNT and PETN recovery from the crystal-spiked surfaces is, on average, noticeably higher than that from the solution-spiked samples, again suggesting that it is easier to recover these explosives in their crystalline forms rather than if they are dispersed from a solution. For the crystal-spiked fabrics, the crystals will give rise to a smaller explosives:surface area ratio than with the solution-spiked fabrics. This will mean a smaller number of possible interactions between the crystal and a surface, relative to individual molecules dispersed about a surface from a solution spike. It therefore seems logical that higher recoveries will be observed from a crystal-spiked surface than a solution-spiked surface. This is also in agreement with the findings of Fletcher *et al.* [68], detailed earlier.

It is of interest to note that the error bars present on this graph (with an average range of 1.29 %), representing the standard deviation amongst the three repeat measurements, are higher than those in Figure 3.10 from the solution-spiked surfaces (with an average range of 0.93 %). This suggests that there is more variability when recovering explosive crystals from a surface than when recovering explosives deposited from a solution.

The fabrics displayed in Figure 3.10 and Figure 3.11 are displayed in increasing order of roughness, moving from left to right (based on the surface roughness measurements detailed in Chapter 2). For the recovery of RDX crystals from the different fabrics in Figure 3.11, it can be seen that the recoveries tend to be from the rougher surfaces on the graph, towards the right-hand side of the graph. AFM work detailed in Chapter 2 found a higher adhesion of RDX to smoother surfaces, so this recovery result is in agreement with the AFM results, suggesting that the low recoveries from the smoother surfaces may be affected by the high adhesion of RDX to the smoother surfaces.

One major point of note is that, in the present work, 70 µL of a mixed solution of 0.33 mg/mL each TNT, RDX and PETN was used to spike the respective surfaces, meaning 23.3 µg of each explosive was deposited onto each solution-spiked surface (with slightly less deposited onto each crystal-spiked surface, taking into account sub-100 % crystal transfer). The surfaces used for analysis in this work measured approximately 10 × 15 cm, with the explosives spiked into the centre of the surfaces to cover an area of approximately 2 × 2 cm, i.e. an area of 4 cm^2. This equates to an approximate density of each explosive of around 6 $\mu g/cm^2$. This value is much lower than that cited by Almaviva *et al.* as being representative of an explosive-contaminated fingerprint in contact with fabric (100-400 $\mu g/cm^2$ [47]). It is very encouraging that in the present work, traces of explosives at much lower levels than this could successfully be recovered using the contact heater. This reinforces the notion that the contact heater is a useful tool for the examination of clothing and other textiles suspected of bearing explosives traces.

3.3.8 A comparison between explosives adhesion and recovery

The work presented in Chapter 2 investigated the adhesion of explosives to a variety of surfaces, and the work presented in the current chapter has assessed the recovery of the same explosives from these surfaces. If the observations from both studies are then combined, an assessment of the relationship between an explosive's adhesion to a surface and its recovery from the same surface can be determined. If an explosive displays a high adhesion to a surface,

it may be more difficult to break these adhesive forces to enable recovery, and conversely, if an explosive displays low adhesion to a surface, higher recoveries may be obtained due to the weaker adhesive forces.

This is reflected in Figure 3.12, which shows the recoveries of TNT from immediately-sampled crystal-spiked surfaces against the adhesion of TNT crystals to these surfaces, as outlined in Chapter 2.

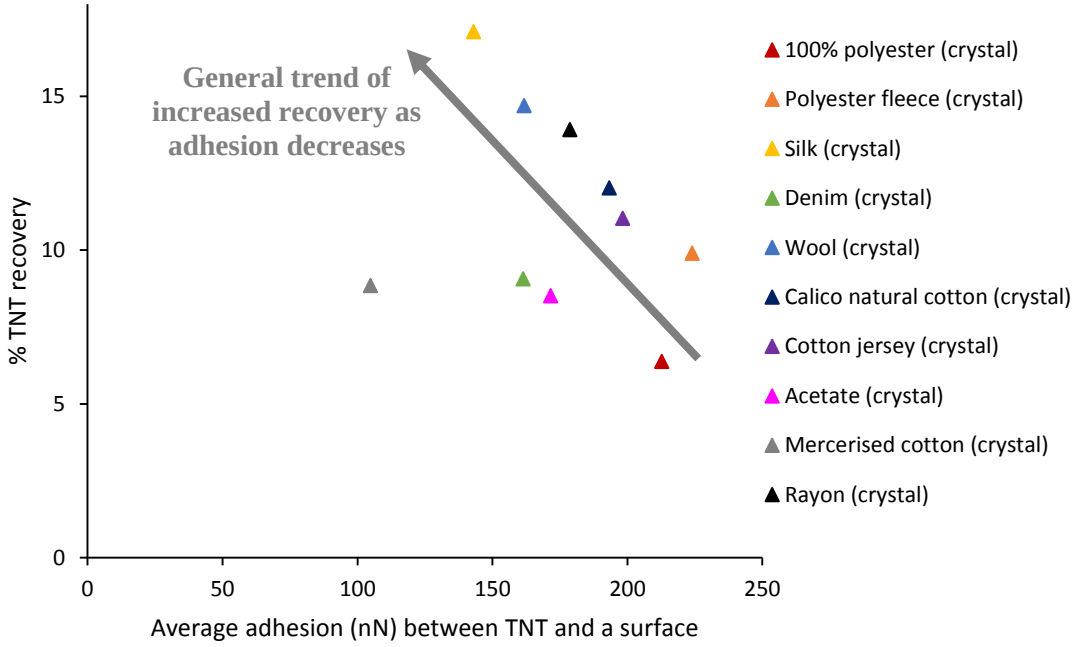

Figure 3.12: Graph showing TNT adhesion to 10 textile surfaces against their immediate-sampling recoveries using the contact heater, following crystal-spiking

From Figure 3.12 it can clearly be seen that there is a general trend of increased TNT crystal recovery as the adhesion to a surface decreases. This suggests that the AFM work presented in Chapter 2 is a useful method for assessing likely TNT crystal recoveries from different surfaces, with a higher recovery likely from those surfaces to which TNT crystals display the lowest adhesion.

Figure 3.13 displays the TNT recoveries from immediately-sampled solution-spiked surfaces against the adhesion of TNT to these surfaces.

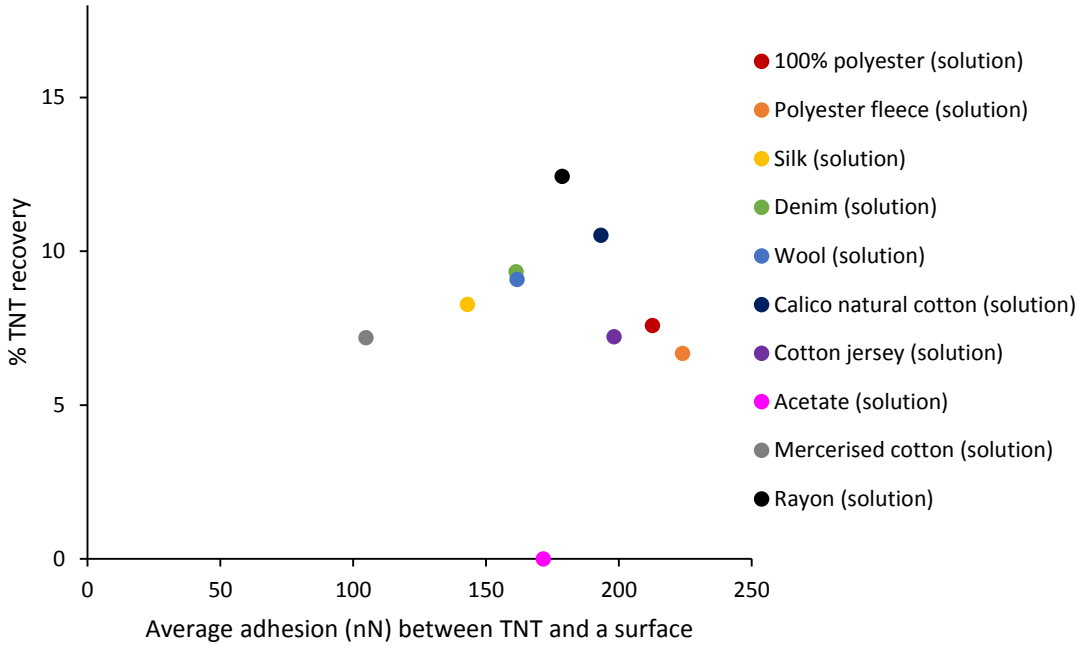

Figure 3.13: Graph showing TNT adhesion to 10 textile surfaces against their immediate-sampling recoveries using the contact heater, following solution-spiking

Unlike for the TNT crystal-spiked surfaces, there appears to be no clear trend in Figure 3.13 between the adhesion of TNT to a surface and its recovery following solution-spiking of the surfaces. Similar TNT recoveries were obtained from all surfaces solution-spiked with TNT. As mentioned, the spiking solution dissolved the acetate, which is the likely explanation for the 0 % recoveries obtained from this solution-spiked surface. A higher TNT recovery was obtained from eight out of the 10 crystal-spiked surfaces, compared to the solution-spiked surfaces. This is in agreement with the findings of Gillen [68], discussed earlier, who found larger particles were more easily dislodged from a surface.

Figure 3.14 shows the recoveries of PETN from immediately-sampled crystal-spiked surfaces against the adhesion of PETN crystals to these surfaces, as outlined in Chapter 2, with Figure 3.15 showing the recoveries of PETN from immediately-sampled solution-spiked surfaces against the adhesion of PETN crystals to these surfaces.

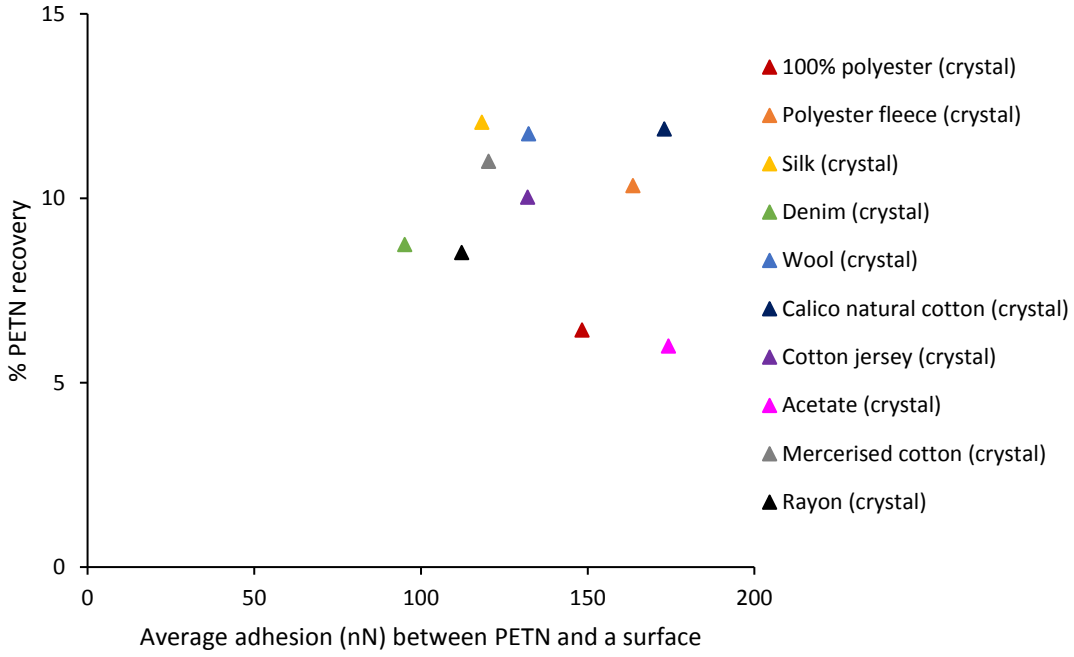

Figure 3.14: Graph showing PETN adhesion to 10 textile surfaces against their immediate-sampling recoveries using the contact heater, following crystal-spiking

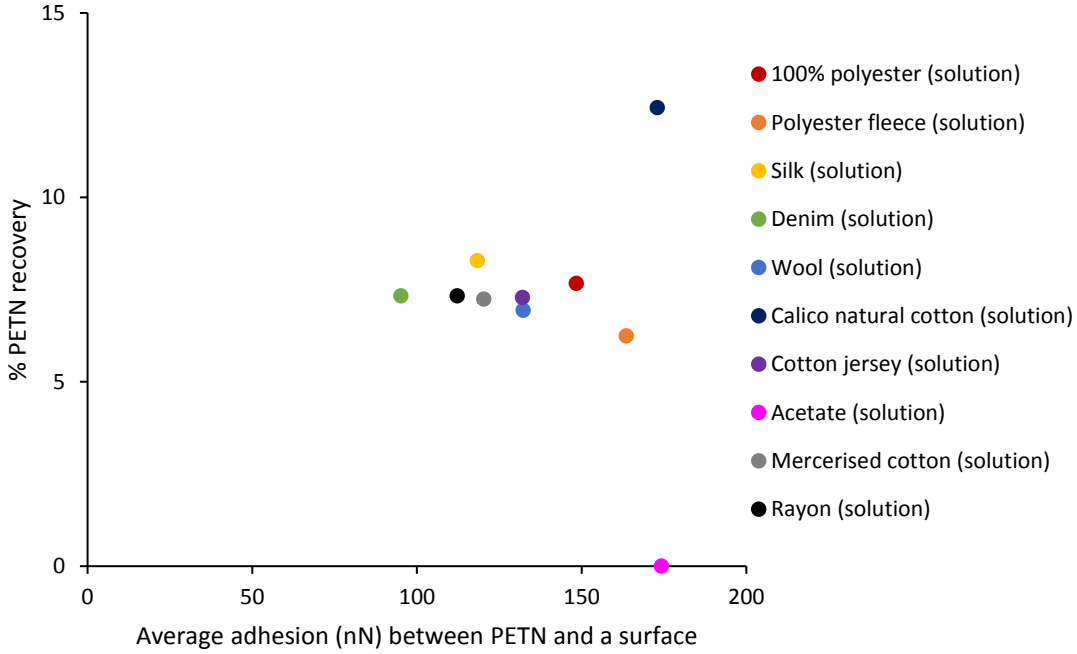

Figure 3.15: Graph showing PETN adhesion to 10 textile surfaces against their immediate-sampling recoveries using the contact heater, following solution-spiking

With these PETN recoveries, there is no clear relationship between PETN adhesion and recovery from a surface, from either the solution-spiked or crystal-spiked samples. Although the majority of the textiles gave higher PETN recoveries following crystal-spiking, 100 %

polyester and calico natural cotton gave higher PETN recoveries from the solution-spiked surfaces. A similar graph was not created to display RDX recoveries against adhesion due to the low, often non-recoveries obtained for RDX.

3.3.8.1 TNT recoveries from aged solution- and crystal-spiked surfaces

Figure 3.16 displays the TNT recoveries from five surfaces, each solution spiked and aged under various conditions. It can be noted that in each case (with the exception of aluminium), the highest recoveries were obtained from the 'immediate sampling' condition. This is to be expected, as the TNT will have had the least time to undergo volatilisation or degradation.

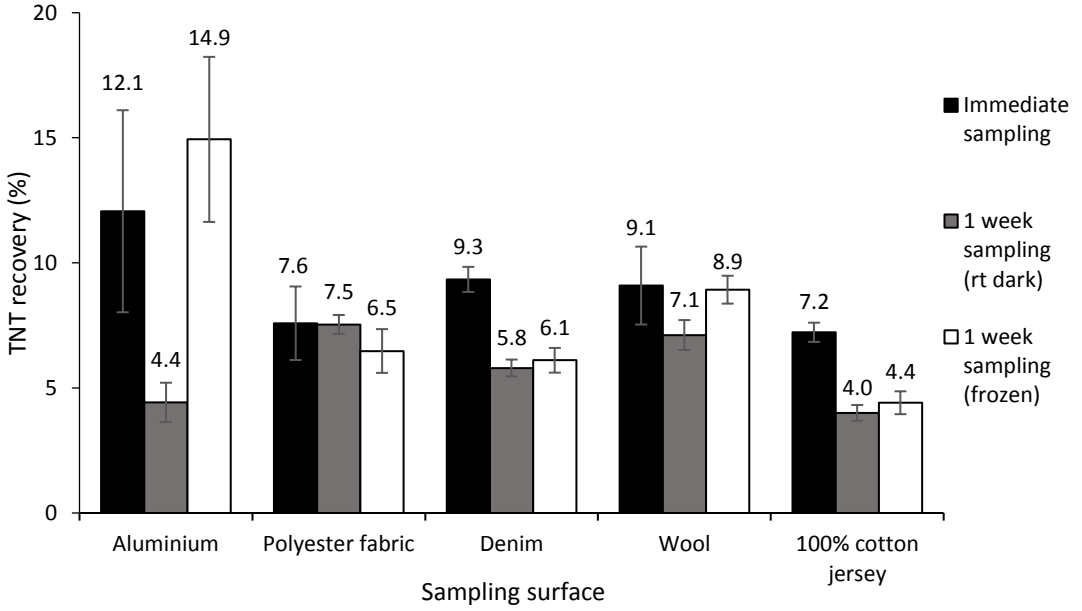

Figure 3.16: TNT recoveries from aged solution-spiked samples obtained using the contact heater. Error bars show standard deviations of 3 replicates for a given surface

The TNT recoveries from the samples stored in the dark at room temperature all show a decrease in TNT recovery, relative to the day 0, 'immediate sampling' recoveries. This decrease was very slight for polyester, whereas the decrease was much higher for the other surfaces. For the cotton-based surfaces (denim and cotton jersey), the percentage decreases relative to recoveries following immediate sampling were similar by around 38 % and 44 %, respectively.

Figure 3.16 also shows that, from the one week aged samples stored in the dark at room temperature, wool showed a decrease of approximately 22 % compared to its immediate sampling recoveries. This percentage decrease in TNT recoveries is approximately half that of

the cotton-based denim and cotton jersey surfaces. This may have several explanations - the TNT may have showed a higher stability on the wool, relative to the cotton-based surfaces, meaning it did not undergo as much degradation on the wool. Alternatively, the TNT may have developed a higher adhesion to the cotton-based surfaces over time, relative to the wool, resulting in lower TNT recoveries over time from the cotton surfaces than the wool. A third, contrasting hypothesis is that the TNT may have shown a lower adhesion to the cotton-based surfaces over time, meaning a greater proportion of the TNT volatilised away from the cotton-based surfaces over time.

Comparing the recoveries from aluminium with immediate sampling vs. sampling after storage for one week in the dark at room temperature, a significant decrease (approximately 64 %) in the recovered levels of TNT can be observed. It is postulated that this is due to the TNT's volatilisation over time. No additional peaks were observed to indicate degradation had occurred.

From the spiked, frozen samples, in four out of five cases, a higher recovered level of TNT was seen relative to the samples aged for one week at room temperature. This finding suggests that the lower storage temperatures resulted in a lower degree of TNT volatilisation. However, Figure 3.16 also demonstrates that immediate sampling of a fabric exhibit upon receipt into a forensic laboratory is likely to be the best method to ensure maximum recoveries of explosive residues.

Figure 3.17 displays the TNT recoveries from four crystal spiked textile surfaces under a range of storage conditions. For the denim, wool and cotton jersey surfaces, much higher recoveries of TNT were obtained from the surfaces sampled immediately after spiking, compared to those sampled after storage for one week at room temperature. This is in agreement with the results from Figure 3.16.

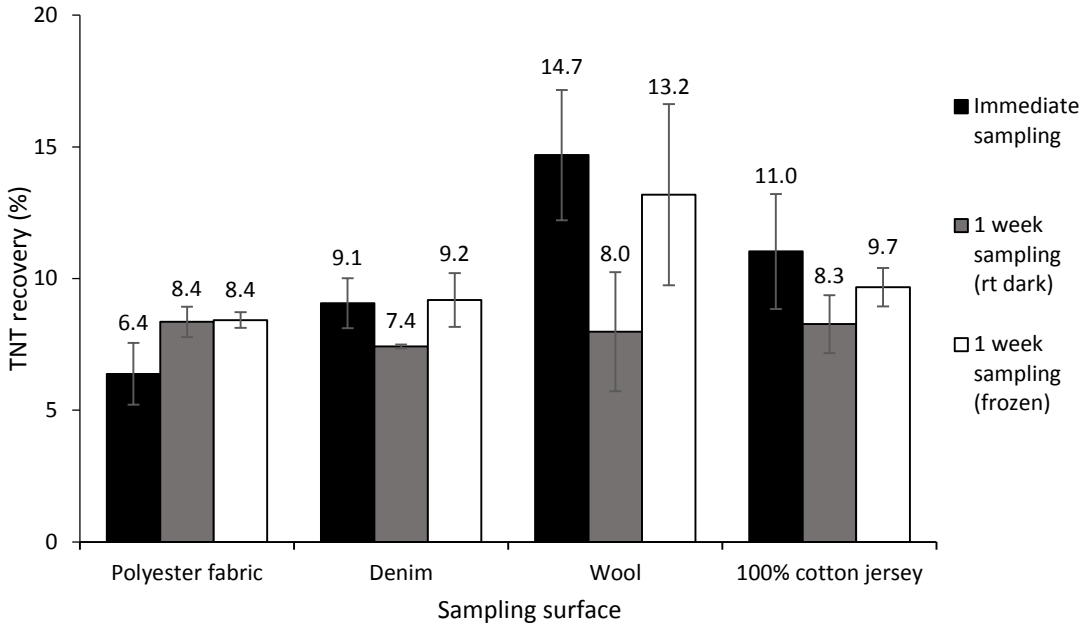

Figure 3.17: TNT recoveries from aged crystal-spiked samples obtained using the contact heater. Error bars show standard deviations of 3 replicates for a given surface

For each textile surface, the samples stored in the freezer gave TNT recoveries which were either equal to, or higher than, the recoveries from the samples stored at room temperature. This result is confirms that the storage of samples in a freezer prior to analysis, rather than at room temperature, is of great benefit in conserving any explosive residues present on a surface.

It can be seen from Figure 3.17 that for wool-based samples, TNT recoveries after storage in the freezer for one week were only approximately 10 % lower than the recoveries from wool-based samples sampled immediately following spiking. Cotton jersey showed a similar decrease of approximately 12 % after storage in the freezer for one week, whereas the decrease relative to the immediate sampling recoveries was approximately 25 % from the samples stored at room temperature. Denim showed an almost identical recovery of TNT from those samples sampled immediately after spiking and those sampled following one week's storage in the freezer.

The aged crystal-spiked samples seem to exhibit greater recovery levels over time relative to the solution-spiked samples. This may be due to the crystals having a smaller surface area:volume ratio compared to the individual molecules resulting from the solution spikes, so fewer explosive molecules are physically available to undergo volatilisation from a spiked sample. Alternatively, if the decrease over time were due to degradation, rather than volatilisation, then again the explosives resulting from the solution-spiked sample would be exposed to a larger surface area of the spiked surface, meaning a greater possible exposed area from which to undergo degradation. However, no extra peaks were observed in the

corresponding chromatograms, suggesting a significant degradation phenomenon was not responsible for the observed decreases in recovery.

3.3.8.2 PETN recoveries from aged solution- and crystal-spiked surfaces

Figure 3.18 displays PETN recoveries from five solution-spiked aged surfaces stored under various conditions.

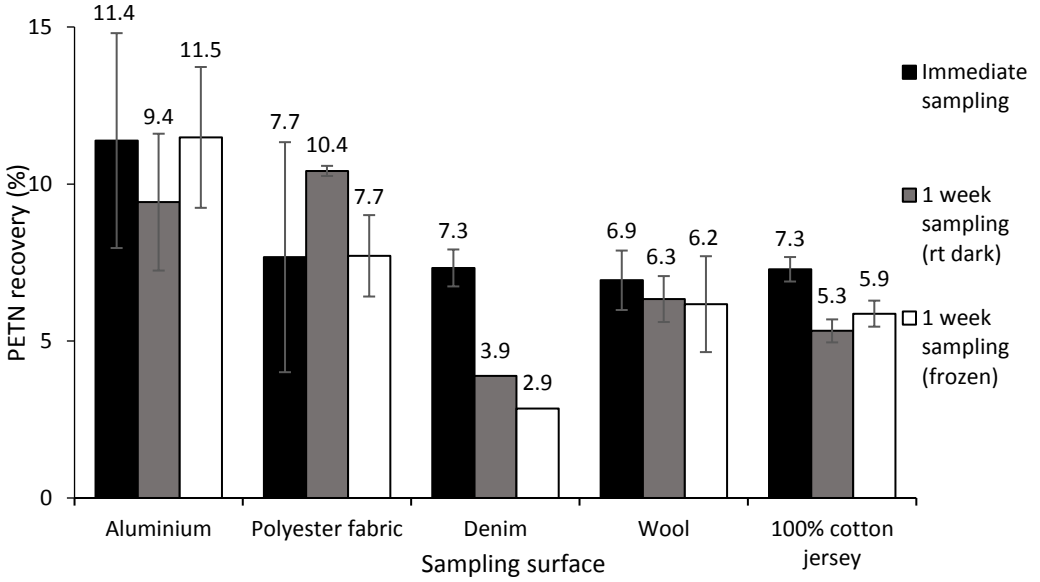

Figure 3.18: PETN recoveries from aged solution-spiked samples obtained using the contact heater. Error bars show standard deviations of 3 replicates for a given surface

Very similar recoveries of PETN were obtained from the four fabrics following the immediate sampling from the surfaces, whereas higher recoveries of PETN were obtained from the aluminium samples. This therefore shows similarities to the TNT recoveries from these five solution-spiked surfaces. Another point to note about aluminium is that it is a much better conductor of heat compared to the fabrics investigated. When the sampling head was applied to the fabrics, they tended not to heat significantly, whereas when the 120 °C sampling head was applied to the aluminium foil, the foil began to heat up, which will assist in the volatilisation of the PETN from the aluminium's surface.

After storage for one week in the dark at room temperature, a general decrease in PETN recoveries was observed, relative to the immediate sampling recoveries. These decreases were approximately 18 % for aluminium, 47 % for denim, 9 % for wool and 27 % for cotton jersey, relative to their immediate sampling recoveries. The recovery patterns for PETN in Figure

3.18 therefore show similarities with the recoveries of TNT displayed in Figure 3.16, with the explosives appearing to be stable on wool, whereas on cotton-based fabrics such as cotton jersey and denim, much greater decreases in recovery were observed over time. It should be noted that the recovery results for denim after ageing for one week at room temperature do not have error bars of relative standard deviation as no recovery was obtained from denim for some of the replicate samples.

By comparing the PETN recovery results (Figure 3.18) to the TNT recovery results (Figure 3.16) after one week storage at room temperature, it can be seen that the decrease in PETN recoveries are lower than the decrease in TNT recoveries. This is in agreement with the explosives' vapour pressure, with TNT having a higher vapour pressure than PETN and thus being more likely than PETN to lose mass over time when stored at room temperature. The results from the PETN experiments after storage in the freezer for one week indicate almost identical PETN recoveries were obtained from aluminium following either immediate sampling, or sampling after storage for one week in the freezer. This suggests that storage of aluminium-based samples in a freezer mitigates PETN loss or degradation, compared to storage of such samples at room temperature, which showed lower recovery levels.

Like aluminium, polyester also shows a similar trend and almost identical PETN recoveries were observed from polyester after either immediate sampling, or after storage in the freezer for one week. This result suggests that storage of polyester samples in a freezer will assist in mitigating any potential loss or degradation of PETN. As was the case with TNT, wool continues to appear to be a surface from which explosives loss or degradation is minimal. A minimal reduction in PETN recoveries from wool was observed for the one week aged samples at either storage temperature. This observation is in agreement with previous literature suggesting that wool is a good surface for capturing and retaining traces of nitrate esters such as PETN [145].

For cotton jersey, it can be seen that a decrease in recoveries was observed for both sets of aged spiked samples relative to the recoveries when sampling immediately after spiking, though higher recoveries were observed from the samples stored in the freezer, rather than at room temperature. This result is in agreement with the general results seen so far.

Figure 3.19 displays the recoveries of PETN obtained from four types of crystal-spiked surfaces. For the immediate sampling recoveries, the same order of recovery is observed as for the TNT crystals shown in Figure 3.17 with the highest recovery from wool, followed by the cotton jersey, then from denim and the lowest recovery from polyester fabric.

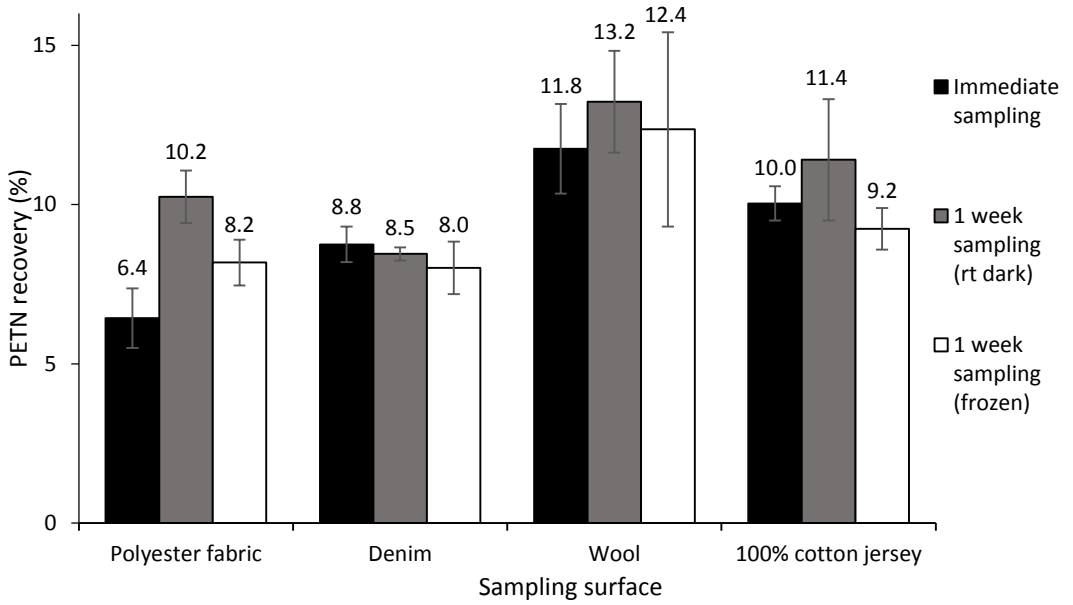

Figure 3.19: PETN recoveries from aged crystal-spiked samples obtained using the contact heater. Error bars show standard deviations of 3 replicates for a given surface

For the one week room temperature dark samples, an increase in PETN recovery was seen compared to the levels of PETN recovery from those samples sampled immediately after spiking. On average, a decrease was seen in the recoveries of PETN from each of the samples stored in a freezer for one week, compared to those stored at room temperature for one week. This result is unusual and an obvious explanation is not apparent. In general, as indicated in Figure 3.19, recovered PETN levels from the different surfaces and storage conditions have remained quite stable across all of the conditions investigated. This perhaps suggests that PETN is more stable under a variety of conditions than TNT, as in some cases large decreases in TNT recoveries were observed following storage and ageing.

3.3.8.3 RDX recoveries from aged solution- and crystal-spiked surfaces

RDX was only recovered from one solution-spiked sample, indicating that it is difficult to recover solution-spiked RDX from the surfaces examined in this work. Figure 3.20 displays the RDX recoveries from four crystal-spiked surfaces, under a range of storage conditions. In general low RDX recoveries were recorded, though these crystal-spiked recoveries were higher than the analogous solution-spiked RDX recoveries.

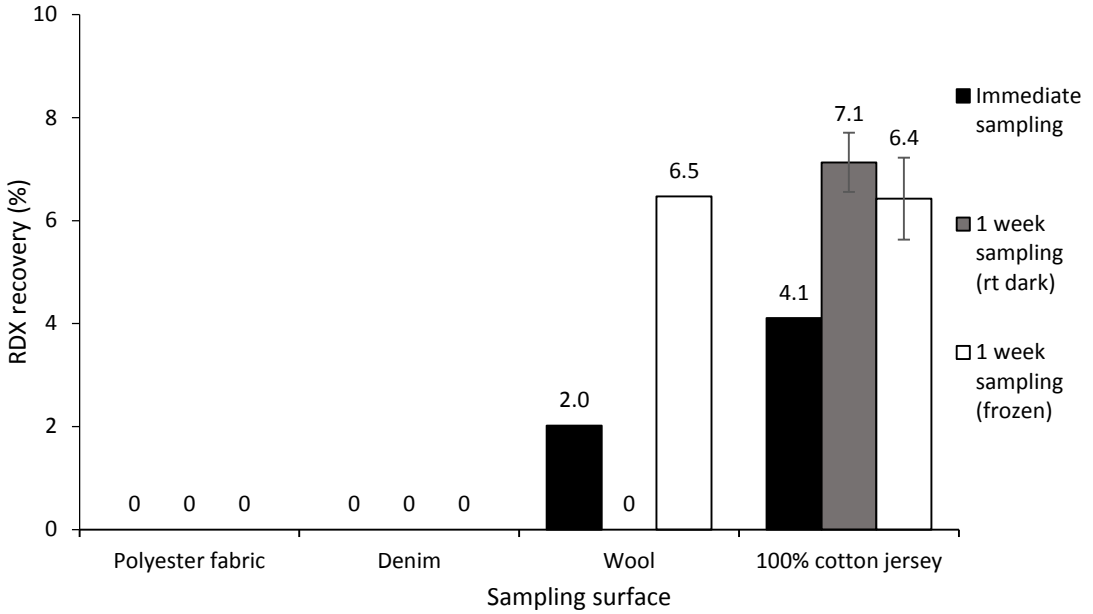

Figure 3.20: RDX recoveries from aged crystal-spiked samples obtained using the contact heater. Error bars show standard deviations of 3 replicates for a given surface

3.3.9 Comparison with vacuum sampling

The main difference between contact heater sampling and vacuum sampling is the use of a heated interface during contact heater sampling, which is used to volatilise any explosives present prior to recovery. In vacuum sampling, which is performed at room temperature, the surface is agitated continually using the end of a glass sampling tube, in an attempt to physically, rather than thermally, dislodge any explosives present on a surface. In the current work, the contact heater's vacuum pump was used for all vacuum samples, to enable a direct comparison between contact heater recoveries and vacuum sampling recoveries when using a vacuum pump of equal strength. In this vacuum sampling work, three fabric surfaces were chosen to be analysed: polyester, cotton jersey and wool. These were chosen as a representative subset of the ten fabrics sampled using the contact heater, as they had given rise to 'low', 'medium' and 'high' explosives recoveries, respectively, during contact heater sampling.

Figure 3.21 shows a comparison between TNT recoveries from crystal-spiked, immediately sampled cotton jersey, wool and polyester samples obtained using the contact heater and vacuum sampling.

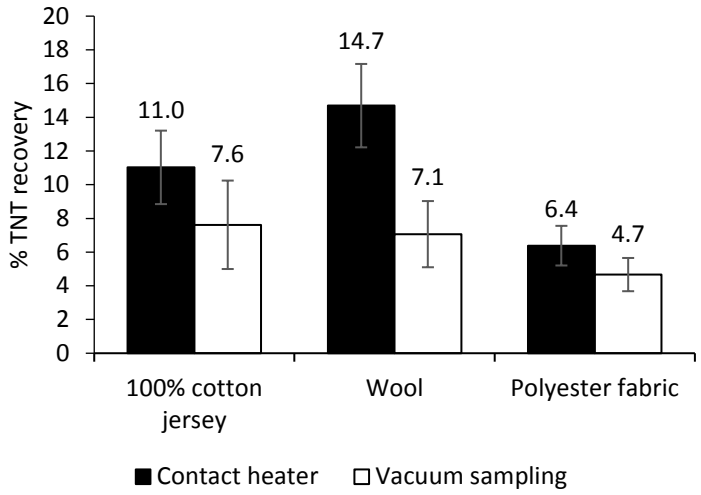

Figure 3.21: A comparison of crystal-spiked TNT recoveries obtained using the contact heater and vacuum sampling, sampling immediately after spiking. Error bars show standard deviations of three replicates

From Figure 3.21 it can clearly be seen that significantly lower TNT recoveries were obtained when vacuum sampling the three surfaces, compared to contact heater sampling the three surfaces. For example, the average TNT recovery from wool using the vacuum sampling technique was less than half that obtained from wool using the contact heater (7.1 % vs. 14.7 %). As mentioned earlier (Table 3.12), TNT has the highest vapour pressure at the contact heater sampling temperature of 120 °C out of the three explosives used in this work, so it is likely that this high vapour pressure has contributed to its volatilisation and thus higher recoveries than from the vacuum samples. The results in Figure 3.21 suggest that heating and contact heater sampling a TNT-contaminated fabric is likely to give higher recoveries than vacuum sampling a fabric at room temperature.

Figure 3.22 compares PETN recoveries from contact heater and vacuum sampled surfaces.

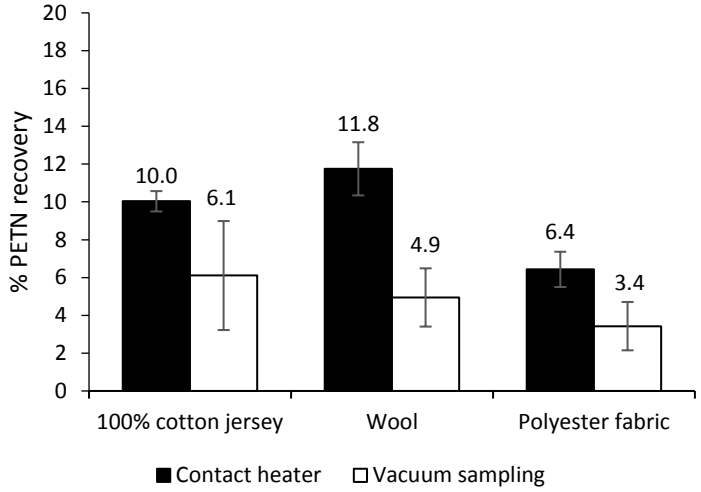

Figure 3.22: A comparison of crystal-spiked PETN recoveries obtained using the contact heater and vacuum sampling, sampling immediately after spiking. Error bars show standard deviations of three replicates

As was the case with the TNT recoveries (Figure 3.21), significantly higher PETN recoveries were obtained when contact heater sampling than when vacuum sampling. This is also likely to be due to PETN's relatively high vapour pressure. As with TNT, Figure 3.22 suggests that contact heater sampling fabrics suspected of bearing traces of PETN is likely to give rise to higher recoveries than vacuum sampling such fabrics.

Finally, Figure 3.23 compares RDX recoveries from contact heater and vacuum sampled surfaces.

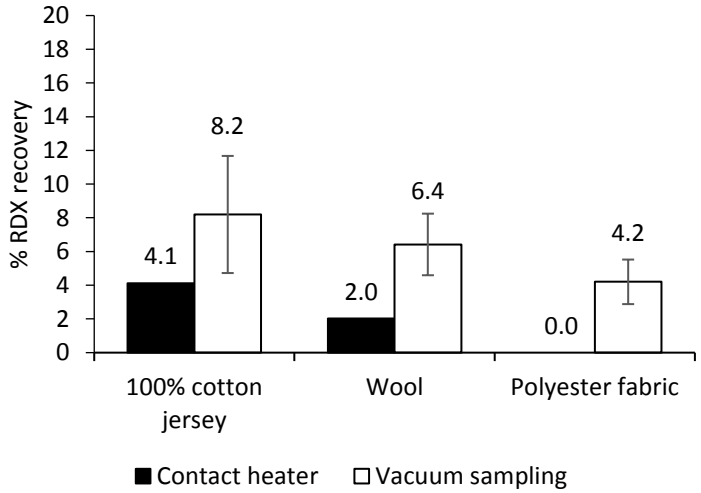

Figure 3.23: A comparison of crystal-spiked RDX recoveries obtained using the contact heater and vacuum sampling, sampling immediately after spiking. Error bars show standard deviations of three replicates

Unlike with the TNT and PETN recoveries vacuum sampling gave significantly higher recoveries of RDX, compared to the recoveries obtained when contact heater sampling. This is likely due to RDX's low vapour pressure which meant that the RDX may not undergo significant levels of volatilisation prior to recovery. As satisfactory RDX recoveries were obtained from the vacuum sampling experiments, but much lower/zero RDX recoveries were obtained from the contact heater experiments, this suggests that physical abrasion of a surface is beneficial for recovering RDX from textiles, compared to the application of thermal energy.

Interestingly, differences in the trend of recovery can be observed between the contact heater and vacuum sampling recoveries for the three explosives. From the contact heater samples, the highest recoveries tended to be obtained from wool, and the lowest from polyester. However, for the vacuum samples, the highest recoveries were obtained from the cotton jersey, and the lowest recoveries from the polyester. Although this work has investigated the possibility of a relationship between the adhesion of an explosive to a surface and its recovery from a surface, the differing recovery patterns obtained when contact heater or vacuum sampling suggest that other factors may also play a role in the recovery of TNT, PETN and RDX from fabrics.

For the contact heater samples it is possible that the trend in recoveries may depend on purely the adhesion of an explosive to a surface, shown in Chapter 2 to be influenced by the roughness of a surface. Wool was the roughest surface sampled and hence a low adhesion was expected, which seems to be in agreement with the high contact heater recoveries from wool. On the other hand, polyester was the smoothest of the three surfaces sampled, and a high adhesion was expected, which is in agreement with the low contact heater recoveries from polyester. Although it is therefore possible that contact heater recoveries may be affected by an explosive's adhesion to a surface/surface roughness on a micro-scale, it is proposed that the factors accounting for the trend in vacuum sampling recoveries are due to a more macro-scale factor, outlined below.

One such macro-scale factor is a fabric's mesh size. The cotton jersey and polyester used have almost identical mesh sizes, whereas wool has the highest mesh size (see Table 3.11). It may be thought that a smaller mesh size would be better able to trap explosive residues, and a larger mesh size would be more susceptible to explosive residue loss. If this were the case, the highest vacuum sampling recoveries would have been expected from wool, as it has the largest mesh size. However, for each explosive, wool gave the only second highest vacuum sampling recoveries, with the highest recoveries of each explosive obtained from the cotton jersey vacuum sampled fabrics. This therefore suggests that mesh size alone cannot be deemed

responsible for the observed trend in vacuum sampling recoveries.

Another factor to be considered alongside a fabric's mesh size is the degree of elasticity of the fabrics. The wool and polyester were both fairly rigid fabrics, without any 'give'. The cotton jersey was a ribbed material with a lot of stretch perpendicular to the ribbing which allowed for the material to 'flex'. This action may have acted to loosen any bound explosive residues and 'flick' them towards the vacuum tube. This hypothesis is supported by results from the first cotton jersey vacuum sample, whereby sampling was performed against the direction of stretch, meaning little flexing of the fabric could occur. This gave relatively low explosive residue recoveries (see Figure 3.24).

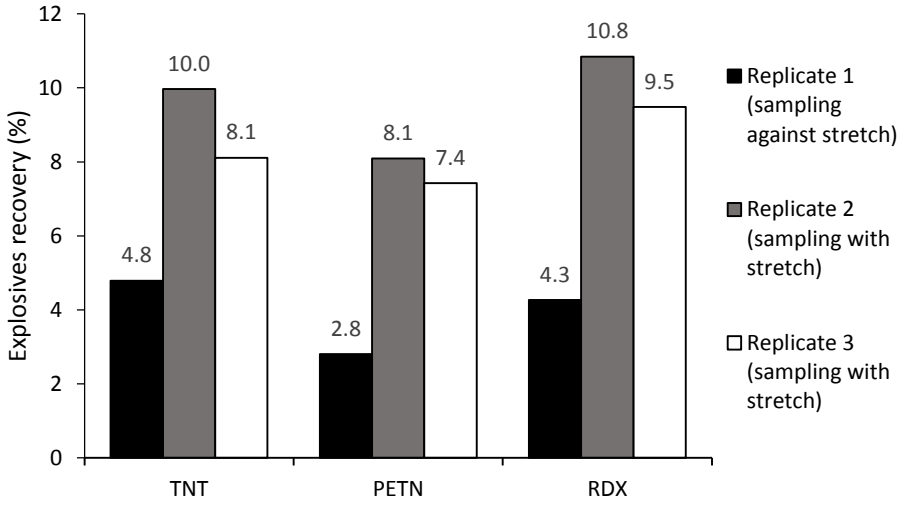

Figure 3.24: TNT, PETN and RDX recoveries from crystal-spiked cotton jersey (for individual vacuum sampling replicates 1, 2 and 3)

For the second and third cotton jersey samples, vacuum sampling was performed 'with' the direction of the stretch of the fabric, and in these cases much higher explosive residue recoveries were obtained (see Figure 3.24) – approximately double those obtained when sampling against the give of the fabric. Unfortunately, due to the limited number of vacuum sampling cartridges provided for this work, this finding could not be explored further. Based on these preliminary observations, the results suggest that when vacuum sampling a stretchy fabric, it may be worthwhile to sample 'with' the direction of stretch, to stretch and distort the fabric as much as possible to loosen any explosive crystals for recovery and enable any bound explosives to be 'flicked' from the fabric into the vacuum sampling tube.

3.4 Conclusions and future work

This work has shown that the contact heater is suitable for recovering TNT and PETN from a variety of surfaces, but is less successful at recovering RDX. Based on the results presented above, it can be concluded that a number of factors contribute towards the successful recovery of explosive residues from fabrics. The vapour pressure of an explosive appears to be the most important factor when contact heater sampling. If an explosive has a low vapour pressure, such as RDX, then the contact heater may struggle to recover it. On the other hand, the contact heater proved successful for the recovery of much higher vapour pressure explosives, such as TNT and PETN. Higher recoveries of TNT were obtained compared to PETN; this agrees with their respective vapour pressures, with TNT having a higher vapour pressure than PETN.

In general, higher recoveries were obtained when contact heater sampling crystal-spiked, rather than solution-spiked, surfaces. The ageing experiments showed that TNT, PETN and RDX display good stability on a range of surfaces in several storage environments, with storage in a freezer, rather than at room temperature, being of benefit to maximise recoveries. Future work could investigate longer storage periods following spiking, to assess how longer-term storage affects recoveries.

For the vacuum samples, the magnitude of explosive residue recovery was similar for each of the three explosives from the different fabrics, suggesting that vapour pressure is less important for recoveries when vacuum sampling, compared to contact heater sampling. Instead, for vacuum sampling, it may be the mesh size and flexibility of the fabric that is more important. For example, wool's mesh size is approximately twice that of polyester, and consistently higher recoveries were obtained when vacuum sampling wool compared to polyester. On the other hand, although cotton jersey's mesh size is approximately the same as polyester's, much higher average recoveries were obtained. This is proposed to be due to the stretch present within the ribbed cotton jersey fabric, enabling explosive crystals to be 'flicked' from the surface when it was stretched during vacuum sampling. This suggests that when vacuum sampling, the highest recoveries may be expected when sampling a stretchy fabric with a large mesh size.

Vacuum sampling and contact heater sampling appear to be complementary techniques, with the contact heater being more successful at recovering some explosives (TNT and PETN), whereas the vacuum sampling was more successful at recovering other explosives (RDX). For this reason, it may be worthwhile in future to sample fabrics using two, or even three techniques, in order to ensure that, if a mixture of explosives is present on a surface, all of the

different explosives are recovered. One such sampling sequence example may be: 1) contact heater sampling, 2) vacuum sampling, and 3) solvent extraction.

Importantly, this work has shown that there is no easy way to recover explosive residues from fabrics. Instead, recoveries depend on the type of explosive present, their vapour pressure, the type of fabric they are deposited on and the nature of their deposition, in addition to the fabric's degree of stretch and mesh size. This reinforces the difficulties that may be encountered with regards to explosive residue recoveries from porous surfaces, and reinforces the fact that further research is necessary in this area to continually improve observed recoveries.

Chapter 4 The effect of storage conditions on the stability of explosives in simulated post-explosion soils

4.1 Introduction

Soil typically consists of sand, silt, clay and organic matter [161], with these proportions varying depending on the soil's locality. Different soils can therefore have very different chemical and physical properties. The clay component of soil comprises a number of species, including silica, iron, aluminium, titanium oxides and phyllosilicate minerals [102], and the organic matter may be formed from decomposing plants and small animals, among other sources. Soils may also contain other debris such as pebbles, gravel, grass, moss and sticks; for this reason, soils are intrinsically heterogeneous [161].

As discussed in Chapter 1, explosive residues are a common soil contaminant at a range of sites, including military training and firing ranges and areas associated with landmine detonations [73-77]. As many explosives are toxic and can have adverse environmental effects, a large body of research has been directed towards the detection and remediation of such explosive residues in soil. TNT, HMX and RDX have been a key focus of the degradation and remediation research conducted to date as these are common components of many explosives. Existing explosive residue bioremediation research can broadly be classified into two groups, the first involving historical field-samples of explosives-contaminated soil [74-76, 86-91], and the second starting with blank, explosives-free soil, with explosives spiked into the soil to assess their degradation and transformation [10, 77, 78, 83, 85, 92-108].

In comparison to this broad set of bioremediation research, very little research has investigated the degradation of 'newly-deposited' explosive residues from the detonation of an explosive. As soil from the vicinity of vehicle bombings is likely to be a good source of explosive residues [8] and is therefore of potential evidential value, the present work is concerned with investigating the degradation of 'newly-deposited' explosive residues following an explosive incident.

Typically, forensic soil samples suspected of containing explosive residues have been collected and transported to a laboratory for analysis [74, 77]. However, over the last number of years, research has been directed towards the development of at-the-scene techniques for

the rapid detection and identification of explosive residues in soil. For example, Ma *et al.* [111] developed a technique enabling the direct mass spectrometric detection of explosive residues in soils, with detection limits as low as 1 ppb, and Choodum *et al.* [112] proposed a novel approach for the quantitative analysis of TNT in soil using an iPhone in conjunction with a colorimetric test for TNT in soil. More recently, Capka *et al.* [113] developed a miniaturised liquid chromatograph involving chemiluminescence detection capable of detecting nitramine and nitroester explosives in soil in under 8 minutes. These in-field sampling techniques are promising and there will continue to be an expansion of research in this area given the advantages of rapid identification to an active criminal investigation. However, it is believed that for the foreseeable future, the majority of soil samples will continue to be transported back to laboratories for analysis [74, 77, 162], until in-field sampling instruments can be commercialised, further miniaturised, show applicability to a wider range of explosives [39, 163] and be available for a competitive price [33], in addition to having stringent quality control requirements to ensure the result is collected in the absence of any contamination [33], meaning it will be accepted by the courts. In particular, the laboratory analysis of soils also allows more detailed analyses to be performed. However, as previous research has shown that explosive residues can undergo degradation in soils within just a few hours [10], it would be of great benefit to assess a variety of storage conditions with the aim of minimising the loss of any explosive present prior to its detection.

A number of processes may affect the stability or attenuation of explosive residues in soil. As highlighted in Chapter 1, the biodegradation of explosive residues by soil-borne microbes and bacteria is one of the major pathways for the attenuation of explosive residues in soil [75, 78-85]. Microbial activity in soils can be either aerobic, requiring oxygen to occur, or anaerobic, without requiring oxygen to occur. Almost all previous research investigating the degradation of explosive residues in soil has involved the storage of soil samples with an air headspace [10, 77, 78, 85, 89, 93-95, 98, 104, 106], thus allowing aerobic microbial degradation to take place. However, storage under a nitrogen headspace may have the potential to minimise the biotic degradation and transformation of explosive residues by preventing aerobic microbial degradation pathways [88, 164-170].

Moshe *et al.* [88] investigated the effect of a nitrogen headspace on explosive residue degradation in soil samples. The authors enriched soil samples containing TNT, RDX and HMX by adding molasses and a nutrient-containing solution to form slurries. Interestingly, degradation of each of the explosives was observed despite the anaerobic conditions, suggesting that anaerobic microbial degradation of the explosive residues may have occurred. Although Moshe's work concerns the use of a nitrogen headspace for soil-based slurries, no

reference could be found in the literature where much drier, unsaturated soil samples (such as those recovered from a post-explosion scene) were stored under a nitrogen headspace.

Whereas nitrogen purging soil samples is likely to only affect any aerobic microbial activity, a comprehensive sterilisation technique is likely to eliminate all aspects of microbial activity, and may prevent explosive residue degradation in post-blast soil samples. Ainsworth *et al.* [96] investigated the transformation of TNT and RDX in steam-sterilised soils, finding that TNT underwent abiotic transformation. Similarly, Larson *et al.* [104] investigated the fate of TNT and RDX in six soils. The authors compared sterilised and non-sterilised soils, and concluded that TNT and RDX transformation occurred in both the sterilised and non-sterilised soils, though the transformation levels were higher in the non-sterilised soils. Later, Sheremata *et al.* [94] investigated the fate of RDX in agricultural topsoil, comparing the rate of RDX sorption and transformation in both non-sterilised and sterilised soils. In the non-sterilised soil, the level of RDX dropped dramatically after two weeks, with the RDX completely disappearing within five weeks. High recoveries of RDX were obtained even after five weeks with the sterilised soils. It should be noted that in each of these previous studies the soil samples were sterilised *prior* to the addition of explosives. No studies have investigated soil *already* containing explosives before sterilisation, which is representative of a real-life post-explosion situation.

In addition to microbial-based attenuation, explosive residues may undergo adsorption to many potential sorbents within a soil matrix, such as organic carbon, microorganisms, humic material, and surfaces present in the clay fraction of soils [73, 90, 92, 93, 96, 102, 106, 109, 171, 172]. TNT [171, 173] and RDX [96] have both been reported to undergo adsorption to organic carbon in soil. The interactions of explosive residues with clay minerals in soil have also been explored [73, 93, 101, 102, 105], with high adsorption coefficients reported between TNT and clay minerals (e.g. K_d = 21500 for adsorption onto Montmorillonite clay [105]), and comparatively lower coefficients between RDX and clay minerals (e.g. K_d = 1.2 for adsorption onto Montmorillonite clay [105]). It is clear from the results from previous research in this area that the attenuation of explosive residues within a soil sample is a highly complex process.

Additionally, by storing soil samples at low temperatures, the rate of microbial degradation of any explosive residues may be reduced. However, although a large proportion of research investigating the degradation of explosive residues in soil has stored soil samples at room temperature [77, 83, 88, 89, 92, 96, 99-101, 103, 104, 108], comparatively little research [10, 95, 98] exists in the literature where researchers have trialled different storage temperatures to assess the effect of temperature on the stability of explosive residues in soil samples. One recent example comes from DeTata *et al.* [10], who investigated the fate of a variety of

explosives in three different soils. The majority of the soil samples were stored at room temperature, though one soil type was also spiked and stored refrigerated or frozen, with the explosive residues displaying a higher stability in the samples stored at lower temperatures. The authors concluded it would be useful to assess the stability of explosive residues under different storage conditions in a wider variety of soils.

The aim of this chapter is to further investigate the current understanding of the fate of explosive residues when stored at various temperatures. In addition, as many explosives are susceptible to microbial degradation, the storage of soil samples under a nitrogen headspace is examined in this chapter as a potential method to increase the stability of the explosive residues over time. This chapter then examines the fate of explosives deposited into soil sterilised *after* being spiked with explosives. The results of this work will enable an assessment of the role of soil sterilisation on the stability of explosive residues within a soil sample.

In this work, an aqueous solution of TNT, RDX and PETN was spiked into 5 g portions of three different soils, and the samples stored in one of five conditions: 1) storage in the dark at room temperature (20-26 °C), 2) refrigerated (1 °C), 3) frozen (-20 °C), 4) nitrogen-purged then stored in the dark at room temperature, and 5) gamma-irradiated and stored in the dark at room temperature. Samples were extracted periodically over six weeks, and the level of each explosive quantified. These experiments enabled an assessment to be made of the effectiveness of a variety of possible storage conditions and soil sample treatments for minimising or preventing explosive residue degradation.

4.2 Experimental

4.2.1 Solvents and chemicals

Acetonitrile (UV grade) was Honeywell, Burdick & Jackson® Brand. Milli-Q water (18.2 MΩ cm^{-1}) was obtained from a Sartorius Arium 611VF water purification system. Explosive standards were obtained from LECO Australia, Castle Hill, NSW, and included the following: PETN, 1000 µg/mL in methanol; 2,4,6-trinitrotoluene, 1000 µg/mL in acetonitrile; RDX, 1000 µg/mL in acetonitrile; 2-amino-4,6-dinitrotoluene (2-ADNT), 1000 µg/mL in acetonitrile; 4-amino-2,6-dinitrotoluene (4-ADNT), 1000 µg/mL in acetonitrile; 1,2-dinitrobenzene (1,2-DNB; internal standard), 1000 µg/mL in methanol.

4.2.2 Consumables

50 mL amber glass tall round bottles (24 mm) and white ringseal 24 mm polypropylene screwcaps were obtained from Cospak, Welshpool, WA. 5 mL Luer slip syringes (without needle) were Nipro Australia or Terumo brand. PTFE membrane 15 mm syringe filters

(0.2 µm) were Phenomenex brand. Clear precleaned boro I-Chem vials (20 mL) with septa were Thermo Fisher Scientific brand. LC vials were Agilent 2 mL clear screw cap vials or Phenomenex 2 mL clear Verex vials. Syringe needles for nitrogen purging were Terumo single use Neolus needles ($21_G \times 1.5$"). Parafilm "M" Laboratory film (Bemis Flexible Packaging, Neenah, WI) was used to seal nitrogen-purged samples.

4.2.3 Explosives spiking solution preparation

The neat explosive standards (TNT, PETN and RDX at 1000 µg/mL; 2 mL of each) were separately concentrated under nitrogen to a final volume of < 50 µL. Each explosive was then reconstituted using Milli-Q water and the aqueous solutions mixed and made up to a total volume of 200 mL. This aqueous spiking solution had a residual organic solvent content of < 0.1 %. The solution was refrigerated prior to use at 1 °C. Prior to use, the solution was sonicated at room temperature (20 °C) for 10 minutes, and three separate samples taken from the spiking solution and analysed for their levels of TNT, RDX and PETN. An average of these three levels was then used as a reference spiking value to calculate percentage recoveries from the aged samples.

4.2.4 Soil preparation

Spearwood soil was obtained from the Soil Laboratory of ChemCentre, WA. Native and landscape soils were obtained from Soils Ain't Soils, Perth, WA. The three soils were chosen as they were reported to have different compositions from each other. As such, this would enable an assessment of the explosives within differing soil environments. The native soil was reported to contain sands, red loam and peat, and the landscape soil was reported to contain sands, fertilisers and peat. Analysis of each soil's properties was performed by the Environmental Chemistry Section at ChemCentre, with selected information on the soils' properties displayed in Table 4.1.

Table 4.1: Properties of Spearwood, native and landscape soils used during this work (note that total organic carbon levels are determined independently from sand, silt and clay, thus each row totals > 100 %)

	Total organic carbon (%)	Sand (%)	Silt (%)	Clay (%)
Spearwood soil	0.95	95.5	1.5	3
Native soil	1.21	93.5	2.5	4
Landscape soil	1.76	92	3.5	4.5

Soils were dried in an oven at 40 °C for 48 hours then passed through a 2 mm sieve prior to use. 5 g (± 0.05 g) soil samples were portioned into 50 mL amber glass vials (for the majority

of samples) or clear glass 20 mL I-Chem vials (for the nitrogen-purged and gamma-irradiated samples).

4.2.5 HPLC-UV instrument and method

Analysis was performed on an Agilent 1200 HPLC-UV instrument equipped with a DAD detector using ChemStation Rev. B.04.03-SP1 software. The HPLC column was an Agilent Zorbax Extend-C18 5 µm 4.6 mm × 150 mm column. A flow rate of 1.6 mL/minute was used with a total run-time of 22 minutes. The following mobile phase sequence was used: 0-11.5 minutes, 28:72 acetonitrile:water; 11.5-13 minutes, ramp to 50:50 acetonitrile:water; hold for 4 min; 17-18.5 minutes, decrease to 28:72 acetonitrile:water; hold for 3.5 minutes until end of run, with a constant column temperature of 40 °C. TNT, 2-ADNT and 4-ADNT were detected at 240 nm, with RDX, 1,2-DNB and PETN detected at 210 nm.

Calibration curves with R^2 values greater than 0.998 containing the five analytes of interest (TNT, PETN, RDX, 2-ADNT and 4-ADNT) along with an internal standard (1,2-DNB) were prepared in 52:48 acetonitrile:water to give on-column concentrations of 5, 10, 20, 35, 50 and 100 ng and 10 ng 1,2-DNB using a 10 µL injection. A typical chromatogram (with an on-column concentration of each explosive of 100 ng) obtained using this HPLC method is provided in Figure 4.1.

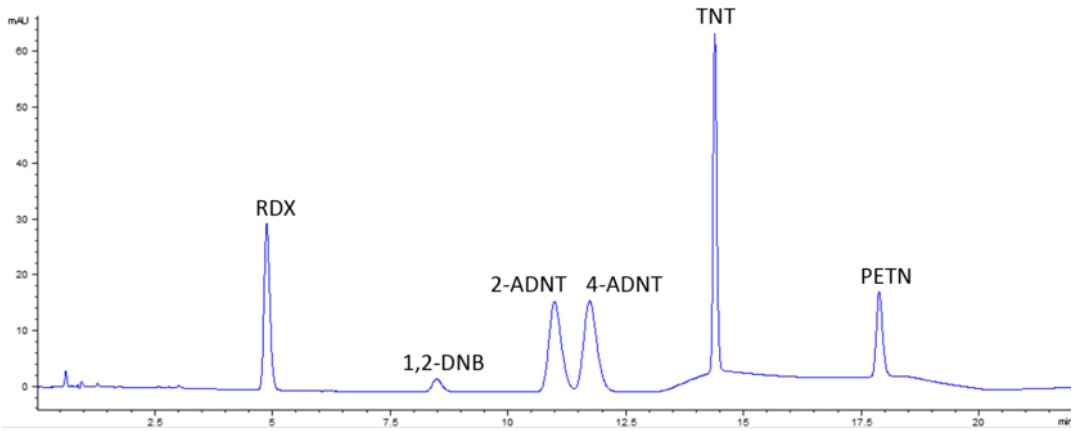

Figure 4.1: HPLC chromatogram at 210 nm showing separation achieved for the 6 compounds using an Agilent Zorbax Extend-C18 5 µm 4.6 mm × 150 mm column. A flow rate of 1.6 mL/minute was used with a total run-time of 22 minutes. The following mobile phase sequence was used: 0-11.5 minutes, 28:72 acetonitrile:water; 11.5-13 minutes, ramp to 50:50 acetonitrile:water; hold for 4 min; 17-18.5 minutes, decrease to 28:72 acetonitrile:water; hold for 3.5 minutes until end of run, with a constant column temperature of 40 °C

4.2.6 Soil extraction study

A mixed explosive spiking solution containing TNT, RDX, PETN, 2-ADNT and 4-ADNT each at 0.2 mg/mL was obtained by mixing equal volumes of 1 mg/mL standards of each

compound. A 50 µL aliquot of this spiking solution (10 µg of each analyte) was spiked onto 7 × 5 g soil samples for each of the three soil types, with an eighth sample used as a control and not spiked. After spiking, the soil samples were left to stand at room temperature (rt; 20-26 °C) for 30 minutes, to allow residual spiking solvent to evaporate. 5 mL acetonitrile was then added to each soil sample bottle, before loosely capping the vials and sonicating for 30 minutes at rt. An aliquot of the resulting soil extract from each sample was filtered through a 5 mL disposable syringe connected to a 0.2 µM syringe filter, with the filtrate collected into a clean test tube. A 500 µL extract of this solution was transferred into an LC vial, before adding 480 µL Milli-Q water and 20 µL of a 0.01 mg/mL acetonitrile-based solution of the 1,2-DNB internal standard, to give an overall volume of 1000 µL and a solvent composition of 52:48 acetonitrile:water. 50 µL of each sample was injected in duplicate onto the HPLC, and the results averaged.

In addition to this acetonitrile-based spike and soil extraction, an aqueous spike extraction was also explored. Spearwood soil was selected as a single soil to analyse. A set of 7 × 5 g Spearwood soil samples were wetted with 0.25 mL Milli-Q water, before the addition of 1 mL of the aqueous spiking solution to each vial, with an eighth sample used as a control and not spiked. Following this, 5 mL acetonitrile was added to each vial, and the vials sonicated at room temperature (20 °C) for 30 minutes, before filtering the resulting extracts through 0.2 µM syringe filters and placing 625 µL of this filtered extract into an LC vial. 355 µL Milli-Q water was added, along with 20 µL of 0.01 mg/mL 1,2-DNB in acetonitrile, to give a final volume of 1000 µL. This gave the same solvent proportion (52:48 acetonitrile:water) as for the previous soil extraction samples. 50 µL of each such sample was injected in duplicate onto the HPLC, and the results averaged.

4.2.7 Sample preparation: Alternate storage temperatures

For the varied storage temperature samples, 5 g (± 0.05 g) of each soil was placed into an amber vial before spiking with 0.25 mL tap water and leaving for three days at room temperature (20-26 °C) to re-establish microbial growth. Following this, 1 mL of the aqueous spiking solution was added, with each spike containing approximately 10 µg each of TNT, RDX and PETN, and the vials placed into their respective storage environments (a sealed box at room temperature, refrigerated at 1 °C or frozen at -20 °C). On each day of spiking using this explosive solution, the solution was sonicated for 10 minutes prior to use, and three separate samples taken from the spiking solution and analysed for their levels of TNT, RDX and PETN. An average of these three levels was then used as a reference spiking value from which to calculate percentage recoveries from the aged samples. Samples were prepared in

duplicate for each time point. Following their designated ageing period, each sample was extracted following the procedure detailed above. The samples stored at room temperature acted as the 'no treatment' samples (i.e. air headspace/non-irradiated samples) against which to compare the nitrogen-purged and gamma-irradiated sample recoveries.

4.2.8 Preparation of nitrogen-purged samples

Following the re-establishment of microbial activity as above in Section 4.2.7, 5g (± 0.05 g) soil samples were spiked with 1 mL of an aqueous explosive spiking solution. Samples were prepared in duplicate for each time point. The spiking solution was sonicated prior to use, to degas the solution and remove any dissolved oxygen from the solution. After capping the vials, the headspace of each sample was purged with nitrogen. This was achieved by piercing the septum of the I-Chem vial lid using a fine needle connected to a nitrogen supply (99.99 % purity), and purging the sample with nitrogen for 15 minutes to ensure that all contained air within the sample had been replaced with nitrogen. An unconnected needle was inserted through the septum to ensure nitrogen flow through the sample.

Nitrogen was applied through a Reacti-Vap Evaporating Unit (Rockford, Illinois) fitted with an Alltech Digital Flow Check HRTM flow meter, operated using DFC Low-Flo 1.01 software and measuring the nitrogen flow using Standard Cubic Centimetres per Minute (SCCM) mode. The evaporating unit contained nine termini for syringe needles, allowing nine vials to be purged simultaneously. The nitrogen flow rate was held at approximately 414 mL/minute, to give an average flow into each of the nine vials of 46 mL/minute (the contained atmosphere within each vial was twice fully displaced with nitrogen each minute). Nitrogen purging was performed for 15 minutes for each set of vials, flushing through with 30 volumes of nitrogen given the 23 mL vial volume, leaving a nitrogen headspace, see Figure 4.2.

Figure 4.2: Photograph of the nitrogen purging setup used during this work

Upon removal of the needles from the 1/8" thick PTFE/silicone septum, the needle holes appeared to self-seal. However, in order to fully ensure that the nitrogen gas would not diffuse out from the samples, the entire flat side of the lid (containing the septum) was covered with a taut layer of Parafilm including the area around the screw threads. Samples were stored immediately in a dark cupboard at room temperature prior to extraction and analysis at their designated time points as detailed above.

4.2.9 Preparation of gamma-irradiated samples

Duplicate 5 g soil samples were pre-wetted and spiked with aqueous spiking solutions as detailed for the nitrogen-purged samples. Samples were then immediately placed into a 2 L metal paint can and irradiated for 16.3 hours to give a total irradiation dose of 70 kGy. The irradiation process was initiated within 30 minutes of soil spiking, i.e. minimal time was allowed for any microbial activity on the spiked explosives between soil spiking and commencement of the irradiation. Gamma irradiation was performed on a MDS Nordon Gammacell 220E irradiator containing cobalt-60 rods. The irradiation dose was verified using a SteriRite Gamma/Ebeam adhesive indicator label (PMA Manufacturing, Penang, Malaysia). At the end of the irradiation time, the samples were stored in the dark at room temperature prior to extraction and analysis at their designated time points. After their designated ageing time, samples were extracted as per the 'no treatment' samples detailed above.

4.3 Results and discussion

4.3.1 HPLC-UV method development

Initially, work was performed to develop a method suitable for separating out RDX, TNT, PETN and the 1,2-DNB internal standard used in this work. A summary of this work is provided in Table 4.2.

Table 4.2: Attempts to improve baseline resolution between TNT, PETN, RDX and 1,2-DNB

Attempt no.	Mobile phase components	Mobile phase ratio	Flow (mL/min)	Column temp. (°C)	Comments
1	Methanol: Water	60:40	1	30	Co-elution of RDX and 1,2-DNB
2	Methanol: Water	60:40	0.8	30	Co-elution of RDX and 1,2-DNB
3	Methanol: Water	50:50	0.8	30	Co-elution of RDX and 1,2-DNB
4	Acetonitrile: Water	50:50	1	30	Co-elution of RDX, 1,2-DNB and TNT
5	Acetonitrile: Water	60:40	1	30	Co-elution of RDX, 1,2-DNB and TNT
6	Methanol: Water	25:75	1	30	Long run time, though separation of RDX and 1,2-DNB peaks
7	Methanol: Water	45:55	1	35	Good separation of all components (RDX, 1,2-DNB, TNT and PETN). 24 minute run time. Slight peak fronting observed on all peaks (suspected due to low miscibility of 10 µL acetonitrile-based sample injection with this mobile phase).
8	Acetonitrile: Water	30:70	1	30	Good peak shapes and separation but long run time required.
9	Acetonitrile: Water	45:55	1	35	Well-separated, symmetrical peaks, 18 minute run time.

It can be seen from Table 4.2, Rows 1-5, that problems were encountered due to the co-elution

of RDX with 1,2-DNB. Alterations to the mobile phase composition, flow rate and column temperature furnished the conditions in Row 9, Table 4.2, which gave rise to good peak separation and a satisfactory run time. Following this, the method was assessed with regards to its suitability to separate 2-ADNT and 4-ADNT from the other four analytes. Unfortunately, co-elution of the isomeric 2-ADNT and 4-ADNT was observed, so work was performed to adjust the HPLC conditions to bring about baseline separation of the two compounds. This is detailed below, in Table 4.3.

Table 4.3: Attempts to separate 2-ADNT and 4-ADNT isomers

Attempt no.	Mobile phase composition	Flow (mL/ min)	Column temp. (°C)	Comments
1	45:55 (isocratic)	1	35	Best conditions from Table 4.2. Gave co-elution of 2-ADNT and 4-ADNT
2	42:58 for 2 min, 50:50 by 6 min, hold (2 min), decrease to 42:58 by 18 min	1	35	Co-elution of 2-ADNT and 4-ADNT
3	42:58 for 3 min, 46:54 by 14 min, 42:58 by 18 min	1	35	Co-elution of 2-ADNT and 4-ADNT
4	30:70 at 0 min, 50:50 by 10 min, 30:70 by 14 min	1	35	Co-elution of 2-ADNT and 4-ADNT
5	40:60 at 0 min, 46:54 by 14 min, 40:60 by 18 min	1	35	Co-elution of 2-ADNT and 4-ADNT
6	10:90 for 1 min, 70:30 by 10 min (hold for 2 min), 10:90 by 18 min	1	35	Co-elution of 2-ADNT and 4-ADNT
7	30:70 at 0 min, 45:55 by 9 min (hold for 3 min), 55:45 by 14 min, 30:70 by 18 min	1	35	Co-elution of 2-ADNT and 4-ADNT
8	30:70 (isocratic)	1	35	Almost baseline separation of 2-ADNT and 4-ADNT. Long run time; 2-ADNT and 4-ADNT had only just eluted by 18 min.
9	30:70 (isocratic)	1	40	Almost baseline separation of 2-ADNT and 4-ADNT. Slightly faster run – 2-ADNT and 4-ADNT eluted by 16 min.
10	30:70 (isocratic)	1.4	40	Almost baseline separation of 2-ADNT and 4-ADNT. Slightly faster run – 2-ADNT and 4-ADNT eluted by 12 min.
11	30:70 (isocratic)	1.4	40	Almost baseline separation of 2-ADNT and 4-ADNT. Slightly faster run – 2-ADNT and 4-ADNT eluted by 12 min.
12	30:70 (isocratic)	1.6	40	Almost baseline separation of 2-ADNT and 4-ADNT. Slightly faster run – 2-ADNT and 4-ADNT eluted by 10 min.

It can be seen from Table 4.3, Row 12, that using an isocratic mobile phase of

30:70 acetonitrile:water throughout the analysis, the compounds were eluted in less than 10 minutes with baseline separation very nearly achieved. However, it was not feasible to maintain this isocratic mobile phase throughout runs designed to separate all six analytes of interest – earlier work had shown that PETN (the slowest compound to elute) required a much higher proportion of organic solvent in the mobile phase to bring about elution within a satisfactory time.

For this reason, the conditions optimised in Table 4.3 for the separation of 2-ADNT and 4-ADNT were used as the starting point for the first stage of a gradient-based mobile phase sequence. This starting point was built upon by developing a second half to add to the first half already developed in Table 4.2, with the aim of increasing the percentage of acetonitrile during the second half of the sequence to promote a more rapid elution of the TNT and PETN.

Experiments incorporating these initial conditions for 2-ADNT and 4-ADNT analysis, followed by an increase in the percentage of acetonitrile used, to bring off the TNT and PETN, are therefore detailed below in Table 4.4 (N.B. A reduction in the initial mobile phase from 30:70 acetonitrile:water to 28:72 acetonitrile:water was also performed in order to achieve complete baseline separation of the two ADNT isomers).

Table 4.4: Development of a gradient sequence to combine with the optimised procedure developed for the separation of 2-ADNT and 4-ADNT

Attempt no.	Mobile phase composition	Flow (mL/ min)	Column temp. (°C)	Comments
1	28:72 for 12 min, 70:30 by 14 min (hold for 1 min), 28:72 by 17 min	1.6	40	Good separation of all 6 analytes; all analytes eluted by 18 min. Steep gradient during increase in % organic content of mobile phase introduced undesirable large bump into chromatogram.
2	28:72 for 12 min, 50:50 by 14 min (hold for 1 min), 28:72 by 17 min	1.6	40	Good separation of all 6 analytes; PETN elution very slow at 29 min. Significantly increased run time from previous row.
3	28:72 for 12 min, 50:50 by 13.5 min (hold for 3.5 min), 28:72 by 18.5 min	1.6	40	Good separation of all 6 analytes; all analytes eluted by 20 min.
4	28:72 for 11.5 min, 50:50 by 13 min (hold for 4 min), 28:72 by 18.5 min	1.6	40	Good separation of all 6 analytes; all analytes eluted by 20 min. Slightly better peak shape by introducing mobile phase composition gradient 0.5 min earlier than in previous run. Final run time 22 min.

The conditions detail in Row 4, Table 4.4, were used as the final conditions for all subsequent analyses. Figure 4.1 (earlier) shows a chromatogram obtained using this final method.

4.3.2 Soil extraction study

The majority of research focusing on the detection of explosive residues in soil is based on the US Environmental Protection Agency (EPA) Method 8330 [174] which details the extraction of a range of explosive residues from soil, with detection using High Performance Liquid Chromatography-Ultraviolet detection (HPLC-UV) [175]. The method involves an 18 hour sonication of 2 g soil samples in 10 mL acetonitrile. More recently, an updated version of Method 8330 was proposed in the form of EPA Method 8330B [174], capable of detecting a greater number of explosives, including PETN. EPA Methods 8330 and 8330B were primarily developed for the analysis of field-contaminated soils collected from military training activities [174]. A number of studies have therefore reported the use of either EPA Method 8330 or 8330B for the extraction of explosive residues from field-contaminated soils [74-76,

87, 92, 98, 161]. Some studies have also utilised these methods for the extraction of explosive residues from blank soils spiked with explosives, to resemble field-contaminated soils [85, 93-95, 99-101, 106, 107].

Variants of the EPA methods have also been reported. For example, Oxley *et al.* [77] extracted 5 g soil samples using 5 mL acetonitrile, sonicating for 12 hours at 10 °C. This method is therefore a shortened version of the EPA methods. Recently, DeTata *et al.* [10] reported the use of a 30 minute sonication period for 5 g soil samples using 10 mL acetonitrile, prior to HPLC analysis. In their work, the authors spiked blank soils with explosives prior to their extraction and analysis. Although this sonication time is significantly shorter than that recommended in the EPA methods, it is unlikely that explosives which have been spiked onto a blank soil and extracted days or weeks later will be as tightly bound to soils which have been contaminated in the field and are being extracted months or years later [10].

In the present work, a combination of the conditions of DeTata [10] and Oxley [77] was used. A sonication time of 30 minutes was used, for a 5 g soil sample extracted with 5 mL acetonitrile. Firstly, the efficiency of the planned recovery method was assessed to confirm that the conditions were sufficient to recover the majority of spiked explosives from the three soils used in this work. This extraction efficiency was examined using all three soil types. For each soil, a set of 7 × 5 g soil samples was spiked with 10 µg each of TNT, RDX, PETN, 4-ADNT and 2-ADNT, with an eighth sample for each soil type not spiked, and used as a control. These control samples confirmed the absence of all of the spiked analytes from the original soils, prior to spiking. 2-ADNT and 4-ADNT (common TNT degradation products) were included in these extraction efficiency studies as it is likely that they may have formed by the end of the six week ageing period. The results from these extraction efficiency experiments are displayed in Figure 4.3.

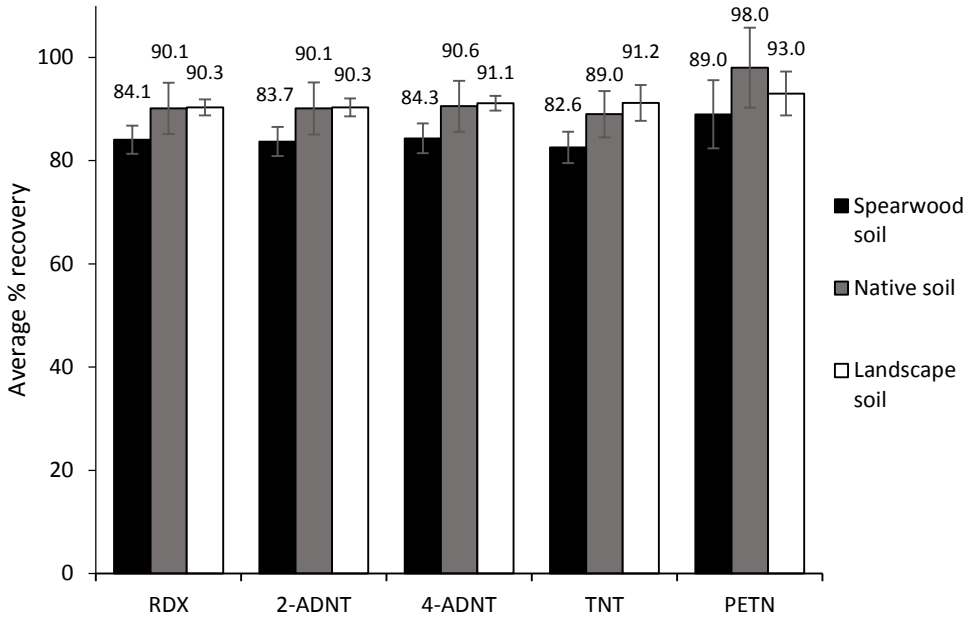

Figure 4.3: Average recoveries of explosives from the three different soils examined in this work. Error bars show the standard deviations within a set of 7 soil samples

It can be seen from Figure 4.3 that high recoveries of each analyte were obtained from each of the three different soils, with low standard deviations within a set of seven extracted soil samples. This extraction method using 5 mL acetonitrile and a 30 minute sonication period was therefore used for all subsequent soil extractions. Slightly lower recoveries of each analyte were obtained from the Spearwood soil, compared to the landscape and native soils. This may be due to inherent chemical and microbiological differences between the different soils (see Table 4.1), giving rise to different degrees of interaction strength between the explosives and the three soils.

For these soil extraction validation experiments, soil samples were spiked using an acetonitrile:methanol-based spiking solution, whereas for the ageing experiments, soils were spiked with a primarily aqueous (> 99.9 % water) spiking solution. In addition to these samples, a set of Spearwood samples was spiked using the aqueous spiking solution (detailed earlier in the experimental section), to compare the explosives recoveries between the two different spiking solutions. This ensured that the spiking and extraction method planned for the spiked soil samples was highly efficient. An aqueous spiking solution, containing a total percentage of < 0.1 % acetonitrile, was used to spike the soil samples rather than an organic solvent-based solution as the presence of acetonitrile has been shown to affect the rate of explosive residue degradation in soils [10, 95]. Spearwood soil was chosen for this extra soil extraction study given the lower explosive recoveries from the acetonitrile-based spiked samples (see Figure 4.3), and was therefore deemed the most difficult soil from which to extract the explosives. It should be noted that, as these soil samples were spiked using a three-

component aqueous spiking solution containing only TNT, PETN and RDX, no ADNT recoveries were obtained from these extractions from the aqueous-spiked samples. The results from this aqueous soil extraction study are displayed in Figure 4.4.

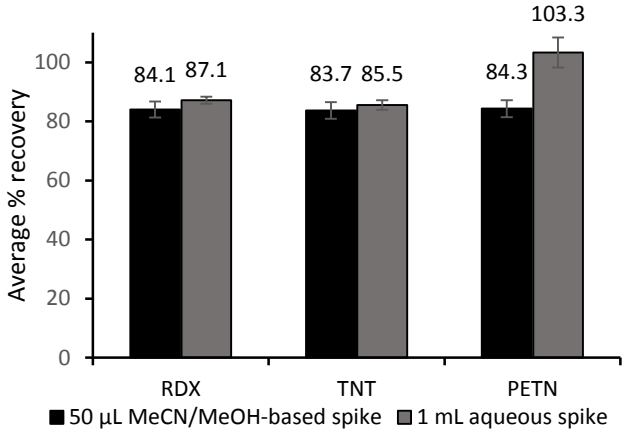

Figure 4.4: Comparing recoveries of RDX, TNT and PETN from Spearwood soil after acetonitrile:methanol or aqueous soil spiking. Error bars show the standard deviations within a set of 7 soil samples

Each spiking solution gave similar recoveries of the three explosives from Spearwood soil, with slightly higher recoveries from the aqueous-spiked samples. This confirmed that the planned extraction technique was a suitable method for recovering the explosives from the soils.

4.3.3 An overview of processes contributing to the attenuation of explosives in soil

Before discussing the pattern of loss of the explosives under investigation in this chapter, a more detailed overview of explosives attenuation pathways in soil will first be provided to enable a better understanding of the overall results obtained. A number of interlinked processes are associated with the fate of explosive residues in soil. These can be broadly categorised into processes which influence the transport of explosive residues in soil (including dissolution, adsorption and volatilisation) and processes which influence the transformation of explosive residues in soil (including photolysis, hydrolysis, reduction and biotransformation) [109]. The relationship between these processes is displayed in Figure 4.5, below.

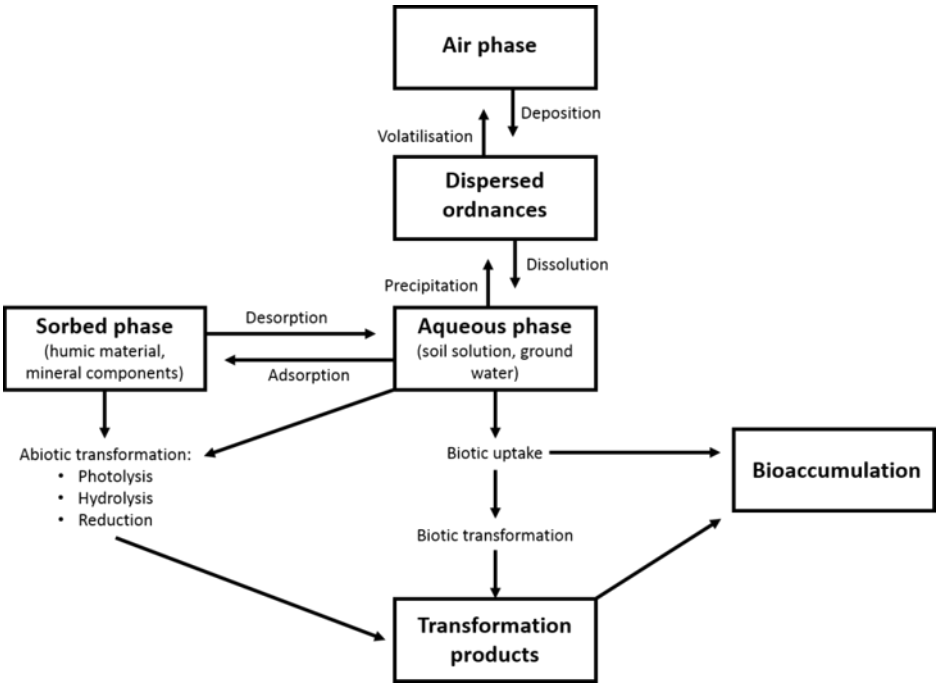

Figure 4.5: Flow chart illustrating the possible fates of explosive residues in the environment (adapted from [109])

4.3.3.1 Processes influencing the transport of explosives in soil

It can be seen from Figure 4.5 that explosive residues in soils may undergo volatilisation into the atmosphere. However, as the TNT, RDX and PETN used in the current work have very low vapour pressures [73, 109], explosives loss due to volatilisation can be considered to be negligible.

Explosive residues in soils may also undergo dissolution by dissolving in any water present in the soil [73, 109]. Dissolution of explosive residues within soil samples is the key mechanism for their dispersal within soil [73], thus previous research has involved producing aqueous batch samples to assess explosive residue degradation following simulated runoff into groundwater [100, 101]. It has been determined that, from 3 °C to 33 °C, the rate of explosives dissolution doubles with every 10 °C rise in temperature [109].

Adsorption is another possible mechanism of explosive residue attenuation in soils. Adsorption can be defined as the process of a dissolved chemical (a solute) accumulating on a particle's surface (a sorbent) [73]. Such sorption interactions may include hydrogen bonding, ion exchange, chemisorption and hydrophobic partitioning, with the extent of observed adsorption dependent on both the physicochemical properties of the solute and sorbent, as well as the environmental conditions present [73, 109]. In the context of the present work, the explosives under analysis in this work (the solutes) are likely to encounter many potential

sorbents within a soil matrix. These include organic carbon, microorganisms, humic material, and surfaces present in the clay fraction of soils, including mineral components, metal oxides and hydroxides [73, 90, 92, 93, 96, 102, 106, 109, 171, 172]. In the following paragraphs, research regarding the adsorption of explosive residues to different soil fractions will be briefly outlined.

A number of researchers have established that explosive residues commonly undergo binding and sorption to organic carbon, a key constituent of many soils. For example, Yamamoto *et al.* [92] looked at the sorption of TNT, RDX and 2,4-DNT to several soils, concluding that the explosives showed a higher sorption to soils with a higher proportion of organic carbon. Similar results were reported by Dontsova *et al.* [102], Alavi *et al.* [106] and Drzyzga *et al.* [172]. These studies concluded that explosive residues preferentially sorb to organic carbon with TNT > HMX > RDX [73, 96, 106]. No mention could be found in the literature as to the potential interactions of PETN with organic carbon in soil, though it is likely that its interactions would be more similar to those of RDX than TNT, as both analytes are non-aromatic compounds.

In the present work, the three soils used had different total organic carbon contents (see Table 4.1), with the total organic carbon content decreasing in the order Landscape > Native > Spearwood. Given this, if the explosives spiked into the soils were undergoing losses solely due to adsorption to organic carbon, then it is likely that a greater degree of loss would be observed for landscape soil, followed by native soil and finally Spearwood soil. However, it is unlikely that the attenuation of explosive residues in soils is due solely to organic carbon. It should also be emphasised that the three soils all had very low carbon contents (approximately 1 %, see Table 4.1). For this reason, further possible attenuation pathways will be outlined below.

In addition to organic carbon, many researchers have explored the interactions between explosive residues and different mineral surfaces in soil. Clay is the finest fraction of soil, with particle sizes < 0.002 mm [176]. Due to its very fine particle size, clay is deemed the most reactive soil fraction, with the greatest likelihood of adsorbing explosive residues [102]. The clay fraction of soil typically comprises a variety of compounds, including silica, aluminium, iron, manganese, titanium oxides and hydroxides and phyllosilicate minerals [102]. Due to this wide variety of compounds present in the clay fraction, it is perhaps unsurprising that explosive residues have been shown to have high affinities to clay minerals [93, 101, 105, 171]. Previous research has investigated the interactions of nitroaromatic compounds, such as trinitrotoluene, with mineral surfaces. High adsorption coefficients were reported [105], attributed to the formation of electron donor-acceptor complexes between the electron-

donating oxygen atoms of the minerals' siloxane surfaces and the electron-accepting π-system of the nitroaromatic explosives [93, 102, 105].

Haderlein *et al.* [105] looked at the adsorption between nitroaromatic explosives and RDX and three different clay minerals. The highest adsorption coefficients were found between the nitroaromatic explosives, such as TNT, and the clay minerals, whereas much lower adsorption coefficients were found between RDX and the clay minerals, with the adsorption deemed to be reversible. The authors rationalised the preferential adsorption of TNT, compared to RDX, with the clay mineral surfaces as being due to the formation of η-π complex systems, in which oxygen atoms from the siloxane surfaces of clay minerals act as electron donors towards the electron deficient π-electron system of the TNT, which acts as an electron acceptor, to give an electron donor-acceptor complex [105]. A possible schematic of this interaction is shown in Figure 4.6.

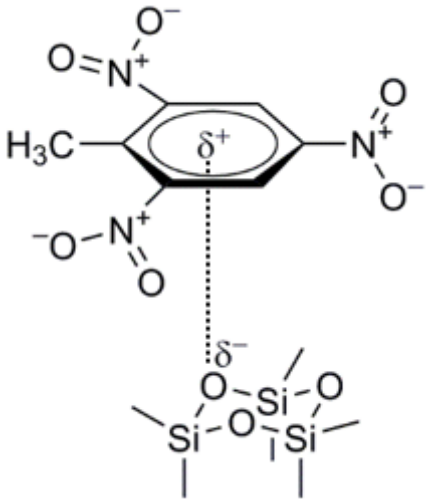

Figure 4.6: Proposed η-π complex formation between TNT and a generic siloxane surface

In addition, compared to TNT, lower adsorption coefficients were obtained for the reduction products of TNT, attributed to the transformation of electron-withdrawing nitro groups to electron-donating amino groups, resulting in the formation of a weaker electron donor-acceptor complex [105]. Interestingly, isomer effects were also observed, for example 2-ADNT displayed a higher adsorption coefficient than 4-ADNT, attributed to steric effects.

In addition to the proposed electron donor-acceptor complexes which may form between TNT and mineral surfaces to give high adsorption coefficients, hydrogen bonds [73] and complexation between soil cations (such as K^+) and TNT [93] have also been proposed as further explanations for TNT's high binding capacity to soils.

In contrast to TNT and other nitroaromatic explosives, RDX has been reported to display much

lower affinities towards clay minerals in soil [73, 93, 101, 105], attributed to the non-aromaticity of RDX, meaning strong η-π electron donor-acceptor complexes cannot form [93]. Alternative interactions have been proposed between RDX and minerals present within the clay fraction of soil. These include hydrogen bonding between the nitro groups of RDX and surface hydroxyl groups in soil [93, 96], as well as van der Waals interactions [96]. A possible hydrogen bond which may form between RDX and surface hydroxyl groups is illustrated in Figure 4.7. Hawari [93] assessed the adsorption coefficients between RDX and HMX and clays, observing higher adsorption coefficients for HMX. The authors propose that this is due to HMX containing an extra NO_2 group compared to RDX, meaning each molecule of HMX has an extra possible interaction with clay in soil compared to RDX.

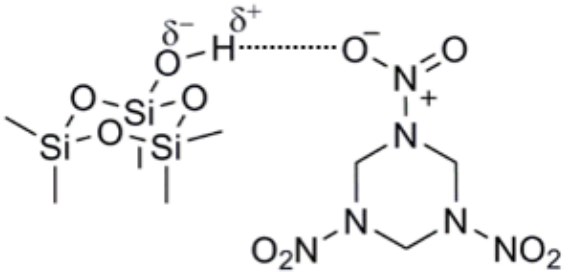

Figure 4.7: Proposed hydrogen bonding interaction between RDX and surface hydroxyl groups

Currently, no literature can be found which discusses the interactions of PETN in soil. However, as PETN is a nonaromatic compound containing four O-NO_2 groups, it is probable that its interactions will be similar to those of HMX and RDX, meaning it will display lower sorption affinities towards soil than nitroaromatic compounds such as TNT. As PETN contains four nitro groups, compared to RDX's three, this may mean that PETN will display a higher sorption to clay minerals in soils than RDX.

Finally, when considering the nature of interaction between explosive residues and mineral surfaces in soils, some thought must be directed towards the age of the mineral surface itself, rather than solely its chemical composition [73, 101]. For example, it has been reported that fresh mineral surfaces show a higher geochemical reactivity than weathered surfaces, and that organic compounds show preferential affinities to fresh reactive surfaces than weathered ones [101]. Douglas *et al.* [101] investigated this phenomenon by assessing the behaviour of TNT and RDX in combination with fresh and weathered surfaces, finding a greater rate of loss with the fresh surfaces. The authors ultimately concluded that this loss was due to enhanced transformation due to the presence of the fresh surfaces, rather than solely a loss due to enhanced adsorption. This finding is also likely to be of significance with regards to the freshly fractured soil likely to originate following an explosion (explored further in Chapter 5).

In the present work, the landscape soil was found to have the highest clay content (Table 4.1), followed by the native and finally Spearwood soil. For this reason, if explosive residue loss within the soils was due solely to adsorption onto mineral surfaces, then the greatest loss would be expected from the landscape soil samples, and the least from the Spearwood soil samples.

In addition to the non-covalent adsorption interactions of explosive residues with soil constituents, research has also shown that explosive residue transformation products, particularly the amino derivatives of TNT, can undergo irreversible covalent binding with the humic acids forming part of the organic carbon content of soil [86, 93, 102, 177-179], meaning it may be problematic to extract these transformation products using simple solvent extraction [86]. Thorn and Kennedy [177] propose that the TNT amino-transformation products (including 2-ADNT and 4-ADNT) undergo nucleophilic addition to carbonyl and quinone groups within the humic acid component of soil. It is therefore possible that a proportion of any observed TNT loss is due to its amino transformation products becoming irreversibly bound to soil components.

4.3.3.2 Processes influencing the transformation of explosives in soil

As can be seen from Figure 4.5, photolysis is a possible pathway for the attenuation of explosive residues within soil. It is likely that photolysis will only have an effect on explosive residues close to the surface of a soil [73]. In the present work, efforts were made to limit the exposure of the spiked soil samples to sunlight, by storing soil samples in amber glass vials or in a dark cupboard.

Figure 4.5 shows that explosive residues may undergo hydrolysis within a soil environment. However, this typically requires a strongly alkaline environment [73], not likely to be present in the three soils under investigation in this work.

Explosive residues in soil may also undergo abiotic reduction [73, 110, 179]. This process typically requires the presence of electron donor species to act as solid catalysts to activate the reduction reaction. Such species include reduced iron and sulfur species, clay minerals and some organic molecules [73, 110]. This process is most likely for nitroaromatic explosives [110].

The sequential abiotic reduction of TNT's three nitro groups has been reported [73, 110, 179]. During the initial reduction step, to give a monoamino dinitrotoluene, reduction at the 4- or para position is regioselectively favoured [73, 110, 179]. This initial reduction has been found to occur much more rapidly than subsequent reduction steps to the di- and tri-amino

compounds [110], with highly reducing conditions required to form the triaminotoluene. Once formed, this triamino product is unlikely to be detected in soil samples due to its likely immobilisation with soil components or microbial degradation [179]. In addition, the amino reduction products may couple to form dimers [110].

Abiotic RDX reduction has also been shown to occur, via formation of mono- (MNX), di- (DNX) and tri-nitroso (TNX) compounds [73, 179]. This process destabilises the reduction products, and may cause ring cleavage and mineralisation of the original molecule. Alternatively, this ring cleavage may also occur without the initial formation of the nitroso intermediates. This process is illustrated in Figure 4.8.

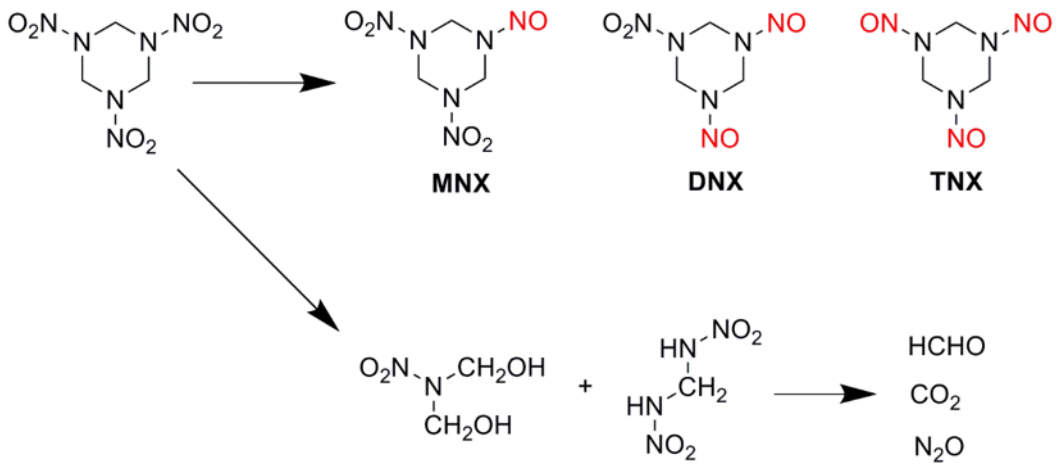

Figure 4.8: Transformation pathways of RDX (adapted from [85])

Little is known about any abiotic reduction processes of PETN. However, it is likely that its nitro groups may undergo similar reduction processes as RDX, to form nitrite esters which can ultimately undergo further reactions, with mineralisation likely.

Finally, biodegradation of explosive residues by soil-borne microbes and bacteria is one of the major pathways for the attenuation of explosive residues in soil. In the current work, soil samples were dried at 40 °C prior to use, before rewetting three days prior to spiking to allow microbial populations to re-establish within the soils [10, 95, 98]. Although microbial activity is low in dried soils, bacteria can remain dormant and can become active again after rewetting the soil [180].

RDX has been shown to biodegrade following enzymatic attack under both aerobic and anaerobic conditions [73, 109]. Less is known about the biodegradation of PETN. Literature suggests that one bacterial strain studied caused the reduction of two PETN nitro groups to hydroxyl groups [109]. Other work has examined the NAD(P)H-based biotransformation of organic nitrate esters (i.e. the same class of compound as PETN), finding that an initial

reduction to a nitrite ester occurred, followed by hydrolysis to the corresponding alcohol [181]. As many of the enzymatic processes for the degradation of explosive residues in soil are believed to involve NAD(P)H-based processes [109], it is likely that this pathway also occurs for the biodegradation of PETN in soils.

TNT has been shown to rapidly biodegrade in the presence of a variety of bacteria [109]. TNT biodegradation can occur under both aerobic and anaerobic conditions [109]. The initial transformation products are aminodinitrotoluenes (either 2-ADNT or 4-ADNT). This reduction involves NAD(P)H-dependent non-specific nitroreductase enzymes [109]. Following this initial reduction, further reduction can occur, to give the corresponding diamino (2,4-diamino-6-nitrotoluene and 2,6-diamino-4-nitrotoluene) and triamino products (2,4,6-triaminotoluene). This overall process of sequential reduction is illustrated below, in Figure 4.9.

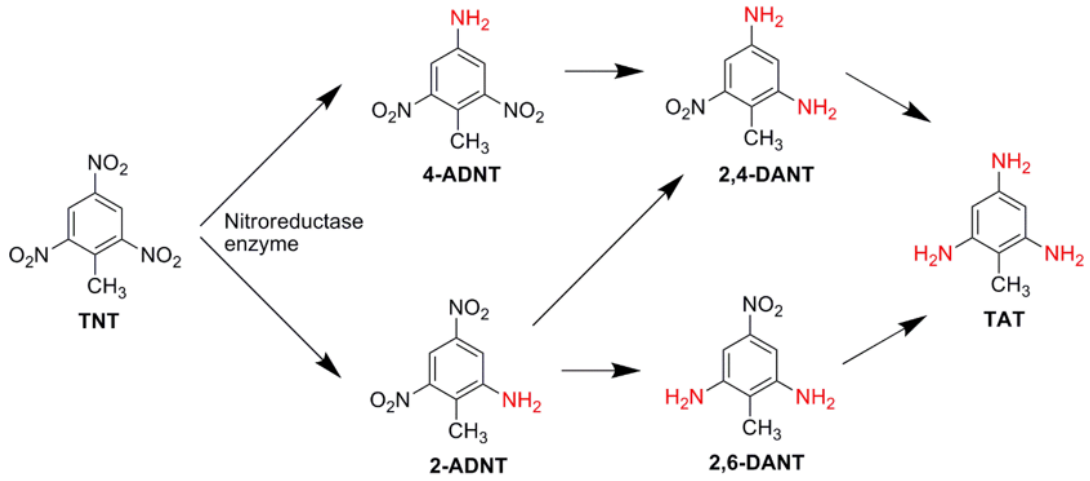

Figure 4.9: Sequential reduction pathway for TNT to form TAT (adapted from [177])

TNT, and other nitroaromatic compounds, are highly susceptible to reduction by bacteria. This is due to the electronegativity of the nitro group oxygen atoms, causing polarisation of the N-O bond to leave a partial positive charge on the nitrogen atom. The electrophilic nature of the nitrogen atom allows for the rapid reduction. Reduction of the first nitro group of TNT, to give a monoaminodinitrotoluene, is the most rapid of these reduction reactions [110], with 4-ADNT reported to form in greater quantity than 2-ADNT [92]. This regioselective reduction is thought to be due to steric effects from the methyl group at the 1-position [109, 110]. However, as was the case for the amino transformation products forming from the abiotic reduction of TNT, it has been suggested that these compounds can again undergo covalent binding to soil components [92, 109]; an irreversible process. This means that the total quantities of recovered/extracted TNT, 2-ADNT, 4-ADNT and further reduction products may not equal the initial number of moles of TNT in the starting sample [92].

In reality it is likely that a complex combination of these processes is responsible for the loss of explosive residues in soil over time. In the following section, the pattern of loss of a particular explosive in a particular soil will be reported for the range of conditions investigated throughout this work, and a discussion made based on the most likely factors responsible for these results, based on the possible attenuation pathways outlined above.

4.3.4 Storage at different temperatures

In the current work, the stability of explosive residues in soil samples was explored at three temperatures: room temperature, 0-1 °C and -20 °C, to determine whether the degradation trends observed in the current work reflect those determined from the previous research in this area. A maximum storage time after spiking of six weeks was used in this work, in line with previous recommendations [95]. The results from the six week experiment examining the effect of alternative soil storage temperatures are detailed in the following sections for each analyte examined.

4.3.4.1 TNT

Figure 4.10 displays TNT recoveries from landscape, native and Spearwood samples stored at room temperature, refrigerated and frozen.

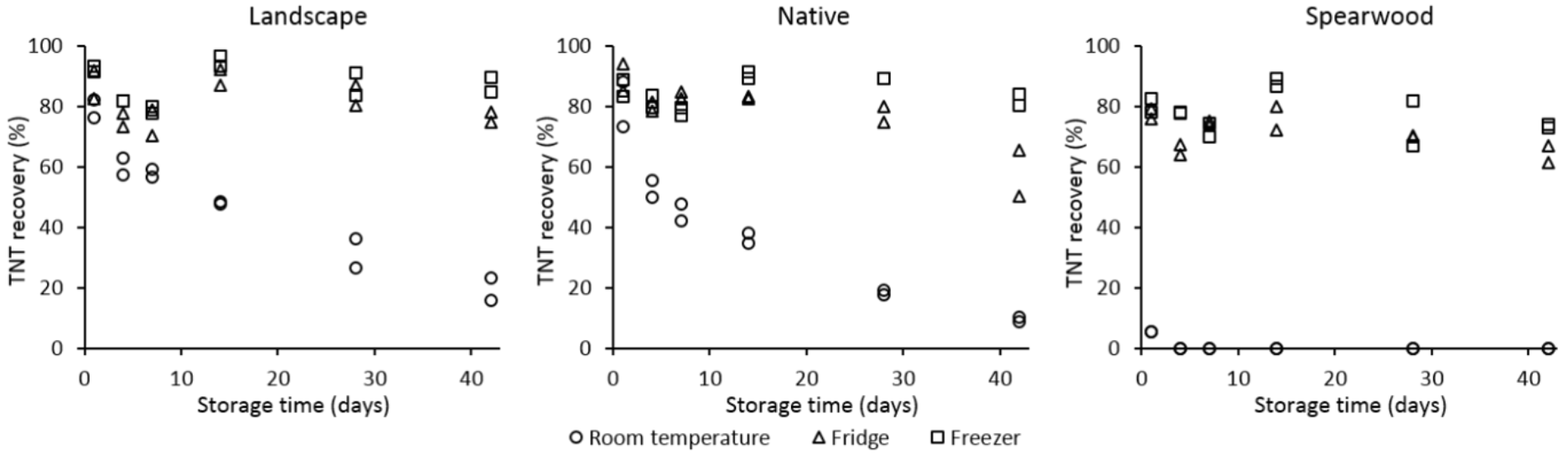

Figure 4.10: TNT recoveries from spiked landscape, native and Spearwood samples, stored at room temperature, refrigerated and frozen and extracted over 42 days

.

Figure 4.10 shows that storing samples containing TNT at decreased temperatures, particularly in a freezer, significantly inhibits the loss of TNT after six weeks, compared to storage at room temperature. Storage at decreased temperatures is believed to lower the rate of metabolism of any contained bacteria, thus slowing the rate of reduction of TNT's nitro groups [10, 95, 98]. It should be noted that for these 'aged' sample sets, the first extraction and analysis time point was one day after spiking. For this reason, no recovery values are plotted for day zero. It is likely that the day zero recovery values would fall in the region of those obtained from the 'Soil extraction study', presented in Figure 4.3.

A comparison of the room temperature results from the three soils indicates that there was a very rapid loss of TNT from the Spearwood samples, with almost complete loss after just one day, whereas the decrease in TNT recoveries proceeded more slowly in the landscape and native soils, with TNT recovery possible after six weeks. It is highly likely that these observed differences in the rate of TNT loss are due to differences in the rate of microbial degradation and transformation of TNT in the different soils. This can be seen by comparing the levels of 4-ADNT recovered from the different soils over six weeks (see Figure 4.11). 4-ADNT is presented, rather 2-ADNT, as 4-ADNT is the major reduction product of TNT, and 2-ADNT the minor reduction product [92, 109, 110]. In the current work, 4-ADNT levels were consistently higher than those of 2-ADNT.

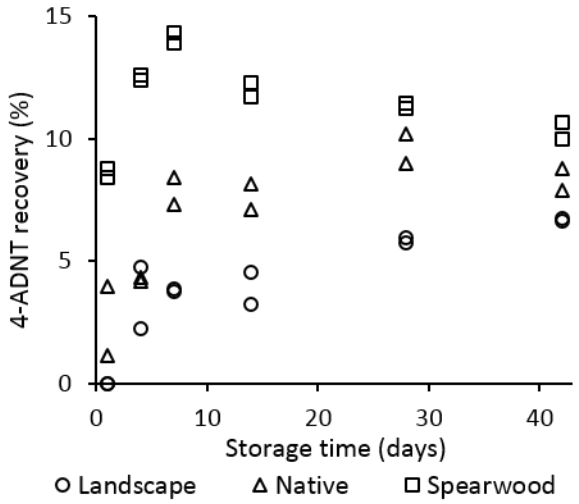

Figure 4.11: 4-ADNT recoveries from spiked landscape, native and Spearwood samples, stored at room temperature and extracted over 42 days

Figure 4.11 indicates that the rate of 4-ADNT formation was lowest in the landscape soil over the six weeks, followed by the native soil, with the highest recoveries from the Spearwood soil. This follows the trend in TNT loss from the three soils. As 4-ADNT is primarily a microbial degradation product of TNT [92, 109, 110], this supports the theory that the majority of the observed TNT loss was due to microbial degradation. Also interesting to note is that by

comparing the percentage of TNT recovered over time against the percentage of 4-ADNT recovered at the same time point, a discrepancy exists, i.e. the sum is less than 100 %. This indicates that another attenuation process or further reduction to the related di- and triaminotoluenes is also occurring. It is also possible that, as discussed earlier, some of the formed 4-ADNT and 2-ADNT may have undergone irreversible covalent binding to the humic acids present in the soils [177], to give a reduction in their overall recovery. Much lower 4- and 2-ADNT levels were observed over time from the samples stored in the fridge and freezer, likely due to the low temperatures preventing microbial activity within the soils.

4.3.4.2 RDX and PETN

Figure 4.12 displays RDX (top row) and PETN (bottom row) recoveries from the same set of landscape, native and Spearwood samples. RDX recoveries remained fairly consistent over time from all of the respective soil samples, with little variation across the range of storage temperatures. However, in all samples, even after one day, the RDX recovery is only approximately half of the initial quantity spiked into the soils. As demonstrated by the soil extraction study detailed earlier (see Figure 4.3), almost quantitative RDX recoveries were obtained. This suggests that some initial adsorption or transformation has occurred during the first day of sample storage. Previous authors have proposed interactions between RDX and minerals present within the clay fraction of soil. These include RDX undergoing hydrogen bonding between its nitro groups and surface hydroxyl groups in soil [93, 96], as well as van der Waals interactions [96]. These interactions may contribute towards the observed reduction in RDX recoveries. It can also be seen from Figure 4.12 that some fluctuations are present in the recoveries of RDX and PETN from the respective soil samples, in particular those stored at room temperature. The complex composition of soil [161] means that the individual soil samples used may have had some variations between them, which may have contributed to the observed fluctuations in Figure 4.12.

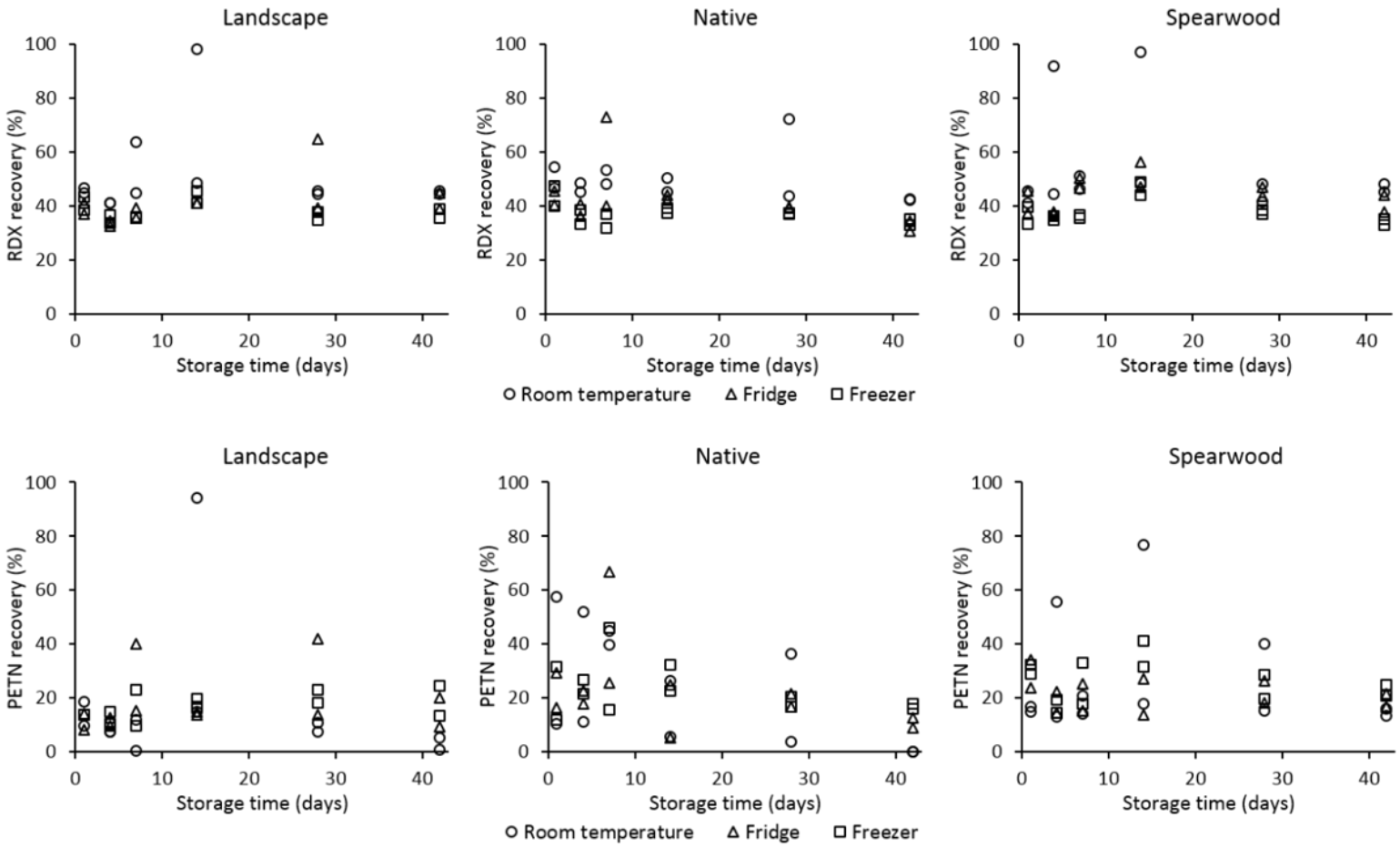

Figure 4.12: RDX (top row) and PETN (bottom row) recoveries from spiked landscape, native and Spearwood samples, stored at room temperature, refrigerated and frozen and extracted over 42 days

PETN recoveries from each soil show broadly the same trends, with PETN levels remaining relatively low and stable over time. As was the case for RDX, low initial PETN recoveries can be seen from each of the samples, again possibly the result of an adsorption process, such as hydrogen bonding of the PETN to soil components, in a similar manner to that proposed between RDX and the soils. As each molecule of PETN has an extra NO_2 group compared to RDX, this may increase the extent of adsorption occurring between PETN and the soils.

Overall, low temperatures have been shown to mitigate TNT degradation, decreasing the rate of formation of the microbial degradation product 4-ADNT. Temperature effects appeared to have a greater influence on TNT recoveries from the soils, compared to RDX and PETN. These results show that the storage of soil samples suspected of containing explosive residues at low temperatures (i.e. frozen) is the most suitable practice for storing soil samples that may contain explosive residues.

4.3.5 Storage under a nitrogen headspace

Nitrogen purging of the spiked soil samples prior to storage was examined to mitigate the biotic degradation and transformation of explosive residues by minimising or eliminating microbial activity in the stored soil samples. The present work allows for an assessment of the degree of aerobic degradation of TNT, PETN and RDX compared to their anaerobic degradation, and whether or not purging samples with nitrogen mitigates aerobic degradation. The recoveries of explosive residues from the nitrogen-purged samples prepared in this work are outlined below.

4.3.5.1 TNT

Figure 4.13 shows the TNT recoveries (top row) from spiked, nitrogen-purged landscape, native and Spearwood soils, in addition to the 4-ADNT recoveries (bottom row) from the respective samples. The results are compared to the previously-discussed room temperature samples under air, with no nitrogen purging.

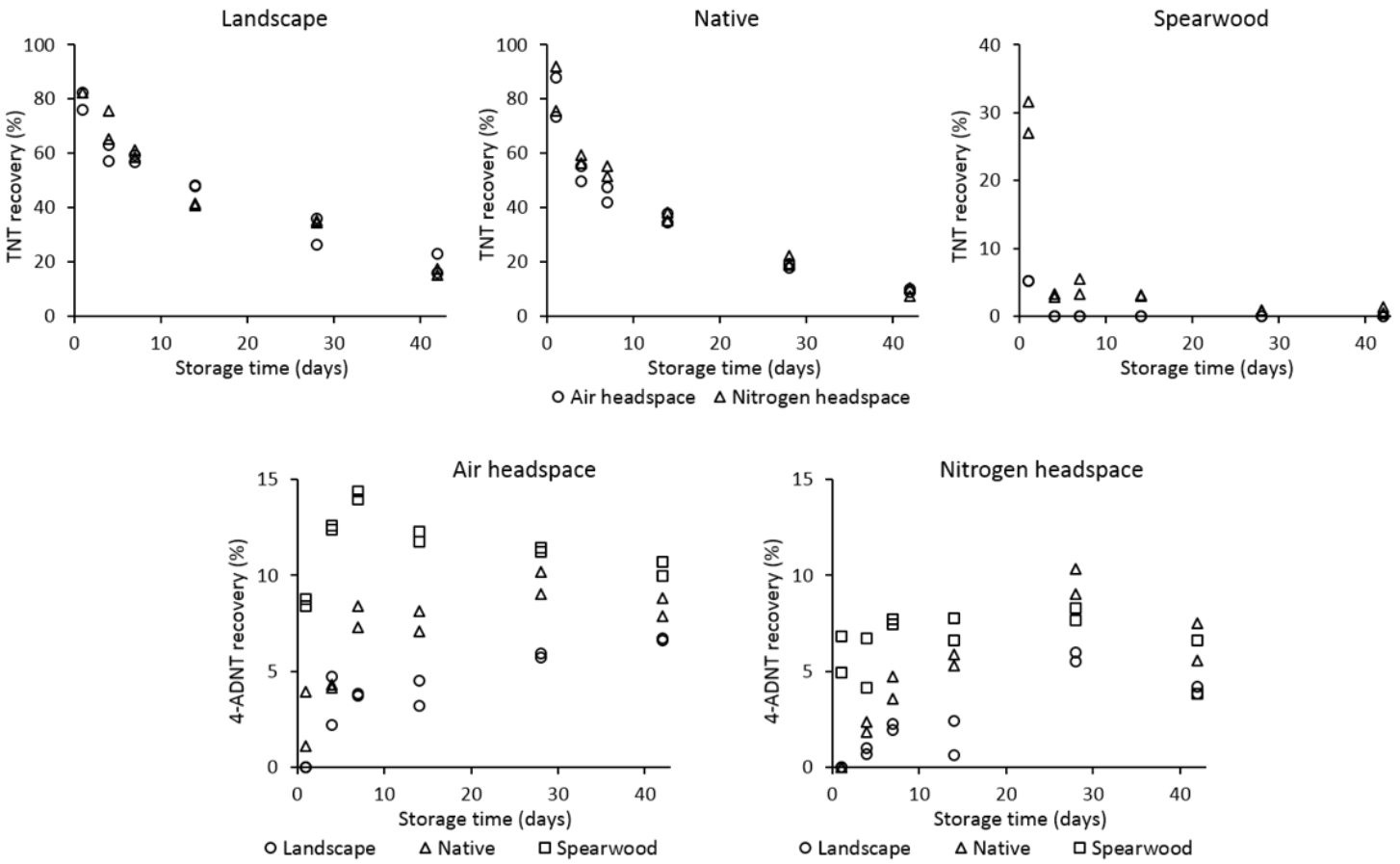

Figure 4.13: TNT recoveries (top row) and 4-ADNT recoveries (bottom row) from spiked then nitrogen-purged landscape, native and Spearwood samples, stored at room temperature and extracted over 42 days. Note the different y-axis scale for the Spearwood samples to more clearly illustrate recovery differences between the nitrogen-purged vs. air headspace samples

.

From Figure 4.13 it can be seen that storage under nitrogen gave only a minor improvement at best for TNT recoveries, with the level of recovered TNT over time comparable to that from the comparative samples stored under air.

Overall, the slight increase in TNT recoveries from the nitrogen-purged samples suggests that the nitrogen headspace has had some effect on aerobic microbial degradation and transformation processes. In particular, an enhancement of TNT stability can be seen from the Spearwood soil samples, with recoveries still possible after 14 days when stored under a nitrogen headspace, rather than the one day following storage under the more typical air headspace. However, as the TNT levels still decreased over time from each soil, and 4-ADNT formation was observed over time from the nitrogen-purged samples, anaerobic microbial degradation processes have still occurred.

4.3.5.2 RDX and PETN

Figure 4.14 displays RDX (top row) and PETN (bottom row) recoveries from landscape, native and Spearwood samples after nitrogen purging. The results are compared to the previously discussed room temperature samples under air, with no nitrogen purging.

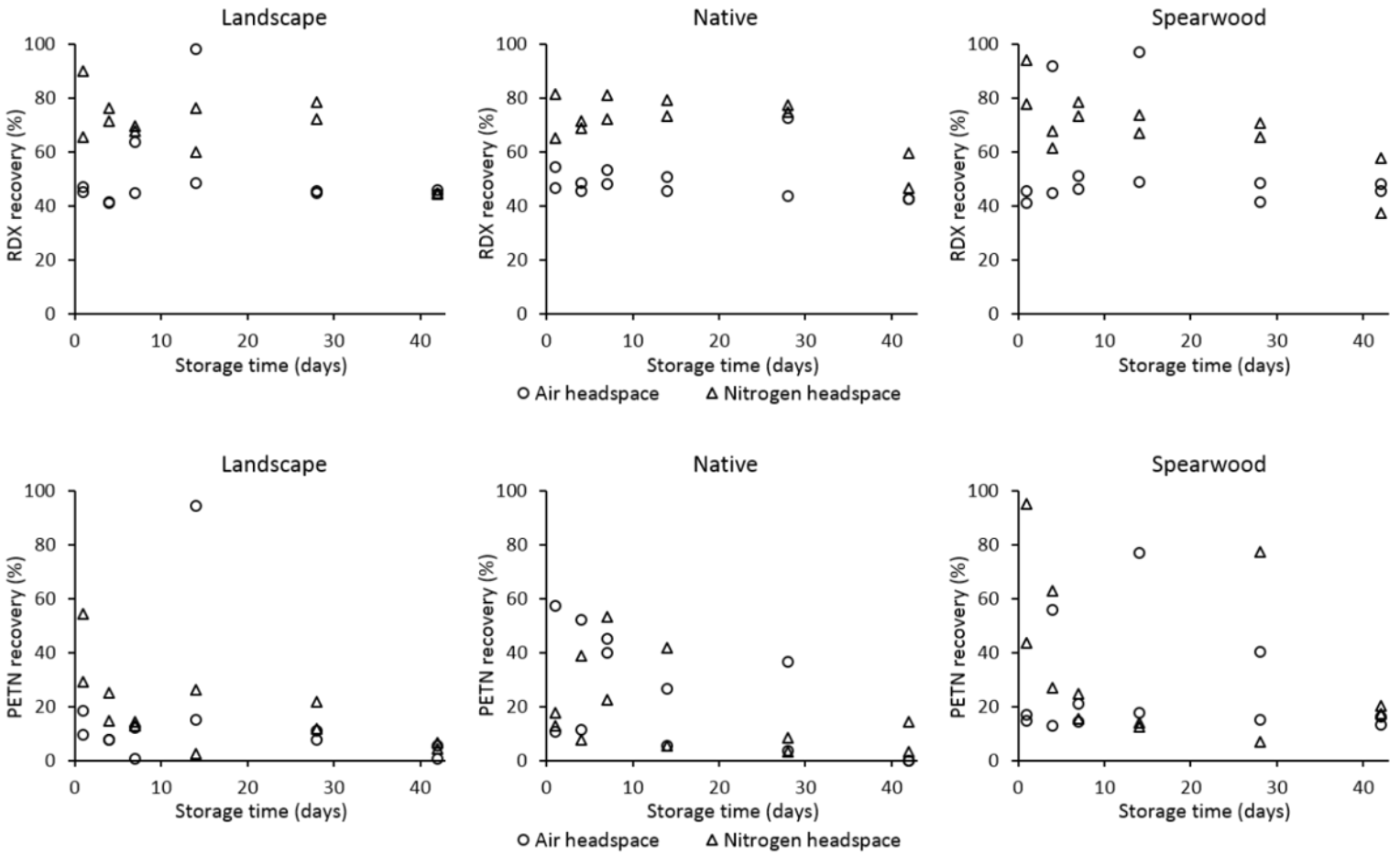

Figure 4.14: RDX (top row) and PETN (bottom row) recoveries from spiked then nitrogen-purged landscape, native and Spearwood samples, stored at room temperature and extracted over 42 days

.

Whereas nitrogen purging appeared to only give a small difference in the recoveries of TNT, it can be seen from Figure 4.14 that storage under nitrogen appears to have had a much more pronounced effect on RDX recoveries, with significantly higher RDX recoveries across the majority of the time points from the nitrogen-purged samples when compared to the comparative samples stored under air. This suggests that the nitrogen purging is useful in mitigating aerobic RDX degradation. As was the case for Figure 4.12, it can be seen that some fluctuations are present in the recovered RDX and PETN levels, which may be due to slight variations in the composition of the individual 5 g soil samples used.

With regards to PETN, it can be seen from Figure 4.14 that for each condition, the recoveries of PETN are relatively low over time, with the initial day one recoveries significantly lower than the recoveries from the soil extraction studies (see Figure 4.3 and Figure 4.4). This may be due to an initial adsorption phenomenon occurring between the PETN molecules and soil constituents. As was the case for RDX, higher PETN recoveries can be observed from the nitrogen-purged samples compared to the control group, suggesting that a nitrogen headspace may be slowing the rate of anaerobic bacterial degradation.

4.3.6 Storage following gamma irradiation

The use of soil sterilisation as a means of mitigating explosive residue degradation has been explored by a number of researchers [88, 93, 94, 96, 104, 108, 182], with these studies demonstrating that soil sterilisation is a useful technique to mitigate the microbial transformation or degradation of explosive residues. Though soil sterilisation can only target the biological aspect of transformation by eliminating bacteria present in the soil, rather than preventing abiotic transformations from occurring, soil sterilisation may have the potential to be a useful technique for prolonging the stability of explosive residues in soil.

Importantly, it should be noted that for all of the studies cited above, the soil samples were sterilised *prior to* the addition of explosives. No studies can be found in which soil *already* containing explosives was sterilised, and the transformation of the explosives monitored, which is more representative of a real-life situation. For this reason, in the present work, investigations into the effect of sterilisation on the stability of any explosives present were performed, as an assessment of the viability of soil sterilisation in limiting explosive losses is critical.

McNamara *et al.* [183] assessed the chemical and biological effects of gamma irradiation on soils during the sterilisation process. The authors outline that the mechanism of soil sterilisation can be either direct, where ionisation causes damage to bacterial cell DNA, or indirect, where bacterial cellular water undergoes radiolysis to form H, OH and HO_2 radicals,

which may promote breakages in bacterial DNA strands. The authors suggest that a 70 kGy irradiation dose should be sufficient to kill the vast majority of bacteria, including radio-resistant bacteria, though the review also reports that a side-effect of such an irradiation dose may be short-term temperature increases of up to 60 °C. McNamara also mentions that enzymes are less susceptible to bacteria, meaning that even if bacteria are killed using gamma irradiation, their intracellular enzymes may still remain and show activity within soils. The explosive residue recoveries from the gamma-irradiated samples prepared in this work are outlined in the following section.

4.3.6.1 TNT

Figure 4.15 compares the TNT (top row) and 4-ADNT (bottom row) recoveries obtained from the previously-discussed non-irradiated room temperature samples and gamma-irradiated landscape, native and Spearwood samples stored at room temperature and extracted over six weeks.

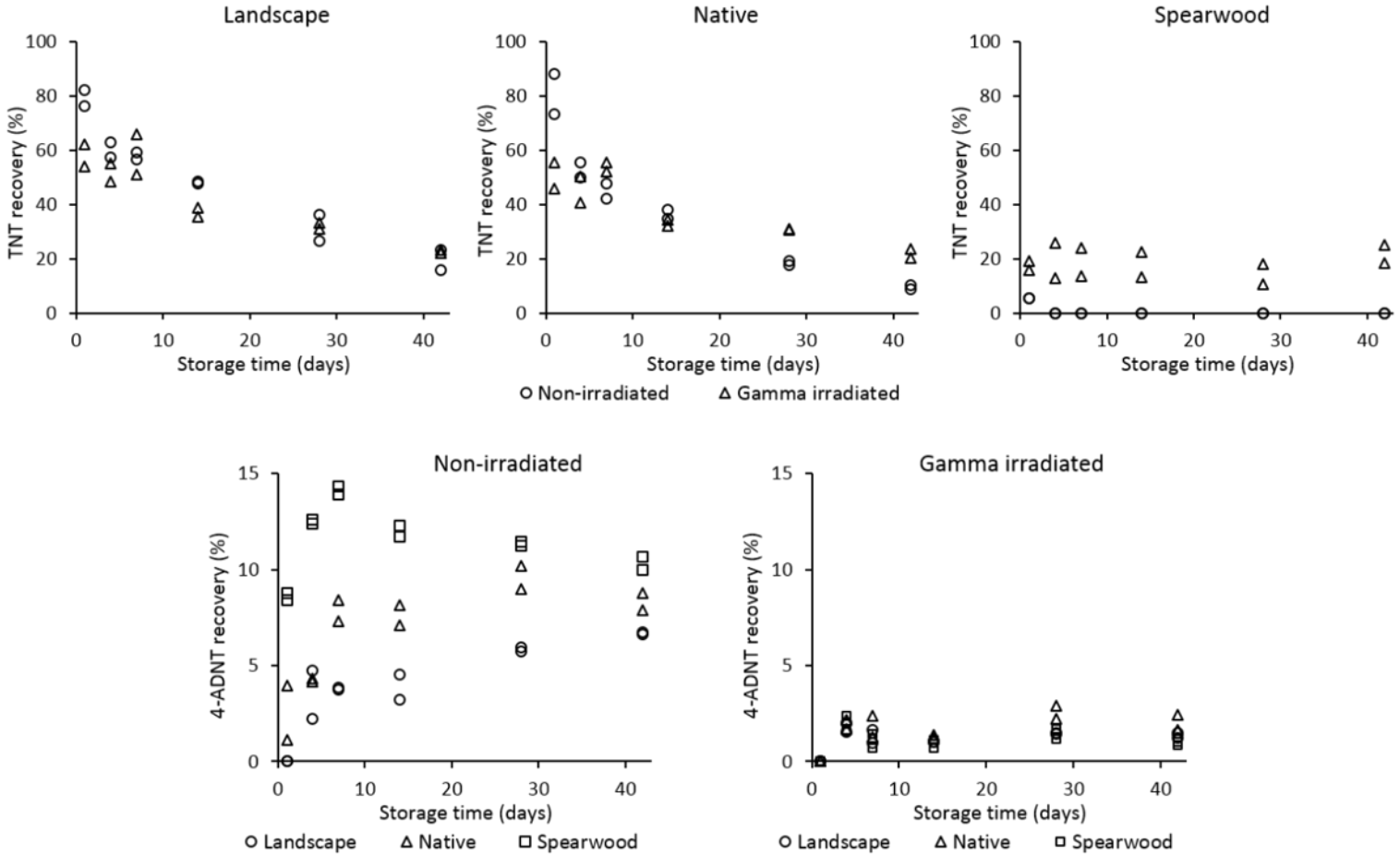

Figure 4.15: TNT (top row) and 4-ADNT (bottom row) recoveries from spiked then gamma-irradiated landscape, native and Spearwood samples, stored at room temperature and extracted over 42 days

.

From Figure 4.15, similar trends can be observed from the landscape and native soils, with the rate of TNT loss from the gamma-irradiated samples slower than from the non-irradiated comparative samples. It is interesting to note that the irradiation process appears to have reduced the day one TNT recoveries from the landscape and native soils, compared to the non-irradiated samples. This suggests that the gamma irradiation process has caused the degradation of a significant proportion of the TNT in the landscape and native soils. In the present work, the soil samples contained 20 % water *w/w* at the time of irradiation. This water may therefore have undergone radiolysis during the irradiation process to form radical species [183], which may have reacted with the TNT within the samples. Similarly, as the irradiation process is also likely to cause a temperature increase within the samples [183], this may have reduced the required activation energy of the nitroreductase enzymes of any bacteria in the soil [184, 185], giving a faster rate of TNT transformation and thus a reduction in the day one TNT recoveries following the gamma irradiation. Although the rate of TNT loss is slowed in the gamma-irradiated landscape and native soil samples, there is still a low but detectable drop in TNT levels over time. Ruling out any possible biotic explanation, this is attributed to abiotic processes such as adsorption to organic carbon and mineral surfaces in clay.

The Spearwood samples display a very different trend from the landscape and native soils. TNT recoveries over six weeks remain stable - in contrast to the TNT recoveries from the irradiated landscape and native samples, where TNT levels slowly decreased over time. If the TNT loss in the gamma-irradiated samples was solely a function of the gamma irradiation, then it would be expected that identical proportions of TNT would be lost from each of the soils. However, the widely differing day one TNT levels observed following the gamma irradiation suggests that this loss has a dependence on a property inherent to the soil itself; potentially the level of bacteria present in the soil.

If the Spearwood soil contained higher bacterial populations than the landscape and native soil (as suggested by 4-ADNT recoveries presented earlier), then this would result in a larger proportion of the TNT being transformed, and thus lower initial TNT recoveries, which was observed. However, following the completion of the cumulative gamma irradiation process, all of the contained bacteria will have been killed, and it is likely that this has caused the stable TNT levels observed in the irradiated Spearwood soil samples.

Figure 4.15 also shows a side-by-side comparison of 4-ADNT recoveries over time from non-irradiated compared to gamma-irradiated samples. As before, the reported recoveries of 4-ADNT are given as a percentage of the initial quantity of TNT spiked into the soils indicating the percentage conversion via reduction of the TNT to 4-ADNT at a given time point.

Significant differences are observed, with the levels of 4-ADNT in the gamma-irradiated samples remaining low and relatively constant over time, indicating the irradiation process was successful in killing all of the bacteria in the soils. The low levels of 4-ADNT observed in the three gamma-irradiated soils may have formed during the early stages of the 16.3 hour irradiation process, as the applied radiation is cumulative and thus the 70 kGy dose required to ensure the complete eradication of all of the contained bacteria would only have been reached by the very end of the irradiation time, indicating that there would have been the opportunity for any bacteria present to begin TNT transformation during the early stages of the irradiation process. In addition, the irradiation process generates heat, which may assist in catalysing the TNT reduction process to form 4-ADNT. As the levels of 4-ADNT remain stable over time following irradiation, this lends strong support to the notion that 4-ADNT formation within the soils can solely be attributed to microbial action, rather than abiotic reduction processes.

4.3.6.2 RDX and PETN

Figure 4.16 displays the RDX (top row) and PETN (bottom row) recoveries obtained from non-irradiated room temperature samples and gamma-irradiated samples extracted over six weeks.

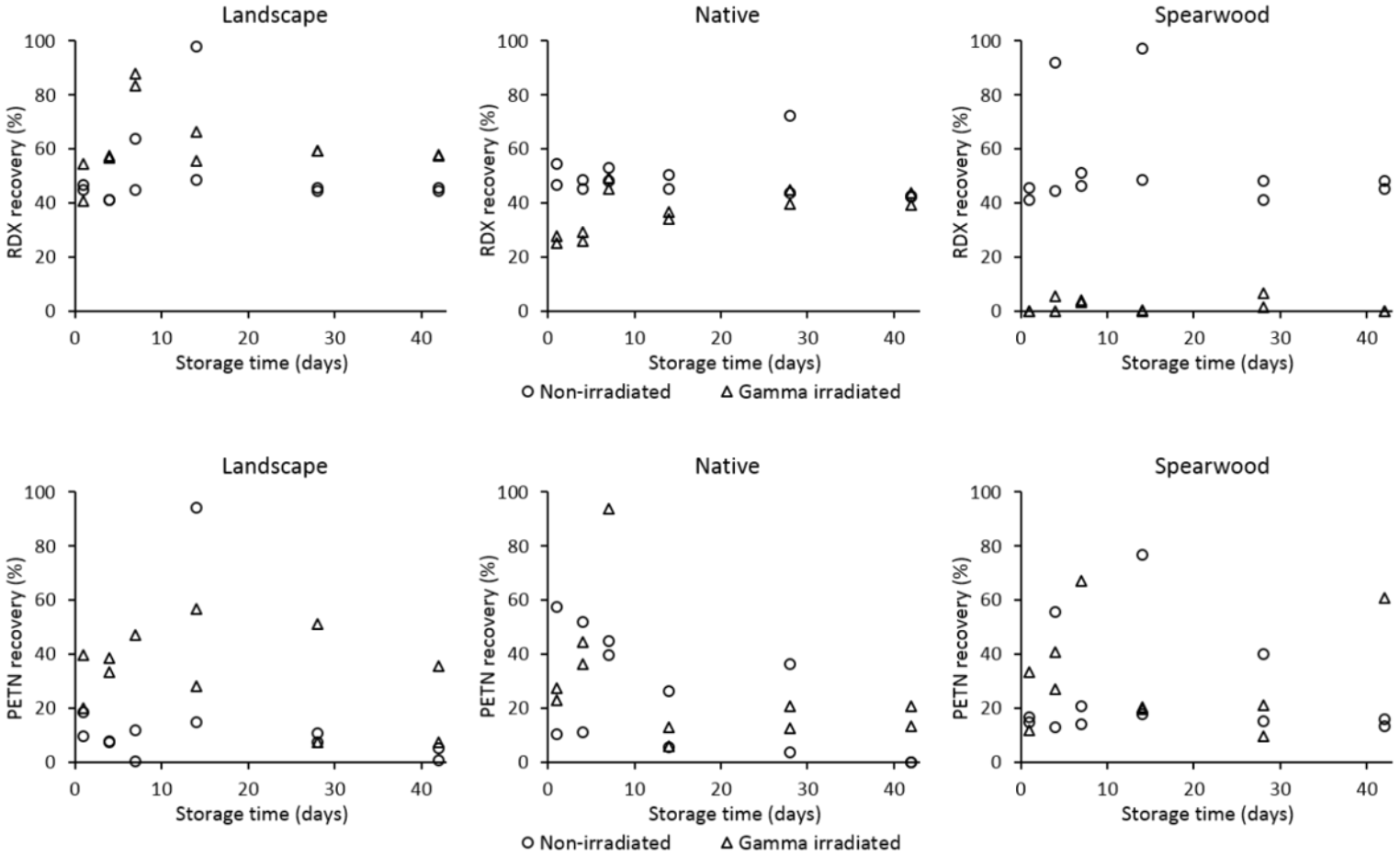

Figure 4.16: RDX (top row) and PETN (bottom row) recoveries from spiked then gamma-irradiated landscape, native and Spearwood samples, stored at room temperature and extracted over 42 days

For the landscape soil samples higher RDX recoveries were obtained from the gamma-irradiated samples at each time point compared to the non-irradiated samples. In contrast, for the native soil samples, the opposite trend is observed, with the gamma irradiation process appearing to have had a more detrimental effect on RDX present within the native soil samples, compared to the landscape soil.

Similarly, the gamma irradiation process had a significant effect on RDX recoveries from the Spearwood samples. This phenomenon was also observed for the TNT recoveries from this soil, supporting the view that a property of the soil is responsible for this discrepancy. Intriguingly, the RDX recoveries from the gamma-irradiated Spearwood samples have become almost negligible at each sampling time point. It is hypothesised that the low RDX recoveries from the irradiated Spearwood samples can be attributed to higher levels of bacteria within the soil compared to the landscape and native soils.

The gamma-irradiated samples broadly show stable PETN recoveries (Figure 4.16), with the gamma-irradiated samples generally giving no clear advantage or disadvantage for PETN recoveries over the non-irradiated comparative samples. The slight discrepancies in the recoveries of RDX and PETN are likely due to slight variations in the composition of the individual soil samples used throughout this work.

From the results presented here, it is clear that gamma-irradiating samples can have a severely detrimental effect on any explosive residues contained within a sample. This is the first known piece of work where soils have been sterilised after spiking with explosives, and the results have clearly shown that although in the case of samples containing TNT, gamma irradiation can prevent the formation of microbial degradation products, it can give detrimental results for samples containing RDX. It is therefore not a viable technique to stabilise explosive residues present in soil samples as the nature of explosive residues present in a soil sample is likely to be unknown prior to extraction.

A number of extra peaks were observed in all of the HPLC chromatograms of the gamma-irradiated samples which were not observed in any of the non-irradiated or nitrogen-purged samples. These peaks suggest the gamma irradiation process promotes a different explosive residue transformation pathway compared to that of the non-irradiated and nitrogen-purged samples. These extra peaks occurred across all of the three soils used during the gamma irradiation studies. An example chromatogram containing these extra peaks (labelled a-f) is provided in Figure 4.17, along with UV-Vis spectra in Figure 4.18 for the six peaks labelled a-f.

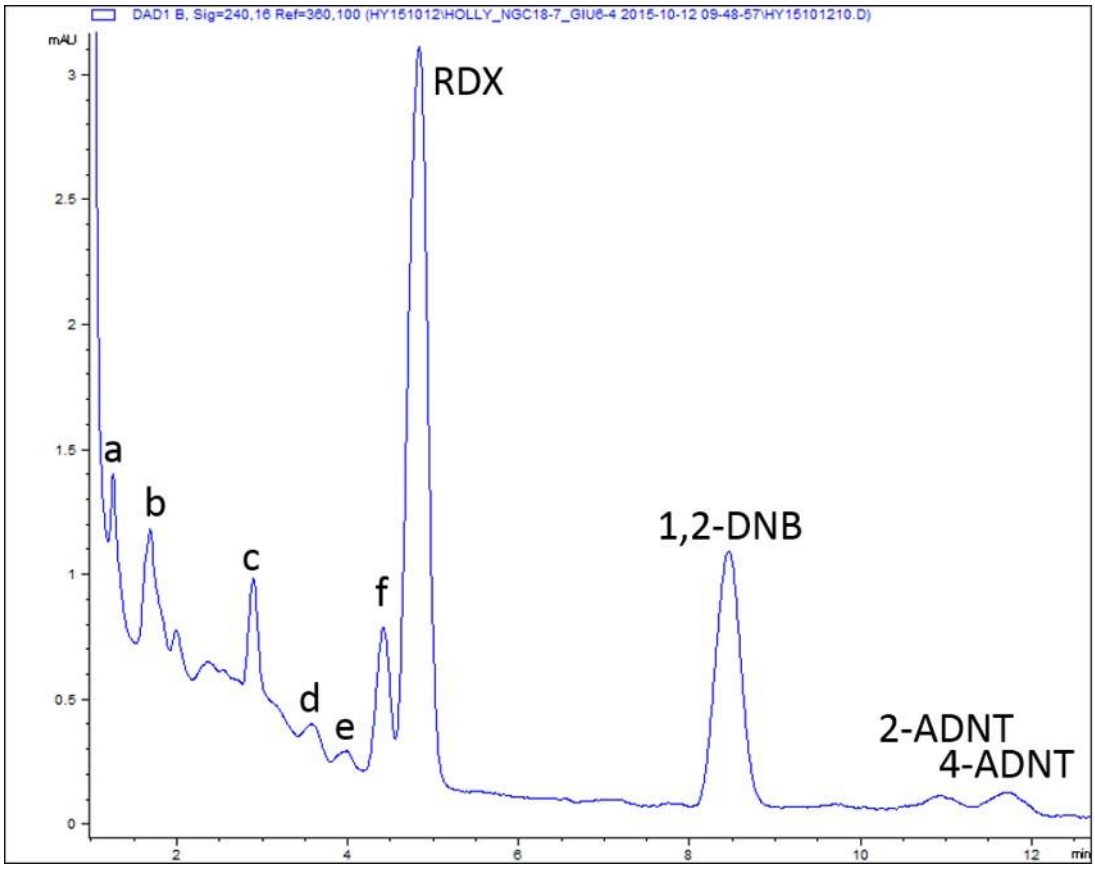

Figure 4.17: Section of chromatogram displaying six extra unknown peaks (labelled a-f) from a gamma-irradiated soil sample. Chromatogram was obtained using an Agilent Zorbax Extend-C18 5 µm 4.6 mm × 150 mm column. A flow rate of 1.6 mL/minute was used with a total run-time of 22 minutes. The following mobile phase sequence was used: 0-11.5 minutes, 28:72 acetonitrile:water; 11.5-13 minutes, ramp to 50:50 acetonitrile:water; hold for 4 min; 17-18.5 minutes, decrease to 28:72 acetonitrile:water; hold for 3.5 minutes until end of run, with a constant column temperature of 40 °C

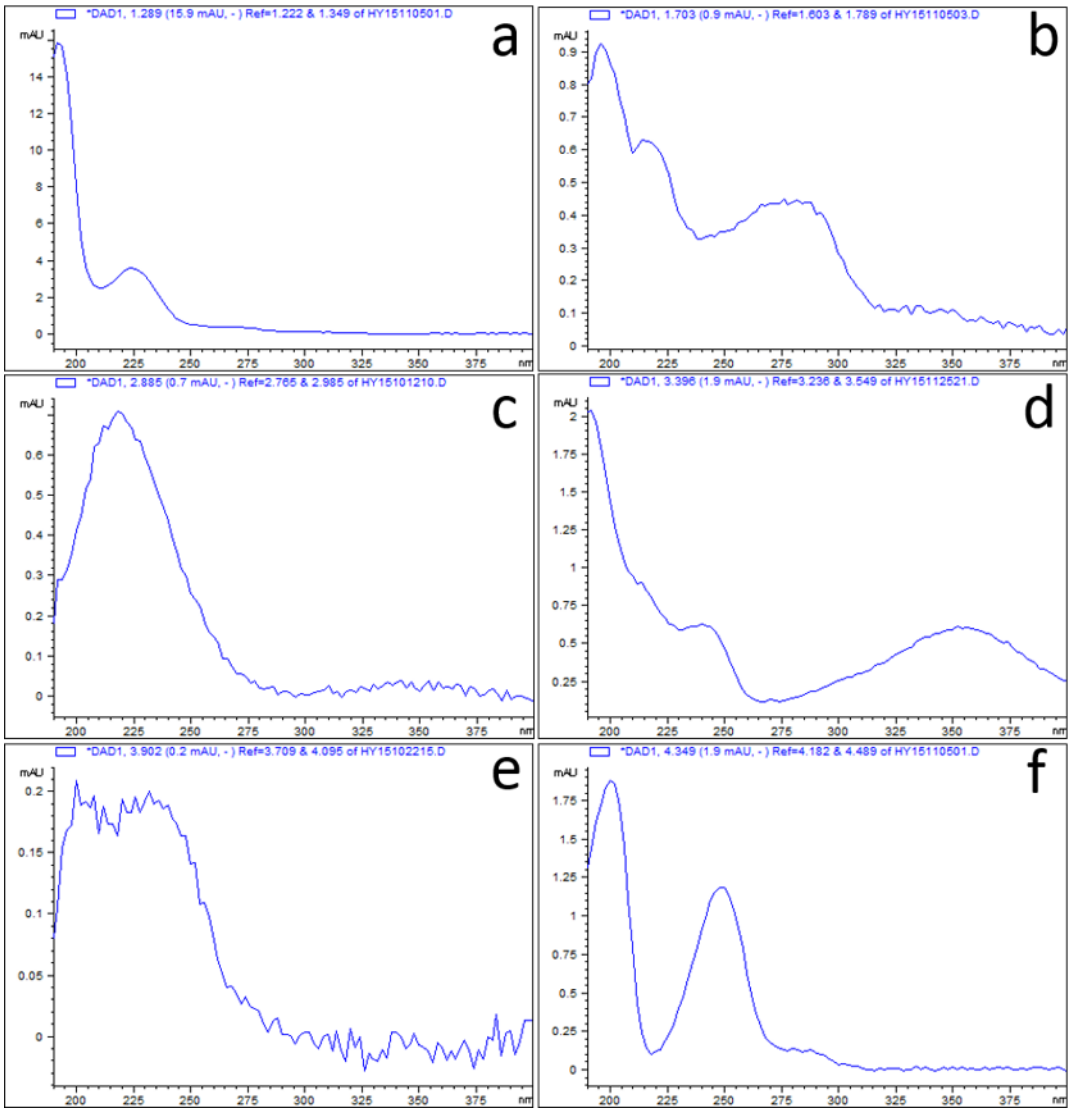

Figure 4.18: UV-Vis spectra of unknown compounds a-f from gamma-irradiated samples. UV-Vis spectra were extracted from a chromatogram obtained using an Agilent Zorbax Extend-C18 5 µm 4.6 mm × 150 mm column. A flow rate of 1.6 mL/minute was used with a total run-time of 22 minutes. The following mobile phase sequence was used: 0-11.5 minutes, 28:72 acetonitrile:water; 11.5-13 minutes, ramp to 50:50 acetonitrile:water; hold for 4 min; 17-18.5 minutes, decrease to 28:72 acetonitrile:water; hold for 3.5 minutes until end of run, with a constant column temperature of 40 °C

It is known that RDX can undergo reduction to its mono-, di- and tri-nitroso derivatives, so it is possible that three of these new peaks correspond to these nitroso derivatives. No UV-Vis spectra for these compounds could be found in the literature, meaning it is not possible to definitely assign specific peaks to these three compounds. It is possible that this could be achieved using a mass-spectral based technique such as LC-MS.

Two new peaks were observed across a very small number of nitrogen-purged samples, indicating possible degradation or transformation products. These peaks typically had a very

low intensity and gave rise to very poor-quality UV-Vis spectra (not shown), so it was difficult to determine their origin.

4.4 Conclusions

This work has shown that different explosives may have different degradation and transformation pathways in soils, and the fate of explosive residues in soil also has a strong dependence on the nature of the soil itself. From assessing the rate of 2- and 4-ADNT formation in the different soils used during this work, it appears that the populations of bacteria in the soils increase in the order landscape < native < Spearwood. For TNT in particular, in the Spearwood soil, a very rapid rate of degradation was observed at room temperature and therefore represents the 'worst-case-scenario' which this work aims to prevent from occurring. Generally, lower PETN recoveries were observed compared to the recoveries of RDX. This may be due to PETN being more susceptible to reduction of its nitro groups compared to RDX.

An enhanced TNT stability was observed over time from soil samples stored at lower temperatures, particularly those stored in the freezer, compared to samples stored at room temperature, so all soil samples suspected of containing explosive residues must be stored at low temperatures prior to analysis. Nitrogen purging of explosives-spiked soil samples in some cases enhanced stability of the explosives assessed in this work. Results relating to the use of gamma irradiation were dependent upon the type of soil used, in addition to the type of explosive. For example, a very large attenuation of the initial TNT and RDX levels was observed in the gamma-irradiated Spearwood soil samples, compared to the landscape and native soils.

To investigate whether it is solely the high temperatures of the gamma irradiation (in conjunction with the respective bacterial loadings of the soils) responsible for the observed large losses of TNT and RDX following gamma irradiation, or whether this observed decrease also has a dependence on any radical ions formed during the gamma irradiation process, one possible method of exploring this would be to prepare a further set of samples and store them at elevated temperatures (in the short term) to mimic the initial temperature increase occurring during the gamma irradiation process. The samples could then be stored at room temperature for six weeks, analogous to the samples presented here. If temperature (in combination with bacteria present in the soils) were the main cause of the losses, then the results should mirror those displayed here for gamma irradiation. However, if the presence of radicals was also necessary to bring about such a dramatic decrease in the levels of TNT and RDX, then a difference would likely be observed in the recoveries over time.

Related to this, additional future research should investigate gamma irradiating dry, spiked

soil samples, to understand whether an enhanced stability of the explosive residues was obtained. The primary mechanism for the success of gamma irradiation to kill soil bacteria is via the formation of radical species, such as from the radiolysis of water, to damage bacterial structures and DNA. However, in the present work, soil samples were spiked using an aqueous solution of explosives, meaning an excess of water was present, which could have undergone radiolysis to form a very large number of radical species which may have contributed towards the degradation of the contained explosives. Therefore, if this was the case, then a reduced rate of explosive degradation may be seen in spiked drier, gamma-irradiated soils. On the other hand, drying soils before irradiation may lead to the loss of any volatile explosive residues present. Freeze-drying spiked soils and then assessing explosive residue recoveries would also be an interesting piece of future research.

Finally, it is acknowledged that in the present work, soils were spiked using solutions of explosives, which may not perfectly represent explosive residue loading to soils using an actual detonation process. Chapter 5 therefore extends this chapter's research and compares the degradation rates of the explosives from solution-spiked soil samples with those from the same soils spiked using actual detonations.

Chapter 5 An investigation into the stability of explosives deposited into soils using a detonation process

5.1 Introduction

As discussed in Chapter 4, previous research has investigated the stability of explosives in soils by spiking pristine soil samples with solutions of explosives [10, 77, 78, 83, 85, 92-108]. In contrast, comparatively little research has been undertaken to examine the fate of explosive residues deposited in soil following an actual detonation process. The detonation process may alter the degradation rate of the explosive compound once deposited into the soil. Further research examining the degradation process of explosive residues in soil samples collected post detonation is therefore crucial to determine the optimal sample collection and storage procedures to ensure the highest possibility of recovery of any deposited explosive residue.

To date, limited literature exists regarding the loading of explosive residues onto soils using a controlled detonation process. Early work by Oxley *et al.* [77] reported controlled detonations of TNT over soil by detonating a TNT charge 60 cm above a tray of soil. 5 g samples of soil were taken and stored at room temperature, monitoring the degradation over 96 days. These experiments involved a poorly-functioning device leading to very high levels of TNT deposition into the soils (approximately 80 mg in each 5 g soil sample), and a very long TNT half-life was observed, potentially due to such high levels of TNT causing a toxic effect towards any TNT-degrading bacteria within the soils.

Following this, Douglas *et al.* [100] buried Composition B (containing TNT, RDX and HMX) in three different blank soils, before detonating the explosives and storing the resulting explosives-fortified soils as slurries (often referred to in the literature as aqueous batch samples [100, 101, 107]) to simulate explosive residue runoff from contaminated sites into groundwater, analysing the samples periodically. The authors proposed that it is likely that a detonation event creates fresh mineral surfaces within soils (termed soil fracturing), due to shock forces from the detonation which shatters the soil particles, and that these fractured surfaces may induce a faster rate of explosive residue degradation. However, these Composition B trials did not specifically look for any evidence of soil fracturing.

Douglas *et al.* later investigated this hypothesis by comparing the degradation rates of

explosive residues in fractured and non-fractured (pristine) soils [101]. The authors dried three soil samples at 100 °C for 24 hours, before crushing subsamples of the different soils using a piston, to simulate detonation-induced fracturing. Scanning electron microscopy (SEM) analysis of the soils revealed the presence of newly-fractured surfaces. Both fractured and pristine soil samples were then spiked with solutions of TNT, RDX, HMX and 2,4-DNT, and excess water added to form slurries, before being analysed periodically. The explosive residues showed a greater decrease in concentration over time in the supernatant of the slurries formed from fractured soils than those formed from the pristine soils. This finding is important as the majority of previous work investigating the degradation of explosive residues in soils used pristine, non-fractured soil, so conclusions drawn using pristine soil may not be applicable to fractured soils.

Douglas *et al.* [101] provided a suggestion for the explosives' more rapid loss in fractured soil. Analysis of the soils following the fracturing showed morphological changes such as more angular surfaces, finer particles and microfracturing. These fresh mineral surfaces and microparticles are known to be more geochemically active than weathered surfaces, with organic compounds displaying a greater affinity for fresh surfaces [186, 187]. The authors argued that enhanced nitramine and nitroaromatic adsorption and transformation were likely to have occurred on these fresh surfaces, resulting in a greater loss over time compared to the pristine soils.

As this soil fracturing had been performed using a piston, rather than a detonation process, Douglas *et al.* also performed experiments where pure mineral phases were fractured by the detonation of explosives [107]. Similar evidence of fracturing was observed from these trials, suggesting that soil fracturing can indeed occur when an explosive charge is detonated when in contact with soil. In these studies [100, 101], slurries were formed from the explosives-spiked soils, and the fate of the explosive residues was monitored over time. The samples can therefore be thought to represent explosive residues leaching into groundwater, meaning the results may be more applicable for long-term bioremediation research of contaminated soil, rather than the preservation of explosive residues in drier, post-explosion soils. Additionally, by drying samples of the soils at 100 °C [101], the authors are likely to have substantially reduced any dormant microbiological activity within the soils [188]. Based on these observations, further research into the fate of explosive residues in fractured soil would be beneficial.

This chapter examines the fate of explosive residues in detonation-spiked soil samples that are more representative of those collected from the vicinity of vehicle bombings. In a vehicle bombing, it is unlikely that any explosives used would be in contact with the soil beneath the

car at the time of detonation, as a gap would be present between the explosives and the soil. Oxley's setup [77], in which a charge was suspended a short distance (60 cm) over a layer of soil, can therefore be thought to represent a simulated car bombing. Alternatively, detonating a charge in contact with soil, such as in Douglas *et al.*'s work [100], is more representative of a landmine detonation. Although Douglas reported evidence of soil fracturing from these simulated landmine detonations, Oxley *et al.* did not investigate whether or not soil fracturing had occurred in their simulated vehicle bombing setup. For this reason, the first aim of this work was to assess whether explosives must be detonated in contact with soil to induce fracturing, or whether fracturing could also be induced using explosives detonated a short distance above soil (such as in a vehicle bombing).

The majority of work looking at the degradation of explosive residues in soil has used TNT, RDX and HMX [77, 100, 101, 107]. In contrast, little is known about the degradation of PETN in soil [79]. An additional aim of this work was therefore to investigate the soils spiked with PETN, a common organic explosive found in military explosives and commercial detonators. This involved preparing a number of detonations with soil samples collected and stored under various conditions, then analysed periodically. Pentex D boosters, containing TNT and PETN, were used as the explosive charge. This work will provide insight into the stability of PETN in soil samples, to determine whether this is a suitable explosive to monitor post blast. Rather than storing the soils as aqueous batch samples, as performed by Douglas *et al.*, samples were stored as much drier soil samples, to better represent typical soil samples collected from the vicinity of vehicle bombings. The TNT and PETN recoveries and degradation rates from these experiments are compared to the analogous solution-spiked results presented in Chapter 4.

Results from solution spiked studies (Chapter 4) showed that TNT in particular underwent much more rapid degradation in the Spearwood soil compared to the landscape and native soils. The formation of the TNT degradation products 2-ADNT and 4-ADNT, primarily microbial transformation products, suggested that the differing rates of degradation and transformation observed in the three different soils may have been due to differences in the soils' microbial populations and numbers. However, it is also possible that the physical structure of each soil may have affected the rate of TNT degradation and transformation. Investigation of the soil's physical structures may also enable a comparison to be made between pre- and post-blast soils, to determine what effect a detonation has on a soil's structure. Although previous analysis by scanning electron microscopy (SEM) has been performed to look at the effects of a detonation on the exterior of soil aggregates [101], no work has investigated the effect of a detonation on the internal structure of a soil. An understanding of the internal architecture of the different soils used and exposed to detonations

in this work may allow hypotheses to be drawn regarding the rate and nature of explosive residue degradation and transformation observed. This chapter therefore also examines the effect of a detonation on the internal structure of soil particles. For this, a novel technique, micro computed tomography, was employed.

5.2 X-Ray micro computed tomography (µCT) scanning

Knowledge of the micro-scale properties of soils, such as a soil's pore structure, porosity and pore connectivity, may be useful for understanding the microbiological processes taking place in soil [189]. A number of techniques can be used to investigate these physical properties of soils including gas adsorption methods, permporometry and microscopic analysis of resin-filled thin-sections of soil aggregates [189, 190]. These techniques are time-consuming, and have a major disadvantage in that they may perturb or even destroy the very property (such as pore structure) being measured. Similarly, the techniques can only provide limited data on the structure and distribution of pores [190], instead mainly providing information on pore size.

X-ray micro computed tomography (µCT) scanning is an emerging technique in the area of soil analysis on both a macro- and micro-scale. The technique involves imaging a sample on a rotating stage whilst exposed to X-rays. Although a proportion of the X-rays will be absorbed by the object of interest, with denser regions absorbing a higher proportion of the X-rays, some X-rays will fully penetrate the object and then hit (illuminate) an X-ray sensitive screen. This process is illustrated in Figure 5.1. Materials of higher density or atomic number give rise to brighter pixels in the resulting X-ray images [116, 190]. Photographs of this illuminated screen are taken throughout the sample's rotation within the X-ray cabinet, resulting in the collection of a large number of images detailing an object's interior structure from many angles [114, 189].

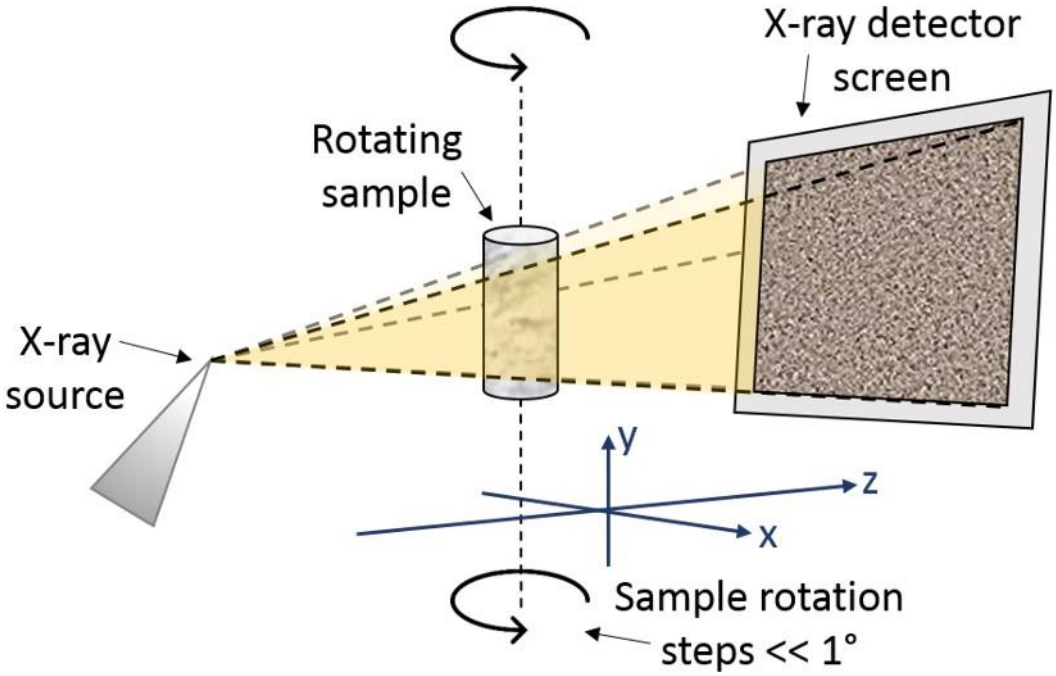

Figure 5.1: Schematic representation of a typical µCT analysis

The resulting series of images can then be reconstructed using an image processing program, to generate a 3D visualisation of the internal structure of the scanned object of interest, as well as stacked 2D images of the object from three different perpendicular viewpoints [189]. For soils, pore space (i.e. air) has the lowest density, followed by water, with mineral components having the highest densities [116]. Figure 5.2 displays images of soils analysed using µCT scanning throughout this thesis. The soil particles depicted in Figure 5.2 measured 1-2 mm in diameter.

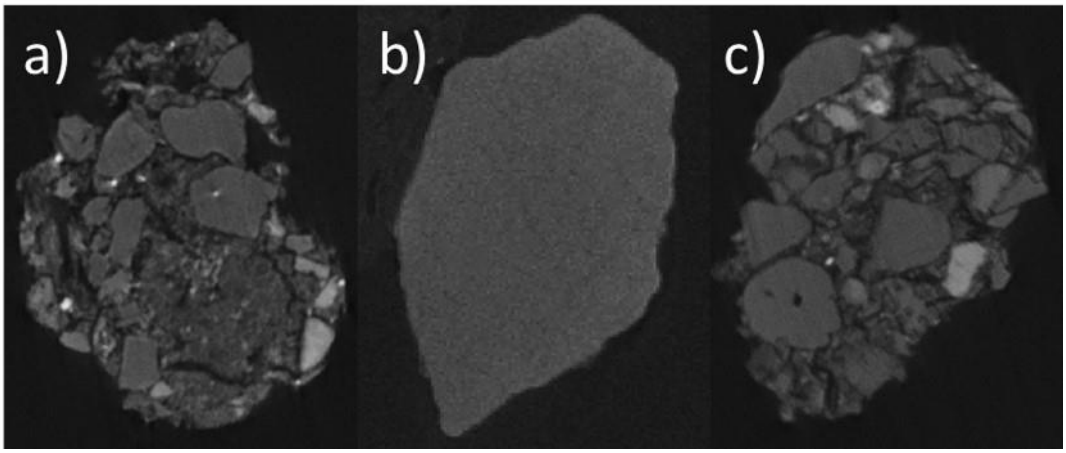

Figure 5.2: Example images of the internal architecture of a) Landscape, b) Spearwood and c) Native soils, obtained using µCT scanning

These high resolution visualisations provide valuable information on the internal architecture of soil aggregates, such as pore size, distribution and connectivity [116, 189, 190]. Such

visualisations can therefore provide insight into the micro-scale habitat of bacteria in soil [116, 190], and may enable pathways to be inferred about the mode of transport and operation of these bacteria. As well as providing valuable information about a soil's internal structure, one of the major benefits of µCT scanning is that it is a non-destructive technique, enabling the properties of soil aggregates to be examined *in situ*, without the risk of any damage [189, 190].

An increasing quantity of research has been directed towards soil analysis using µCT-based methods. Nielsen [114] developed a non-destructive method to analyse soil micro features such as porosity and pore size distribution, focusing on the inter-aggregate properties (i.e. the spacing present *between* soil aggregates in a cylinder filled with dried soil). Several researchers have taken µCT scanning further, to investigate the internal architecture of *individual* soil aggregates, typically sized between 1-5 mm.

Peth *et al.* [115] used Synchrotron-based µCT to quantify the morphological features of the pore networks present in two air-dried aggregates, each approximately 5 mm in diameter. The authors looked at pore size distributions amongst a range of other parameters. Similarly, Nunan *et al.* [116] also used µCT to investigate soil pore geometry. The authors collected soil samples from pasture land which was subjected to three different treatments (control, sewage sludge and biocide treated), and determined the aggregates' porosity and pore shape, with a view to investigate any structural variability of the aggregates due to different microbial habitats.

More recently, a comprehensive study by Akbari *et al.* [190] assessed the role of soil pore size on the biodegradation of hexadecane present in soils. The authors characterised the aggregate's pore size and pore distribution using a combination of µCT and N_2 adsorption techniques, as well as assessing the ability of hexadecane-degrading bacteria to pass through porous membranes bearing different pore sizes. Ultimately, the authors found that hexadecane biodegradation only occurred if pores were 5 µm or larger, concluding that bioaccessible pores had a diameter of > 4 µm. However, to date, no work has been performed using µCT scanning for the analysis of explosives-damaged soils, which is explored in this chapter.

5.3 Experimental: Detonations and degradation experiments

5.3.1 Solvents and chemicals

Acetonitrile (UV grade) was Honeywell, Burdick & Jackson Brand®. 18.2 MΩ cm^{-1} Milli-Q water was obtained from a Sartorius Arium 611VF water purification system. Explosive standards were obtained from LECO Australia, Castle Hill, NSW, and included the following:

PETN, 1000 µg/mL in methanol; 2,4,6-trinitrotoluene, 1000 µg/mL in acetonitrile; 2-amino-4,6-dinitrotoluene, 1000 µg/mL in acetonitrile; 4-amino-2,6-dinitrotoluene, 1000 µg/mL in acetonitrile; 1,2-dinitrobenzene (internal standard), 1000 µg/mL in methanol.

5.3.2 Consumables

50 mL amber glass tall round bottles (24 mm) and white ringseal 24 mm polypropylene screwcaps were obtained from Cospak, Welshpool, Western Australia. 5 mL Luer slip syringes (without needle) were either Nipro Australia or Terumo brand. PTFE membrane 15 mm syringe filters (0.2 µm) were Phenomenex brand. 4.5 L HDPE plastic jars for storing wetted soil samples for the range day trials were obtained from Silverlock Packaging. Ezy Tarp 1.8 × 2.4 m tarpaulins with pegs, Grunt 200 µm black heavy duty builders' film (2 × 20 m) and QiQ-Tidy 55 Litre metal bins were obtained from Bunnings, Western Australia. 25 g Pentex™ D Boosters and Orica Exel™ non-electric detonators were kindly supplied by the Western Australia Police Tactical Response Group – Bomb Response Unit. The same batches of soils were used for these experiments as those used in Chapter 4.

5.3.3 HPLC-UV parameters

Analyses were performed using the same instrument and analytical conditions as described in Chapter 4.

5.3.4 Preliminary detonation trials

Throughout this work, all detonations were performed in conjunction with the Western Australia Police Tactical Response Group – Bomb Response Unit at either Orange Grove Shooting Association, Gosnells, Western Australia, or Wooroloo Prison Farm, Wooroloo, Western Australia. Preliminary detonation trials were performed to determine the most suitable charge position for later experiments and to assess explosive loadings onto soil following a detonation. 2 kg soil samples of the three dried, sieved soils were weighed out into 4.5 L plastic screw-cap bottles. Two bottles were prepared for each of the three soils. Three days prior to the detonations, 100 mL tap water was added to each bottle (with the mass of spiked water equalling 5 % of the total soil mass). Each bottle was then manually tumbled for five minutes until the water appeared to be dispersed evenly throughout the soil. The soils were then stored at room temperature for three days prior to being used. This process has been shown to adequately re-establish microbial activity within soils [95]. For these initial detonations, two conditions were explored: detonations performed over soil, or detonations performed in contact with soil. The procedures for the two conditions are outlined below.

5.3.4.1 Detonations over soil

A new tarpaulin was placed on the ground, and a 2 × 2 m piece of black plastic film placed on top. A 1 × 1 m square was marked in the centre of the black plastic using 1 m lengths of string. The tarpaulin and black plastic film were then secured to the ground using heavy-duty tape. The pre-wetted soil was sprinkled evenly across the black plastic film, ensuring the soil remained within the pre-marked 1 × 1 m area. Using pickets and string, a 25 g booster connected to a detonator was suspended 50 cm above the centre of the square of soil (with the booster placed perpendicular to the plane of the layer of soil), before the charge was detonated. Figure 5.3a shows the typical setup used for a detonation over a layer of soil, with Figure 5.3b illustrating a typical detonation.

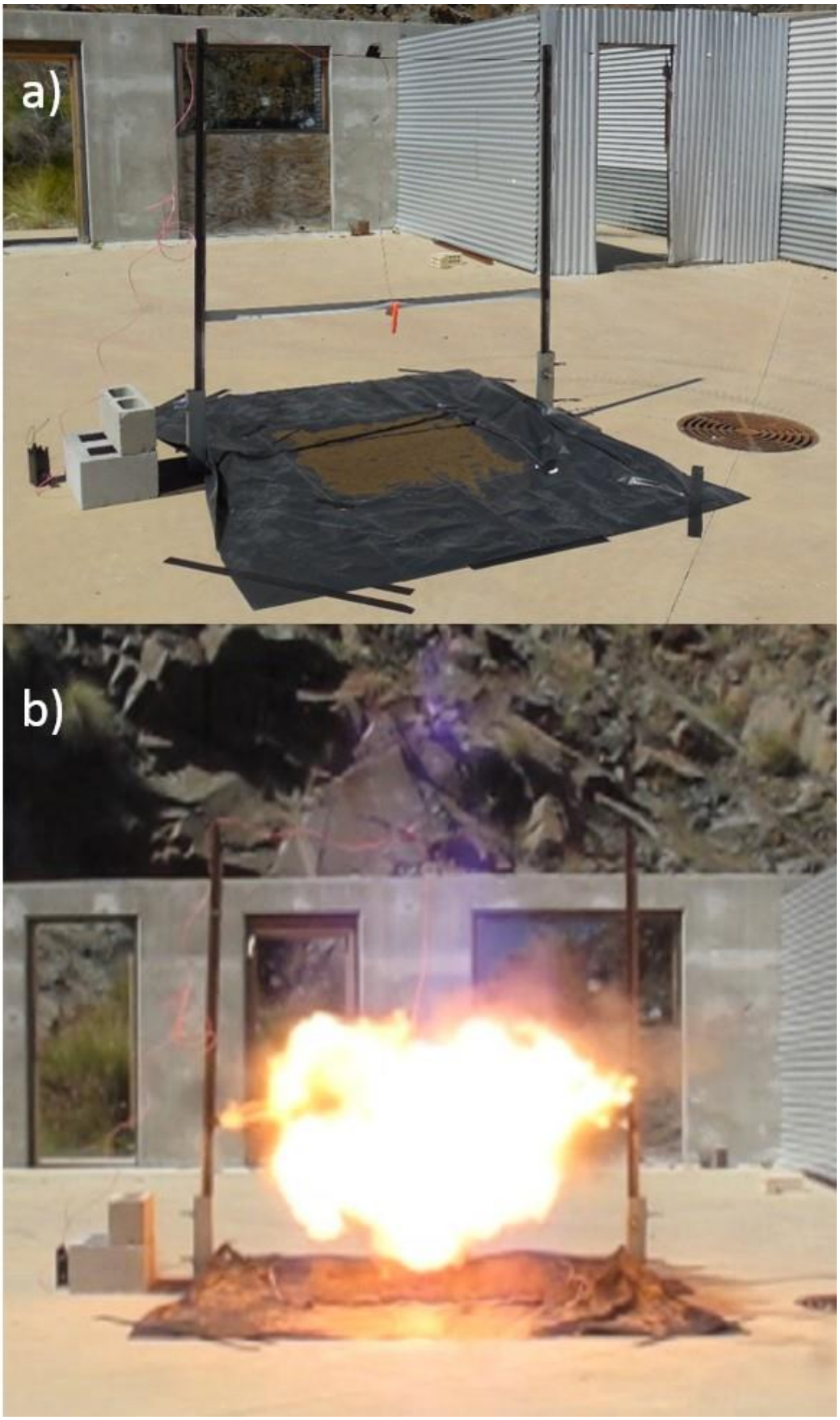

Figure 5.3: a) Photograph of the experimental setup used for detonations over a layer of soil. Orange casing in centre of image contains the explosive charge, and b) Still image from video of a detonation performed over a layer of soil

Following detonation, the post-blast soil was poured back into its original plastic tub prior to transportation to the laboratory for analysis.

5.3.4.2 Detonations in contact with soil

For the initial setup, a new tarpaulin was placed on the ground, and a 2 × 2 m piece of black plastic placed on top. The tarpaulin and black plastic film were then secured to the ground using heavy duty tape. A 55 L metal bin was placed in the centre of the black plastic film, and an additional piece of black plastic film was used to line the bin. Following this, the soil was placed at the bottom of the bin, and the charge, connected to a detonator, inserted approximately 3 cm into the soil. The charge was detonated, and the soil was poured back into its original tub ready for transportation to the laboratory for analysis. The bin lids were not used during the detonations. Following the first such detonation of this type, a slight modification was made for the subsequent two detonations. The bottom two thirds of the bin was filled with bricks and then lined with black plastic film, before adding the soil, in order to position the soil closer to the top of the bin and reduce the confinement of the booster. Figure 5.4a illustrates this modified charge in contact with soil experimental setup, with Figure 5.4b illustrating the result of the initial (unmodified) detonation process of this type.

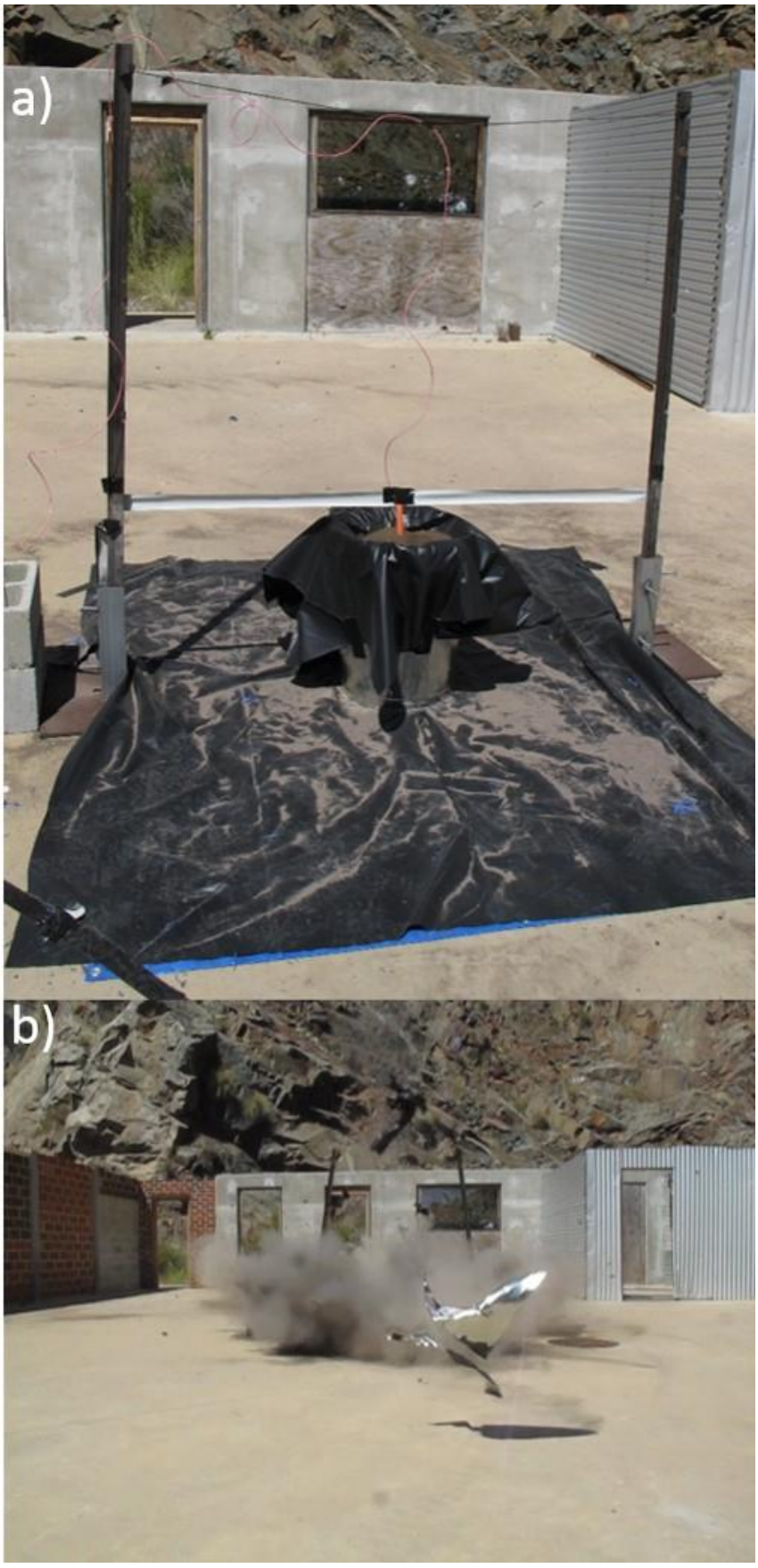

Figure 5.4: a) Photograph of the modified setup used for charge in contact with soil detonations. Orange casing contains the explosive charge, and b) Still image from a video of the initial (unmodified) charge in contact with soil detonation

5.3.5 Sample processing after preliminary detonation trials

Prior to analysis, each container of soil was weighed to determine the percentage of soil recovered from each blast. This was referenced with respect to the dry mass of the starting soils, prior to wetting, as it was apparent during the detonations that the water used to wet the soils to re-establish microbial activity had evaporated during the trials. Three 40 g samples of each soil were taken using the cone and quarter method [191] for later size fraction analysis. Following this, each container was manually tumbled for 10 minutes to homogenise the soil samples prior to analysis.

Six 5 g (5 ± 0.05 g) soil samples were collected from each of the different detonation conditions. A 1.25 mL aliquot of water was added to each vial to replace the evaporated initial water content of the soils, to give a water content equal to that used in the solution-spiked soils of Chapter 4. Following this, each soil sample was extracted and analysed to determine the levels of explosive residues present and their degree of homogeneity within the bulk soil sample. Extraction and analysis was performed in an analogous fashion to that performed in Chapter 4.

An additional sample was taken from each of the bulk post-blast soil samples and analysed using SEM to assess whether any of the detonations had given rise to soil fracturing. Instrumental procedures and parameters for these SEM studies are outlined in more detail in Section 5.3.10 below.

5.3.6 Final detonation conditions for ageing studies

A 1 kg sample of each of the three dried, sieved soils was weighed into a 4.5 L plastic screw-cap bottle. Three days prior to the detonations, 50 mL tap water was added to each bottle (with the mass of spiked water equalling 5 % of the total soil mass). Each bottle was then manually tumbled for five minutes until the water appeared to be dispersed evenly throughout the soil. The soils were stored at room temperature for three days prior to the detonations.

All detonations were performed over a layer of soil, based on the procedure used for the earlier detonations. In an attempt to increase the loading of explosive residues onto the soils, three sequential detonations, each using one booster, were performed over each soil. Following the first and second detonations in each set of three detonations, any soil which had been displaced outside the pre-marked 1 × 1 m square, but remained on the black plastic film, was shaken back into the pre-marked square prior to the next detonation, to ensure that the soil was directly beneath the booster. Following the detonations, the samples were immediately transported

back to the laboratory, where they were stored in a freezer at -20 °C prior to splitting into 5 g aliquots (see Section 5.3.7). The time between detonation and the soils reaching the laboratory was approximately two hours.

5.3.7 Sample processing post detonation

The individual samples of soil from the respective detonations were split into 5 g aliquots (with this entire process completed within two hours of the soils reaching the laboratory). Each soil was passed through a 2 mm sieve, to remove any extraneous material not present prior to the detonations (mostly consisting of dried plant matter from the detonation site due to the negative pressure phase of the detonation). The bulk soil samples were then weighed, to determine the percentage soil recovery, before three 40 g samples of each soil were taken using the cone and quarter method for size fraction analysis.

The remaining soil was poured into a disposable aluminium tray and mixed thoroughly for 10 minutes using a disposable plastic spoon, until the soil was homogeneous in appearance. A set of 6 × 5 g (± 0.05 g) samples was then taken to quantify the levels of TNT and PETN which had been deposited onto each of the soils using the method described previously. A misfire occurred over the native soil and deposited significantly higher quantities of explosive residues into the native soil. Thus, following extraction and filtration of the native soil samples, the extracts were further diluted 1:10 using the same overall solvent composition, and the injection volume was reduced to 5 µL, in contrast to the 50 µL injection volume used for the Spearwood and landscape soils.

5.3.8 Preparation of post-blast samples for ageing studies

Following the final set of detonations, samples were prepared for ageing studies: 36 × 5 g (± 0.05 g) samples were split into 50 mL amber glass bottles for each of the detonations. 1.25 mL water was added to each vial, to replace the evaporated initial water content of the soils, to give a water content equal to that of the comparative solution-spiked soil samples of Chapter 4. For each soil, 12 samples were stored at room temperature, 12 refrigerated at 1 °C and 12 frozen at -20 °C, with two samples from each soil analysed at time points of 1, 4, 7, 14, 28 and 42 days.

5.3.9 Soil size fraction determination

To determine the size fractions of the pre- and post-blast soils, three aliquots of each pre- and post-blast soil (each at least 40 g) were prepared using the cone and quarter method [191]. After drying overnight in an oven at 60 °C, each aliquot of soil was passed through

progressively finer sieves (> 1 mm, 0.495-1 mm, 0.250-0.495 mm and < 0.250 mm), to determine the percentage by mass of each size fraction of the soils. Details of the sieves used are as follows: 250 µm sieve: mesh no. 60, aperture 250 µm, Endecotts Test Sieves Ltd, London, England; 495 µm sieve: mesh no. 32, The Tyler Standard Screen Scale, The W.S. Tyler company, Cleveland, Ohio; 1000 µm sieve: Mesh no. 16, The Tyler Standard Screen Scale, The W.S. Tyler Company, Cleveland, Ohio. Extraneous material including any large pieces of black plastic or brick originating from the experimental setup were manually removed before weighing.

5.3.10 SEM analyses of soils

Preliminary SEM analysis was performed on an Obducat CamScan 3200LV SEM using Helios software. Secondary Electron Imaging (SEI) and Backscattered Electron Imaging (BEI) images were captured using a scan speed of S4, gun voltage of 25 kV and emission of 92 µA. Further SEM analysis was undertaken using a Carl Zeiss Sigma VP Field Emission Gun Scanning Electron Microscope coupled to a Bruker Quantax 400 Energy Dispersive Spectrometer equipped with an Xflash 5030 Silicon Drift Detector. Analysis was carried out using an accelerating voltage of 20 kV in variable pressure mode, with a mix of 40 % Secondary Electron and 60 % Backscattered Electron. Samples were prepared for this procedure by rinsing a small amount of soil with distilled water and ethanol, before oven-drying the samples for 10 minutes at 40 °C. The cleaned soils were then transferred onto an SEM stub and sputter coated using a thin layer of platinum prior to analysis. Figure 5.5 illustrates stages during preparation of the SEM stubs for analysis.

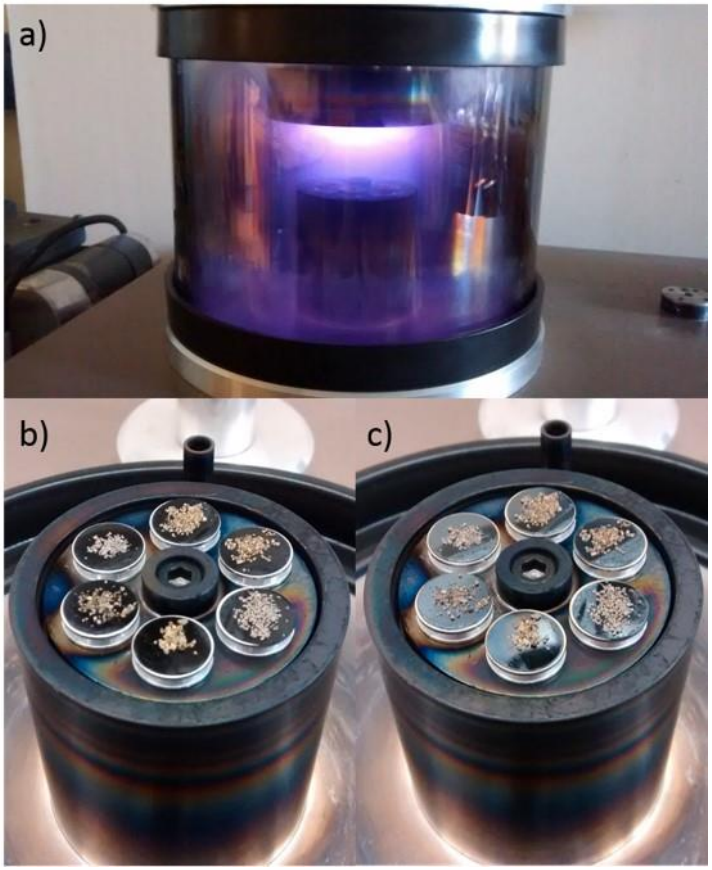

Figure 5.5: Stages present during preparation of the soils for SEM analysis, showing a) plasma formation during coating of the SEM stubs, b) the uncoated stubs, and c) the stubs after a light coating of platinum

5.4 Experimental: µCT analyses

5.4.1 Sample preparation

Intact, dried soil aggregates (1-2 mm) were selected from each of the nine conditions (landscape, native and Spearwood soils, either pre-blast, post-blast detonated in contact with soil, or post-blast detonated above soil), with a total of three aggregates analysed from each condition.

The aggregates were prepared using two separate methods prior to µCT scanning. In the first method, a small piece of double-sided adhesive tape was placed over the tip of a plastic micropipette tip and smoothed into place. The tape was gently touched to the chosen aggregate, to mount the aggregate onto the pipette tip. The base of the pipette tip was mounted vertically into a metal sample stage clip, prior to insertion into the scanner. In later scans, a folded piece of foam was inserted into the clip beneath the pipette tip, to provide some friction and minimise any potential slippage of the pipette tip during the 360° rotation required for the scans.

In the second method, individual aggregates were gently placed into the hollow centre of a

plastic micropipette tip and the pipette tip tilted vertically, to allow the aggregate to naturally fall and be held in place by the angled walls of the pipette tip. Prior to mounting into the sample stage clip, the pipette tip was inserted into an inverted pipette tip to provide sufficient height for the sample stage clip to avoid hitting the X-ray source during its rotation. Images of two soil aggregates prior to µCT scanning are provided in Figure 5.6.

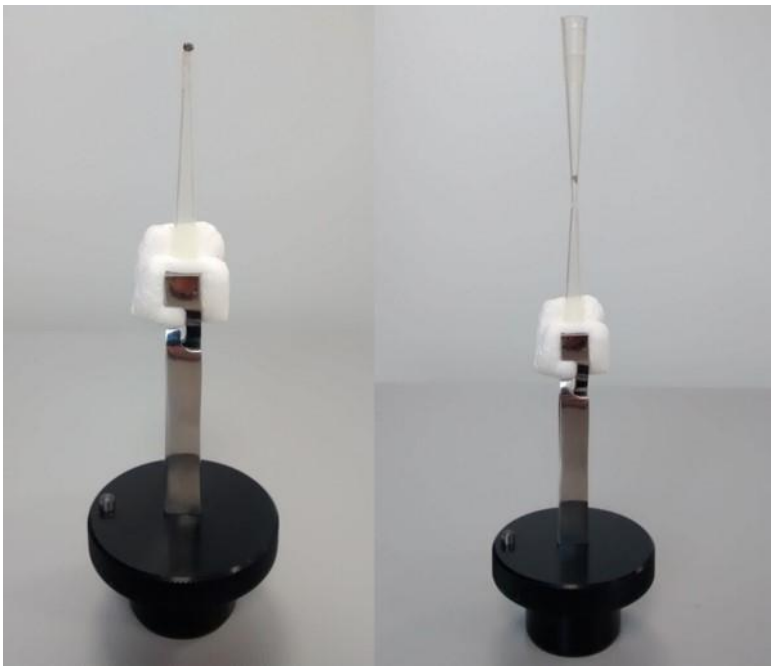

Figure 5.6: Setup showing soil aggregates prepared for µCT scanning, with (left) an aggregate mounted on the end of a pipette tip, and (right) an aggregate contained within a pipette tip

5.4.2 µCT data acquisition

Scanning was performed on a Nikon XT H 225 ST µCT scanner, fitted with a static tungsten reflection target, and running Nikon Metrology X-TEK Inspect-X Version XT 4.3.1 software. The scanning procedure involved placing the sample holder into the stage and securing it in place. The aggregate was then located on the screen and magnified such that upon a 360° rotation of the sample, the aggregate edges spanned approximately 90 % of the screen, which had a 2000 × 2000 pixel resolution. The Image Optimisation parameters were adjusted manually to improve the contrast of the aggregate on the screen. Typical parameters used include: Beam energy 150 kV; Beam current 193 µA; Power 29 W; Exposure 2 f.p.s.; Gain 18 XdB. Following this, a new shading correction was created prior to the scan. Each scan was acquired using four frames per projection at 1440 (occasionally 720) projections, to give a total acquisition time of 48 minutes. No X-ray filters were applied during acquisition.

5.4.3 Image reconstruction

Although the Inspect-X software associated with the µCT scanner is capable of performing

automatic reconstruction of the resulting image stacks, this tended to determine an inaccurate centre of rotation, resulting in slightly blurred reconstructions. For this reason, reconstruction was performed separately from the scans, using Nikon Metrology X-TEK CT Pro 3D Version XT 4.3.1. Once a satisfactory centre of rotation had been achieved, the resulting data was sent for reconstruction in the Nikon Metrology X-TEK CT Agent program, Version XT 4.3.1, opting for a Floating Point volume, Full Range attenuation scaling and no Volume Graphics data import conversion. No beam hardening presets were used during the reconstruction. Following reconstruction, the new VGL file was opened in VGStudio MAX Version 2.2.6, importing the volume in an unsigned 16 bit format. An image stack from one of the three available projections (Front, Top or Right) was then exported in Tiff format prior to further image processing using the ImageJ program.

5.4.4 Thresholding

The saved image stacks were imported into ImageJ Version 1.50b. Prior to performing any porosity calculations, thresholding was performed. This is an essential step to indicate to the image processing software which areas of the image correspond to pore space (i.e. air), and which correspond to solid aggregate material, such as mineral surfaces. The threshold value was determined for five slices within a stack (taking precedence from Pajor *et al.* [192]). In the current work, representative slices from 10, 30, 50, 70 and 90 % of the way through the stack were used, manually adjusting the histogram if necessary to ensure that adequate delineation of the soil and pore space had been achieved. An average was then taken of these five threshold values and applied as an averaged global threshold across the entire image stack.

5.4.5 Volume analysis and porosity determination

Porosity percentages of the different aggregates were calculated using the ImageJ BoneJ plug-in (primarily designed for calculating bone density), Version 1.4.1. The first step in this process was to ensure that a suitable threshold had been applied (see Thresholding section above). Following this, suitable regions of interest (ROIs) had to be defined which would encompass the entire aggregate volume. For this, 30 regions of interest were defined in each image stack, approximately every 17 slices, using the ‘Create Selection’ feature. This feature selected all detected edges present within an image (including the edges of pores entirely contained within the centre of an aggregate). In order to calculate overall porosity, selection of solely the edges of the aggregate was required, rather than any internal edges present within an aggregate. For this reason, any selected internal edges were manually removed from the selection using the ‘Selection Brush’ tool. An example of an aggregate slice progressing through these stages (original aggregate slice, thresholded slice, and selection before and after its internal edges were removed) is displayed in Figure 5.7.

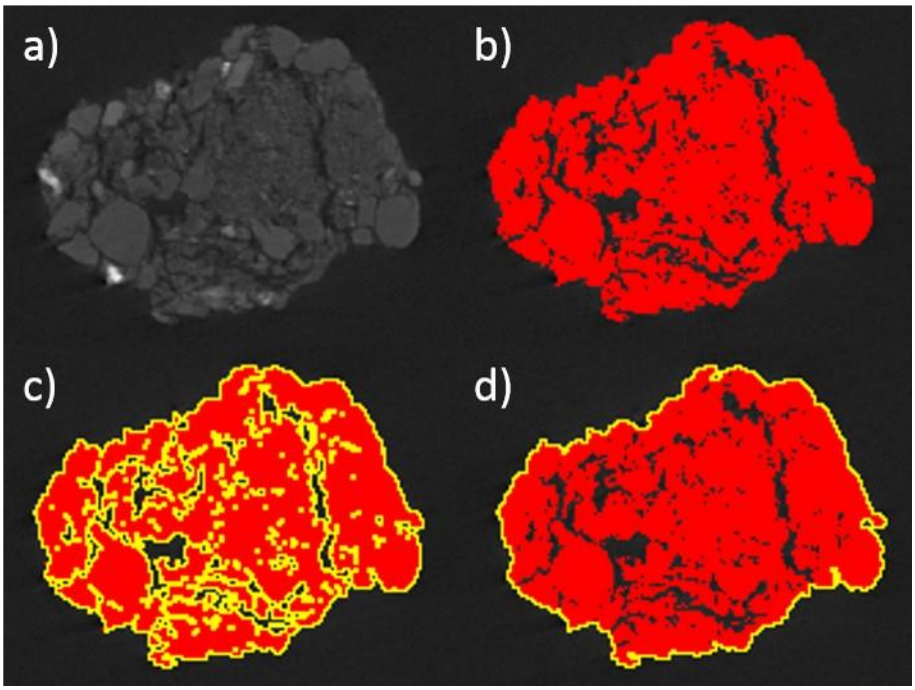

Figure 5.7: Images of a landscape aggregate slice, showing a) the original slice; b) the slice after thresholding; c) the thresholded slice following the 'Create Selection' command; and d) the thresholded aggregate slice with solely its external edge selected

At this stage, the modified selection was added into the ROI manager. This process was repeated across 30 evenly-spaced slices through the aggregate, with each new selection added into the ROI manager. The 'Interpolate' feature within the ROI manager was then used to generate an ROI for each individual slice.

The Volume Fraction option from the BoneJ plug-in was used to calculate the porosity within the defined regions of interest. This was performed using the Surface algorithm, with a surface resampling value of six. During this calculation, the ROI manager was used to ensure that the porosities were calculated for the pre-defined regions of interest. This generated a value designated BV/TV (arbitrarily referring to Bone Volume/Total Volume), indicating the proportion of solid material within the defined volume of interest (i.e. a value of 0.8 would indicate a volume of interest was 80 % solid and 20 % air).

5.5 Results and discussion

5.5.1 Soil degradation and fracturing

5.5.1.1 Sample processing after preliminary detonation trials

A key aim of the preliminary detonation trials was to assess whether or not fracturing would be evident in soils from two distinct charge detonation positions (with the charge detonated either over or in contact with soil). Additionally, these trials were used to assess the degree of

explosive residue loading onto the soils resulting from the detonations so that later experiments could be adjusted to deposit explosive residues at a similar spiking level to those used in Chapter 4.

Duplicate subsamples were stored for each set of storage conditions and analysis time points. A previous study by Oxley *et al.* [77] used triplicate subsamples; however, duplicate subsamples were used in this study to reduce the required sample numbers. Additionally, to assess the degree of homogeneity of the collected soils immediately after mixing, six subsamples were taken and extracted, and the relative standard deviations (RSDs) of the contained explosive residues calculated to enable an assessment of the homogeneity achieved within the bulk sample after mixing.

The same batch of Pentex D boosters, reported to contain TNT, PETN and RDX [193, 194], was used for all detonations performed during this study. In order to determine the proportions of TNT, RDX and PETN present within these boosters, a sample was taken from a booster and analysed. This analysis also enabled assessment of whether any additional species were present prior to the detonations, such as TNT degradation products or manufacturing impurities (e.g. 2-DNT). Analysis revealed a TNT:PETN ratio of approximately 76:24 by mass within the booster (see Table 5.1). This ratio is broadly in agreement with the Safety Data Sheet provided (Table 5.1). Interestingly, the Safety Data Sheet also reports the presence of between 0 and 60 % RDX, however RDX was not detected. Similarly, no RDX was detected from any of the post-detonation samples generated during this work. This is likely due to the manufacturer listing RDX as a possible additional component on the safety data sheet to account for any impurities arising from manufacture, or to protect their compositions from being used by other manufacturers.

Table 5.1: Comparison between reported and detected components of Pentex D boosters used in controlled detonations

Component	Reported proportion [193, 194] (%)	Detected proportion (%)
TNT	35-70	75.6
PETN	0-60	24.4
RDX	0-60	0

5.5.1.2 Preliminary range day

Table 5.2 contains information on the percentage of soil recovered from trials where the boosters were detonated over a layer of each respective soil, along with the average observed TNT and PETN levels recovered from the soil and associated RSDs.

Table 5.2: Soil recoveries from detonations where a booster was detonated over a layer of soil, average TNT and PETN levels per kg collected soil, and RSDs of the detected TNT and PETN levels

Soil	Native	Spearwood	Landscape
Initial mass (g)	2000	2000	2000
Post-blast mass (g)	1877	1945	1506
% soil recovery	93.9	97.3	75.3
Average TNT recovery (mg/kg)	0.8	1.1	0.1
RSD of TNT recoveries (%) (n=6)	29.8	12.7	55
Average PETN recovery (mg/kg)	0.5	0.9	0.6
RSD of PETN recoveries (%) (n=6)	67.9	18.8	36.7

It can be seen from Table 5.2 that an almost quantitative mass recovery of the native and Spearwood soils was obtained following these detonations, with a significantly lower recovery from the landscape soil. The native and Spearwood soils gave similar TNT recoveries of approximately 1 mg/kg, whereas much lower levels were detected from the landscape soil. The reason for this is unclear, as the boosters used throughout these trials were from the same batch and comparable levels of PETN were recovered from each of the soils. Ultimately, the results displayed in Table 5.2 highlight that even when trying to perform ‘controlled’ detonations to deposit explosive residues into soil, this practice is still much less ‘exact’ than spiking soils using solutions of explosives, and variable levels of explosive residues may be deposited even when all conditions are kept as similar as possible.

High relative standard deviations in explosive residue recoveries (mg of explosive residues per kg of soil) of up to 68 % were observed within the sets of six soil samples analysed for each of the three soils, which indicated that the soil preparation step undertaken prior to soil portioning (manual tumbling) was not adequate.

Table 5.3 contains data for the preliminary detonations where a booster was detonated in contact with the three soils.

Table 5.3: Soil recoveries from detonations where a booster was detonated in contact with soil, average TNT and PETN levels per kg collected soil, and RSDs of the detected TNT and PETN levels

Soil	Native	Spearwood	Landscape
Initial mass (g)	2000	5500	4000
Post-blast mass (g)	217	5328	618
% soil recovery	10.85	96.87	15.45
Average TNT recovery (mg/kg)	0.5	0.1	0.1
RSD of TNT recoveries (%) (n=6)	20.3	6.7	7.3
Average PETN recovery (mg/kg)	0.1	0	0
RSD of PETN recoveries (%) (n=6)	62.3	0	0

The first detonation trial, involving native soil, gave rise to a very low soil recovery, and resulted in the destruction of the metal bin used to contain the soil at the time of detonation. During this first trial, the soil was placed in the base of the bin. Confining the soil and charge in this manner increased the explosive effect which expelled the majority of the soil from the scene, resulting in low soil recoveries. For the following two detonations (Spearwood and landscape), larger quantities of soil were used in an attempt to diffuse the explosive power generated by the booster. In addition, rather than placing the soil within the base of a bin, a new bin was filled approximately two-thirds full using layers of bricks, and the soil placed on top of these bricks (separated using a layer of black plastic). In this modified setup, there was still a mound of soil held within the bin, into which the tip of the booster could be placed, but the confinement of the charge and the resulting blast effect were reduced. This change in procedure resulted in nearly 97 % of the Spearwood soil being recovered. A lower recovery was obtained from the landscape soil as the detonation force caused the bin to fall over and spill, thus losing the majority of the soil.

Soil samples were mixed in a disposable aluminium tray for 10 minutes prior to splitting off into aliquots for analysis. The relative standard deviations of the recovery of TNT (mg/kg of soil) for the three soil samples (Table 5.3) were acceptable using this method. It can also be seen from Table 5.3 that very low PETN recoveries were obtained from these three soils. Analysis of the collected soil samples from this initial range day revealed the presence of low levels of 2-ADNT and 4-ADNT (approximately 0.05 mg/kg) in the native soil sample in which the booster was detonated in contact with the soil. As the soils were extracted within a few hours of the detonations, this indicates that degradation of the deposited TNT had begun to occur very rapidly and highlights the importance of mitigating the degradation of explosive residues as the transformation of TNT can occur within only a few hours.

SEM analyses were performed on the pristine and post-blast soils to assess for soil fracturing. Figure 5.8 compares the typical appearance of the pristine landscape, native and Spearwood soils (Figure 5.8a, c and e, respectively) against the appearance of post-blast landscape, native and Spearwood soils (Figure 5.8b, d and f, respectively), in each case with the explosive detonated in contact with the soils.

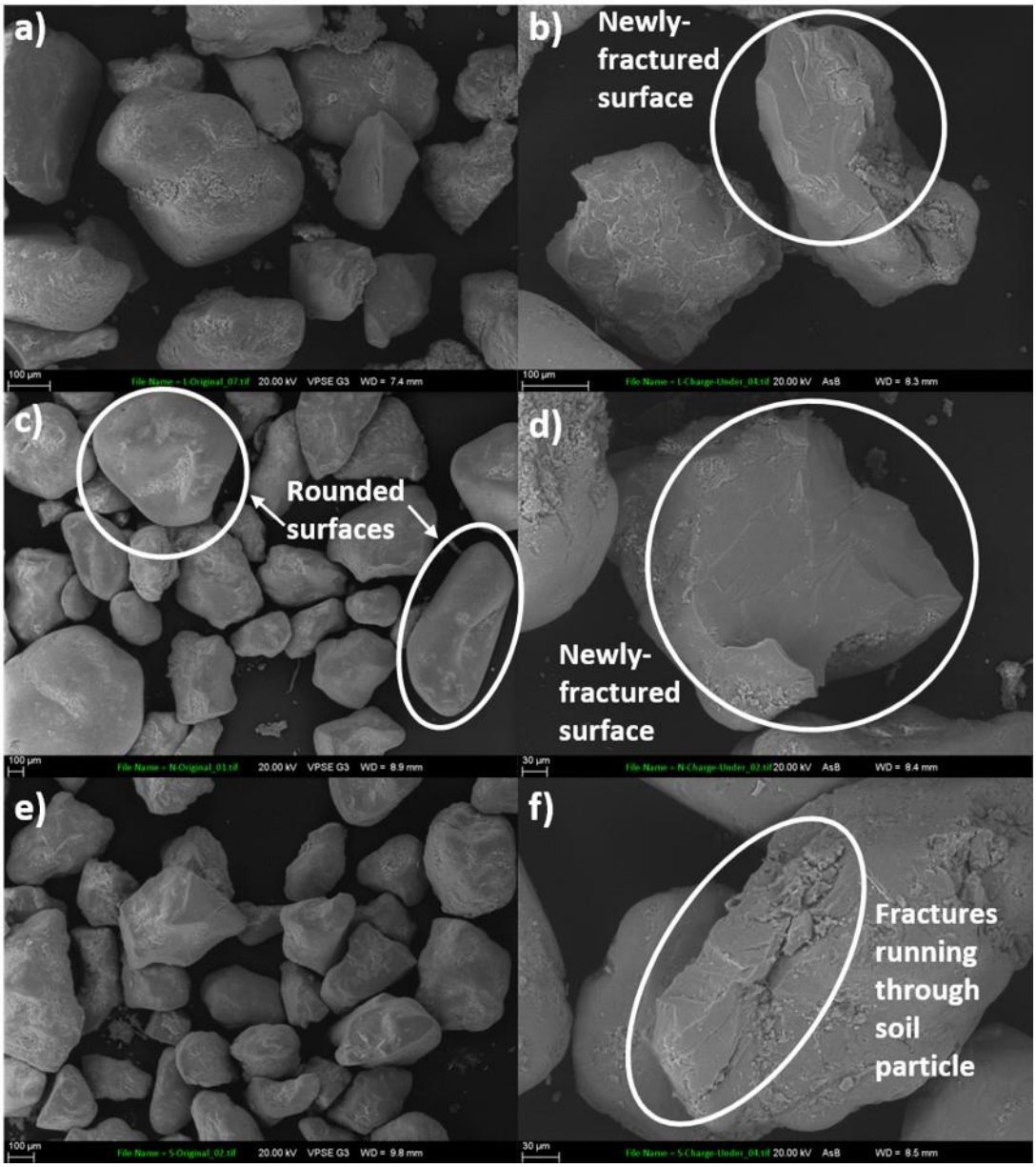

Figure 5.8: SEM images of a) pre-blast landscape soil, b) post-blast landscape soil, c) pre-blast native soil, d) post-blast native soil, e) pre-blast Spearwood soil and f) post-blast Spearwood soil. In each of the post-blast soils illustrated in this figure, the explosive was detonated in contact with the soils. Newly-cleaved planes and fractures are visible within each post-blast soil. Note that the post-blast soils are displayed at a higher magnification than the pre-blast soils, to more clearly illustrate the detonation-induced damage to the soils. Source: Evelyne Delbos, James Hutton Institute

It can be seen from Figure 5.8 that fresh mineral surfaces are exposed in each post-blast soil.

In addition to SEM analyses, pre- and post-blast soils from these initial detonation trials were also subjected to size fraction analysis to assess what effect fracturing had on the soil particle sizes. These size fraction analyses were performed by sieving triplicate coned and quartered soil samples through progressively finer sieves, and determining the proportion by mass of each size fraction.

These particle size fraction analyses of the pre- and post-blast soils revealed a tendency of the soils to shift to a smaller average particle size following detonations, particularly for the landscape and native soils, an effect which was more pronounced when the explosive charge was detonated in contact with the soils rather than above the soils (Figure 5.9). As smaller particles will have a larger surface area to volume ratio, the data from Figure 5.9 suggests that the surface areas of the landscape and native soils increased following each of the detonations.

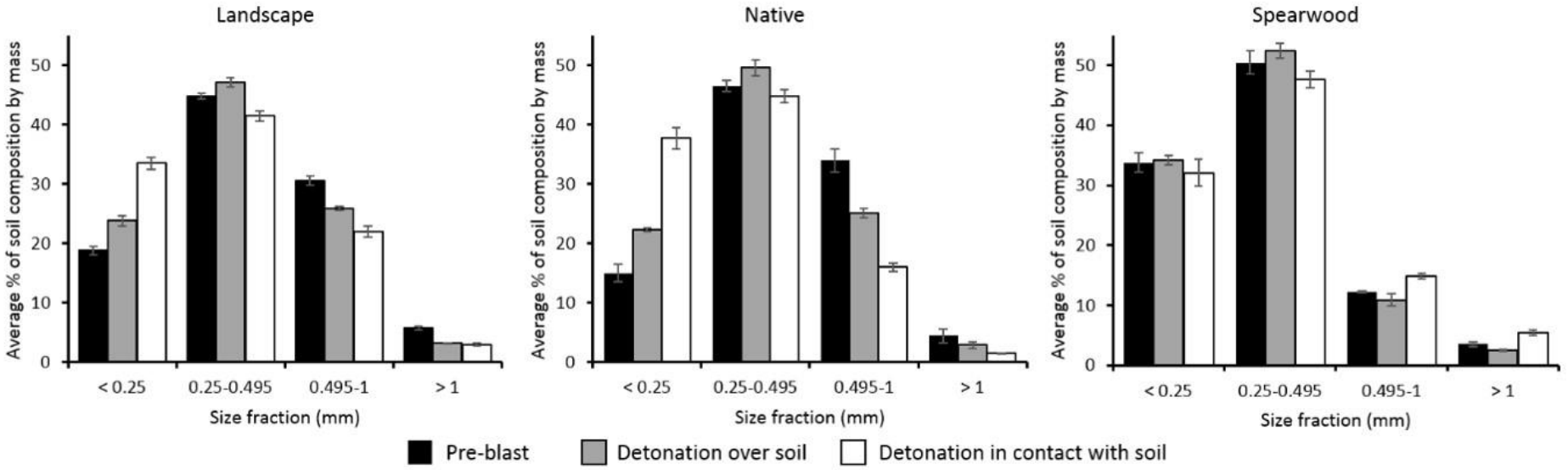

Figure 5.9: Size fraction distributions for pre- and post-blast landscape, native and Spearwood soils following preliminary range day, with charges detonated either over, or in contact with, the soils. Error bars show the standard deviation between triplicate samples

The highest degree of fracturing occurred in the native soil sample where the booster was detonated in contact with the soil. In these samples, 2-ADNT and 4-ADNT were detected from initial extracts of the soil, though these were not observed in any of the other samples collected from this initial range day. It is therefore possible that the large increase in surface area which occurred due to the detonation contributed towards the transformation of some of the TNT to its reduction products.

5.5.1.3 Final detonations

This work ultimately aimed to investigate the degradation of explosive residues following simulated vehicle bombings, due to their increasing prevalence. For this reason, the detonation setup most representative of a vehicle bombing was used for the final range day's detonations, with the explosive charge detonated over a layer of soil. During extraction of the soils and quantification of the explosive residues present, analysis by HPLC-UV revealed that the levels of TNT and PETN in the Spearwood and landscape soils fell within the limits of the calibration range prepared for this work. This allowed for extraction and analysis to be performed in the same manner as for samples from the preliminary detonation trials. The native soil had significantly higher levels of TNT and PETN (approximately 100 times higher than those in the Spearwood and landscape soils), causing the peak areas to exceed the calibration range. Dilution of the native soil extracts as described in Section 5.3.7 was therefore performed prior to analysis.

To enable a meaningful comparison between the degradation of explosives in the solution-spiked soils of Chapter 4 and the detonation-spiked soils of this chapter, similar loadings of explosives were desired from the two spiking methods. In Chapter 4, solution-spiked explosives loadings of 2 mg/kg of TNT and PETN were used. As shown earlier in Table 5.2, the levels of explosive residues deposited in the soils during the preliminary detonation trials ranged from 0.1 to 1.1 mg/kg TNT, with an average of 0.67 mg/kg. For PETN, the levels ranged from 0.5 to 0.9 mg/kg, with an average of 0.67 mg/kg. These levels are approximately three times lower than the explosive loadings used in Chapter 4. For this reason, adjustments to the detonation procedure were made which included using three boosters detonated in succession over each soil, and a reduction in soil mass from 2 kg to 1 kg. Table 5.4 contains information on the resulting explosive residue loadings from the three soils used for the final set of detonations.

Table 5.4: Soil recoveries and levels of TNT and PETN in the native, Spearwood and landscape soils from the second, final range day

Soil	Native	Spearwood	Landscape
Initial mass (g)	1000	1000	1000
Post-blast mass (g)	815	724	712
% soil recovery	81.5	72.4	71.2
TNT recovery (mg/kg)	343.2	5.7	5.9
RSD of TNT recoveries (%)	25.4	47	10.5
PETN recovery (mg/kg)	391.3	6.8	3.2
RSD of PETN recoveries (%)	25.3	55.6	13

For the landscape and Spearwood soils, the average concentration of TNT within the soils had increased to 5.8 mg/kg – an approximately nine-fold increase compared to the initial range day. Similarly, for PETN in these two soils, the average concentration was 5 mg/kg; an approximate seven-fold increase. The TNT and PETN levels in the native soil were significantly higher than those in the landscape and Spearwood soils. This was attributed to the misfire of one of the three boosters detonated over the native soil, where the detonator functioned but the booster low-ordered in an incomplete detonation (see Figure 5.10), leaving higher quantities of explosive residues dispersed throughout the soil.

Figure 5.10: Booster casing following misfire over native soil

Table 5.4 illustrates that varied relative standard deviations were obtained for the recoveries of TNT and PETN levels (mg/kg of soil) within the soil samples extracted from the final range day. RSDs of approximately 10 % were obtained for the landscape soil, indicating a relatively even distribution of the two explosives within the soil. For the native soil, higher RSDs of around 25 % were obtained. This increase may be attributed to the booster misfire, which likely resulted in the deposition of large explosive crystals over the soil. If, for example, two explosive crystals were present in one extracted soil sample, whereas only one was present in another extracted soil sample, then this may have led to the high RSDs. However, the reason

for the high RSD values for the Spearwood soil is unclear – all boosters detonated efficiently over this soil, and the soil was subjected to the same soil homogenisation method as the native and landscape soils. The high RSDs of the TNT and PETN levels within the Spearwood soil samples resulting from this range day should therefore be borne in mind when assessing the degradation results over time. It may be expected that larger discrepancies within the results for the Spearwood soil may be seen, compared to the landscape and native soils.

During this work, a total of 15 boosters were detonated. Following each detonation, the levels of explosive residues deposited into the collected soils were quantified. This information enabled an assessment to be made of the detonation efficiency of the 15 detonations, to give an idea of the proportion of explosives which may survive a typical detonation.

This assessment was performed using the following method: Each booster used was reported to contain 25 g of a mixture of TNT and PETN [193, 194]. Based on analysis of a sample of the booster contents from this batch of boosters (see Table 5.1), these components were present in a ratio of 75.6 % TNT and 24.4 % PETN. This suggests approximately 18.9 g TNT and 6.1 g PETN present within each booster. In addition, the detonators used to initiate the boosters contained 0.79 g PETN [195], giving a total mass of PETN per detonation of 6.89 g.

For the six detonations performed during the preliminary detonation trials, a single booster and detonator were used over each soil sample. The detected TNT and PETN levels could therefore be directly related to the initial quantities of TNT and PETN present in the starting booster-detonator pairs, taking precedence from the procedure of Oxley *et al.* [77]. For the soil samples from the second, final, range day, three booster and detonator pairs were detonated in succession over each of the three soils. In this case, the absolute mass of TNT and PETN recovered from each soil was divided by three, to obtain the average mass of TNT and PETN deposited into the soil from each of the three successive detonations. The combined overall results were then averaged, to give an average mass of TNT and PETN remaining following a detonation, referenced with respect to the initial masses of the explosives used. This provided a percentage of the explosives which had survived each detonation, and thus the detonation efficiency of each explosion. These calculated detonation efficiencies are displayed in Table 5.5.

Table 5.5: Average calculated detonation efficiencies from 12 detonations

Explosive	Calculated detonation efficiency from 12 detonations (%)
TNT	99.995
PETN	99.989

It can be seen from Table 5.5 that the detonations performed throughout this work demonstrated very high efficiencies. Several assumptions must be taken into account when assessing these values - for example, this calculation assumes that each soil captured all of the intact explosive residues following the detonation. However, it is likely that some residues will have dispersed away from the soil due to the force of the explosion, so for this reason the values quoted in Table 5.5 should be taken as an upper estimate of the detonation efficiencies obtained. For these calculations, the masses of TNT and PETN from the native soil of the final range day were not included, as a misfire occurred over this soil and resulted in the deposition of significantly higher TNT and PETN levels in the soil compared to the other detonations. The detonation efficiency of the misfire is therefore calculated separately below, for comparison.

The low-order detonation was the first in a series of three successive detonations over the native soil sample during the final range day. In calculating the detonation efficiency of the misfired detonation, the overall mass of TNT and PETN deposited in this native soil after the three detonations was determined. Then, the calculated average mass of TNT and PETN remaining from a non-misfired detonation (determined from Table 5.5) was subtracted twice from this value, to account for any TNT and PETN resulting from the two successful detonations, thus giving the approximate masses of TNT and PETN remaining due to the misfire. Calculating the detonation efficiency of the misfire gave the results in Table 5.6.

Table 5.6: Approximate detonation efficiency of TNT and PETN from a misfired detonation

Explosive	Calculated detonation efficiency from misfired detonation (%)
TNT	98.530
PETN	95.393

It can be seen from Table 5.6 that this misfire still produced a very high detonation efficiency, with efficiencies for TNT and PETN above 95 %. Previous researchers have also calculated the detonation efficiencies of TNT. Oxley *et al.* [77] report the detonation efficiency of a 75 g TNT charge as being 71 %, which the authors attribute to a poorly-functioning device. On the other hand, Jenkins *et al.* [196] examined the detonation efficiency of TNT from a landmine containing 75 g TNT. The authors reported a TNT detonation efficiency of 99.992 %. This value is almost identical to the value of 99.995 % calculated from the majority of detonations performed in this work (Table 5.5), suggesting that these calculated detonation efficiencies are relatively accurate.

Based on these results and the findings of Jenkins *et al.* [196], it can be seen that explosives may detonate with very high efficiency, in some cases leaving intact explosive residues at less

than 0.01 % of their initial mass. This may equate to only a few milligrams of explosive residues being recovered in soil following a detonation (for example, in this work, 0-3 mg was the typical detected range of explosive residues remaining following a detonation). The likely deposition of such low quantities of explosive residue into soil is problematic, as any degradation or transformation of these explosive residues may bring the level of intact explosive residues below their limit of detection during a typical instrumental analysis. This presents a major challenge, and highlights the need to identify the optimum conditions for the transportation and storage of soil samples suspected of containing explosive residues, in order to maximise their stability prior to analysis.

SEM analysis was performed on the post-blast soils following the second range day to assess whether fracturing had occurred. As for the soils from the preliminary detonations, newly-fractured mineral surfaces could be seen in each post-blast soil sample, supporting the idea that soil fracturing had occurred.

Figure 5.11 shows the size fraction distributions of the three soils before and after the final range day.

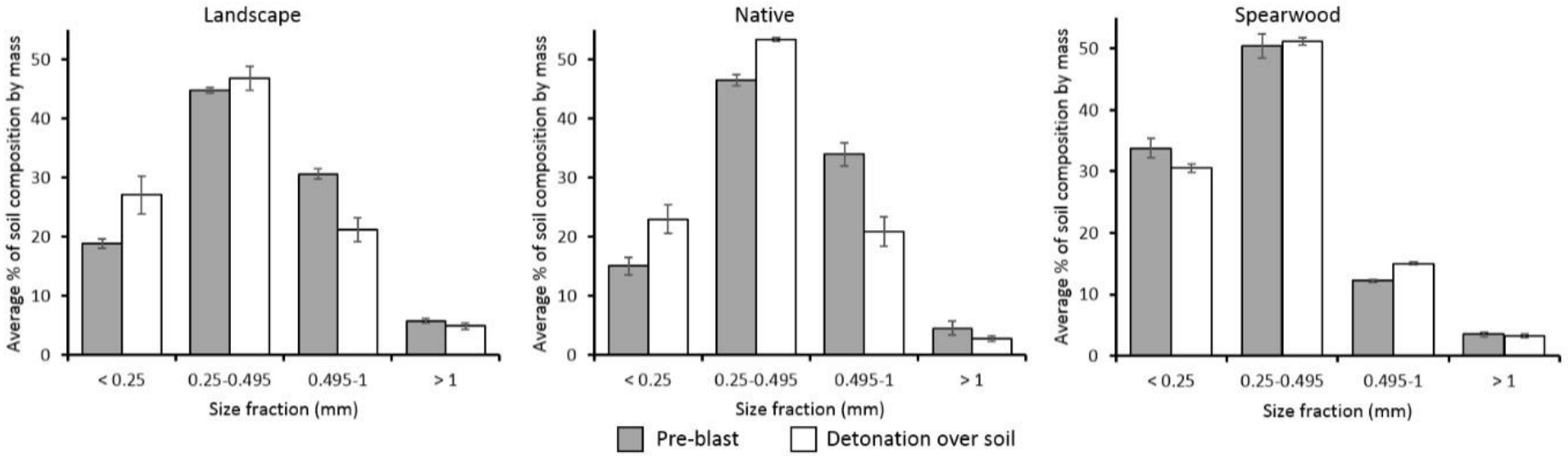

Figure 5.11: Size fraction distributions of landscape, native and Spearwood soils, before and after the final set of detonations. Error bars show the standard deviation between triplicate samples

It can be seen from Figure 5.11 that similar post-blast changes in the size fraction distribution have occurred for each of the soils, compared to those from the preliminary set of detonations (Figure 5.9). A general shift to a smaller particle size is evident from the landscape and native soils. As finer soil particles are more geochemically reactive [102], it is possible that this shift to finer particles compared to the pristine soils used for the solution-spiked experiments of Chapter 4 will give rise to a faster rate of explosive residue transformation.

For the Spearwood soil, as before, no significant change was observed between the pre-blast and post-blast soil size fractions. However, evidence of fracturing could be seen from the SEM images of the Spearwood soil after this second set of detonations (see Figure 5.12), indicating that SEM analyses may provide a better means of determining whether a soil has undergone fracturing compared to size fraction analyses.

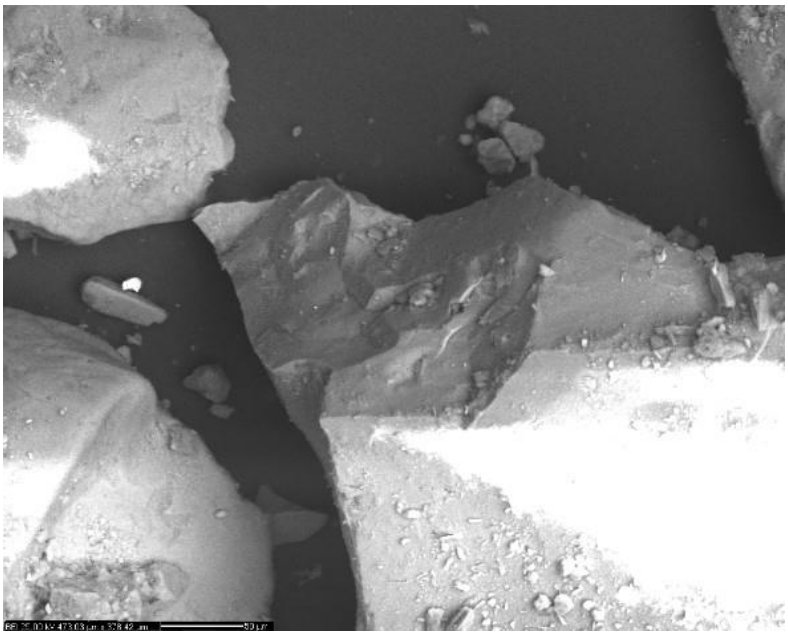

Figure 5.12: Fracturing present on a Spearwood soil sample following the final set of detonations

This research confirms that SEM analysis on soils samples can be undertaken to confirm that an explosive event has indeed taken place, which may be useful in the event that the blast seat has been disturbed or its location is not clear.

5.5.2 µCT analyses

In the present work, three aggregates were scanned for each of the nine respective conditions used throughout this work. Example slices through pre-blast landscape, native and Spearwood soils are provided in Figure 5.13.

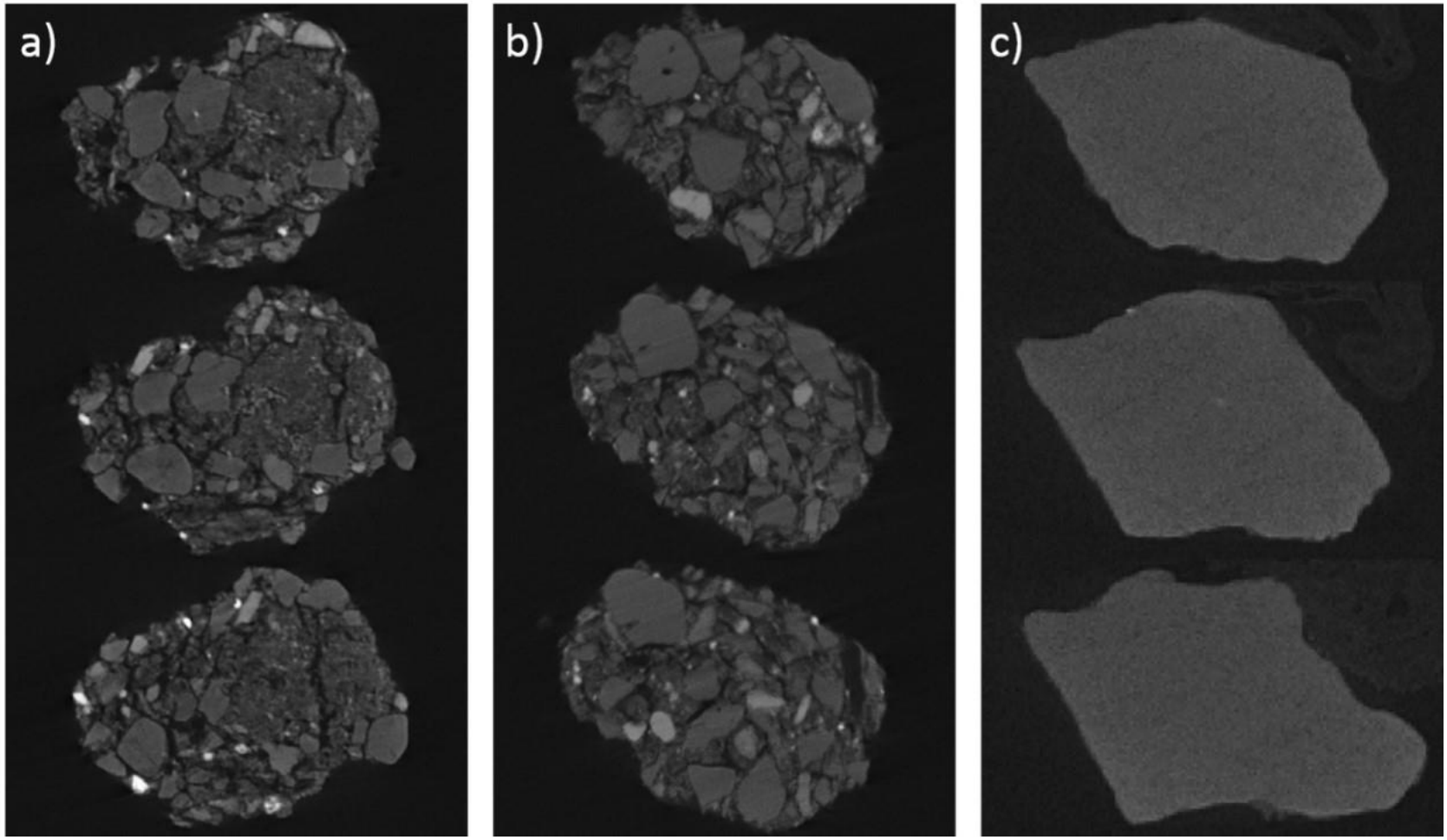

Figure 5.13: Example slices taken from a) a pre-blast landscape soil aggregate; b) a pre-blast native soil aggregate; and c) a pre-blast Spearwood soil aggregate

The use of three aggregates is comparable to previous research. For example, Peth *et al.* [115] analysed two aggregates, one each from two different soil locations. Akbari *et al.* [190] analysed a total of six soil aggregates with four from one soil and two from another. Finally, Nunan *et al.* [116] analysed fifteen aggregates – five each from three different soil treatments. In the current work, due to high demand for the µCT instrument and thus very limited instrument availability, three aggregates were analysed for each individual soil condition. This choice of three aggregates was thought to give a satisfactory balance between time required and data output.

Two different methods were used within this work to prepare the aggregates for scanning. The first method involved mounting aggregates onto the tip of a disposable micropipette using double sided adhesive tape, taking precedence from the work of Akbari *et al.* [190]. The main benefit of this method is that the aggregate can easily be placed directly in front of the X-ray source with no extraneous material present, meaning no extraneous material has to be removed from the images during subsequent image processing. However, this method also bears a number of limitations including the loss of adhesion of the tape during scanning, which resulted in blurred images. Additionally, the mounted aggregates were very fragile and were difficult to store safely in case the aggregates needed to be re-scanned at a later date.

The second method used for aggregate analysis involved placing the aggregate into the inside of a plastic pipette tip. This protected the aggregate during its storage following scanning, meaning it would be easier to re-scan later, if necessary. However, this method had the drawback that the aggregate was surrounded by plastic, which needed to be removed in subsequent image processing programs prior to more detailed analyses. In this work, aggregates were initially analysed using the first approach, shifting to the second approach for later analyses.

The first step in CT image processing when determining aggregate porosity is to perform a thresholding step. This is an essential step to indicate to the image processing software which areas of the image correspond to pore space (i.e. air), and which correspond to solid aggregate material, such as mineral surfaces (often referred to as ‘void’ and ‘solid’ voxels, respectively). This process can be especially challenging for heterogeneous materials.

In Akbari *et al.*’s work [190], the authors investigated a number of different thresholding techniques, ultimately opting for an indicator Gaussian thresholding technique with additional modifications. This technique is very lengthy and complex, and adds considerable time onto an already lengthy scanning and reconstruction cycle. Pajor [192], on the other hand, reported a much quicker and simpler thresholding technique for 3D datasets that involved averaging

the threshold value determined by ImageJ for the pore-solid interface across five randomly selected slices for a given sample. The authors reported that this method gave porosity values close to the bulk sample's overall porosity. In the interests of time and simplicity, Pajor's [192] thresholding technique, using an averaged threshold value from five randomly-selected slices, was therefore adopted in the current work. An example of an image thresholded using this technique is provided in Figure 5.7.

One of the aims from µCT scanning the soils was to assess the porosity of the aggregates, to determine whether differences existed between aggregates from the different soils and treatment conditions. Although soil aggregates tend to have irregular shapes, the majority of previous researchers in this field [115, 116, 192] have determined aggregate porosity by looking solely at a regularly-shaped (e.g. cuboid/cylindrical) sub-section of an aggregate, typically from the very centre, presumably due to limitations present in image processing programs. Other researchers [114] have interpolated an overall three-dimensional porosity value from porosities calculated from a two-dimensional soil slice obtained during µCT scanning. These approaches do not account for the entire volume of a soil aggregate's structure, which may lead to unreliable conclusions due to an aggregate's heterogeneity and structural variability [116]. In fact, work done by Akbari [190] has shown that soil aggregates have a higher density in the centre of an aggregate compared to the edges, resulting in biased calculated porosities if only a subsection from the centre of an aggregate is analysed. Akbari *et al.* reported that the porosity of a cube from the centre of a specific aggregate was found to be 14 %, whereas when the porosity of the entire, same aggregate was calculated, this value nearly doubled to 26 %. It is therefore clear that an aggregate's entire volume should be considered before any meaningful conclusions can be drawn regarding its porosity.

In the present work, a method was therefore developed to analyse an aggregate's entire volume using the available software. This method involved the use of the BoneJ plug-in for the image processing program ImageJ, more commonly used for determining bone density, and is described earlier in more detail in the experimental section (Section 5.4.5).

ImageJ's 'Create Selection' feature enables the selection of an aggregate's external edges, in addition to any internal edges caused by the presence of pores. These internal edges can then be removed from the selection using the selection brush feature, opting to add the selected pixels to the selection, which enables the external edges of the aggregate present in the selection to be loaded as a 2D image (a 'slice').

As each µCT scan results in the collection of several hundred slices to represent each aggregate, it is time-consuming to select the edges of the aggregate on each individual slice to

add into the Region of Interest (ROI) manager contained within the ImageJ software. Therefore, an alternative approach was developed whereby 30 evenly-spaced regions of interest were defined on 30 slices within each aggregate, with one each on the first and last slice, to create a total of 29 equally-sized sections within each aggregate. The 'Interpolate' feature within ImageJ was then used to determine the aggregate edges on intermediate slices. The proposed technique was validated prior to its implementation for the porosity determination of each of the scanned aggregates to ensure that the procedure did not influence the overall calculated porosity. This validation involved processing a set of images from the same aggregate three times, each time staggering the defined regions of interest by a small number of slices, to determine whether this alteration affected the calculated porosity. Table 5.7 contains the resulting porosities for a representative aggregate using this staggered approach.

Table 5.7: Calculated aggregate porosities using the three staggered ROI sets for region of interest interpolation and subsequent porosity calculations

ROI set	% porosity
1	8.7
2	8.8
3	8.6

It can be seen that the calculated porosities are almost identical, indicating that the ROI interpolation method is suitable for the determination of porosity, regardless of the slice locations for initial ROI definition.

An example set of interpolated selections is shown below (Figure 5.14), with the first and last images (top left and bottom right, shown in red) being images where a selection was created and manually adjusted to remove any internal edges, and the intermediate images (yellow) bearing selections created with the 'Interpolate ROIs' feature within ImageJ. It should be noted that ordinarily at this stage within the developed porosity calculation procedure, thresholding would already have been performed, creating a red mask across the solid areas of the aggregate on each slice (such as in Figure 5.7). However, in Figure 5.14, selections were captured on non-thresholded images, to show the detail and complexity within each aggregate slice.

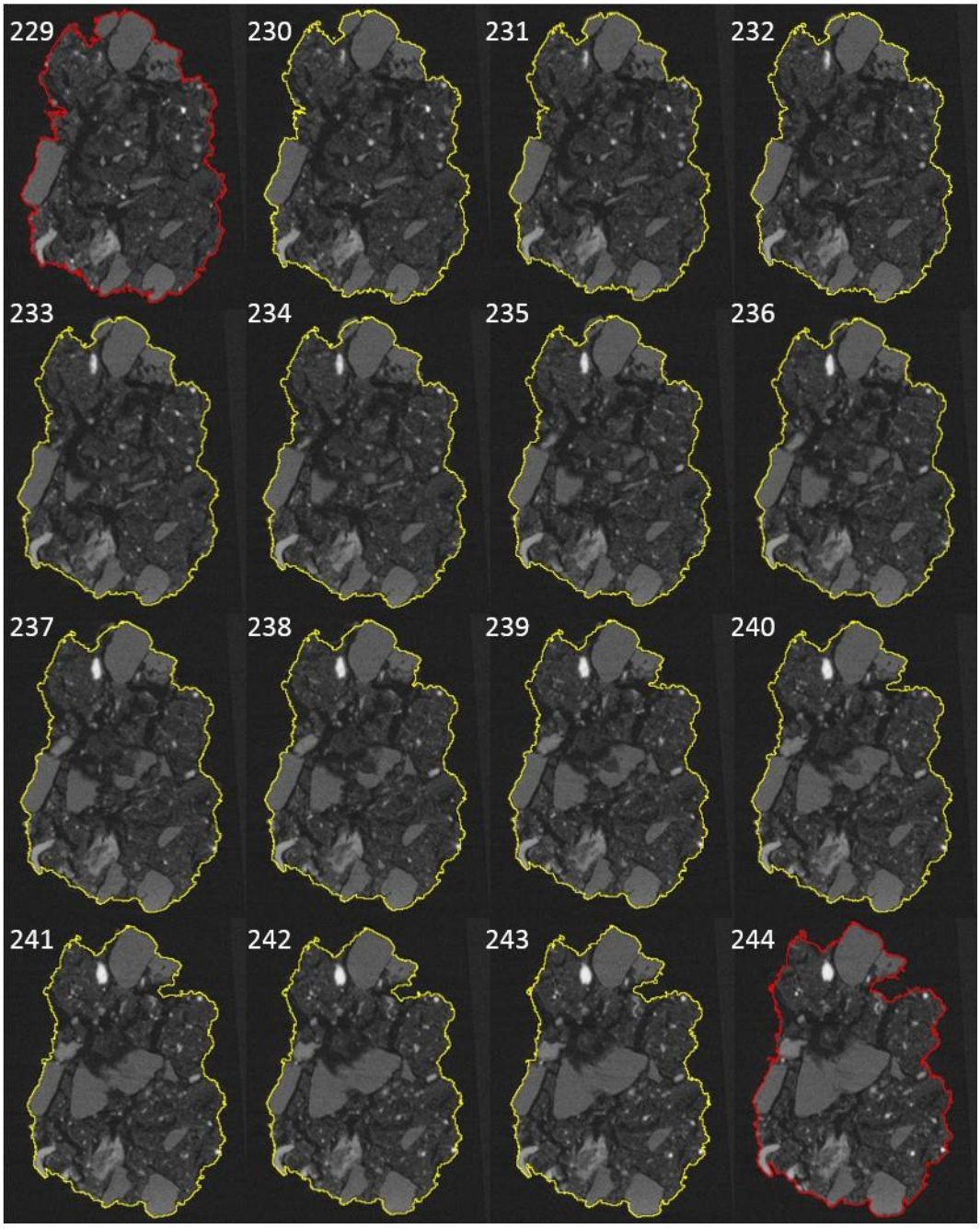

Figure 5.14: Aggregate images bearing manually selected (red) and interpolated (yellow) selections across 16 aggregate slices

It can be seen from Figure 5.14 that the Interpolate ROI function within ImageJ is excellent for creating representative interpolated selections. This figure, coupled with the porosity calculation validation detailed earlier (Table 5.7) produces a suitable approach to calculate the porosities of the aggregates resulting from this work (Figure 5.15).

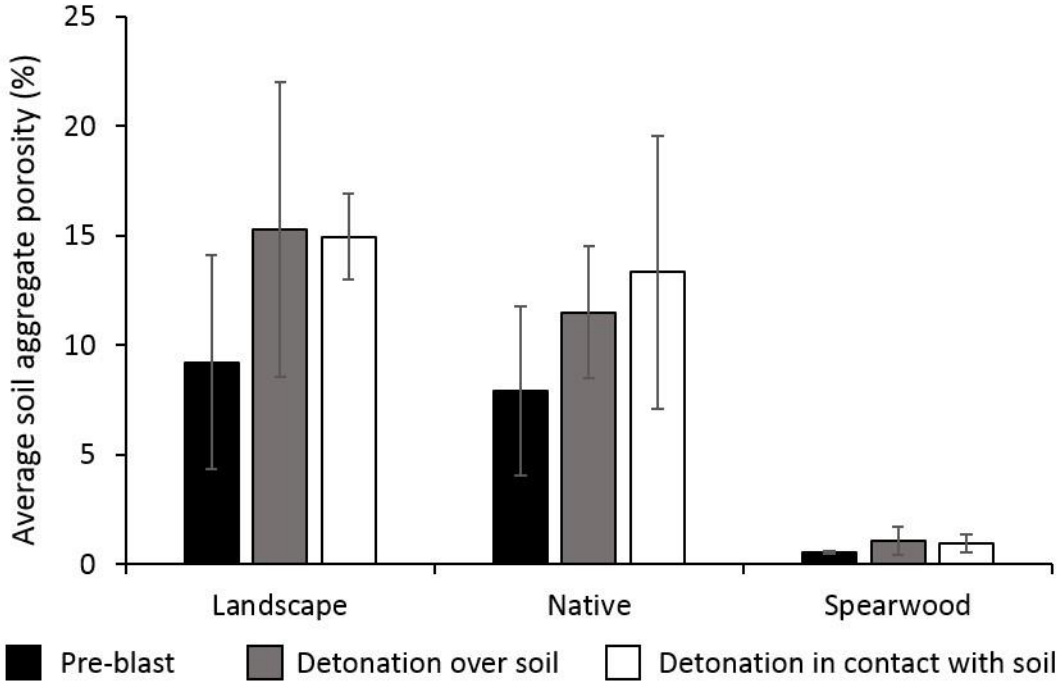

Figure 5.15: Calculated average porosities from the pre- and post-blast landscape, native and Spearwood soil aggregates analysed. Error bars show standard deviations between triplicate samples

Of the three types of soil subjected to µCT analyses in this work, it was evident that the Spearwood soil samples had a very different internal structure to the landscape and native soils (see Figure 5.13). The Spearwood soil samples are composed of mainly solid material, with few pores present which was confirmed with the calculated low porosities of Spearwood soil in Figure 5.15. Additionally, it was seen from the CT images that the Spearwood soil samples were much more internally homogeneous than the landscape and native soils.

In contrast, the landscape and native soils had much more heterogeneous internal structures (see Figure 5.13), with a large number of pore spaces. This is reflected well in the pre-blast porosities determined for the different aggregates, with the landscape and native soil aggregates displaying similar average porosities of approximately 9 % and 8 %, respectively, compared to the Spearwood soil, displaying an average pre-blast porosity of below 1 %.

An understanding of the internal architecture of soil aggregates, particularly with regards to their porosity, is important in establishing a link between soil microorganisms and their interactions with the soil itself, or any contained contaminants [115, 189]. Many key chemical, biological and physical processes occurring in soils are facilitated by its pore structure [189]. In recent years, µCT imaging has been used to investigate pore networks within soil aggregates, yielding information on parameters such as pore size, bioaccessible pore volumes and pore connectivity, and thus potential movement pathways of bacteria, water, oxygen and

nutrients through soils [115, 116, 190].

Pajor *et al.* [192] found that pore volume and connectivity affected the rate of fungal spreading in soils, and Nunan *et al.* [116] found that the internal structure of soils is highly heterogeneous, meaning complex soil-microbe interactions are likely. Interesting work by Marchuk *et al.* [189] investigated changes in soil aggregate pores depending on the proportion of cations bound to the soil aggregate. They found that pore parameters such as total porosity and pore connectivity were influenced by both a cation's valence and its prevalence in the soil, with soils with higher Ca^{2+} and Mg^{2+} levels displaying well-developed pore structures and connectivity compared to those predominantly containing Na^{+} or K^{+}.

Finally, as briefly outlined earlier, very recent work by Akbari *et al.* [190] assessed the role of soil pore size on the biodegradation of petroleum hydrocarbons in soils. The authors started with two types of hexadecane contaminated soil, and performed μCT and N_2 adsorption analyses to investigate the soil's internal architecture, pore sizes and structures. The authors also assessed the ability of bacteria to pass through porous membranes of specific pore sizes. The results showed that hexadecane biodegradation only occurred if pores were 5 μm or larger; consequently, only pores > 4 μm were deemed to be bioaccessible.

This finding was thought to be due to migration of the hexadecane into the soil's pores, initiated by an initial binding of the hexadecane onto the soil's mineral surfaces and subsequent movement of the hexadecane deeper into the aggregate structure. Depending on the pore size in which the hexadecane settled, this may be too small for access by bacteria, protecting the hexadecane from biodegradation. The authors hypothesise that the presence of very small (< 4 μm) pores within a soil may lead to a high bioremediation endpoint for the compound of interest, as a given fraction of the compound of interest would remain inaccessible to any bacteria present.

The authors also note that for coarse grained soils of a lower internal porosity (e.g. fine sands and gravel, such as the Spearwood soil used in this work), then the bioremediation endpoint for any contaminants of interest is likely to be dictated by the rate of biodegradation of the compound itself, rather than being affected by the fraction of the compound held in pores. If a soil has low/negligible porosity, then a negligible proportion of the compound of interest is likely to be encapsulated in pores at any one time. Ultimately, the authors concluded that assessing a soil's microstructure in this way was useful for qualitatively assessing the bioremediation properties of a soil.

With this in mind, it was hypothesised that the explosive residues deposited onto the soils may migrate within the pores present in the soil aggregates used. Depending on the pore sizes, and

the sizes of typical explosives-degrading bacteria present in the soils, this increases the likelihood that a greater proportion of the explosive residues will have become inaccessible to the soil bacteria, potentially leading to a longer duration of explosive residue stability. One of the most common genus of bacteria isolated from soils associated with TNT bioremediation is the aerobic *Pseudomonas* bacteria genus [80, 110]. Typical *Pseudomonas* bacteria have a size range from 1-5 μm [197], or larger as the bacteria can often aggregate or form chains [197], increasing their overall size. It is likely therefore that the bacteria present within the soils will have been unable to access pore sizes smaller than this.

By comparing the average pre- and post-blast porosities (Figure 5.15), it can be seen that the detonation process gives rise to a higher average porosity within the analysed aggregates. This is likely due to damage to the internal structure of the aggregates, creating larger pores within the soils. Example images of aggregates which appear to display cracks as internal damage are displayed in Figure 5.16.

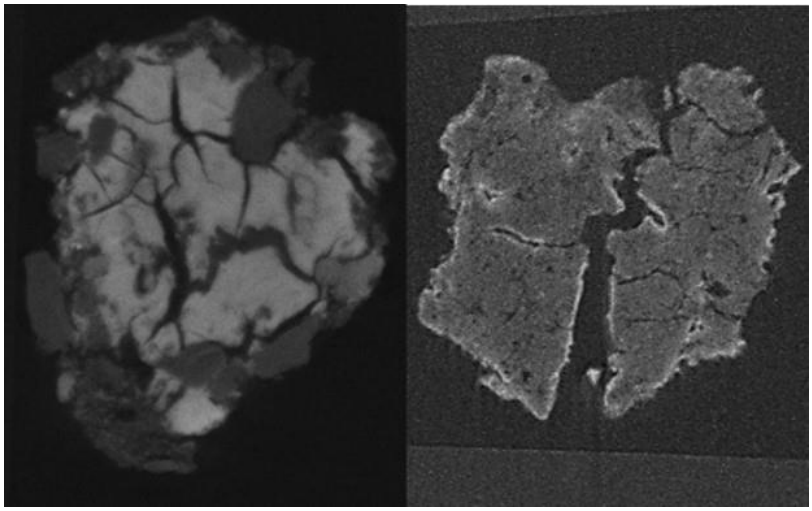

Figure 5.16: μCT images taken from post-blast aggregates displaying large cracks throughout the aggregate structures

An overall increase in porosity of the aggregate also increases the contained pore size, meaning that any TNT present within the pores is likely to be more bioaccessible by any bacteria within the soils, increasing the rate of degradation. The validity of this hypothesis is explored in the following section, by comparing the rates of explosive residue degradation between the solution-spiked soils of Chapter 4 and the detonation-spiked soils of the current chapter.

5.5.3 A comparison of the rate of TNT transformation between solution-spiked and detonation-spiked soils

As in Chapter 4, soil samples were stored at three temperatures: room temperature (20 °C), in a fridge at 1 °C and in a freezer at -20 °C. A maximum storage time after spiking of six weeks was used in this work, in line with previous recommendations [95]. Figure 5.17 displays the TNT recoveries obtained from landscape and Spearwood soil samples spiked using a controlled detonation process and subsequently stored at room temperature, in a fridge and in a freezer, extracted at various intervals over six weeks.

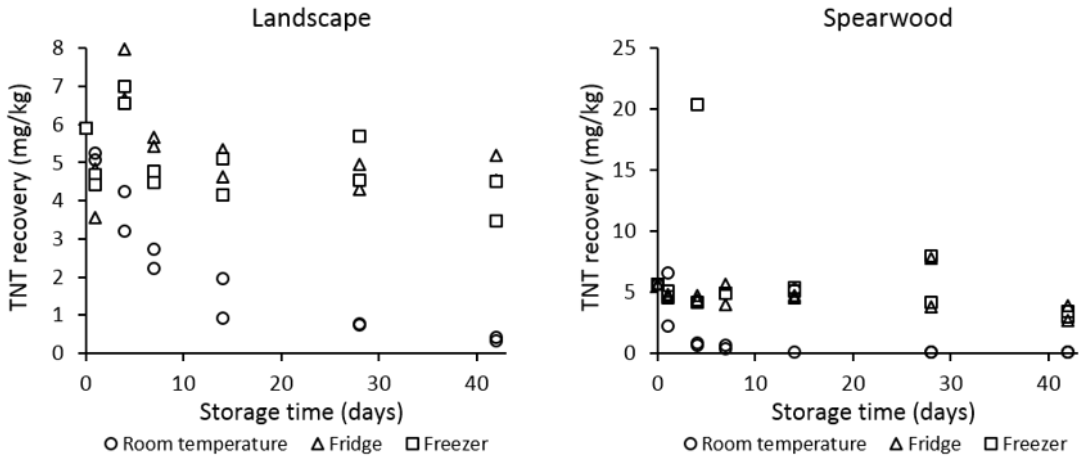

Figure 5.17: TNT recoveries obtained from post-blast landscape and Spearwood soil samples stored at three temperatures, extracting over six weeks

As evident from Figure 5.17, the levels of recovered TNT in the landscape soil samples remain broadly stable over time for those samples stored in the fridge and freezer, whereas the recovery levels from the samples stored at room temperature steadily decrease. The TNT levels in the Spearwood samples also remain relatively stable in the refrigerated and frozen samples, however a much faster decrease in TNT recovery over time is observed at room temperature compared to the landscape soil. The anomalous day four results for one of the freezer-based samples which shows TNT recovery of approximately 20 mg/kg, is most likely due to the presence of a large crystal of explosive within the soil sample. Overall, these results follow the same overall trend as seen for the solution-spiked samples in Chapter 4, but further investigation is required to directly compare the rate of TNT loss from the solution-spiked and detonation-spiked samples, to assess whether any significant differences are present.

In the solution-spiked samples of Chapter 4, TNT was spiked at a level of 2 mg/kg. For the recoveries depicted in Figure 5.17, a slightly higher quantity of TNT was spiked into the soils, given the limited control over the detonation-based spiking process. For this reason, as the

magnitude of TNT spiked into the soils differed, simply superimposing the solution-spiked room temperature recoveries onto the results in Figure 5.17 does not provide a meaningful comparison to be made between the degradation rates.

Alternatively, by averaging the TNT loss in mg/kg between each of the respective analysis time points for the solution-spiked results of Chapter 4 and the detonation-spiked results of the current chapter, a more robust assessment of whether the rate of TNT loss differed significantly between the samples resulting from the two spiking methods can be determined (Figure 5.18). Two outlying results were removed from the Spearwood detonation-spiked results prior to this calculation, as these are attributed to the presence of large, discrete TNT crystals within the soil samples which would have otherwise impacted any conclusions. The high relative standard deviations between the levels of TNT (mg/kg of soil) detected in the six samples used to assess TNT homogeneity within the post-blast soils (Table 5.4) reinforces the likelihood that these outliers were due to heterogeneously-distributed TNT crystals.

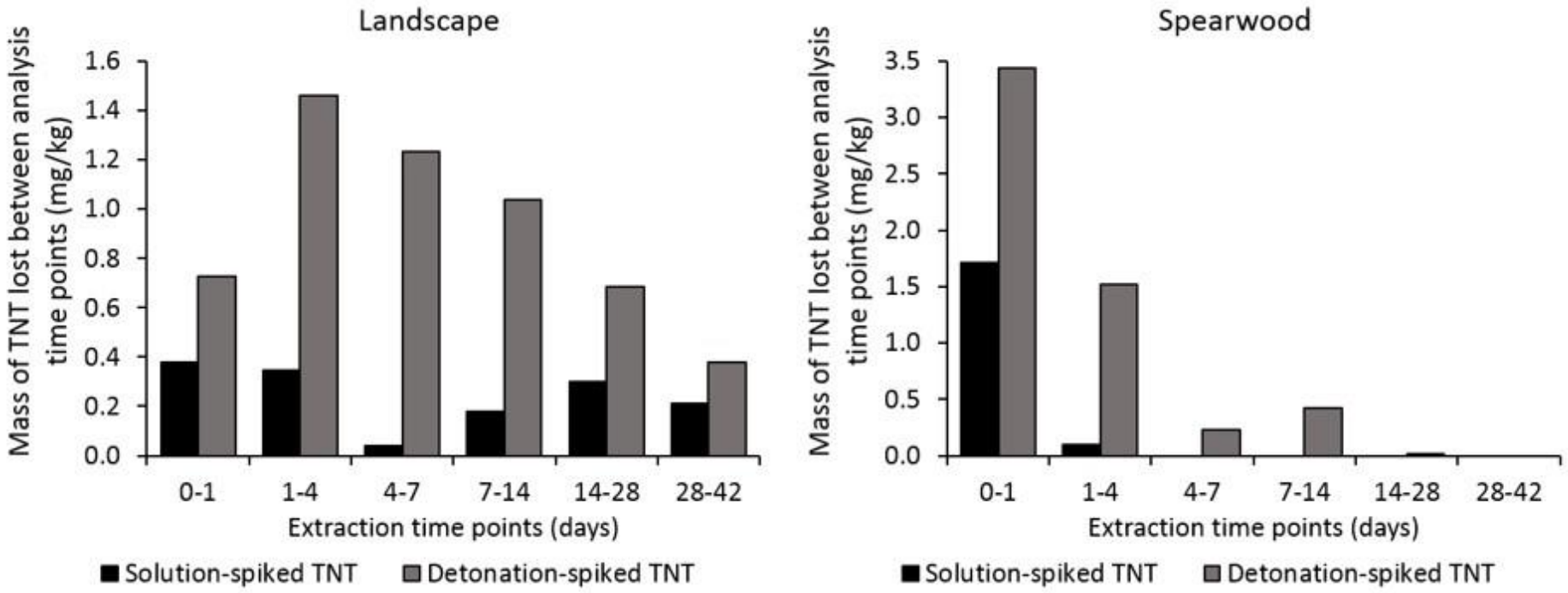

Figure 5.18: Average (n=2) TNT loss between the analysis time points used for this work, from spiked pre-blast and post-blast samples

.

It can be seen from Figure 5.18 that in the solution-spiked landscape soil samples, TNT is lost gradually over the six week timespan of this study. In contrast, in the solution-spiked Spearwood samples, the majority of the TNT spiked into the samples was lost within the first day following sample spiking; while at the same time, the rapid emergence of a TNT microbial degradation product (4-ADNT) was seen. As shown from the µCT images presented earlier, the internal structure of these two soils is very different, with many pores present within the landscape soil, but almost no pores observed within the Spearwood soil (Figure 5.13). Taking into account the findings of Akbari *et al.* [190], who reported that soil pores may act as a 'sink' for hexadecane in soils, preventing its biodegradation, this raises the possibility that the pores within the landscape soil act as a 'sink' for the TNT, with the TNT migrating into the pores of the landscape soil and thus becoming less accessible for microbial degradation, leading to a resultant longer TNT half-life in the landscape soil.

In contrast, as the Spearwood soil has very few fine pores within its grain structure, any TNT spiked into the soils would have remained on the surface of the soil particles and would have been fully exposed to the microbes within the soil, making it susceptible to very rapid microbial degradation.

It can also be seen from Figure 5.18 that a much faster rate of TNT loss was observed from the detonation-spiked soils compared to the solution-spiked soils, and this coincided with an increase in the soil aggregates' porosity in the post-blast soils (Figure 5.15). These results suggest a detonation-induced phenomenon is responsible for such a significant increase in the rate of TNT loss from the post-blast soils. It is highly likely that the increase in porosity observed in the post-blast soils facilitated bacterial movement through the soil aggregates, making it easier for the bacteria to access the TNT and bring about its transformation.

The discussion so far has related to TNT deposition into soils following an efficient detonation. However, as discussed, a misfire occurred during one of the detonations over native soil. In this case, even in the native soil samples stored at room temperature, high levels of TNT were still observed after six weeks (Figure 5.19). This is in contrast to the results from the landscape and Spearwood soils, where the TNT recovery level fell substantially over the six weeks (Figure 5.17).

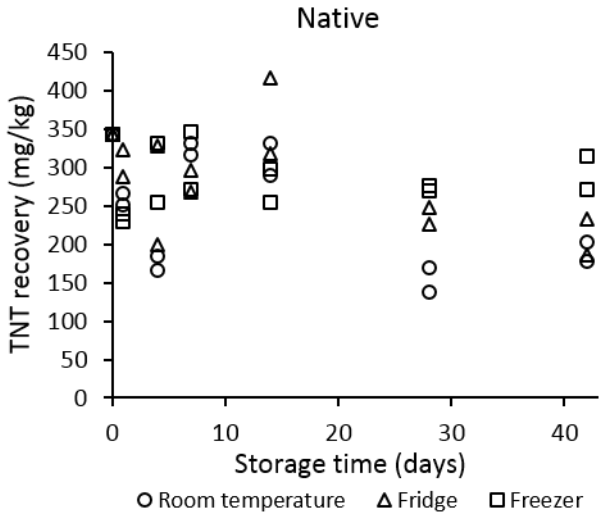

Figure 5.19: TNT recoveries obtained from post-blast native soil samples stored at three temperatures, extracting over six weeks

The misfire over the native soil resulted in the deposition of significantly larger quantities of TNT into the soil (approximately 60 times the level deposited into the landscape and Spearwood soils). It may have been thought that the high levels of TNT initially present would mean that any decrease in TNT recovery on the order of that observed in the landscape and Spearwood soils would not be easily discerned, due to the magnitude of the y-axis for the native soil sample. However, by comparing the levels of the TNT degradation product 4-ADNT recovered from the room temperature samples of these three soils (Figure 5.20), it is clear that a different phenomenon occurred in the native soil.

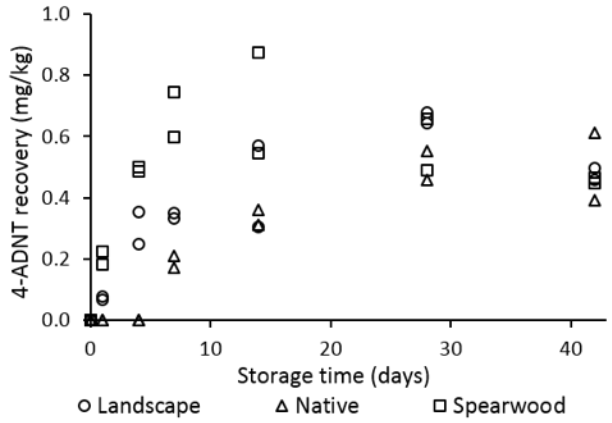

Figure 5.20: 4-ADNT recovery from controlled detonation-spiked landscape, native and Spearwood soils stored at room temperature and extracted over six weeks

With such high initial levels of TNT within the native soil samples, it was anticipated that this would lead to a corresponding increase in the rate of TNT transformation and thus an enhanced rate of formation of 4-ADNT. This was not the case, and it was not until day seven that any 4-ADNT recovery was observed in the native soil, whereas 4-ADNT was recovered from the

landscape and Spearwood samples after just one day. This is possibly due to the high levels of TNT having an inhibitory effect on any TNT-transforming bacteria within the native soil, and that this time lapse is due to the bacteria adjusting to their heavily TNT-contaminated environment before beginning transformation of the TNT. Singh [89] has shown that high levels of TNT may have a toxic effect on bacteria in soils, and it is likely that this is the case in the native soil, accounting for the lower rate of observed microbial degradation. Other work [77] has also reported a prolonged TNT half-life due to high levels of TNT in soil and related bacterial inhibition processes.

This finding raises an interesting consideration with respect to the overall aim of this work. The motivation behind this research was to try to preserve *low* levels of explosive residues present in soil. However, as demonstrated both in this work and by previous studies [77], misfires can occur, which are likely to deposit significantly higher quantities of explosive residues into soil. In the case of TNT, high levels may exhibit a toxic effect on any bacteria present, which unexpectedly slows the rate of TNT degradation. Regardless of this, sample collection and storage should be conducted based on a 'worst-case-scenario' - that low levels of TNT are present in the sample and that the transformation process is very rapid.

Figure 5.21 displays the PETN recoveries obtained from landscape, native and Spearwood soils, respectively, with samples stored at room temperature, in a fridge and in a freezer.

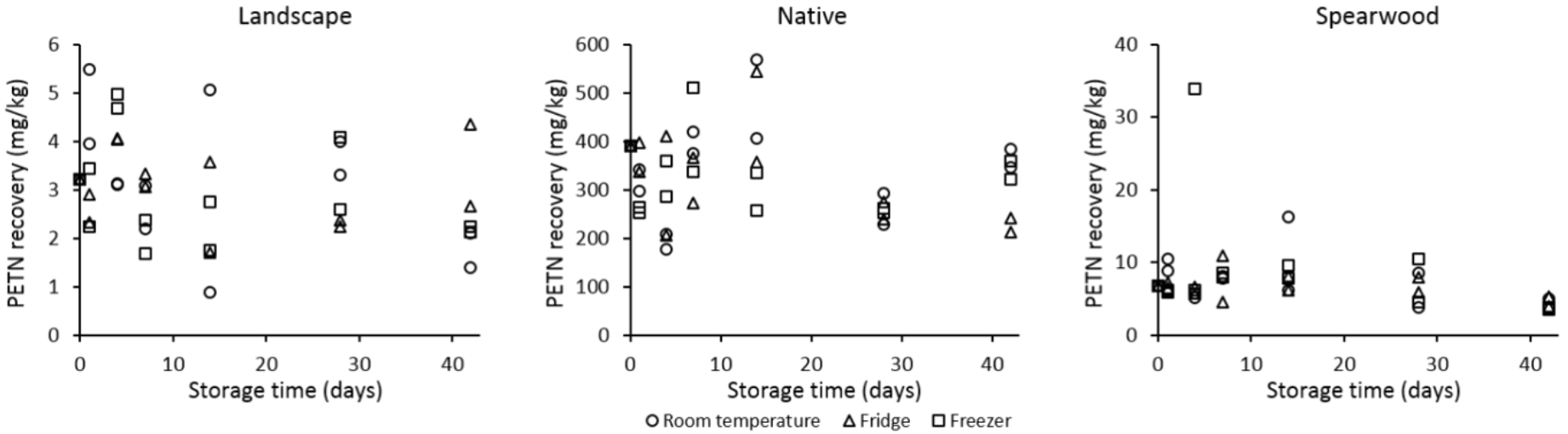

Figure 5.21: PETN recoveries from controlled detonation-spiked landscape, native and Spearwood soils stored at room temperature and extracted over six weeks

For the solution-spiked samples from Chapter 4, relatively low (around 20 %) PETN recoveries were seen over time from the soils. However, the PETN recoveries from the detonation-spiked samples shown in Figure 5.21 show that the PETN levels remain fairly stable over time with respect to the day zero samples. This suggests that some differences exist between the stability of PETN spiked into soils using an aqueous solution, and PETN spiked into soils using a controlled detonation. The detection of PETN in soil samples across a range of soils and sample storage temperatures following deposition from an actual explosion is encouraging, as it means that PETN residues deposited into soils from detonating cord, for example, may still be detected over a long period of time, even if TNT undergoes more rapid degradation.

In the current work, spiked soil samples were stored at three different temperatures: room temperature, refrigerated (1 °C) and frozen (-20 °C). TNT recoveries in particular were consistently higher over time from the refrigerated and frozen soils than those stored at room temperature (Figure 5.17). In contaminated soils within the environment, the geographic location of the soil may therefore have an influence on the rate of TNT loss. In a cooler climate or an area with limited direct sunlight, the results of Chapter 4 and the current chapter suggest that TNT loss would occur much more slowly. In contrast, TNT loss would be expected to occur more rapidly in warmer climates.

5.6 Conclusions and future work

This work aimed to assess whether simulated bombings were capable of giving rise to soil fracturing. Comparative detonation setups, with explosives detonated either in contact with three different soils or 50 cm above the three soils, showed via SEM that fracturing occurred in each case, exposing fresh mineral surfaces within the soils. In addition to this, detonations gave rise to a smaller soil particle size, and the use of a novel μCT procedure revealed that detonations increased the overall porosity of the soil aggregates. The implications of this have been explored in the current work.

The results from this chapter suggest that pores present within some soil types may act as ‘sinks’ for soil contaminants such as TNT, reducing its availability for microbial degradation and transformation. It was also found that TNT transformation occurred much more rapidly in post-blast soils than in analogous solution-spiked soils (Chapter 4). It is proposed that this is due to the detonation process causing internal damage to soil aggregates, resulting in increased porosities and larger pore sizes which would then become more bioaccessible to any bacteria present within the soils.

Fifteen detonations were performed in this work, with an average TNT detonation efficiency

of 99.995 %. This illustrates that only minute quantities of explosive residues are likely to be deposited in soils following a detonation using a commercial explosive, highlighting the importance of maximising their stability prior to sample extraction and analysis. Based on the results of this work, freezing samples between collection and analysis proved the most effective means of reducing explosive residue loss. Interestingly, this work has illustrated that high TNT levels in soil may act in a toxic manner towards soil bacteria, which may decrease the rate of TNT degradation and transformation. When comparing the attenuation of PETN in solution-spiked and controlled detonation-spiked soil samples, the PETN displayed a higher stability in the soil samples spiked using an actual detonation process.

Further research in this area should involve the use of a wider range of explosives to determine the degradation and transformation patterns of alternative explosives in soils. Additionally, it would be of interest to perform actual vehicle bombings to evaluate the degree of observed soil fracturing and explosive residue loading. Finally, it would also be useful to compare explosive residue loadings into soils from explosives strapped beneath a car, to explosive residue loadings into soils from explosives detonated within a vehicle, such as in the passenger foot well of a car, to compare the degree of explosive residue loadings and severity of soil fracturing resulting from the different charge position.

Chapter 6 Development of a gel polymer-based sensor for the electrochemical detection of TNT

6.1 Introduction

An ability to quickly and easily detect TNT directly at a wide range of locations, such as at post-explosion scenes, and, from a bioremediation aspect, in soil and groundwater, is highly desirable. As demonstrated in Chapters 4 and 5, explosive residues can undergo very rapid degradation in soils, which may be exacerbated by any time involved in transporting samples to a laboratory prior to extraction and analysis. On the other hand, on-site sampling using portable detection equipment offers the significant benefit of immediate analysis at or near the site of sample collection, which should reduce the degree of any explosive residue degradation prior to analysis. A number of portable detection methods are available for the on-site detection of explosive residues, such as TNT, as outlined in Chapter 1. Electrochemical sensors in particular are highly suitable for use as portable detection instrumentation as they are cheap, lightweight, can be miniaturised, have low power requirements and provide high sensitivity [129, 130, 136, 198, 199]. In addition, due to their speed of analysis, they offer the possibility to perform real-time monitoring. Currently, electrochemical techniques are not routinely used for the analysis of forensic explosives samples, though they show excellent potential for use as sensitive, fast, cheap and portable at-the-scene detection techniques. This chapter provides an overview of electrochemical techniques and their utility in explosives detection, before describing the development of a novel gel polymer-functionalised thin-film electrode for the electrochemical detection of TNT from aqueous samples.

6.1.1 Electroanalytical chemistry

Electrochemistry can be defined as the study of chemical phenomena associated with charge transfer [200]. In this chapter, dynamic electrochemistry techniques are employed for the detection and sensing of TNT. Dynamic electrochemistry involves the study of electron transfer between (typically) metallic electrodes and reactant molecules in the solution-phase [201].

A number of different electrochemical methods can be used: potentiometric (measurement of equilibrium potentials), amperometric (measurement of current) and conductometric

(measurement of conductivity) [202]. The work presented in this chapter investigates the use of amperometric techniques for the detection and analysis of TNT. Electrochemical sensors require an electrolyte – an ionically conducting medium. The role of the electrolyte is to transport charge, provide contact between the electrodes and solubilise the reactants and products to enable efficient mass transport to occur [203]. The technique involves applying a potential (measured in Volts) between two electrodes, and measuring the resulting current due to redox process(es) associated with the target analyte. The recorded current corresponds to specific redox reactions of an analyte molecule, and the potential at which it occurs provides some specificity regarding the identity of the compound. The magnitude of the recorded current typically corresponds to the concentration of the compound present [136, 198, 202, 204].

6.1.2 Voltammetry

Voltammetric techniques are a sub-class of amperometry. Voltammetry involves the measurement of electrical current as a function of applied voltage (potential). Typically, a three-electrode setup is used, with a working electrode (WE; where the electrochemical reaction of interest occurs), a reference electrode (RE; which provides a stable reference potential with respect to the potential at the WE), and an auxiliary counter electrode (CE; where the opposite cell reaction occurs) [201]. Often these setups involve relatively large electrodes (approximately 80 mm long × 6 mm diameter) immersed into a beaker containing the analyte of interest in an electrolyte solution. Figure 6.1 illustrates a typical three-electrode setup with counter, working and reference electrodes.

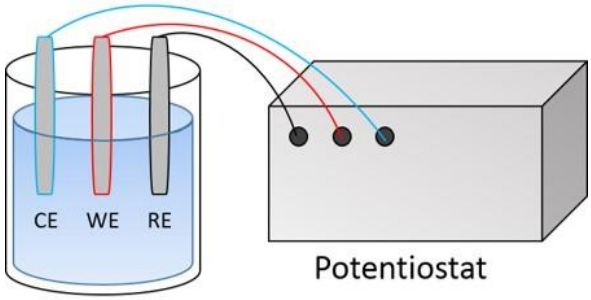

Figure 6.1: Schematic of a conventional 'three-electrode' setup including counter (CE), working (WE) and reference (RE) electrodes in a 'beaker-type' cell, connected to a potentiostat

A number of parameters may influence electrode reaction dynamics, including the electrode potential, the redox reactions of the analyte of interest (i.e. ease of oxidation or reduction), the properties of the electrode surface, the structure of the electrode-solution interface where electron transfer occurs and analyte transport between bulk solution and the electrode (mass transport).

In order for an electrode reaction to occur, the analyte species must be transported to the WE surface. Mass transport concerns the movement of an analyte from bulk solution towards an electrode surface, as well as movement of the reaction products away from the electrode. Three different processes can influence mass transport: diffusion, convection and migration [201].

Diffusion occurs to reduce compositional heterogeneities in a solution when uneven concentration distributions are present. Analyte species diffuse from an area of high concentration in the bulk, to an area of low concentration at the electrode surface. *Convection* occurs when a mechanical force acts on a solution. This may be either natural convection, due to thermal or density gradients naturally present within a solution, or forced convection, achieved through the application of external forces such as stirring or bubbling gas through a solution. *Migration* occurs as a result of an electrostatic force induced in the electrode-solution interface caused by a drop in electrical potential between the two phases. In the majority of experiments performed in the present work, only the diffusion aspect of mass transport is relevant, with the convection and migration aspects of mass transport kept negligible (i.e. without the use of a stirrer bar).

Many WEs have diameters in the millimetre to centimetre range; so-called 'macroelectrodes'. However, microelectrodes are also available. Microelectrodes are typically around 10 μm in diameter, and offer the significant benefit of being able to analyse very small sample volumes. As the current measured is a function of electrode area, the current at a microelectrode is much lower than at a macroelectrode. Due to the geometry of the electrode, radial diffusion quickly dominates. The result is that a much faster rate of mass transport will occur at microelectrodes compared to macroelectrodes [201], generating higher current density and better sensitivity due to a higher signal to noise ratio.

A number of different materials have been used as a WE for electrochemical explosives analysis, with the resulting voltammetric performance suggested to strongly depend on the WE material [199]. The vast majority of previous electrochemical research involving explosives analysis has involved the use of glassy carbon electrodes [124, 125, 128, 133, 199, 205-228], likely due to their ease of use and functionalisation, robust nature and good analyte responses. A number of other electrode materials have also been reported for the electrochemical detection of explosives, including gold [138, 199, 207, 210, 229-233], carbon fibre [199, 234, 235], copper [236], platinum, nickel and silver [210].

Although the use of glassy carbon electrodes for explosives sensing appears to be the most widely reported in the literature [124, 125, 128, 133, 199, 205-228], it is difficult to construct glassy carbon into integrated planar electrodes [237]. However, a number of other electrode

materials (such as gold) have been miniaturised into planar electrodes. These combine working, reference and counter electrodes into a miniaturised, planar interface, providing ease of use and portability, with the potential to be used for explosives detection 'at-the-scene' [138]. These miniature electrodes take two common forms: screen-printed electrodes (SPEs) [121-123, 126, 132, 238] and thin-film electrodes (TFEs) [138, 239]. In the present work, the decision was made to utilise a commercial gold thin-film electrode (Au-TFE) (Micrux Technologies, Oviedo, Spain, http://www.micruxfluidic.com). Figure 6.2 illustrates the size and electrode layout of these TFEs.

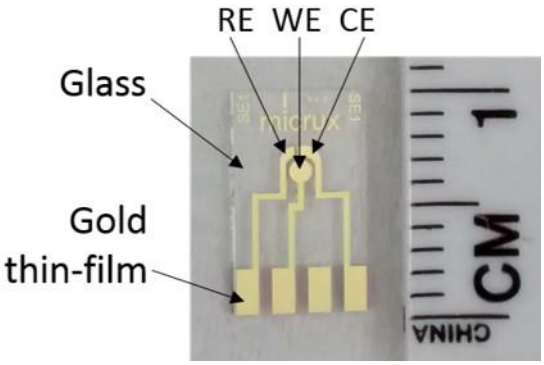

Figure 6.2: Photograph of the gold thin-film electrodes used throughout this thesis, containing planar working electrode (WE), reference electrode (RE) and counter electrode (CE)

These planar electrodes offer electrode surfaces made entirely of gold (i.e. with no binders present), and a small WE area (approximately 1 mm diameter). The use of a miniature planar integrated electrode means that only very small aliquots of electrolyte (a few microlitres) are required for analysis [138, 239, 240].

6.1.3 Background to the electrochemical techniques used in this chapter

A number of different electrochemical techniques can be applied for explosives detection, including cyclic voltammetry (CV), square wave voltammetry (SWV) and chronoamperometry. Cyclic voltammetry involves sweeping from a starting potential (E_1) to a final potential (E_2), before reversing the direction of the sweep and scanning back to the original potential (E_1). A schematic illustrating the variation in applied potential as a function of time for such a CV experiment is shown in Figure 6.3.

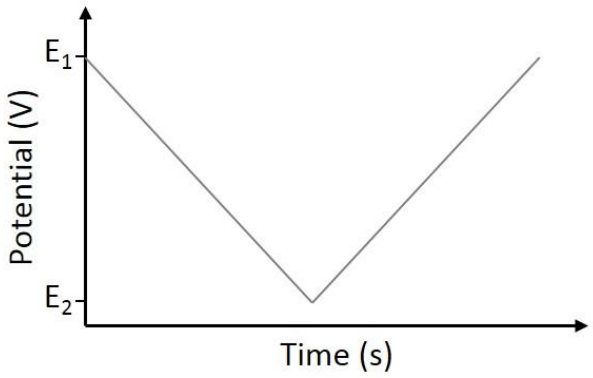

Figure 6.3: Variation of the applied potential vs time during a cyclic voltammetry experiment

For the redox couple A + e^- ⇌ B, species A will undergo reduction to species B between E_1 and E_2, before undergoing oxidation back to species A upon the reverse sweep. The output to the experiment is a plot of current vs the applied potential – a cyclic voltammogram. A figure illustrating the typical cyclic voltammogram shape for a fast reversible redox couple is provided in Figure 6.4.

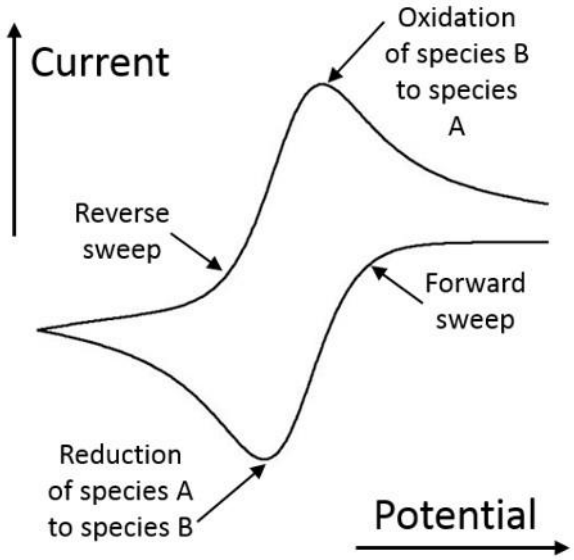

Figure 6.4: Cyclic voltammogram for a reversible reduction reaction, adapted from reference [201]

The Randles-Sevcik equation [241] can be used to describe the relationship between the current and other reaction variables (eq. 2):

$$I_p = 0.4463nFAc_R\sqrt{(nFvD_R/RT)} \quad \textbf{(2)}$$

Where I_p is the current (A), n is the number of electrons transferred, F is the Faraday constant (C mol^{-1}), A is the electrode area (cm^2), c_R is the concentration of analyte (mol cm^{-3}), v is the sweep rate (V s^{-1}), D_R is the diffusion coefficient of the analyte species (m^2 s^{-1}), R is the

universal gas constant (J mol^{-1} K^{-1}) and *T* is temperature (K).

Several CV analyses were performed in the present work. CV is a quick and easy technique to provide information about the system under investigation [201]. In addition to being useful for quantification purposes, CV is an ideal technique for studying electrochemical reaction mechanisms [206]. An example of a cyclic voltammogram showing the sequential reduction of the three nitro groups of TNT, followed by their oxidation on the reverse sweep, is provided in Figure 6.5 [138].

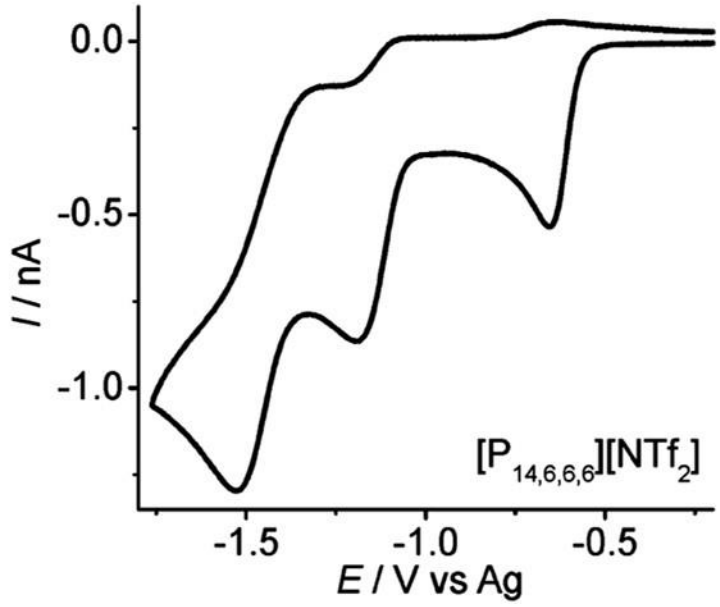

Figure 6.5: Cyclic voltammogram showing the reduction of the three nitro groups of TNT, followed by their corresponding oxidations on the reverse sweep. Figure sourced from Kang *et al.* [138]

Square wave voltammetry (SWV) involves superimposing a square wave on a potential staircase, to give an overall waveform of the form shown in Figure 6.6 [242]. Only the forward sweep is generated in a SWV experiment.

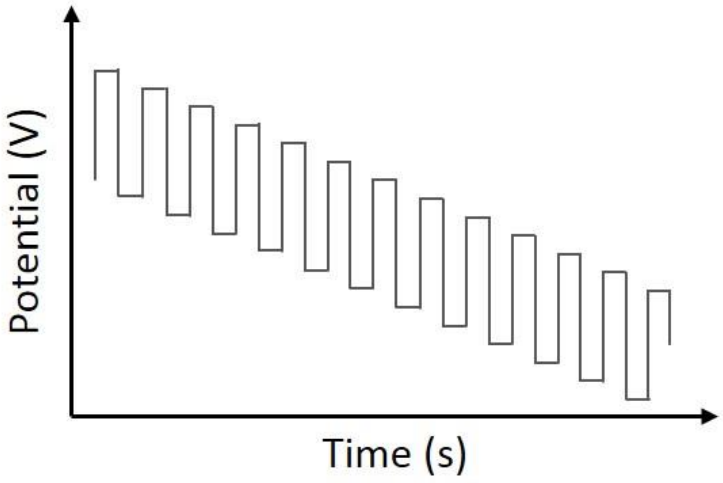

Figure 6.6: Series of short potential steps applied during a square wave voltammetry analysis

During a series of short pulses, the current is measured at the top and bottom of every step, giving currents that correspond to the forward (Ψ_f) and backward (Ψ_b) peaks. The difference ($\Delta\Psi$) is then plotted as the primary result of the SWV scan (see Figure 6.7).

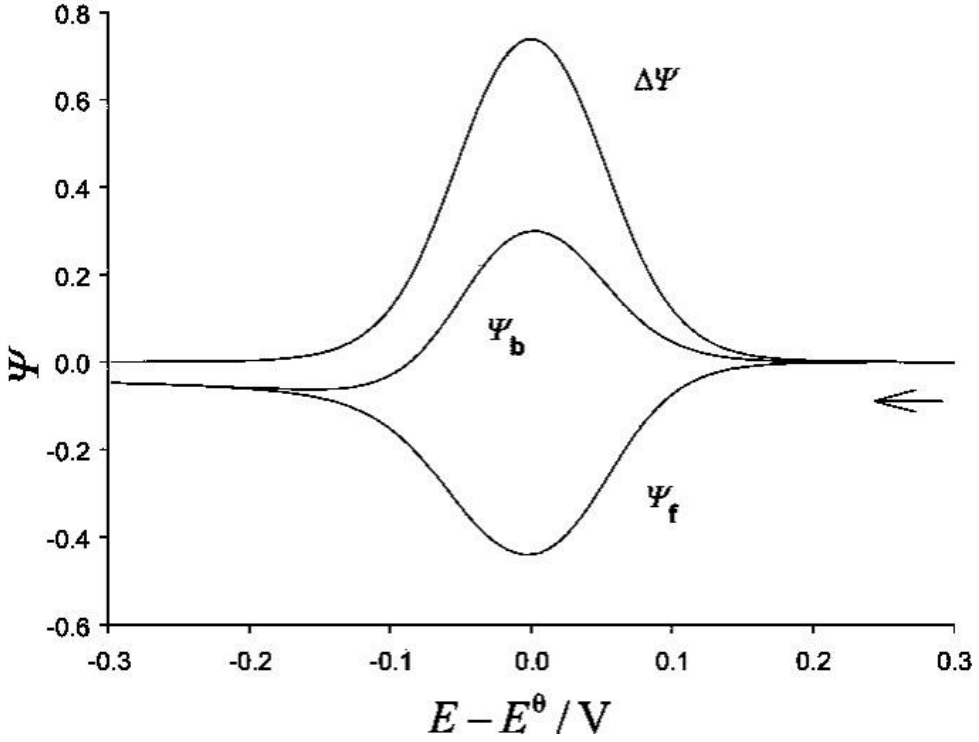

Figure 6.7: Calculation of the overall current ($\Delta\Psi$) resulting from the forward (Ψ_f) and backward (Ψ_b) components during a square wave voltammetric analysis. Figure from reference [243]

The main benefit of SWV is that it minimises capacitive contributions (a phenomenon arising from the subtraction of the backward current from the forward current). This can result in an

improved signal to noise ratio compared to CV, leading to very low detection limits. SWV offers high sensitivity with fast scan rates, meaning it is often the method-of-choice for analytical electrochemistry studies [130, 198, 199, 206, 242]. In the present work, SWV was chosen as the primary technique for TNT analysis, following the TNT-sensing work of Xiao *et al*. [206]. SWV typically gives an electrochemical profile of the reduction steps for species of interest in a sample (i.e. without providing information on their reverse peaks). An example square wave voltammogram showing the sequential reduction of the three nitro groups of TNT is provided in Figure 6.8 [206].

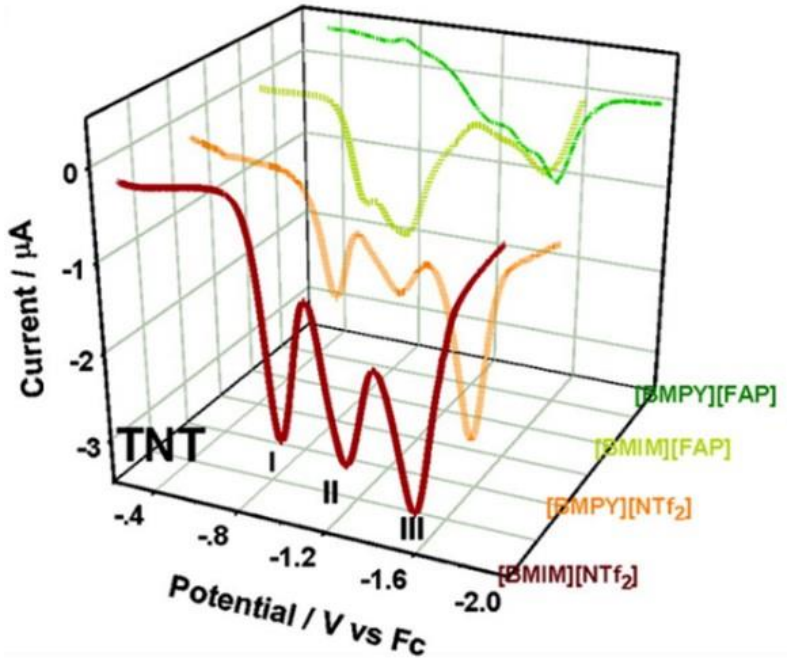

Figure 6.8: Example square wave voltammograms showing the sequential reduction of the three nitro groups of TNT in four different room temperature ionic liquids. Sourced from Xiao *et al.* [206]

SWV has been utilised in a number of studies investigating the electrochemical detection of explosives [203, 206, 234, 244], with a number of other studies opting for CV-based analyses [122, 128, 129, 203, 206, 218, 221-223, 232, 245-247].

Chronoamperometry involves the study of current response over time. The technique involves instantaneously stepping the potential of the WE from E_1 to E_2, and holding at this potential for a fixed amount of time. A schematic is provided in Figure 6.9a. This changes the situation from only species A being present at the WE (at potential E_1), to one where species A undergoes complete conversion to species B (at E_2). This process causes a large current spike, which decreases quickly over time as the diffusion layer thickness gradually increases around the electrode and species A becomes depleted. An example of the experimental output is illustrated in Figure 6.9b.

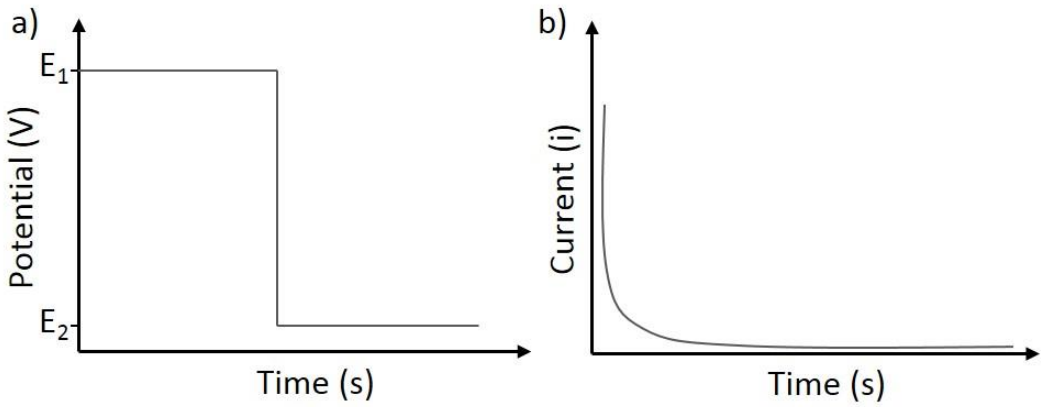

Figure 6.9: a) Instantaneous stepping from potential E_1 to potential E_2 during a chronoamperometric experiment and b) Decrease in current with respect to time during a typical chronoamperometric analysis

For a microelectrode, due to the dominance of radial diffusion, the current decays to a steady-state value – unlike the decay to zero on a macroelectrode. Calculations can then be performed on the resulting current response to determine the initial concentration of species A in the solution by use of the Shoup and Szabo equation [248], displayed below (eq. 3):

$$I = 4nFcDr_e f(\tau) \quad \textbf{(3)}$$

$$f(\tau) \approx 0.7854 + 0.8862\tau^{-½} + 0.2146e^{-0.7823\tau^{-½}} \quad \textbf{(4)}$$

$$\tau = (4Dt/r_e^2) \quad \textbf{(5)}$$

Where I is the limiting current (A), n is the number of electrons transferred, F is Faraday's constant (C mol^{-1}), c is concentration (mol cm^{-3}), D is the diffusion coefficient (m^2 s^{-1}), r_e^2 is the microelectrode radius (m) and τ is dimensionless time.

6.1.4 Explosives analysis using electrochemistry

A wide range of explosives are electroactive and have thus been the subject of electrochemical research. TNT is a particularly good candidate for electrochemical detection due to its redox activity. The majority of electrochemical explosives research to date has focused on TNT detection, both in aqueous samples [122, 124, 125, 128, 129, 132, 133, 205, 208, 210, 213-215, 217-220, 225, 227, 232, 234, 235, 238, 244, 247, 249-254] and in the vapour phase [123, 134, 136, 204, 206, 245, 255, 256]. Although not currently employed as an explosives detection technique in forensic explosives laboratories, electrochemical detection techniques have been compared to established explosives detection techniques, such as EPA Method 8330 (discussed in Chapter 4), and found to give comparable results [222]. This shows the potential of electrochemistry to be developed as a more mainstream explosives detection and

quantification technique. In addition to protic solvents such as water, a small quantity of research has investigated TNT detection in aprotic solvents, such as acetonitrile and ionic liquids [138, 206, 216, 222, 245].

Electrochemical sensors have previously been utilised for the detection of explosives [202]. Papers dating from the early 1980s detail the use of 'coupled' electrochemical techniques for the analysis of nitroaromatic explosives, nitrate esters and nitramines, including TNT, DNT and tetryl [207, 250, 253, 257]. For example, low detection limits of 25 ppb for TNT were reported from a HPLC instrument coupled to an electrochemical detector [253]. Nitro-based explosives in particular are ideal for electrochemical detection due to their inherent redox properties [198, 202], with the nitro groups being easily electrochemically reduced [199]. The reduction pathways of many nitro-based explosives have been reported [130].

As well as TNT, a number of other nitro-based explosives have also been studied using electrochemical techniques. These include DNT [122, 124, 206, 208, 217-219, 222, 244, 251, 253, 255, 258], RDX [132-134, 208, 210, 216, 218, 222, 244, 247, 259, 260], HMX [132, 216, 218, 222, 244], PETN [134, 135, 216, 244, 247, 254, 260], tetryl [216, 253], trinitrobenzene [217], nitrobenzene [233], NG [135, 244], EGDN [135] and picric acid [236]. In addition, electrochemical techniques are also being exploited for the analysis of peroxide-based explosive analytes such as TATP [198, 211, 223, 224, 261-263] and HMTD [223, 246, 261, 263, 264]. These examples illustrate the versatility of electrochemical techniques for explosives analysis.

6.1.5 Electrode miniaturisation

Over recent years, a shift has been seen towards the development and use of miniaturised screen-printed and thin-film electrodes for explosives sensing, likely due to the utility of portable sensors being recognised [129, 136, 198, 199, 202]. Such miniaturised electrodes will remove the need for bulky 'beaker type' cells to be employed for field-sampling. An example of a commercially available portable electrochemical instrument is the blood glucose instruments available for diabetics [246], widely available to purchase. Other portable electrochemical detection devices have also been developed for the detection of heavy metal contaminants in the environment [265-267]. Screen-printed electrodes (SPEs) involve a thick film of (typically) carbon paste (often containing binders/polymers [240]) screen-printed onto a planar substrate such as plastic, ceramic or silicon; the working, reference and counter electrodes are all integrated onto a single strip. Similarly, thin-film electrodes (TFEs) contain lithographically transferred working, reference and counter electrodes on a single strip [199]. Compared to screen-printed electrodes, the electrode surface of TFEs is purely metal-based,

promoting cleaner voltammetry less likely to be complicated by follow-up chemistry from any binders present [240].

These 'self-contained' electrochemical cells show great potential for at-the-scene explosives sensing, and have been reported in a number of recent works. For example, screen-printed electrodes have been used for TNT detection in aqueous samples [122, 238, 244, 247, 251], including a novel 'forensic finger' consisting of a finger sleeve screen-printed electrode for explosives detection at a scene [121], and a screen-printed neoprene suit for underwater TNT detection by divers [252]. Screen-printed electrodes have also been utilised for the detection of TNT vapours [123]. Some of these electrodes are designed to be disposable [122], whereas others have been shown to give reproducible results over a period of 1.5 years [251]. Very recently, Kang *et al.* used gold TFEs to investigate the electrochemical reaction mechanism of TNT in ionic liquids [138].

6.1.6 Electrode functionalisation

Although glassy carbon is a relatively sensitive WE material, recent work has investigated the functionalisation of WEs using a variety of materials. This approach can give rise to enhanced chemical and physical properties of a system, such as increased electrode sensitivity, increased surface area for redox reactions to occur, improved conductivity, catalytic effects and the potential for improved selectivity [128, 130, 198, 205, 268, 269]. A variety of materials for electrode functionalisation have been reported, including graphene and graphite, carbon nanotubes, metal nanoparticles, ordered mesoporous carbon, nanoporous carbon and polymers.

Graphene in particular has been widely used for the modification of electrodes [125, 128, 129, 205, 214, 220, 249] due to its high surface area, high conductivity, chemical stability and its homogenous distribution of electrochemically active sites. In addition, it offers the possibility of TNT pre-concentration, due to the aromatic rings in TNT and graphene being able to undergo favourable interactions (such as π-π interactions, hydrophobic, electrostatic and hydrogen bonding interactions [220]) allowing TNT to adsorb on the graphene surface [129, 130, 220, 249, 269]. Graphene-functionalised WEs have been widely reported to show a higher sensitivity towards TNT than analogous bare metal electrodes. Similarly, carbon nanotubes [215, 217, 249, 251] and ordered mesoporous and nanoporous carbon functionalised electrodes [124, 215] have been used due to their large surface area and enhanced electron transfer ability.

In addition to the substantial work performed with regards to electrode functionalisation with graphene and carbon nanotubes, some recent work has also been performed with regards to electrode functionalisation using conducting polymers [239, 240]. Polymers offer a number of

advantages over graphene and carbon nanotubes – for example, carbon nanotubes are not amenable to large scale production, have short lifetimes and are expensive to produce, whereas polymers do not generally suffer from these limitations [133].

A polymer-based electrode functionalisation method offers the unique benefit of improving an electrode's *selectivity* towards an analyte of interest; this is particularly the case if molecularly imprinted polymers are used. Molecularly imprinted polymers contain recognition sites specific to a target analyte, and offer a stable and robust platform for improving selectivity [198]. Molecularly imprinted polymer-functionalised electrodes have been used recently for improved electrochemical detection of explosives [211, 213, 217, 233, 270], giving highly sensitive and selective analyses using techniques including SWV, CV, and differential pulse voltammetry.

In addition to molecularly imprinted polymers, a number of non-imprinted polymers have been reported for the successful functionalisation of electrodes, giving enhanced explosives sensitivity. These non-imprinted polymers have primarily been 'synergistic' polymers containing aromatic functionalities (such as polyaniline [218, 271] and porphyrin-based polymers [128, 133]), which can undergo preferential interaction with TNT to pre-concentrate the TNT onto the polymer surface prior to its electrochemical detection. On the other hand, a number of non-imprinted, non-aromatic polymers have also been reported to give rise to enhanced TNT sensitivity [126, 219]. Alternative work by Lee *et al.* has reported poly(methyl methacrylate) (PMMA)-functionalised electrodes for their utility in oxygen-sensing applications [239, 240]. In this case, rather than the polymer functionalising the electrode surface itself, the polymer was used to immobilise a layer of room temperature ionic liquid onto the electrode to improve the robustness of the planar electrode system.

6.1.7 Room Temperature Ionic Liquids in electrochemical sensing

Over recent years, there has been a surge of interest towards the use of room temperature ionic liquids (RTILs) as electrolytes for electrochemical reactions. RTILs are salts that exist in liquid form at room temperature [137]. They commonly consist of a bulky organic cation paired with an inorganic or organic counter anion [137]. Figure 6.10 displays the structures of the cations and anion present in the RTILs used throughout this chapter. RTILs show a number of advantageous properties, including low volatility, inherent conductivity, high chemical stability, tunable viscosity, wide electrochemical windows and the ability to dissolve a wide variety of compounds [137, 203, 238, 272, 273].

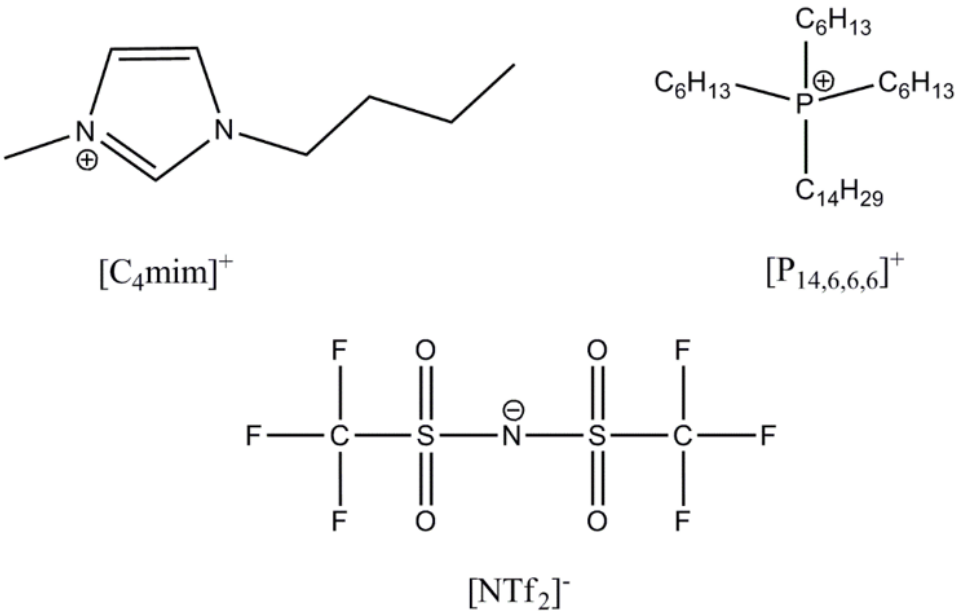

Figure 6.10: Structures of the cations ($[C_4mim]^+$ and $[P_{14,6,6,6}]^+$) and anion ($[NTf_2]^-$) comprising the two room temperature ionic liquids ($[C_4mim][NTf_2]$ and $[P_{14,6,6,6}][NTf_2]$) used in this chapter. Each room temperature ionic liquid contains the same anion

In addition, by careful choice of cation and anion, the physiochemical properties of RTILs can be adjusted to promote hydrogen bonding or π-π interactions with a compound of interest [206, 228]. Some research has also reported that ionic liquids may pre-concentrate vapour-phase analytes [206, 245].

For this reason, a number of researchers have adopted the use of ionic liquids in electrochemical sensors for explosives detection [138, 203, 205, 206, 226, 228, 245, 249, 274]. Recently, Fernandez *et al.* [238] reported the use of screen-printed electrodes in combination with dispersive liquid-liquid microextraction for the detection of TNT in aqueous samples. The process involved generating a water insoluble ionic liquid by adding a water miscible ionic liquid and an ion exchange agent to an aqueous solution containing TNT. After manually shaking, holding in an ice bath and centrifuging the sample, a metathesis reaction occurred between the water miscible ionic liquid and the ion exchange agent, which generated a water immiscible ionic liquid. At the same time, due to TNT's relatively low solubility in water and the high solvating ability of ionic liquids, the TNT originally in the aqueous phase partitioned into the water immiscible ionic liquid layer, with detection limits of 7 μg L^{-1} reported. Although this work seems promising for the detection of TNT in aqueous samples, its portability and ease of use are limited by the complex steps necessary prior to analysis. It would therefore be advantageous if a method could be developed which offered increased portability and ease of use for TNT detection at a scene itself, or in a nearby portable laboratory, such as that used in the Bali bombings [8].

6.1.8 The electrochemical reduction mechanism of TNT in protic vs. aprotic solvents

Chua *et al.* [227] studied the reduction mechanism of TNT in aqueous solution, concluding that a six electron and six proton transfer mechanism occurred for the reduction of each nitro group (i.e. a total of 18 protons and 18 electrons for the three nitro groups in a molecule of TNT). It is important to understand the reaction mechanism as this may aid the development of future electrochemical sensing methodologies for TNT. An example showing a six electron reduction of *one* nitro group in TNT in this manner is displayed in Figure 6.11.

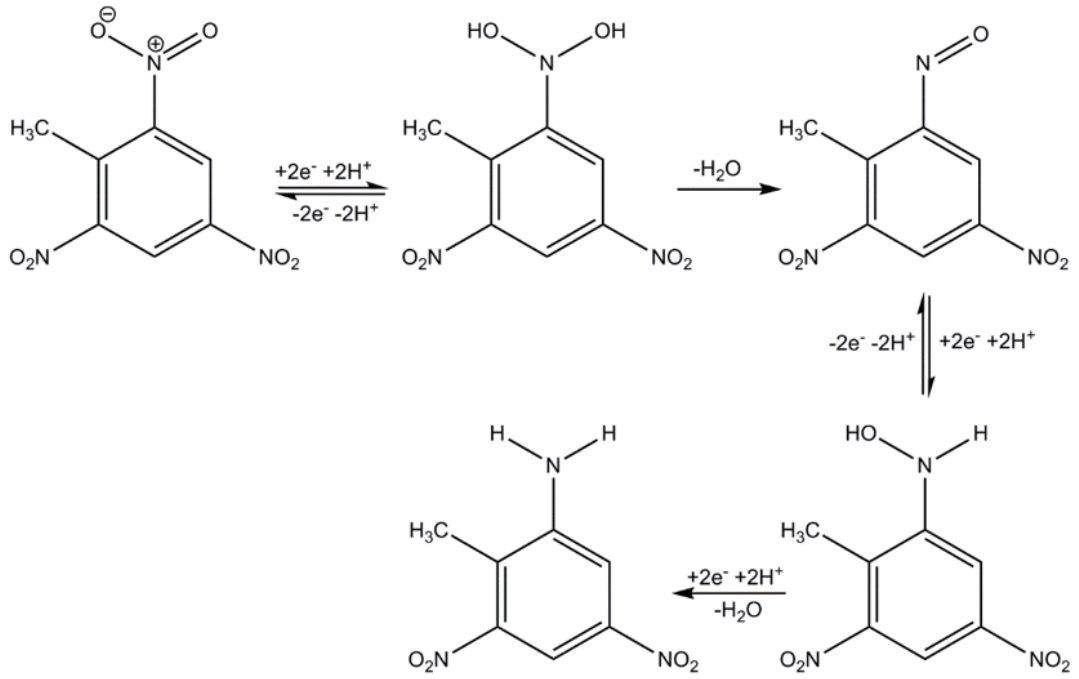

Figure 6.11: Proposed mechanism of TNT reduction in protic solvents, adapted from Chua *et al.* [227]

Kang *et al.* [138] studied the mechanism of TNT reduction in the aprotic RTIL $[C_4mim][NTf_2]$ on both a gold microelectrode and a gold TFE. Three reduction peaks were observed, corresponding to consecutive reduction of the three nitro groups. The electron count corresponding to each peak was calculated to be one, rather than the six electrons reported by Chua *et al.* [227] for reduction in protic media. In this aprotic medium, the radical anion is highly reactive and dimerises, since no protons are present to participate in follow-up chemical steps. An EC_2 mechanism was proposed to account for the dimerisation of the reduced species. A proposed scheme for this dimerisation process is shown in Figure 6.12.

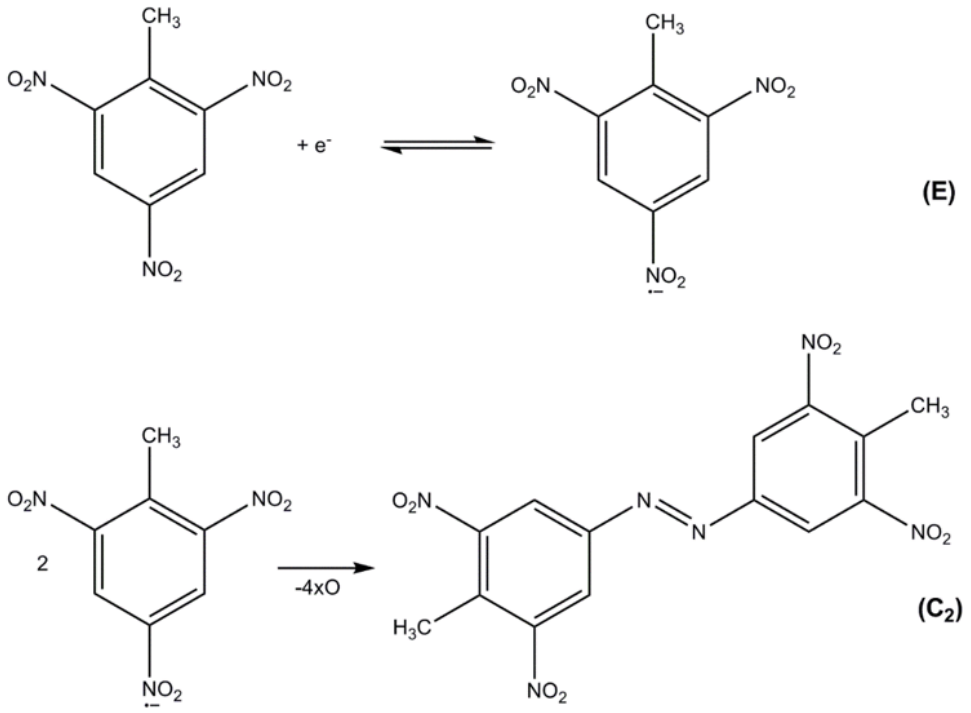

Figure 6.12: Proposed reduction mechanism of TNT in aprotic solvents, adapted from Kang *et al.* [138]. Here 'E' represents the electron transfer step, whereas 'C_2' refers to a second-order chemical step

This knowledge of the reaction mechanism of TNT in aprotic media is beneficial. As EC_2 mechanisms require two species to undergo reaction, the kinetics of the second-order chemical step will be very slow at low concentrations and thus should not be significant at the low TNT concentrations under investigation in the present work.

As the use of ionic liquids for the electrochemical detection of explosives is still an emerging research area, the potential exists for a lot of further research to enhance current capabilities and develop effective, portable electrochemical detectors for explosives. A number of authors have investigated combining ionic liquids with polymers, to immobilise the ionic liquid within a gel matrix and provide physical stability of the electrolyte during sampling [204, 239, 240, 271], leading to the potential for a more rugged and robust electrochemical sensor. For example, Lee *et al.* reported the addition of PMMA to the RTIL [C_2mim][NTf_2] to form a gel polymer electrolyte (GPE) with the aim to construct a robust portable gas-sensor [240]. Lee's work showed that the voltammogram of oxygen reduction in the PMMA/[C_2mim][NTf_2] matrix was less affected by the presence of moisture than the pure RTIL in the absence of the polymer. From this work, it was proposed that polymer/RTIL based GPEs may have the potential for the direct sensing of TNT in aqueous samples or wet soil samples, but that PMMA may not be sufficiently hydrophobic. It was suggested that more hydrophobic polymers and RTILs should be investigated for this purpose.

To date, almost no work has been performed on the use of polymers combined with ionic liquids for explosive detection, and previous studies have focused solely on the detection of solid-phase DNT [121]. This chapter therefore aims to investigate the use of polymer and ionic liquid-functionalised electrodes for the detection of explosives in alternative chemical phases, such as aqueous samples. The development of such a portable electrochemical sensor would potentially be of great utility for at-the-scene explosive residue detection, offering fast analyses, good sensitivity, low cost and ease of use.

6.2 Experimental

6.2.1 Chemicals

Trihexyltetradecylphosphonium bis(trifluoromethylsulfonyl)imide ($[P_{14,6,6,6}][NTf_2]$ – CAS no. 460092-03-9) was kindly donated by Professor Christopher Hardacre, the University of Manchester, UK, and was used as received. 1-butyl-3-methylimidazolium bis(trifluoromethylsulfonyl)imide, 99.5 % ($[C_4mim][NTf_2]$ – CAS no. 174899-83-3) was obtained from IoLiTec (Ionic Liquids Technologies GmbH), Heilbronn, Germany (Lot no. M00250.7-IL-0029). Poly(methyl methacrylate) (PMMA) was obtained from Sigma-Aldrich as a white powder and contained an average molecular weight of approximately 15,000 by gel permeation chromatography (batch no. MKBK0678V). Poly(hexyl methacrylate) (PHMA) was synthesised and purified by Dr Junqiao Lee, Curtin University. A size exclusion chromatogram for PHMA is provided in Appendix C, Figure C.1. 18.2 MΩ cm^{-1} ultrapure water was obtained from a Millipore Pty Ltd ultrapure laboratory water purification system. Acetone (Sigma-Aldrich, 99.9 %) was used for washing electrodes prior to use. A 1000 µg/mL solution of TNT in acetonitrile was obtained from Chem Service, West Chester PA (lot 3196300). A solid TNT sample was kindly donated by the Forensic Science Laboratory at ChemCentre, Perth, Western Australia, and used as received. Ferrocene (98 % purity) was obtained from Sigma-Aldrich and used without further purification. A 25 mM solution of ferrocene was made up in acetonitrile for use as an internal redox couple in selected systems. High-purity nitrogen gas (99.99 %) used for sample purging, and high-purity oxygen gas (99.5 %) were obtained from BOC Gases (North Ryde, NSW, Australia) connected into gas lines of the building (Resources and Chemistry Precinct, Curtin University). A 1 M stock solution of sulfuric acid (prepared with Milli-Q water from a 95-98 wt % sulfuric acid solution, Ajax Finechem, WA, Australia) was used for all TFE activations. > 99.0 % potassium chloride (SigmaUltra) was obtained from Sigma-Aldrich.

6.2.2 Electrochemical experiments

All electrochemical experiments were performed using an Autolab PGSTAT101 potentiostat (Eco-Chemie, Netherlands) interfaced to a computer operating Nova 1.11 software (Eco-Chemie, Netherlands). All analyses were performed inside a custom-built aluminium Faraday cage to reduce background interference.

6.2.2.1 Microelectrode experiments

Initial experiments were performed using a gold microelectrode. Such microelectrodes are more ideal surfaces than TFEs as they can be polished and re-used continuously, unlike the gold TFEs used later. The microelectrode experiments employed a 'home-made' microelectrode with a radius of 10.78 µm, kindly donated by Professor Richard Compton of the University of Oxford, UK. The microelectrode radius was electrochemically calibrated using CV of a 3.3 mM aqueous solution of $K_3[Fe(CN)_6]$ in 0.1 M potassium chloride. Prior to each use, the microelectrode was polished in a figure-8 motion on a set of soft velvet polishing pads (Buehler, Illinois), using sequentially decreasing aluminium oxide particle sizes (3 µm, 1 µm and 0.05 µm, Kemet, Marayong, NSW), with one pad used for each particle size, rinsing the microelectrode with Milli-Q water between each pad, and with acetone and Milli-Q water after the final polish.

A schematic of the microelectrode preparation is provided in Figure 6.13a. For this, a strip of Parafilm "M" Laboratory film (Bemis Flexible Packaging, Neenah, WI) (approximately 1.5 cm) was tightly wrapped around the top of the microelectrode, leaving the gold wire of the microelectrode exposed. A clean section of a plastic micropipette tip was cut and placed over the end of the microelectrode, pressing down to ensure a good seal between the Parafilm and the plastic pipette tip. The outer edge of the plastic pipette tip was then wrapped with a further layer of Parafilm, to provide a sturdy collar around the gold WE of the microelectrode. The microelectrode was inserted into the 'long arm' of a glass T-cell, securing in place using Parafilm. Aliquots (typically 20-25 µL) of ionic liquid-based samples were then pipetted into the plastic collar to cover the gold WE (approximately 1mm layer thickness of RTIL), prior to analysis.

A silver wire (acting as a combined reference/counter electrode) was then inserted into the top of the glass T-cell, to complete the system. Prior to each use, this silver wire was cleaned by sonicating in acetone for five minutes. Upon insertion into the glass T-cell, it was ensured that the tip of the silver wire was immersed into the ionic liquid. Prior to any analyses, the T-cell was evacuated for at least one hour using an Edwards high vacuum pump (model ES 50) to remove any dissolved oxygen, carbon dioxide and water from the sample. A photograph of a

constructed microelectrode in a T-cell is shown in Figure 6.13b.

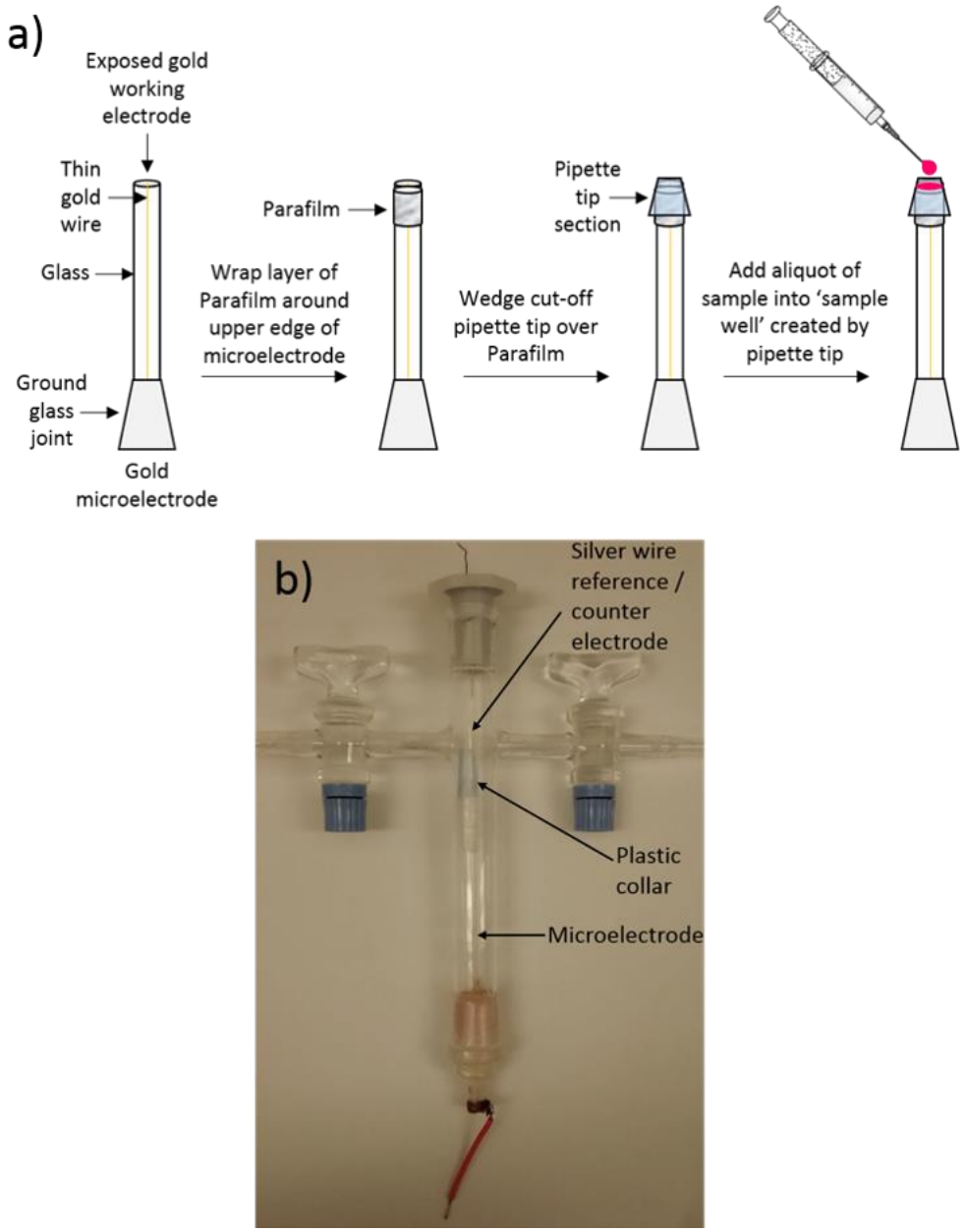

Figure 6.13: a) Schematic of the stages used to prepare the gold microelectrode for use and b) Photograph of a glass T-cell containing a prepared microelectrode and silver reference/counter electrode

SWV optimisation was performed by varying scan frequencies (25, 50, 100, 150, 200 250 Hz), amplitudes (20, 25, 30 mV) and scan rates (50, 100, 400 mV/s) to find the best combination to maximise the TNT peak one reduction current while minimising the corresponding background current.

6.2.2.1.1 TNT extraction efficiency experiments

Although the overall aim of this work was to develop a polymer/ionic liquid matrix for the

extraction of TNT from aqueous samples, initial experiments involved assessing the ability of pure RTILs (i.e. in the absence of polymer) for the extraction of TNT from aqueous samples. This was possible due to the relatively low miscibility of RTILs with water [275]. To identify a suitable volume of ionic liquid to use for these extractions, 100, 200, 300, 400 and 500 µL aliquots of $[C_4mim][NTf_2]$ were individually manually shaken vigorously for 5 minutes with 20 mL volumes of Milli-Q water, before leaving to settle for 5 minutes. Following this, the upper aqueous layer was removed, and the volume of the lower ionic liquid layer measured. A 200 µL aliquot of $[C_4mim][NTf_2]$ was found best to give sufficient volume for use in the microelectrode setup.

Following this, 2 mg solid TNT was added to 20 mL Milli-Q water and sonicated until dissolved. 200 µL $[C_4mim][NTf_2]$ was added, and the vial shaken vigorously for 5 minutes, forming microdroplet dispersions of $[C_4mim][NTf_2]$ within the aqueous TNT solution. The vial was left to settle for 20 hours to allow the $[C_4mim][NTf_2]$ to amalgamate into a single large droplet, before decanting the upper aqueous layer and removing 25 µL of the enriched RTIL layer for analysis on the microelectrode after evacuation for 1 h. A schematic of this process is provided in Figure 6.14.

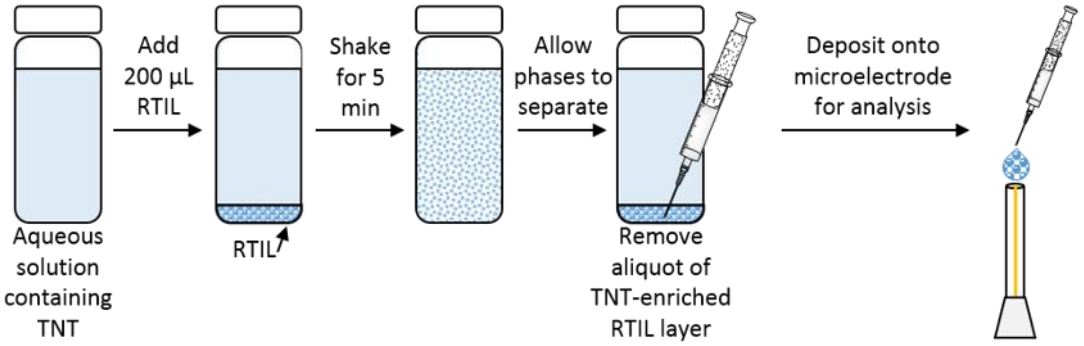

Figure 6.14: Schematic of the process used to extract TNT from aqueous solution by shaking with an aliquot of room temperature ionic liquid (volumes not to scale)

Chronoamperometry was performed to determine the concentration of TNT within the resulting RTIL layer using the diffusion coefficients reported by Kang *et al.* [138] and the software program Origin 7.5 (OriginLab Corporation, Massachusetts, USA), in conjunction with the Shoup and Szabo equation (eq. 3). In addition, an analogous sample was prepared and analysed after a 5 minute settling period. Analogous extraction experiments were performed using 200 µL $[P_{14,6,6,6}][NTf_2]$. With this more hydrophobic RTIL, centrifuging for 10 minutes at 4000 rpm was performed to enhance phase separation of the RTIL layer from the aqueous layer.

6.2.2.2 Thin-film electrode experiments

TFEs with gold working, reference and counter electrodes were obtained from Micrux Technologies, Oviedo, Spain, product no. ED-SE1-Au. A photograph of a TFE is provided in Figure 6.2. All TFE experiments were performed using a custom-made TFE adapter (made by Dr Junqiao Lee, Curtin University). An image of the adapter is provided in Figure 6.15.

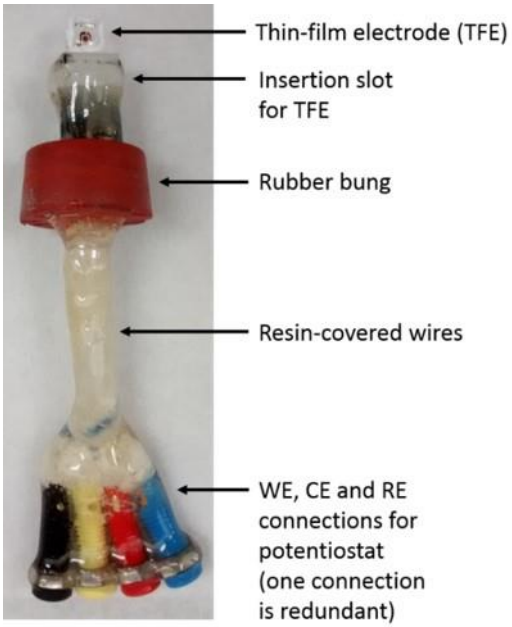

Figure 6.15: Schematic of the custom-made thin-film electrode adapter used throughout this work

All TFEs were electrochemically activated prior to use as recommended by the manufacturer. This involved placing a 12 µL aliquot of 1 M sulfuric acid onto the TFE, to cover the three electrodes, before performing repeated CV scans (approximately 100 scans) at 1000 mV/s between potentials of approximately 1.1 V and -1.2 V. This induced the formation of bubbles of hydrogen gas to clean and activate the electrode surface. Following this, the TFE was removed from the adapter and washed with excess Milli-Q water and acetone, before drying under nitrogen.

For TFE experiments in the absence of a polymer, 2 µL aliquots of the RTIL sample were deposited onto the TFE. For those involving a polymer, 3 µL aliquots of gel polymer were deposited (giving an approximate gel polymer diameter of 2.5 mm on the TFE). This was due to the higher viscosity of the gel polymer compared to the RTILs, meaning less spreading occurred upon addition to the TFE and thus a larger volume was required to fully cover all of the three electrodes.

All CV experiments were performed at a scan rate of 100 mV/s. Unless otherwise stated, all TFE experiments were performed in a glass ‘8-cell’ under a constant stream of nitrogen gas

(0.2 L/minute, modulated with a gas flow meter), with all samples purged under nitrogen for at least 20 minutes prior to analysis (see Figure 6.16). The TFE is inserted into one slot of the '8-cell' using the rubber bung shown in Figure 6.15, with the remaining slots sealed using glass stoppers.

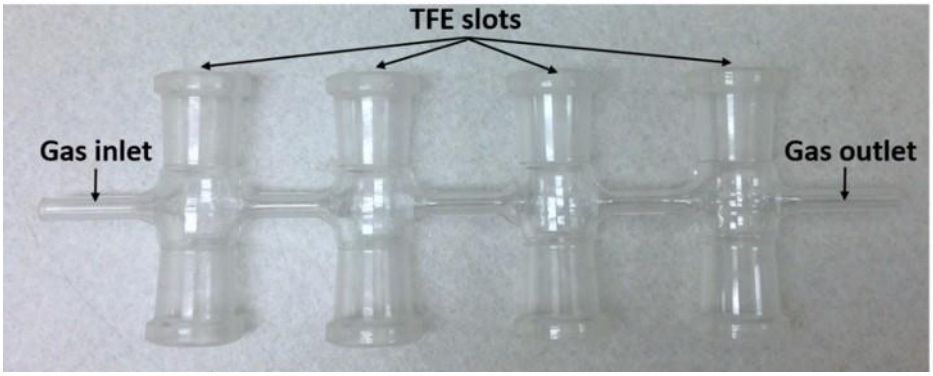

Figure 6.16: Photograph of the glass '8-cell' used during this work (photograph courtesy of Dr Junqiao Lee)

SWV optimisation was performed for TNT on the TFEs in an analogous manner to the optimisation performed on gold microelectrodes. SWV optimisation revealed that conditions of 25 Hz, 25 mV and 100 mV/s were best for both RTILs under investigation on TFEs. 3 mM samples of TNT in $[C_4mim][NTf_2]$ and $[P_{14,6,6,6}][NTf_2]$ were analysed on a TFE under 1) nitrogen, 2) 21:79 O_2:N_2 (obtained using a gas-mixing setup [276]) and 3) air. The samples were purged for at least 20 minutes prior to analysis. Blanks of the RTILs $[C_4mim][NTf_2]$ and $[P_{14,6,6,6}][NTf_2]$ in nitrogen were also analysed under identical conditions.

Assessment of gel polymer mixing ratios

Two ionic liquids ($[C_4mim][NTf_2]$ and $[P_{14,6,6,6}][NTf_2]$) and two polymers (PMMA and PHMA) were investigated for the formation of gel polymers, giving a total of four possible combinations (see Table 6.1).

Table 6.1: Table of RTIL/polymer combinations trialled in this work

		→ More hydrophobic	
		$[C_4mim][NTf_2]$	$[P_{14,6,6,6}][NTf_2]$
↓ More hydrophobic	PMMA	Gel polymer variant 1	Gel polymer variant 2
	PHMA	Gel polymer variant 3	Gel polymer variant 4

Each gel polymer was prepared and tested at 10, 20, 30, 40 and 50 % polymer by mass ($100*m_{polymer}/(m_{polymer}+m_{RTIL})$). Details of the polymer masses and RTIL volumes required for this are provided in Appendix C, Table C.2 to Table C.4. A 12 µL aliquot of each gel polymer dissolved in acetone was dropped onto a clean glass microscope slide (with this technique hereafter termed 'dropcasting'), and left for approximately three hours to allow any residual acetone to evaporate. Following this, the slide was held vertically overnight, to assess the mechanical stability of the mixtures. Those with the highest viscosity were expected to display the highest adhesion to the glass slide, with the glass slide simulating the flat glass substrate present in the gold TFEs.

Assessing gel polymer compatibility with water

The overall aim of this work is to develop a gel polymer-functionalised TFE that will be suitable for immersion into aqueous TNT samples. The three optimum mixing ratios were dropcast onto a glass microscope slide and subjected to the same glass slide test (i.e. holding vertical overnight). The slide was then immersed into a container of ultrapure water (at 21 °C), with the slide periodically removed after various time periods (5, 15, 30, 60 minutes; and 2, 4, 6, 8, 20 hours). Any water droplets surrounding the gel polymer droplets were removed using a lint-free tissue. The glass slide was photographed, then placed into water for a fixed time. Following the final immersion, the glass slide was removed and left to dry naturally at room temperature, photographing after 20 hours and two weeks.

Assessing TNT behaviour in gel polymer films

TNT at a concentration of 3 mM was prepared in the optimum gel polymer ratios. The gel polymer was dissolved using an equal volume of acetone, and 6 µL was dropcast onto a TFE, giving a total volume of TNT-spiked gel polymer of 3 µL, following acetone evaporation. A

photograph of a gel polymer-functionalised TFE, along with a labelled schematic, is provided in Figure 6.17.

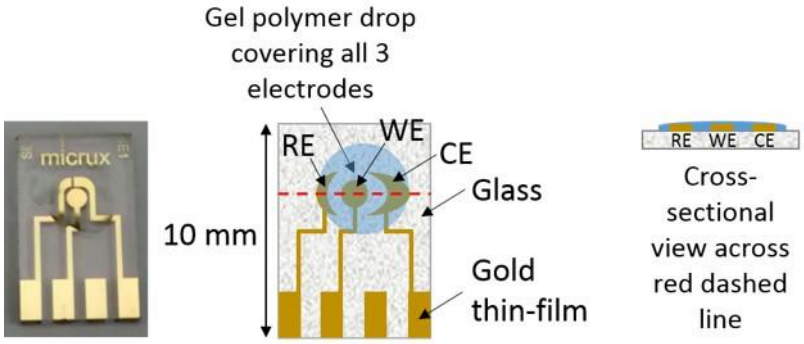

Figure 6.17: Photograph and schematic of a thin-film electrode functionalised with a gel polymer drop formed from a polymer and a room temperature ionic liquid

Prior to analysis, the TFEs were purged with nitrogen either at 0.2 L/minutes for 1 hour, or at 0.1 L/minute overnight. The TNT-spiked gel polymers were then analysed using CV and SWV. Multiple square wave voltammograms were recorded for each sample, with 15 minute intervals between each scan, to assess the long-term stability. Following this, each TFE was immersed in Milli-Q water for 15 minutes and analysed immediately following removal from the water, and after drying under N_2 for one hour at 0.2 L/minute.

A sample of 3 mM TNT and *ca*. 3 mM ferrocene was prepared in 50 % PHMA/$[P_{14,6,6,6}][NTf_2]$ to determine the potential separation of ferrocene and the first reduction peak of TNT. This value (1.2 V) was then used to adjust all voltammetric data so that the TNT peak potential was plotted with respect to ferrocene, with the ferrocene peak adjusted to a fixed potential of 0 V.

Assessing a gel polymer-functionalised TFE for the extraction of TNT from aqueous solution

Prior to use, all gel polymer-functionalised TFEs were dried overnight under nitrogen (0.1 L/minute) to remove any residual acetone. Following this, all TFEs were pre-conditioned with water by immersing them into ultrapure water for 15 minutes, before removal and drying under nitrogen at 0.2 L/minute for one hour.

1 mL aqueous solutions of TNT (at 1, 2, 4, 7 and 10 µg/mL) were prepared in straight-sided 15 × 45 mm glass vials (Grace Division Discovery Sciences, Victoria, Australia). This involved placing aliquots of TNT standard (1000 µg/mL in acetonitrile) into 0.5 mL centrifuge tubes and using a gentle stream of nitrogen to evaporate all residual acetonitrile, leaving an orange residue. Following this, the residue was reconstituted with 400 µL ultrapure water, sonicating to ensure complete dissolution, before transferring the solution into the glass vials.

Each centrifuge tube was then rinsed successively with 3 × 200 µL ultrapure water, transferring these washings into the respective glass vials, to give a total aqueous TNT solution volume of 1 mL at each of the five concentrations. An initial calibration series was prepared by immersing five individual gel polymer-functionalised TFEs into the five vials and placing on a shaker table at 120 rpm for 15 minutes prior to SWV analysis.

Later, a modification was made by using a stirrer bar rather than a shaker table to agitate the solution: A clean miniature stirrer bar was added to the vial containing 1 mL aqueous TNT solution. Following this, a pre-activated gold TFE with a pre-conditioned 3 µL aliquot of gel polymer (50 % PHMA/[$P_{14,6,6,6}$][NTf_2]) was inserted vertically into the vial, ensuring that the gel polymer layer was completely immersed. This was achieved by inserting one end of the TFE into a slit made in the rubber end of a 5 mL disposable syringe plunger. A photograph of this setup is provided in Figure 6.18.

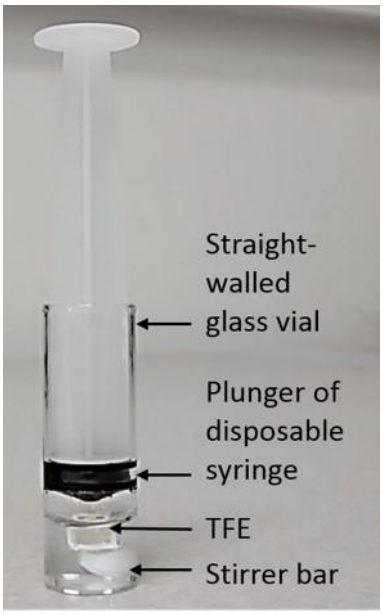

Figure 6.18: Photograph of the setup used for partial TFE immersion into aqueous solutions of TNT

The vial was then placed on a stirrer plate and stirred for 15 minutes at room temperature. The same stirring speeds were used for each sample (1, 2, 4, 7 and 10 µg/mL aqueous solutions of TNT). SWV was performed on both the 'wet' TFE (i.e. immediately after removal from the aqueous TNT solution after 15 minutes stirring) and 'dry' TFE (after drying for one hour under N_2 at 0.2 L/minute).

Later calibration attempts involved an accumulation technique. Aqueous solutions of TNT were prepared at 1 µg/mL and 2 µg/mL by evaporation of the acetonitrile-based TNT standard and reconstitution with ultrapure water. A 50 % PHMA/[$P_{14,6,6,6}$][NTf_2]-functionalised TFE was immersed into a 1.35 mL aliquot of 1 µg/mL aqueous TNT solution using the setup shown

in Figure 6.18. The solution was stirred vigorously for 15 minutes, after which time the TFE was removed. An initial square wave voltammogram was run of the 'wet' gel polymer. In addition, the gel polymer was dried for one hour under N_2 (0.3 L/minute) and a 'dry' square wave voltammogram captured of the TFE following exposure to 1 µg/mL TNT solution.

The TFE was then immersed into another 1.35 mL aliquot of 1 µg/mL TNT, and the process repeated, to give a square wave voltammogram representative of cumulative exposure to 2 µg/mL TNT. Following this, the TFE was successively immersed in fresh aliquots of 2 µg/mL TNT, to give cumulative exposure to 4, 6, 8 and 10 µg/mL TNT. This generated a cumulative six-point calibration curve for the TFE. The procedure was repeated twice more, to give three replicates using the given setup.

To compare TNT detection with the gel polymer-functionalised electrodes against a bare electrode, a bare gold TFE was immersed into each of four solutions: (1) 0.45 mL Milli-Q water, (2) 0.45 mL 0.1 M potassium chloride, (3) 0.45 mL 2 µg/mL TNT in Milli-Q water, (4) 0.45 mL 2 µg/mL TNT in 0.1 M potassium chloride) and SWV analysis was performed using the optimised parameters for gel polymer-functionalised TFEs.

Assessing a gel polymer-functionalised TFE for the detection of TNT vapour

Initial TNT vapour detection experiments were performed using the glass 8-cell (volume 22.5 cm^3) shown in Figure 6.16. Two experiments were performed: 1) static exposure to TNT vapour, and 2) dynamic exposure to TNT vapour. For the static exposure experiments, 40 mg TNT was placed into a small (approximately 2.5 × 2.5 cm) flat nylon mesh bag (constructed from a section of a 'T2 in the bag' nylon mesh bag, Tea Too Pty Ltd, Port Melbourne, Victoria, Australia). An image of this bag is shown in Figure 6.19.

Figure 6.19: Photograph of nylon mesh bag containing 40 mg TNT used for vapour-phase experiments

The mesh bag of TNT was inserted into one end of the glass 8-cell and the stoppers inserted, with the open gas inlet/outlet ends of the 8-cell sealed with Parafilm. An image of the mesh

bag *in situ* is shown in Figure 6.20.

Figure 6.20: Photograph of nylon mesh bag in situ (centre of image) in the glass 8-cell

TNT was allowed to equilibrate overnight at room temperature, before removing a stopper and immediately inserting a rubber bung bearing a TFE adapter and gel polymer-functionalised TFE. SWV analysis was performed after exposure intervals of 0, 15, 30, 60, 90 minutes; 2, 3, 4, 5, 6 hours and overnight (24 h). Dynamic sampling was performed in an analogous fashion, with a flow of nitrogen gas (0.225 L/minute) applied through the gas inlet of the 8-cell (i.e. the 8-cell was fully flushed with 10 volumes of nitrogen gas per minute).

Subsequent vapour-phase experiments involved heating the TNT. A 20 mg TNT sample was placed into the base of a short glass pot (volume 18.5 cm^3). Two small plastic caps (Agilent blue screw cap, part no. 5185-5823; septa removed) were then placed into the base of the glass pot, to act as a stand to hold the TFEs during exposure to the TNT vapour. Following this, three TFEs were placed onto the stand: one functionalised with 3 µL gel polymer (50 % PHMA/$[P_{14,6,6,6}][NTf_2]$), one a bare Au-TFE with 2 µL $[C_4mim][NTf_2]$ and one a bare Au-TFE with 2 µL $[P_{14,6,6,6}][NTf_2]$. Figure 6.21 shows the TFEs in situ.

Figure 6.21: Three Au-TFEs bearing either gel polymer (50 % PHMA/[$P_{14,6,6,6}$][NTf_2]), [C_4mim][NTf_2] or [$P_{14,6,6,6}$][NTf_2] in proximity to 20 mg TNT

The glass pot was then capped with a Teflon lid and placed on a hotplate at 60 °C for four hours, to allow the TNT to volatilise and allow partitioning into the RTILs or gel polymer. Following this, the individual TFEs were removed, purged with nitrogen (0.4 L/minute) for five minutes and analysed using the optimised SWV parameters.

6.3 Results and discussion

6.3.1 Electrochemical detection of TNT on a microelectrode

Throughout this work, gold WEs were utilised, since gold has previously been shown to be less prone to fouling during TNT reduction compared to alternative electrode materials such as platinum [138]. SWV parameters were improved by varying scan frequencies (25, 50, 100, 150, 200 250 Hz), amplitudes (20, 25, 30 mV) and scan rates (50, 100, 400 mV/s) to find the best combination to maximise the TNT peak one reduction current while minimising the corresponding background current. Conditions of 25 Hz, 25 mV and 100 mV/s were found to be best for both RTILs under investigation. Two RTILs were employed: [C_4mim][NTf_2] and [$P_{14,6,6,6}$][NTf_2]. [C_4mim][NTf_2] has previously been demonstrated to be a promising RTIL for TNT analysis at relatively high concentrations [138]. [$P_{14,6,6,6}$][NTf_2] was also investigated as a more hydrophobic RTIL – it was thought that the use of this RTIL may give rise to improved behaviour upon immersion into aqueous samples during the later stages of this work. Figure 6.22 compares square wave voltammograms of TNT in the two ionic liquids. It can be seen that higher peak currents were obtained in [C_4mim][NTf_2] compared to [$P_{14,6,6,6}$][NTf_2] at the same concentration which is likely due to the lower viscosity of the [C_4mim][NTf_2], leading to a higher TNT diffusion coefficient [138]. Diffusion coefficients of TNT in [$P_{14,6,6,6}$][NTf_2] and [C_4mim][NTf_2] are 0.86×10^{-11} m^2 s^{-1} and 2.6×10^{-11} m^2 s^{-1}, respectively [138], reflecting

the different viscosities of the two RTILs. It can also be seen that the first TNT reduction peak lies at a more negative potential in $[P_{14,6,6,6}][NTf_2]$ (-1.10 V) compared to the analogous peak in $[C_4mim][NTf_2]$ (-0.95 V), consistent with that reported previously [138].

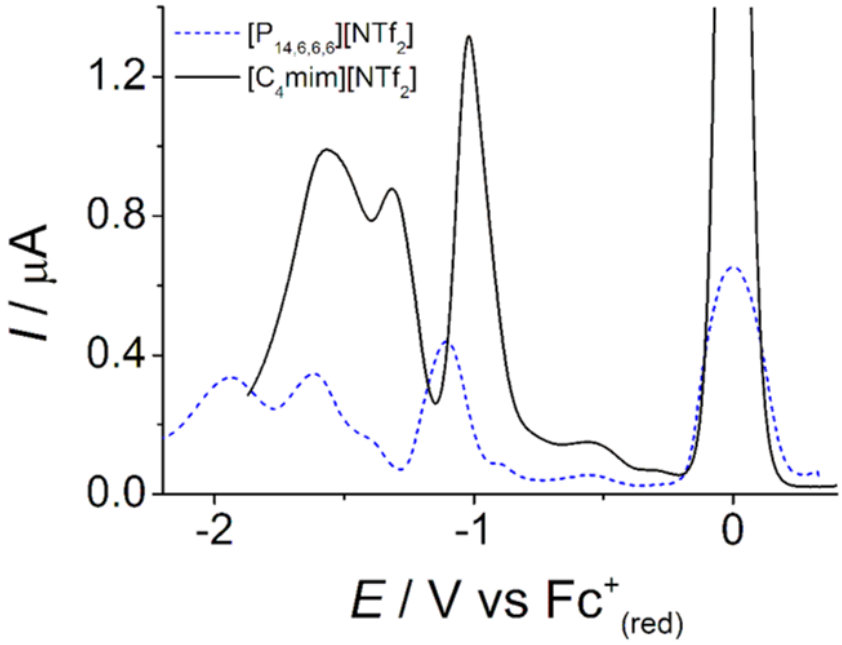

Figure 6.22: Square wave voltammograms on a gold microelectrode (diameter 21.56 µm) at a scan rate of 100 mV s^{-1} for the reduction of 3 mM TNT in $[C_4mim][NTf_2]$ (black solid line) and $[P_{14,6,6,6}][NTf_2]$ (blue dashed line) in the presence of ferrocene (peak at 0 V) using a silver reference electrode. Note that the Fc peak at 0 V is truncated in the $[C_4mim][NTf_2]$ square wave voltammogram to enable a clearer comparison of the TNT currents in the respective RTILs

6.3.2 Assessing gel polymers for TNT pre-concentration from aqueous samples

Prior to introducing polymers into the system, the current work initially aimed to verify that addition of a pure RTIL would also be able to achieve TNT extraction from an aqueous solution. Previous work by Fernandez *et al.* [238] has shown that TNT can be extracted from aqueous samples into an RTIL by generating an RTIL *in situ* in the sample, using a metathesis reaction.

Initial experiments had planned to add a 100 µL aliquot of RTIL to a 20 mL aqueous solution of TNT, to pre-concentrate the TNT from the aqueous solution into the RTIL. It was expected that the TNT would partition into the RTIL upon vigorous shaking, before phase separation and re-accumulation of the RTIL into a single large droplet (analogous to liquid-liquid extraction techniques), an aliquot of which could be deposited onto the microelectrode and analysed. However, initial experiments involving 100 µL of $[C_4mim][NTf_2]$ resulted in no obvious phase separation. $[C_4mim][NTf_2]$ is reported to have a low but measurable miscibility towards water [275], suggesting that all of the $[C_4mim][NTf_2]$ had dissolved into the water. A

further series of shaking experiments were therefore performed to determine a suitable [C_4mim][NTf_2] volume for aqueous extraction (see Table 6.2).

Table 6.2: Results from a series of 5 minute shaking experiments to determine a suitable volume of [C_4mim][NTf_2] to employ

Initial volume of [C_4mim][NTf_2] added (µL)	Recovered volume of [C_4mim][NTf_2] (µL)	Volume [C_4mim][NTf_2] lost (µL)
100	0	100
200	65	135
250	110	140
300	170	130
400	290	110
500	350	150

From Table 6.2 it can be seen that in each shaking experiment, approximately 100 µL of [C_4mim][NTf_2] was lost into the aqueous layer. A 200 µL volume of [C_4mim][NTf_2] was therefore chosen for initial TNT extraction experiments from aqueous samples, to ensure that sufficient RTIL was recoverable for analysis on the microelectrode. An initial shaking experiment was performed involving 200 µL [C_4mim][NTf_2] and a 20 mL saturated aqueous solution of TNT. Immediately after the five minute shaking period, the colourless RTIL layer had taken on a faint pink colour (see Figure 6.23).

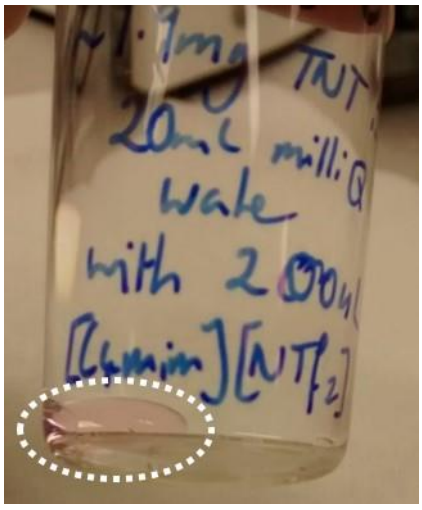

Figure 6.23: Pink-coloured RTIL layer (highlighted with the dashed oval) after shaking 200 µL [C_4mim][NTf_2] with an aqueous solution of TNT

After allowing to fully phase separate for 20 hours, the RTIL layer had turned a darker pink colour; possibly due to chromophoric interactions of the TNT with the RTIL or due to the formation of highly-coloured by-products within the relatively highly concentrated solution (though no additional peaks were observed during analysis).

Chronoamperometry was performed to determine the concentration of TNT within the resulting RTIL layer, and thus the percentage recovery of the TNT, using the diffusion coefficients calculated by Kang *et al.* [138] and the Shoup and Szabo equation [248]. An overall TNT recovery of approximately 28 % was obtained in this system. As an overall darkening of the RTIL layer had occurred over the 20 hour settling time, indicating possible by-product formation, a shorter settling time of five minutes was investigated, with higher TNT recoveries (approximately 40 %) obtained. These high TNT recoveries demonstrate the strong preference of TNT to partition into the RTIL phase from the aqueous phase, and highlight the promising pre-concentration ability of the RTILs. It should be noted that it is likely that a proportion of the TNT is lost in the fraction of RTIL that is miscible with water, leading to the TNT recoveries being less than 100 %.

'Wet' cyclic voltammograms were captured of the newly-separated RTIL phase, prior to evacuation of the glass T-cell, to assess the effects of dissolved oxygen and water within the RTIL. However, these cyclic voltammograms had a shape that was far from ideal and it was difficult to distinguish any obvious peaks from TNT (Figure 6.24a).

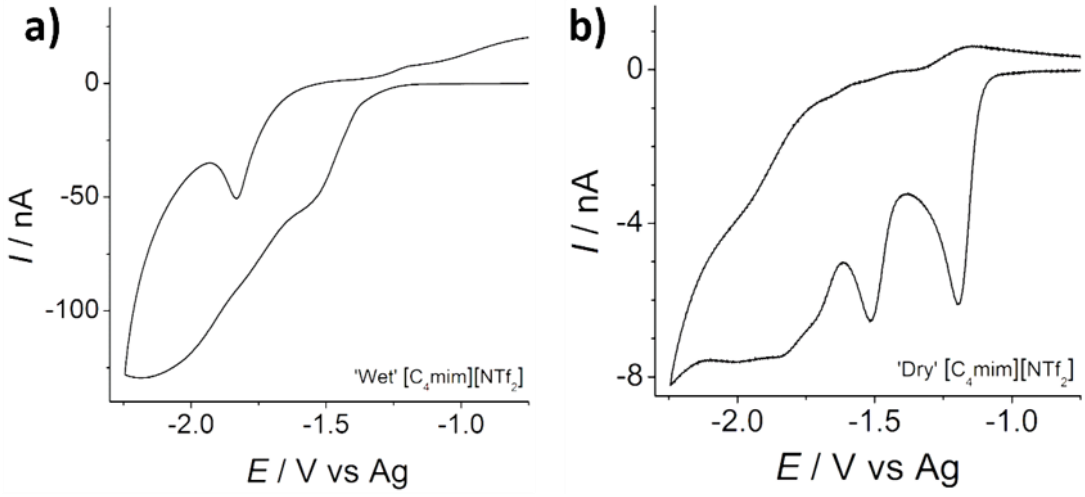

Figure 6.24: a) 'Wet' and b) 'dry' CV analyses of [C_4mim][NTf_2] following shaking with an aqueous solution of TNT. Cyclic voltammograms were captured on a gold microelectrode (diameter 21.56 µm) at a scan rate of 100 mV s^{-1} using a silver reference electrode

Upon evacuation of the system for one hour using a high vacuum pump (to remove dissolved oxygen and water), the resulting voltammetry gave peaks resembling those expected for TNT (Figure 6.24b) under ideal, dry conditions. This suggests that analyses involving [C_4mim][NTf_2] should be thoroughly dried following immersion in water, to enable clearer visualisation of the TNT peaks.

As the shaking experiments with [C_4mim][NTf_2] had shown that a five minute settling time

was sufficient for up to around 40 % TNT pre-concentration into the RTIL, a five minute settling time was used for analogous trials with the more hydrophobic RTIL $[P_{14,6,6,6}][NTf_2]$. Initial shaking experiments of 200 µL $[P_{14,6,6,6}][NTf_2]$ with 20 mL water resulted in the formation of a cloudy emulsion with small droplets of the RTIL spread around the inner surface of the glass vial, as opposed to the single large droplet which had formed with $[C_4mim][NTf_2]$. It was found that 10 minutes centrifuging at 4000 rpm gave sufficient $[P_{14,6,6,6}][NTf_2]$ recovery (130 µL) from an initial volume of 200 µL. Extraction of an aqueous solution of 2 mg TNT in 20 mL water using 200 µL $[P_{14,6,6,6}][NTf_2]$ resulted in the formation of a dark pink RTIL layer following centrifuging (see Figure 6.25).

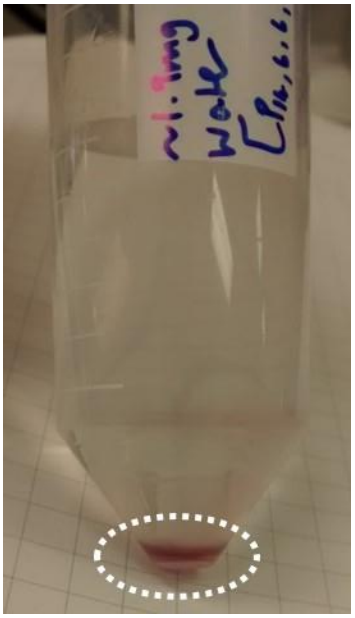

Figure 6.25: Dark pink-coloured RTIL layer (highlighted with the dashed oval) after shaking then centrifuging 200 µL $[P_{14,6,6,6}][NTf_2]$ with an aqueous solution of TNT

This suggests a strong interaction between TNT and $[P_{14,6,6,6}][NTf_2]$ to induce the colour change. In order to ensure this deep pink colour was due to the properties of $[P_{14,6,6,6}][NTf_2]$ itself, rather than an impurity in the centrifuge tube or the centrifuging process, the process was repeated using $[C_4mim][NTf_2]$, but this gave rise to a much paler pink RTIL layer, confirming that a property of the $[P_{14,6,6,6}][NTf_2]$ was responsible for the darkening of the RTIL phase. A 'wet' cyclic voltammogram was run of the newly-separated $[P_{14,6,6,6}][NTf_2]$ phase after TNT extraction from the aqueous solution. Unlike in the $[C_4mim][NTf_2]$, where the 'wet' cyclic voltammogram showed no distinct TNT peaks, two TNT reduction peaks could clearly be distinguished in the wet $[P_{14,6,6,6}][NTf_2]$ sample (Figure 6.26a).

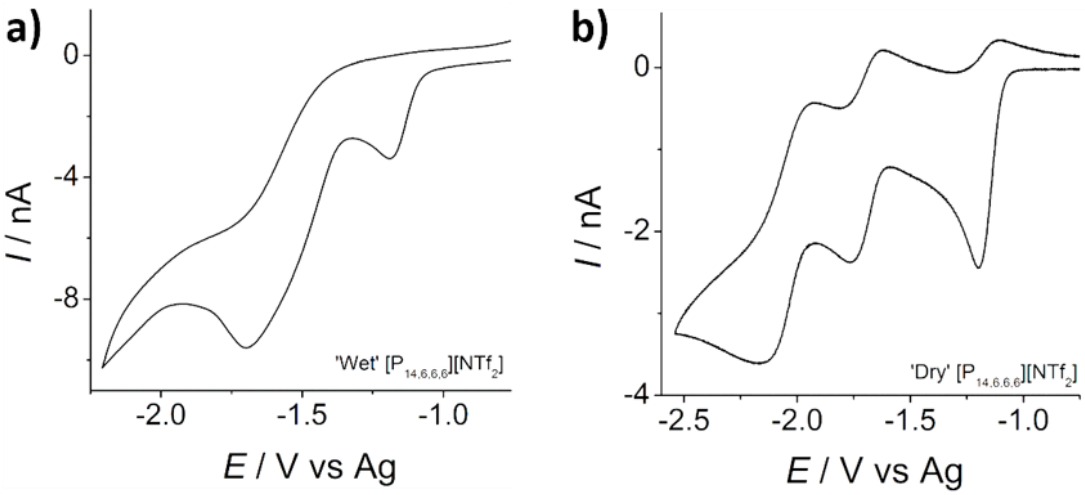

Figure 6.26: a) 'Wet' and b) 'dry' CV analyses of $[P_{14,6,6,6}][NTf_2]$ following shaking with an aqueous solution of TNT. Cyclic voltammograms were captured on a gold microelectrode (diameter 21.56 µm) at a scan rate of 100 mV s^{-1} using a silver reference electrode

This was promising, suggesting that $[P_{14,6,6,6}][NTf_2]$ may need a shorter drying time compared to $[C_4mim][NTf_2]$ in the later stages of this work when immersed into aqueous samples. This is likely to be due to $[P_{14,6,6,6}][NTf_2]$'s higher hydrophobicity relative to $[C_4mim][NTf_2]$. As before, analyses were then performed after evacuating for one hour using a high vacuum pump (Figure 6.26b). Table 6.3 summarises the overall TNT recoveries from these extraction experiments.

Table 6.3: TNT recoveries into RTIL from shaking extraction experiments

RTIL	Separation technique	Separation time	Maximum TNT concentration in RTIL	Calculated TNT concentration in RTIL from chronoamperometry fitting with eq. 3	% TNT transfer from aqueous phase into RTIL
$[C_4mim][NTf_2]$	Natural phase separation	20 hours	~ 80 mM	22.7 mM	~ 28 %
$[C_4mim][NTf_2]$	Natural phase separation	5 minutes	~ 80 mM	32.3 mM	~ 40 %
$[P_{14,6,6,6}][NTf_2]$	10 minutes centrifuging at 4000 rpm	10 minutes (during centrifuging)	~ 80 mM	23.1 mM	~ 29 %

Overall, these experiments showed that $[C_4mim][NTf_2]$ and $[P_{14,6,6,6}][NTf_2]$ are both suitable for the extraction and pre-concentration of TNT from aqueous solution. The next stage was to assess the best polymers for combination with the respective RTILs. As the TNT peaks in the

more hydrophobic $[P_{14,6,6,6}][NTf_2]$ had been shown to be less affected by the presence of moisture (i.e. TNT peaks were visible in the 'wet' samples of $[P_{14,6,6,6}][NTf_2]$), it was hypothesised that this RTIL may be more suitable than $[C_4mim][NTf_2]$ for the planned later stages of this work.

6.3.3 Influence of oxygen on TNT detection

Initial experiments to this point had used a gold microelectrode as it can be polished and re-used, and gives more 'ideal' responses. However, as the ultimate aim of this work was to move towards miniaturised devices, the rest of this chapter involved the use of much smaller, portable TFEs.

As the overall aim was to use the developed electrochemical detection system in 'real-life' environmental conditions, i.e. in the presence of oxygen in air, an assessment was made of 3 mM samples of TNT in both $[C_4mim][NTf_2]$ and $[P_{14,6,6,6}][NTf_2]$ under nitrogen, 21:79 O_2:N_2 and air. Previous work by Xiao *et al.* [206] has shown that the same analyte may give differing responses in different RTILs, and it was therefore considered in this work that one RTIL may be superior for the analysis of TNT in the presence of oxygen. Examples of the resulting cyclic voltammograms captured under the different environmental conditions are provided in Figure 6.27 and Figure 6.28.

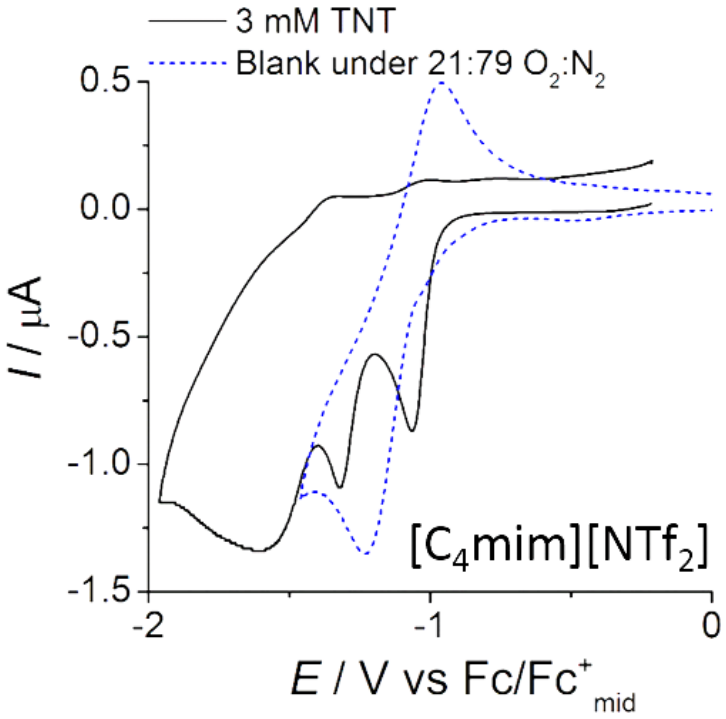

Figure 6.27: Cyclic voltammograms on a gold thin-film electrode (diameter 1 mm) at a scan rate of 100 mV s^{-1} using a gold reference electrode of 3 mM TNT in $[C_4mim][NTf_2]$ under nitrogen (black solid line) and blank $[C_4mim][NTf_2]$ in 21:79 O_2:N_2 (blue dashed line) both referenced against the midpoint of Fc/Fc^+ at 0 V

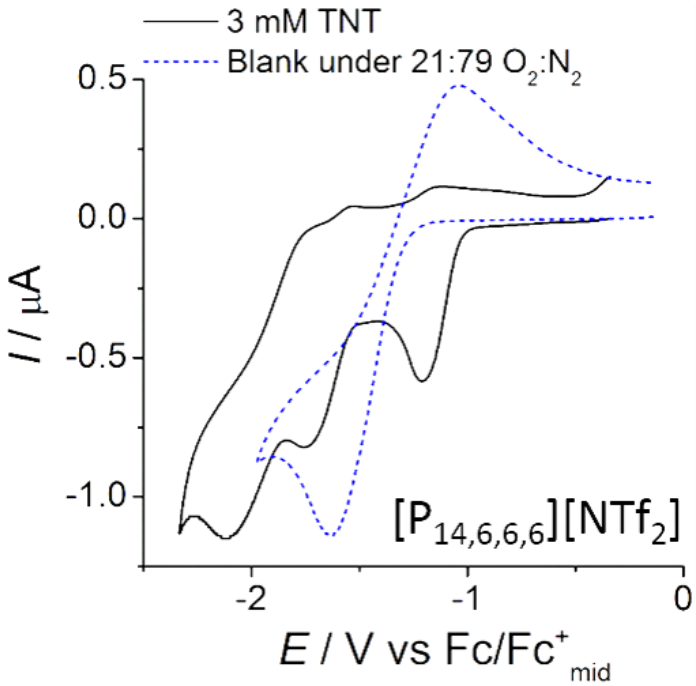

Figure 6.28: Cyclic voltammograms on a gold thin-film electrode (diameter 1 mm) at a scan rate of 100 mV s^{-1} using a gold reference electrode of 3 mM TNT in $[P_{14,6,6,6}][NTf_2]$ under nitrogen (black solid line) and blank $[P_{14,6,6,6}][NTf_2]$ in 21:79 O_2:N_2 (blue dashed line) both referenced against the midpoint of Fc/Fc^+ at 0 V

Based on Figure 6.27 and Figure 6.28 it can be seen that, due to the smaller amount of overlap between the peaks of oxygen and TNT, $[P_{14,6,6,6}][NTf_2]$ is a more suitable RTIL for the analysis of TNT in the presence of oxygen compared to $[C_4mim][NTf_2]$. Coupled with the fact that $[P_{14,6,6,6}][NTf_2]$ also gives better voltammetry in the presence of water, this highlights that $[P_{14,6,6,6}][NTf_2]$ is likely to be a more suitable RTIL than $[C_4mim][NTf_2]$ for use towards this chapter's overall aim of developing an electrochemical sensor for the detection of TNT in aqueous samples.

6.3.4 Gel polymer mixing ratio assessment

After assessing $[C_4mim][NTf_2]$ and $[P_{14,6,6,6}][NTf_2]$ as suitable ionic liquids for the recovery of TNT from aqueous solutions and assessing the response of TNT in the presence of oxygen, the next stage was to introduce polymers into the system. Gelling the RTILs with polymers should give a much more robust, portable TFE which can easily be used for TNT detection at scenes without the need to carry any additional chemicals or to perform any additional sample preparation steps prior to analysis.

In this work, two polymers were assessed: poly(methyl methacrylate) (PMMA) and poly(hexyl methacrylate) (PHMA). Their structures are provided in Figure 6.29.

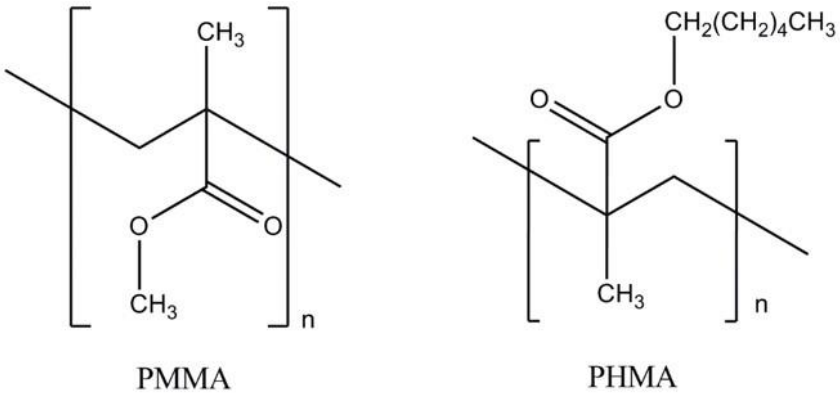

Figure 6.29: Chemical structures of poly(methyl methacrylate) (PMMA) and poly(hexyl methacrylate) (PHMA) used in this work

PMMA is an electrochemically inert polymer [239, 240] and is not anticipated to have a detrimental effect on TNT analyses. PMMA has previously been shown to be suitable for the formation of gel polymers with [C_2mim][NTf_2] for use with a TFE for oxygen sensing [239, 240], so it was thought to be a good starting point for this work. In addition, PHMA was employed as a structurally similar (i.e. also a methacrylate) but more hydrophobic polymer. Table 6.4 details contact angle measurements for the two polymers [277], with a higher contact angle corresponding to a higher hydrophobicity.

Table 6.4: Contact angle measurements of water droplets on PMMA and PHMA [277]

	PMMA	PHMA
Contact angle (°)	80	99

The increased hydrophobicity of PHMA relative to PMMA (due to its longer alkyl chains) may make for a more suitable gel polymer for immersion into aqueous samples, resulting in voltammetry that is less affected by exposure to moisture. For the development of a portable device, it needed to be ensured that the gel polymer used showed a good adhesion to a TFE and would not flow from the TFE during potential transportation to a scene. All polymer/RTIL combinations (see Table 6.1) were prepared at concentrations of 10-50 % polymer by mass and were then dropcast onto a glass microscope slide and held vertical for 12 hours to assess the adhesion properties to glass (see Figure 6.30 and Figure 6.31). It should be noted that when preparing PHMA/[C_4mim][NTf_2] (gel polymer variant 3, Table 6.1), white blobs formed in the mixture, which would not dissolve to give a homogeneous, clear gel polymer. It was not possible to dropcast these gel polymers onto a glass slide. For this reason, the decision was made to exclude the PHMA/[C_4mim][NTf_2] combination, and to move forward with the three successful polymer/RTIL combinations (gel polymer variants 1, 2 and 4, Table 6.1).

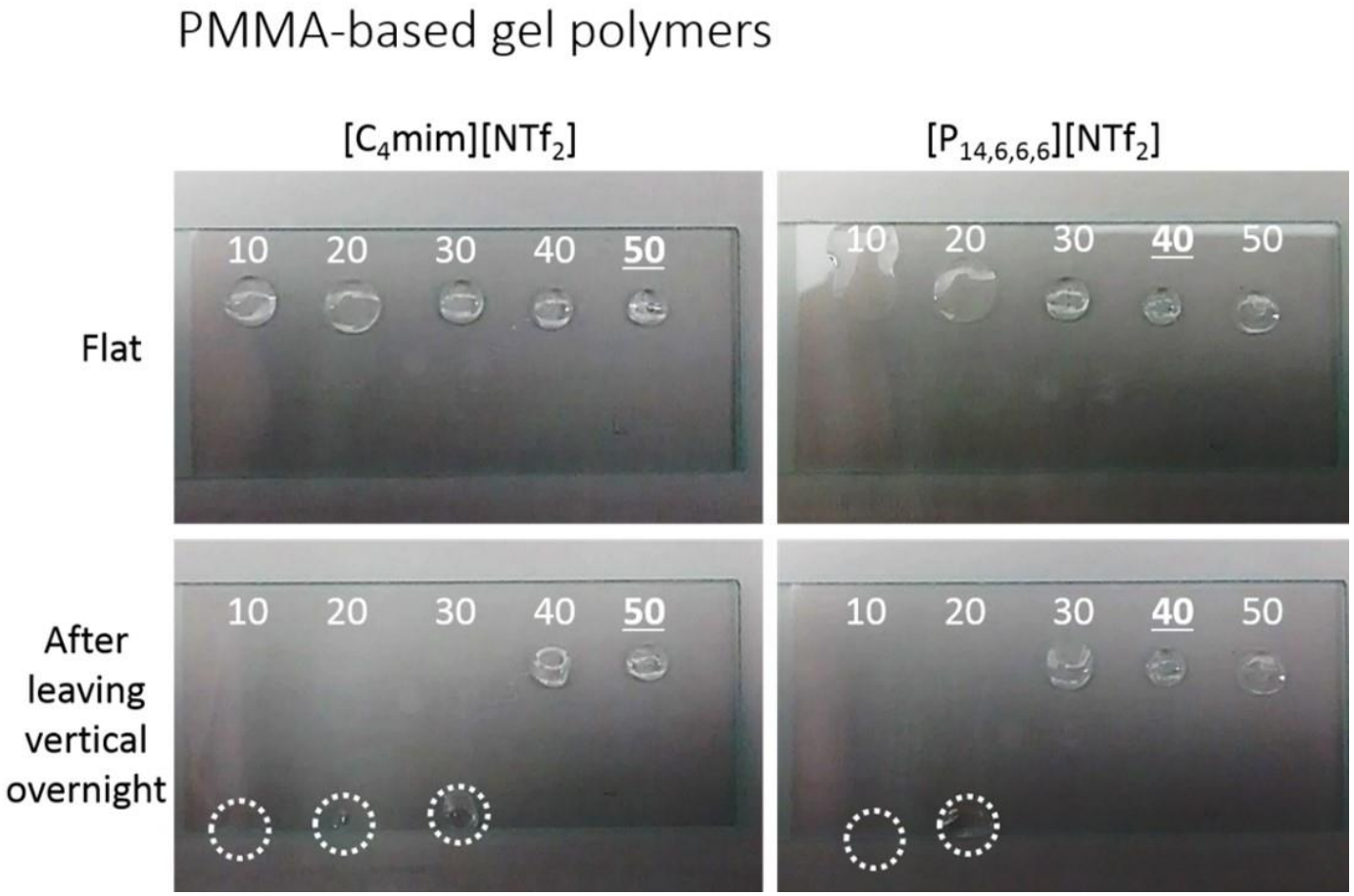

Figure 6.30: Results of the vertical glass slide test for PMMA with [C_4mim][NTf_2] and [$P_{14,6,6,6}$][NTf_2]. Numbers above each droplet indicate the percentage by mass of PMMA. Dashed circles highlight gel polymers with poor adhesion to the glass

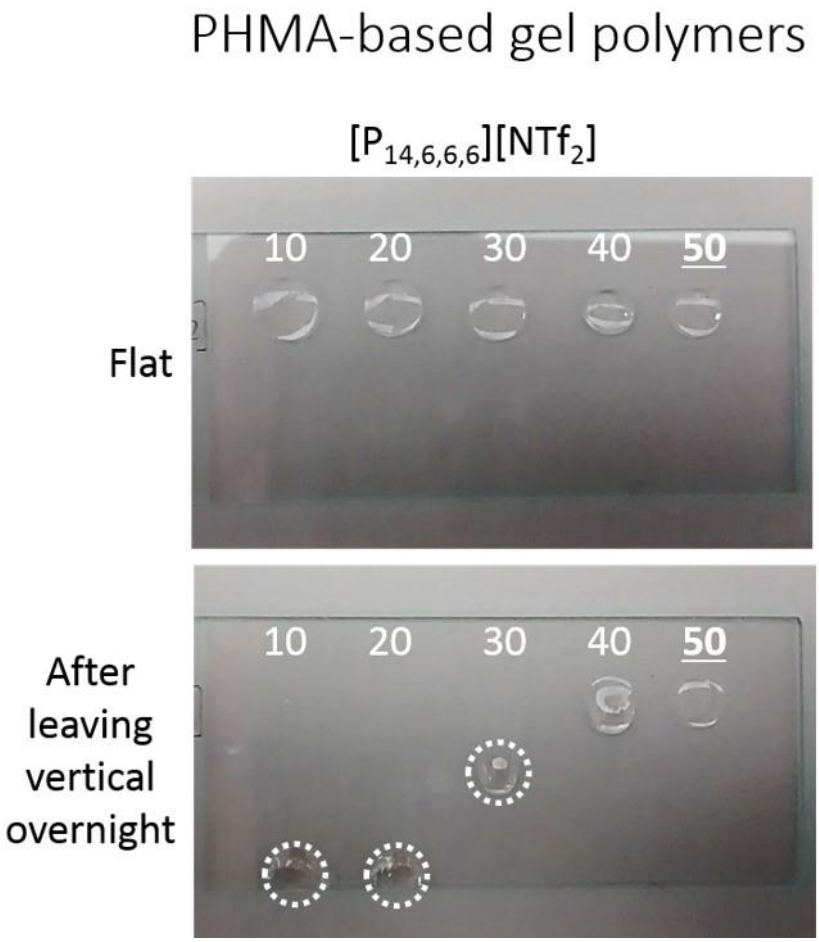

Figure 6.31: Results of the vertical glass slide test for PHMA with $[P_{14,6,6,6}][NTf_2]$. Numbers above each droplet indicate the percentage by mass of PHMA. Dashed circles highlight gel polymers with poor adhesion to the glass

It can be seen from Figure 6.30 and Figure 6.31 that a higher proportion of polymer within the gel polymer mixing ratios tended to give a polymer droplet with a higher viscosity, which decreased the gel polymer's ability to flow and resulted in a mechanically stable gel polymer droplet when held vertically overnight. The underlined polymer mixing ratios in each figure represent those used in later analyses in this work.

6.3.5 Polymer-water interactions

The shaking experiments detailed earlier found that a proportion of RTIL was lost due to dissolution into water. This led to concerns that RTIL may leach out from the gel polymers during their immersion in aqueous samples. For this reason, the three polymer mixing ratios were prepared and dropcast on a glass slide with the intention of assessing their behaviour during and after immersion into water. Figure 6.32 shows photos of the gel polymers with increasing immersion time.

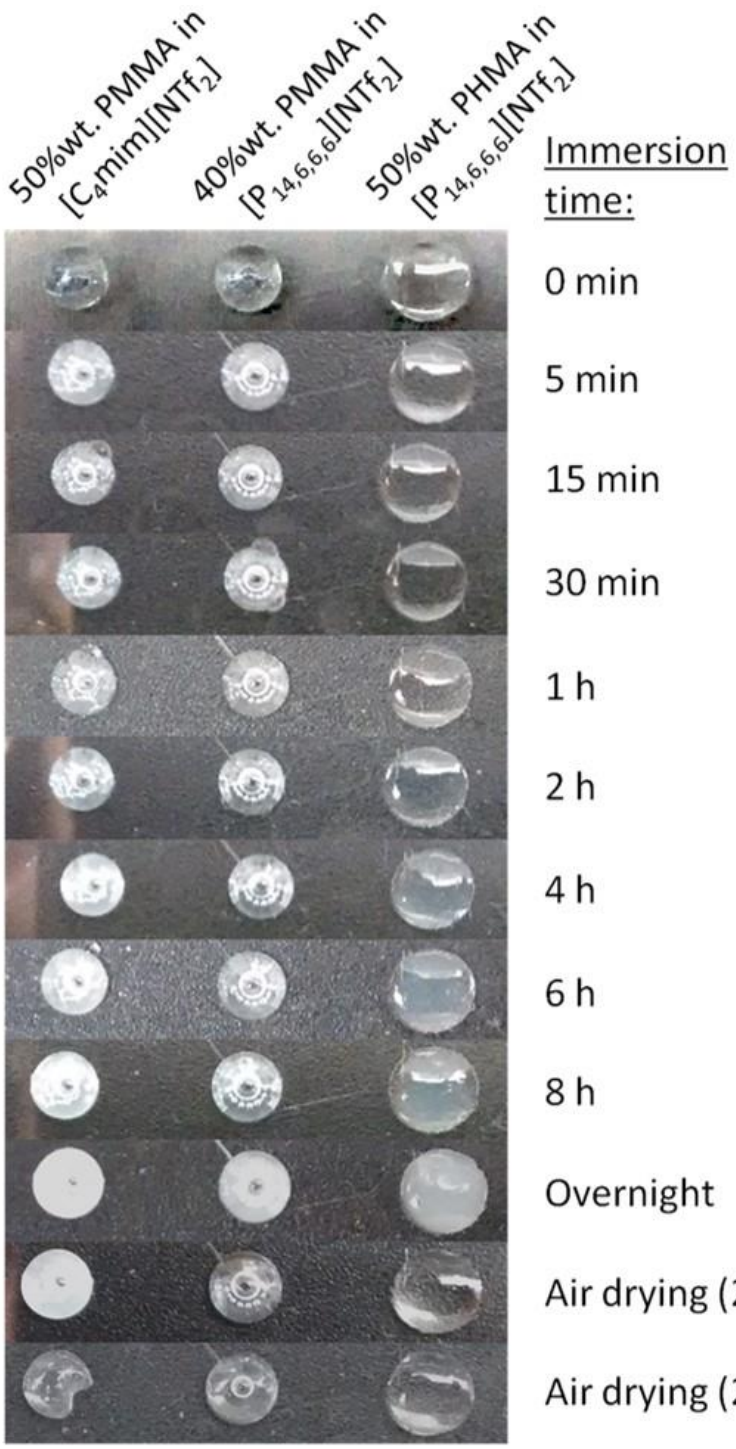

Figure 6.32: Gel polymer appearance after increasing immersion time in ultrapure water, along with appearance following removal and drying at room temperature

From Figure 6.32, it can be seen that all gel polymers began to turn white and opaque at increasing immersion times. The onset of opacity was fastest for the least hydrophobic PMMA and $[C_4mim][NTf_2]$ based gel polymers, whereas the slowest onset of opacity was observed with the most hydrophobic PHMA/$[P_{14,6,6,6}][NTf_2]$-based gel polymer.

It is possible that the white colour was due to some RTIL leaching into the bulk water phase,

with the white colour resembling that of the pure polymers. However, upon closer inspection of the white droplets, their surfaces had a sheen reminiscent of an emulsion. For this reason, it was instead hypothesised that some water molecules had partitioned into the outermost layer of the gel droplet. This conclusion is supported further by the observation that the PMMA and $[C_4mim][NTf_2]$ based gel polymers (the most hydrophilic combination) turned opaque more rapidly than the PHMA/$[P_{14,6,6,6}][NTf_2]$-based gel polymer (the most hydrophobic combination). Table 6.5 details the miscibility of $[C_4mim][NTf_2]$ and $[P_{14,6,6,6}][NTf_2]$ with water [275].

Table 6.5: Water content of $[C_4mim][NTf_2]$ and $[P_{14,6,6,6}][NTf_2]$ under atmospheric and wet conditions. Data from O'Mahony *et al.* [275]

	$[C_4mim][NTf_2]$	$[P_{14,6,6,6}][NTf_2]$
Water content (ppm) under atmospheric conditions	491	328
Water content (ppm) under wet conditions	5680	No data

This information is in agreement with the 'wet' cyclic voltammograms (Figure 6.24a and Figure 6.26a) of TNT in $[C_4mim][NTf_2]$ and $[P_{14,6,6,6}][NTf_2]$. The 'wet' cyclic voltammogram of TNT in $[C_4mim][NTf_2]$ showed a very indistinct voltammogram, with no discernible TNT peaks (Figure 6.24a). On the other hand, the analogous 'wet' cyclic voltammogram of TNT in $[P_{14,6,6,6}][NTf_2]$ showed clear peaks present corresponding to TNT (Figure 6.26a). This is likely to be due to the higher hydrophobicity of $[P_{14,6,6,6}][NTf_2]$ leading to less uptake of water than for $[C_4mim][NTf_2]$.

Images of the glass slide after drying in air for 20 hours and two weeks are displayed in the last two rows of Figure 6.32. It can be seen that after 20 hours drying at room temperature, the PHMA/$[P_{14,6,6,6}][NTf_2]$-based gel polymer and the PMMA/$[P_{14,6,6,6}][NTf_2]$-based gel polymers had started to revert back to their original transparent colour. On the other hand, the PMMA/$[C_4mim][NTf_2]$-based gel polymer required much longer. It is likely that the water penetration layer was more closely confined to the surface for the more hydrophobic gel polymer combination, whereas a thicker water penetration layer was likely for the more hydrophilic gel polymer, corresponding to a longer time to dry out the gel polymer after immersion.

6.3.6 TNT behaviour in gel polymer films

An initial assessment was made of the voltammetry of TNT dissolved directly in the three gel polymer combinations. An overall reduction in the TNT peak current was observed relative to the pure RTILs, likely due to the slower rate of diffusion of TNT in the more viscous gel polymers. Cyclic voltammograms of the same systems all showed highly resistive (i.e. highly

sloping) behaviour and few discernible TNT peaks (Figure 6.33a,c,e). Alternatively, clear TNT peaks (designated i_p) were obtained upon SWV analysis (Figure 6.33b,d,f), with a particularly distinct peak visible in the 50 % PHMA/[$P_{14,6,6,6}$][NTf_2] combination. Generally, the systems showed a high stability upon repeated SWV analysis at fixed 15 minute intervals. In addition, after a 15 minute immersion in water (simulating the TNT immersion experiments planned with blank gel polymer TFEs) and subsequent analysis using SWV, the overall TNT peak current was comparable before and after immersion. This suggests that TNT has a preference for the gel polymer and will remain there following its initial partitioning.

As the 50 % PHMA/[$P_{14,6,6,6}$][NTf_2] combination had consistently shown the best characteristics during the various RTIL and gel polymer assessments made throughout this work, this gel polymer combination was chosen for TNT extraction experiments from aqueous samples (detailed in next section).

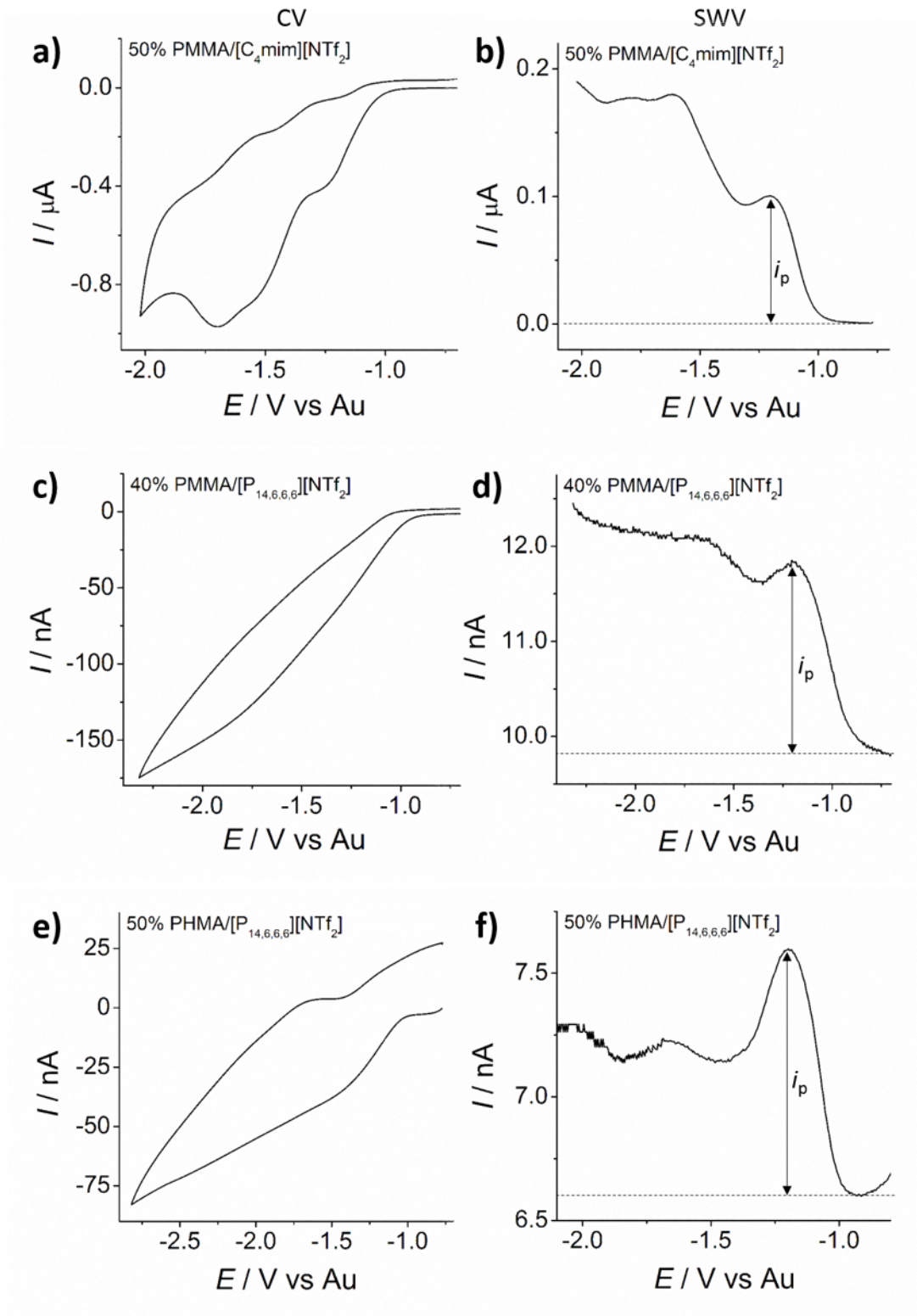

Figure 6.33: Cyclic voltammograms (a, c, e) and square wave voltammograms (b, d, f) of 3 mM TNT in the three best gel polymer ratios identified during this work. All voltammograms were captured on gold thin-film electrodes (WE diameter 1 mm) using a scan rate of 100 mV s^{-1} against a gold reference electrode

6.3.7 Gel polymer films for TNT extraction from aqueous samples

An initial experiment involved immersion of a gel polymer functionalised TFE into 0.5 mL of a static (i.e. with no stirring) 40 µg/mL aqueous solution of TNT in a 0.5 mL centrifuge vial. The TFE was removed and analysed using SWV after 15 minutes, though no TNT peaks were observed from this sample. It was hypothesised that agitation of the solution (e.g. shaking or stirring) would induce a greater flow of TNT across the gel polymer.

For this, initial experiments used a shaker table at 120 rpm to assess the effects of consistent shaking on TNT uptake into the gel polymer. The TFE was immersed in a glass vial containing 1 mL aqueous TNT solution, and subjected to 15 minutes at 120 rpm on the shaker table. The constant movement of TNT across the surface of the gel polymer during shaking was expected to induce faster TNT pre-concentration into the gel polymer compared to the earlier gel polymer-functionalised TFE immersion into a static solution of TNT. A schematic illustrating the mode of action for TNT pre-concentration into the gel polymer is provided in Figure 6.34.

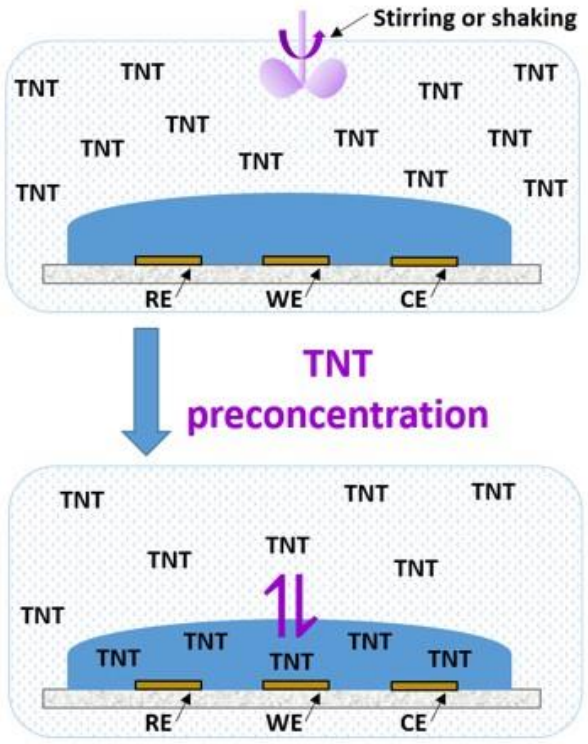

Figure 6.34: Schematic illustrating the TNT pre-concentration from bulk aqueous solution into a gel polymer layer observed in this work

Using the shaker table, approximately 5% of the TNT partitioned into the gel polymer (with this value calculated by comparing the TNT peak current to that obtained from the previous analysis of a 3 mM TNT-spiked gel polymer). Initially it had been planned to record a square wave voltammogram of a 'blank' 50 % PHMA/[$P_{14,6,6,6}$][NTf_2]-functionalised TFE, in order

to background subtract from all subsequent TNT-containing scans using different gel polymer-functionalised TFEs. However, it was observed that the individual gel polymer-functionalised TFEs had very different background currents (Figure 6.35 shows an example of the background currents of five different blank 50 % PHMA/$[P_{14,6,6,6}][NTf_2]$-functionalised TFEs prepared at the same time using the same batch of gel polymer), so the universal background subtraction approach was not viable. Instead, TNT peak currents were measured with respect to the background of each individual gel polymer-functionalised TFE used, with all backgrounds showing no peaks in the expected TNT region.

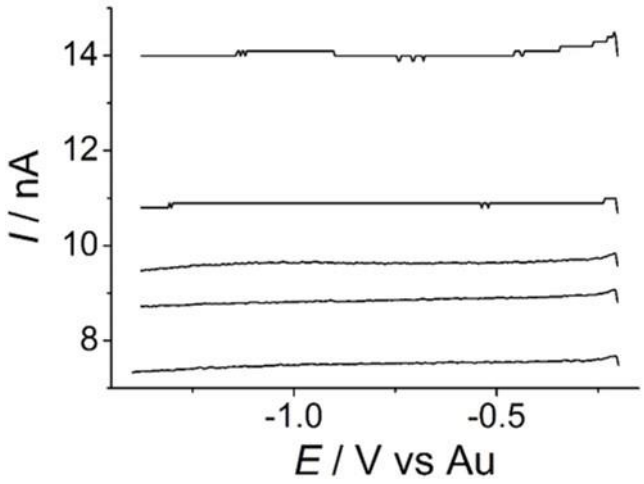

Figure 6.35: Square wave voltammogram currents of five blank gel polymer-functionalised TFEs, prepared in the same batch. Square wave voltammograms were captured at 100 mV s^{-1}, 25 Hz and 25 mV on gold thin-film electrodes (WE diameter 1 mm) against a gold reference electrode

The differences in background current observed in Figure 6.35 are likely due to differences in the individual gel polymer droplets. Although the same volume of gel polymer was dropcast onto each TFE, differences arose due to the individual nature of each dropcasting. For example, the different gel polymer droplets may have had different surface area:volume ratios depending on the exact spreading of the gel polymer upon its contact with the TFE, causing different gel polymer thicknesses.

It was also found that more stable background currents were obtained after immersing a gel polymer-functionalised electrode into ultrapure water for 15 minutes and then drying under nitrogen, compared to a TFE without the water immersion step. This was attributed to the 'pre-conditioning' of the gel polymer, causing it to relax to a more stable polymer structure [278-280].

The shaker table setup was used in conjunction with five individual gel polymer-functionalised TFEs to generate a calibration curve for TNT extraction from aqueous TNT solutions (1, 2, 5, 10 and 20 µg/mL). These concentrations are representative of those reported to have been

found in groundwater around the sites of explosives manufacturing plants [73, 281, 282]. The results of the calibration are shown in Figure 6.36.

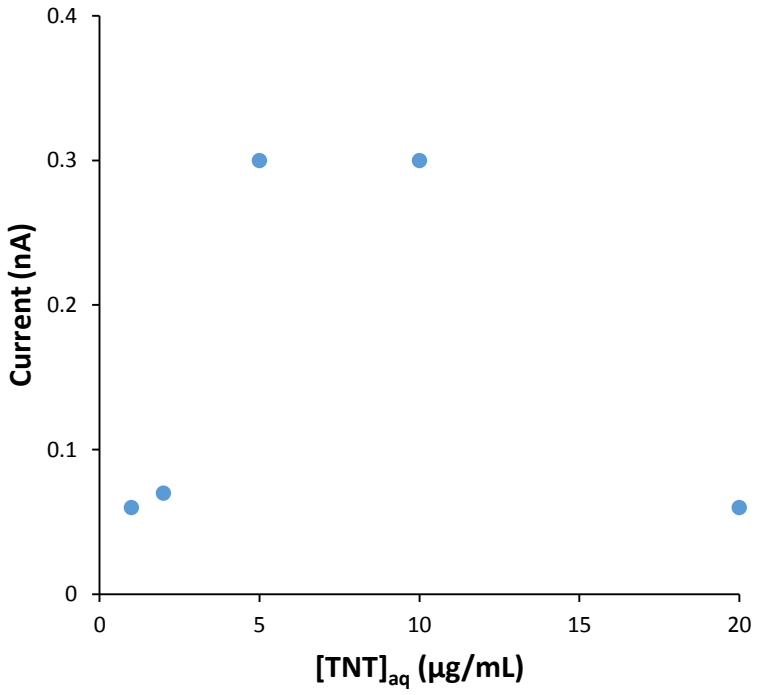

Figure 6.36: Plot of data from initial calibration attempt using a shaker table with different TFEs for each calibration point. Data from square wave voltammograms was captured at 100 mV s^{-1}, 25 Hz and 25 mV on gold thin-film electrodes (WE diameter 1 mm) against a gold reference electrode

The corresponding percentage TNT uptakes for the respective TNT standards are provided in Table 6.6, with these values calculated by comparing the TNT peak current from these calibration standards against the TNT peak current of 3 mM TNT prepared and analysed in the same gel polymer matrix.

Table 6.6: TNT uptake observed into gel polymer films from the respective aqueous TNT calibration standards

TNT concentration in aqueous solution (µg/mL)	TNT peak current (nA)	TNT uptake into gel polymer (g)	% TNT uptake
1	0.06	0.153	15.3
2	0.07	0.1785	8.9
5	0.3	0.765	15.3
10	0.3	0.765	7.65
20	0.06	0.153	0.765

From Figure 6.36 it can be seen that the data is scattered and there are not enough points to draw a meaningful conclusion regarding the success of the calibration attempt. As the use of

separate TFEs for immersion into TNT standards gave rise to a highly scattered calibration curve, a more suitable approach to obtain a linear calibration curve was hypothesised to use the same sensor to obtain an entire calibration curve.

For this, a cumulative TNT calibration curve was planned, in which a TFE would be repeatedly immersed in 1 μg/mL and 2 μg/mL aqueous solutions of TNT, with this design assuming that all TNT remains in the gel polymer over time (due to the much higher solubility of TNT in the gel polymer rather than aqueous solution). For this, a stirrer bar was employed to induce greater movement within the solution and thus a greater amount of TNT partitioning. Rather than fully immersing the TFEs flat into the vial, the TFEs were partially immersed at a vertical angle. The volume of solution was increased from 1 mL to 1.35 mL – this ensured that the stirrer bar maintained a smooth flow throughout the 15 minutes stirring time and did not touch the TFE upon stirring. The repeated exposure of the TFE to TNT should then generate a 'cumulative' calibration curve reflecting overall exposure to 1, 2, 4, 6, 8 and 10 μg/mL TNT. This approach proved much more successful than the use of individual TFEs for the individual TNT calibration standards, giving rise to relatively linear calibration plots.

Recently, these aqueous TNT extraction experiments using gel polymer functionalised TFEs were repeated in duplicate by Dr Junqiao Lee of Curtin University, with a graph of the three combined sets of results generated by this author and Dr Junqiao Lee shown in Figure 6.37. An averaged limit of detection of 0.37 μg/mL was obtained for TNT, generating a linear calibration curve with an R^2 value of 0.9995. This highlights the robustness of the system developed throughout this chapter. In addition, triplicate samples at the highest concentration (10 μg/mL) were analysed separately, with each response comparable to those obtained using the cumulative method (see red points on Figure 6.37). This highlights that quantitative detection is achievable with this sensor.

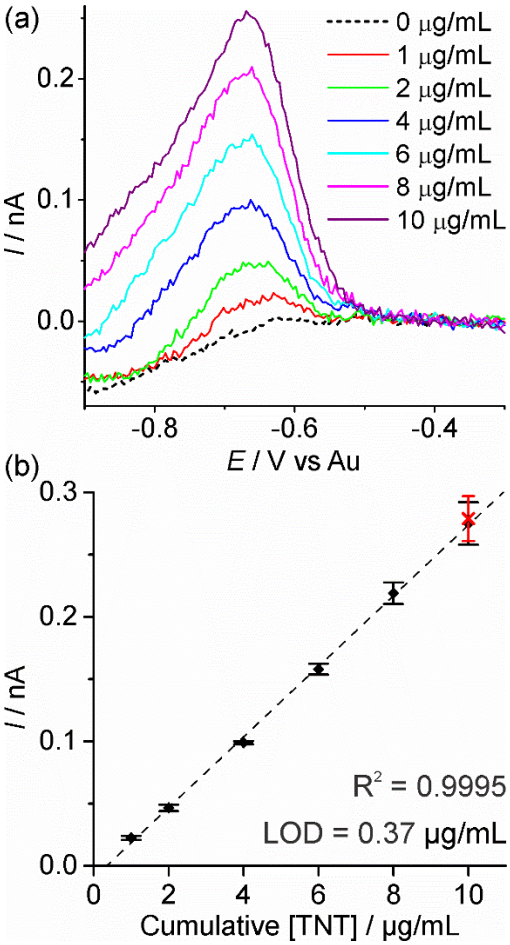

Figure 6.37: (a) SWVs on a gold TFE (WE Ø=1 mm) for the first reduction peak of TNT. TNT was partitioned into the GPE from aqueous phase concentrations of 1-10 µg/mL, each with a 15 minute GPE immersion/stirring time. (b) Corresponding cumulative calibration plot. Error bars correspond to one standard deviation. For comparison, the red cross with error bars represents the results of triplicate experiments using a 10 µg/mL TNT solutions, rather than the cumulative approach depicted using the black points

From the results displayed in Figure 6.37, it is promising that each of the TFEs was capable of uptaking TNT, even from solutions at low concentrations (1 µg/mL) representative of those which may be found in TNT-contaminated groundwater. The averaged limit of detection was 0.37 µg/mL. This limit of detection is comparable to a number of previous papers investigating the electrochemical detection of TNT in aqueous samples [125, 218, 234, 283]. However, the method developed in the current chapter negates the need for buffer solution preparation prior to analysis, as the RTIL acts as the electrolyte for sampling. In addition, as the TFE is disposable, this reduces the risk of any cross-contamination between sample analyses. Though non-electrochemical methods have been reported which offer lower detection limits (e.g. 1.4 ng for TNT using a lab-on-a-chip device driven by microfluidic separation [284]), the current method involves minimal sample preparation and it has the potential to be further improved to reduce the current limits of detection obtained.

A TFE without the gel polymer was used for the detection of TNT directly in aqueous solution (with potassium chloride as a supporting electrolyte), and it was found that no TNT could be detected, confirming that the gel polymer is necessary to pre-concentrate the TNT. In addition, making a separate solution containing supporting electrolyte is not necessary when using the gel polymer-functionalised TFE as the ionic liquid functions as the inbuilt electrolyte. This therefore reduces the complexity of the system and avoids the need to make up solutions prior to analysis.

6.3.8 Gel polymer films for the detection of TNT vapour

In addition to assessing their utility for TNT detection from aqueous samples, the gel polymer-functionalised TFEs were also assessed with regards to their ability to detect vapour phase TNT. If successful, this would broaden the applicability of the developed system. However, no TNT uptake was detected in the gel polymer-functionalised TFE during either the static or dynamic vapour-phase experiments (performed at room temperature). This is perhaps not surprising, due to the very low vapour pressure of TNT (9.15 ppb at 25 °C) [285], which is likely to hinder significant TNT pre-concentration within the gel polymer. The application of heat to the solid TNT sample should promote TNT volatilisation and thus should favour enhanced TNT pre-concentration into the gel polymer. The 'heating' approach (at temperatures of 50, 60 or 120 °C) has previously been used by other researchers to generate measurable quantities of vapour-phase TNT [126, 204, 206], so a heated TNT vapour generation approach was also trialled during the present work. A temperature of 60 °C was chosen, to minimise the hazards associated with heating TNT to higher temperatures. In addition, it was ensured that all crystals of TNT were smaller than its critical diameter (2 mm) [146], to ensure that shock or friction would not induce a detonation.

The two neat RTILs $[C_4mim][NTf_2]$ and $[P_{14,6,6,6}][NTf_2]$ showed detectable levels of TNT uptake during the four hour TNT vapour exposure time (see Figure 6.38). However, a 50 % PHMA/$[P_{14,6,6,6}][NTf_2]$ gel polymer-functionalised TFE, which had been successful for the extraction of TNT from aqueous samples, showed no detectable TNT under the same conditions. This is likely due to the much higher viscosity of the gel polymer than the pure RTILs, in addition to the thicker layer of gel polymer compared to the pure RTILs, factors likely to have prevented significant TNT partitioning into the gel polymer.

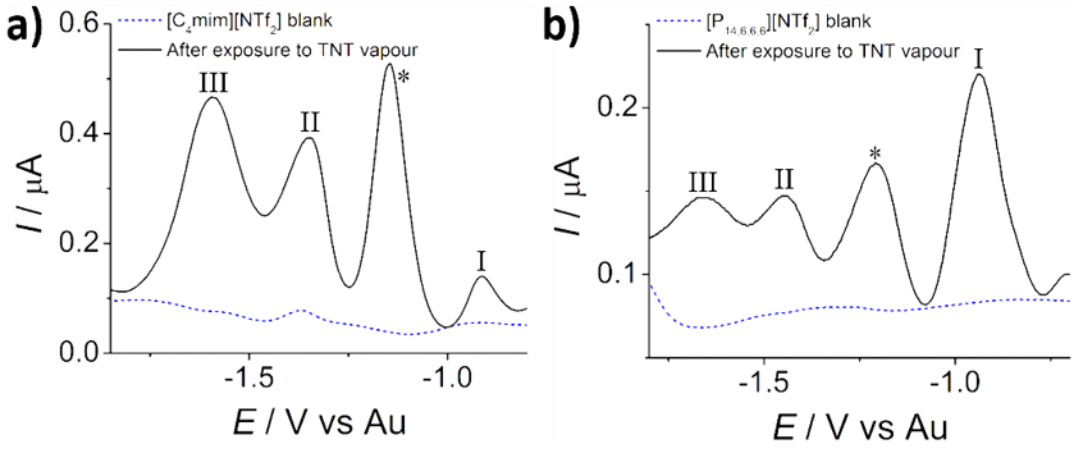

Figure 6.38: TNT vapour phase results in [C4mim][NTf2] and [P14,6,6,6][NTf2], with initial blanks indicated by a dashed line. I, II and III designate the successive reduction of the three nitro groups of TNT; * indicates a probable peak due to oxygen

Previous researchers [126, 206] have reported pre-concentrating TNT vapour aided by nitrogen flow. This approach was briefly investigated in the present work, with a gel polymer-functionalised TFE positioned in the path of nitrogen flow passing through a heated glass pot (70 °C) containing TNT. However, as before, no TNT was detected using this system. It is possible that the use of a much thinner gel polymer film (potentially applied by a spin-casting technique) may favour TNT partitioning from the vapour phase. In addition, it is likely that the use of a less viscous RTIL within the gel polymer would favour TNT uptake from the vapour phase. These ideas would be interesting to explore in future work.

6.4 Conclusions and future work

This main aim of this chapter was to develop a gel polymer-functionalised electrode for the detection of TNT in aqueous samples (i.e. for the detection of TNT in groundwater and soil samples). TNT behaviour was assessed in two RTILs in the absence and presence of oxygen, finding one ionic liquid ($[P_{14,6,6,6}][NTf_2]$) superior to the other ($[C_4mim][NTf_2]$) as its voltammetry was less affected by the presence of oxygen and water.

Following this, a number of gel polymers were assessed with regards to their mechanical stability, in addition to their behaviour upon immersion into water. Using the most suitable gel polymer (50 % PHMA/$[P_{14,6,6,6}][NTf_2]$), a technique was developed for the immersion of the gel polymer-functionalised TFEs in aqueous TNT samples, and a calibration curve was generated using aqueous TNT concentrations typically found in groundwater. The sampling approach is convenient (highly portable and fast – analyses can be performed within 30 minutes, allowing for a 15 minute sampling time and 15 minute drying time), and offers the potential for a new at-the-scene sampling device for TNT detection from aqueous samples. This is of significance, considering that the work outlined in Chapter 4 and Chapter 5

highlighted that explosive residues can undergo very rapid degradation. In addition, early work was performed towards the utilisation of these gel polymer-functionalised TFEs for the detection of vapour-phase TNT.

Future work would be to use molecularly imprinted polymers, as these may give rise to a higher specificity than the non-specific polymers used during this work. It would also be useful to investigate sampling at different temperatures, and the use of more hydrophobic RTILs. By tuning the polymers and RTILs in this manner, it is likely that the developed sensor would be improved, leading to lower detection limits for TNT.

In terms of other future work, spin-casting the gel polymer films is likely to give more consistent gel polymer film thicknesses and more reproducible background currents from different TFEs. In addition, it would be useful to try experiments to aid the detection of vapour-phase TNT using gel polymer-functionalised TFEs; in Chapter 3, use of the contact heater was described for the recovery of explosive residues, including TNT, from textiles. If the gel polymer-functionalised TFEs developed in this chapter could be optimised for the detection of TNT vapour, it is conceivable that they could be incorporated into the sampling head of the contact heater to aid TNT detection from porous surfaces.

Finally, this chapter has focused solely on the detection of TNT. However, it would also be forensically useful to assess this setup with regards to the detection of other electrochemically active explosives, such as RDX and PETN utilised throughout the other chapters of this thesis, to give wider applicability to the developed device.

Chapter 7 Conclusions and Future Work

This thesis describes studies aiming to improve various aspects of forensic explosives recovery, storage and analysis. In order to achieve this aim, significant fundamental studies have been performed to investigate the underpinning science behind explosive residue recovery, storage and analysis.

In terms of recovery, this thesis has demonstrated that crystals of TNT, PETN and RDX tend to show a higher adhesion to smoother surfaces, such as glass, compared to rougher surfaces, such as textiles. This finding will have implications for the design of future explosive residue recovery kits.

In terms of storage, this thesis has demonstrated that current storage conditions used for soil samples containing explosive residues are inadequate and may lead to a rapid rate of explosive residue degradation. More appropriate storage conditions have been identified in this thesis. In addition, the work described in this thesis has also shown that current techniques used to spike soils with explosives for degradation studies do not generate samples which are representative of samples generated following actual vehicle bombings or landmine detonations. The findings from this thesis will therefore influence future explosives degradation studies involving soil samples.

In terms of analysis, a novel electrochemical method has been developed for the extraction and pre-concentration of TNT from aqueous samples. The limits of detection for TNT are on the order of those found in TNT-contaminated groundwater, and this technique therefore shows potential as a new at-the-scene explosive residue detection technique. More detailed conclusions are summarised below for each chapter, in addition to suggestions for future work.

Chapter 2 demonstrated the utility of atomic force microscopy (AFM) to identify surfaces most likely to capture explosive residues following a detonation process. It was found that crystals of TNT, PETN and RDX tend to exhibit a higher adhesion to smoother surfaces, which tended to be non-porous (glass, polypropylene, paint) compared to rougher, textile surfaces. This work utilised undetonated explosive crystals, and useful further work could be performed using similar explosive crystals exposed to a detonation process, as it is likely that the crystals' morphology would change upon exposure to the extreme conditions generated during a detonation process.

The efficacy of the contact heater was evaluated in Chapter 3 with regards to the recovery of

TNT, PETN and RDX from the textile surfaces examined in Chapter 2. For TNT in particular it was found that an inverse correlation exists between the degree of explosives' adhesion to a surface and subsequent explosives recovery from that surface, knowledge which may have a useful bearing on future forensic explosives examinations. The three explosives demonstrated a good stability on the ten textile surfaces over one week, particularly when stored in a freezer. A small-scale comparison between the contact heater and more conventional vacuum sampling revealed the contact heater to be superior to vacuum sampling for those explosives with the higher vapour pressures (TNT, PETN), whereas vacuum sampling was more effective for the lower vapour pressure RDX. Taken together, the work from Chapters 2 and 3 has demonstrated that a targeted approach may help to maximise recoveries of explosive residues when faced with a large quantity of different debris exhibits. This results of this work may also be of interest in terms of designing new swab materials for explosive residue recovery. Useful future work would be to trial the contact heater and vacuum sampling techniques sequentially, to favour maximum explosive residue recoveries from a given textile.

In Chapter 4, work was performed to investigate the stability of explosive residues in soils and examine the ways in which degradation may occur. New storage conditions were proposed to aid the recovery of these explosive residues over longer time periods, as their degradation in soils using current storage methods has been reported within a matter of hours. Three different soils were spiked with an aqueous solution of TNT, PETN and RDX and aged for six weeks, to assess explosive residue recoveries over time. A variety of storage conditions were investigated, with storage in a freezer using a nitrogen headspace deemed to be the most effective. This finding is significant for the storage of soil samples from the vicinity of an explosion scene, prior to analysis. This work was extended in Chapter 5, where the same three soil types were subjected to controlled detonation processes (simulating landmine or vehicle bombing detonations). SEM analyses revealed that both detonation positions caused fracturing of the soil particles, and subsequent µCT analyses showed the detonated soil aggregates had a higher internal porosity. At the same time, a faster rate of TNT degradation was observed in these detonation spiked soils, attributed to facilitated microbial transfer through the more porous post-blast soils leading to a greater bioavailability of the contained explosive residues [190]. These findings have strong ramifications for future investigations into the fate of explosive residues in soils, as it is clear that laboratory simulations do not ideally replicate results from soils exposed to a real-life detonation process. These results also have wider implications in terms of the remediation of explosives-contaminated land, with one possibility being to increase a soil's porosity to enhance the rate of TNT biodegradation.

In order to further establish the role of a soil's specific properties on the rate of explosive

residue degradation, further studies could be performed using a wider array of soils. In addition, in this work, much of the observed explosive residue loss and degradation product formation has been attributed to microbial activity within the soils [75, 78-85]. However, this postulation could only be confirmed by performing some biochemical analyses to culture colonies of bacteria present in the specific soils used within this work, to determine whether the bacteria present are capable of degrading the explosive residues in the manner anticipated. It would also be beneficial to determine the effect of certain additives on the rate of degradation of explosive residues within a soil – for example, some explosives compositions contain aluminium which may have an effect on the rates of explosive residue degradation. In addition, it would be of interest to assess the behaviour and detonation efficiency of improvised explosives in conjunction with soils, as there is little, if any, published literature to this effect. In addition, it would also be of use to identify any degradation products which may form.

A technique for the electrochemical detection of TNT in aqueous samples was developed in Chapter 6. For this, a gold thin-film electrode was functionalised with a mixture of polymer and ionic liquid. Following immersion into aqueous TNT samples, a limit of detection of 0.37 µg/mL was obtained using square wave voltammetry. This method is highly promising for the detection of TNT at post-explosion scenes or for the detection of TNT in soil or groundwater samples from a bioremediation perspective. Importantly, the functionalised electrodes are miniature, low-cost and readily transported in a ready-to-use state, without the need for any activation on-site or the addition of any additional chemicals or complicated sample processing steps. Future research should extend this system to assess its use in detecting other explosives such as PETN and RDX. It would also be of benefit to assess the system in the presence of contaminants to verify its robustness. For example, it would be beneficial to test the developed system using real soil extracts. Following this, the developed apparatus could then be incorporated into a portable device to be used at or near a scene of interest [8, 33]. Looking further ahead, the system could then be subjected to appropriate validation protocols prior to introducing it for use in the field.

References

[1] T. Tamiri, S. Zitrin, Chapter 15: Analysis of explosives by mass spectrometry, in: A. Beveridge (Ed.) Forensic Investigation of Explosions (2nd edition), CRC Press, Boca Raton, FL, 2012, pp. 621-670.

[2] S. Broome, C. Todd, Chapter 6: The management of casework within the United Kingdom Forensic Explosives Laboratory, in: A. Beveridge (Ed.) Forensic Investigation of Explosions (2nd edition), CRC Press, Boca Raton, FL, 2012, pp. 159-195.

[3] R.A. Strobel, Chapter 5: Recovery of material from the scene of an explosion and its subsequent forensic laboratory examination - A team approach, in: A. Beveridge (Ed.) Forensic Investigation of Explosions (2nd edition), CRC Press, Boca Raton, FL, 2012, pp. 119-157.

[4] H.K. Evans, F.A.J. Tulleners, B.L. Sanchez, C.A. Rasmussen, An unusual explosive, triacetonetriperoxide (TATP), J. Forensic Sci., 31 (1986) 1119-1125.

[5] J.-Y. Vermette, Chapter 4: General protocols at the scene of an explosion, in: A. Beveridge (Ed.) Forensic Investigation of Explosions (2nd edition), CRC Press, Boca Raton, FL, 2012, pp. 79-117.

[6] L.F. Kobilinsky, Forensic Chemistry Handbook, John Wiley & Sons, Hoboken, N.J., 2012.

[7] U. Rodoplu, J.L. Arnold, R. Tokyay, G. Ersoy, S. Cetiner, T. Yucel, Mass-casualty terrorist bombings in Istanbul, Turkey, November 2003: report of the events and the prehospital emergency response, Prehosp. Disaster Med., 19 (2004) 133-145.

[8] D. Royds, S.W. Lewis, A.M. Taylor, A case study in forensic chemistry: The Bali bombings, Talanta, 67 (2005) 262-268.

[9] M.M. Houck, Fundamentals of Forensic Science, Academic Press, Burlington, MA, 2010.

[10] D. DeTata, P. Collins, A. McKinley, An investigation into the fate of organic explosives in soil, Aust. J. Forensic Sci., 45 (2012) 71-84.

[11] R. Waddell, D.E. Dale, M. Monagle, S.A. Smith, Determination of nitroaromatic and nitramine explosives from a PTFE wipe using thermal desorption-gas chromatography with electron-capture detection, J. Chromatogr. A, 1062 (2005) 125-131.

[12] S. Doyle, Chapter 13: Quality and the trace detection and identification of organic high explosives, in: A. Beveridge (Ed.) Forensic Investigation of Explosions (2nd edition), CRC Press, Boca Raton, FL, 2012, pp. 539-583.

[13] M. Emmrich, T. Lahrz, W. Spyra, Influence of solvents and gas chromatographic injector conditions on the detectability of nitroaromatic compounds, J. Chromatogr. A, 918 (2001) 121-126.

[14] D.A. DeTata, P.A. Collins, A.J. McKinley, A comparison of common swabbing materials for the recovery of organic and inorganic explosive residues, J. Forensic Sci., 58 (2013) 757-763.

[15] D.A. DeTata, P.A. Collins, A.J. McKinley, A comparison of solvent extract cleanup procedures in the analysis of organic explosives, J. Forensic Sci., 58 (2013) 500-507.

[16] R. Schulte-Ladbeck, P. Kolla, U. Karst, Trace Analysis of Peroxide-Based Explosives, Anal. Chem., 75 (2003) 731-735.

[17] L. Widmer, S. Watson, K. Schlatter, A. Crowson, Development of an LC/MS method for the trace analysis of triacetone triperoxide (TATP), Analyst, 127 (2002) 1627-1632.

[18] J.W. Jardine, Chapter 16: Presentation of explosive casework evidence, in: A. Beveridge (Ed.) Forensic Investigation of Explosions, Taylor & Francis, London, 1998, pp. 469-487.

[19] J. Yinon, Modern Methods and Applications in Analysis of Explosives, Wiley, New York, 1993.

[20] K. Yeager, Chapter 12: Improvised explosives characteristics, detection, and analysis, in: A. Beveridge (Ed.) Forensic Investigation of Explosions (2nd edition), CRC Press, Boca Raton, FL, 2012, pp. 493-538.

[21] B. Mohanty, Chapter 2: Physics of explosion hazards, in: A.D. Beveridge (Ed.) Forensic Investigation of Explosions (2nd Edition), CRC Press, Boca Raton, FL, 2012, pp. 19-52.

[22] R.B. Hopler, Chapter 1: The history, development, and characteristics of explosives and propellants, in: A. Beveridge (Ed.) Forensic Investigation of Explosions (2nd edition), CRC Press, Boca Raton, FL, 2012, pp. 1-18.

[23] G.T. Murray, Chapter 18: The significance of analytical results in explosives investigation, in: A. Beveridge (Ed.) Forensic Investigation of Explosions (2nd edition), CRC Press, Boca Raton, FL, 2012, pp. 725-739.

[24] J.A. Siegel, P.J. Saukko, Encyclopedia of Forensic Sciences, Elsevier, Oxford, 2013.

[25] S. Zitrin, Chapter 9: Analysis of explosives by infrared spectrometry and mass spectrometry, in: A. Beveridge (Ed.) Forensic Investigation of Explosions, Taylor & Francis, London, 1998, pp. 267-314.

[26] BBC News. Shoe bomb suspect 'did not act alone'. 25th January 2002; accessed 14th August 2014. http://news.bbc.co.uk/2/hi/americas/1783237.stm.

[27] BBC News. Brussels explosions: What we know about airport and metro attacks. 9th April 2016; accessed 13th December 2016. http://www.bbc.com/news/world-europe-35869985.

[28] J.E. Chipuk, Attribution of Erythritol Tetranitrate (ETN) Homemade Explosives to Precursor Sources and Synthetic Route via Chemometric Analysis of Multi-Channel Data, International Symposium on the Analysis and Detection of Explosives, The Hague, The Netherlands, 2013.

[29] M. Kunzel, Q.-L. Yan, J. Selesovsky, S. Zeman, R. Matyas, Thermal behavior and decomposition kinetics of ETN and its mixtures with PETN and RDX, J. Therm. Anal. Calorim., 115 (2014) 289-299.

[30] S. Sollid, R. Rimstad, M. Rehn, A. Nakstad, A.-E. Tomlinson, T. Strand, H. Heimdal, J. Nilsen, M. Sandberg, Oslo government district bombing and Utoya island shooting July 22, 2011: The immediate prehospital emergency medical service response, Scand. J. Trauma, Resusc. and Emerg. Med., 20 (2012) 1-12.

[31] B.R. McCord, I. Corbin, E.C. Bender, Chapter 14: Chromatography of explosives, in: A. Beveridge (Ed.) Forensic Investigation of Explosions (2nd edition), CRC Press, Boca Raton, FL, 2012, pp. 585-620.

[32] E.C. Bender, Chapter 11: Analysis of low explosives, in: A. Beveridge (Ed.) Forensic Investigation of Explosions, Taylor & Francis, London, 1998, pp. 343-388.

[33] S. Benson, N. Speers, V. Otieno-Alego, Chapter 17: Portable explosive detection instruments, in: A. Beveridge (Ed.) Forensic Investigation of Explosions (2nd edition), CRC Press, Boca Raton, FL, 2012, pp. 691-723.

[34] E.C. Bender, A.D. Beveridge, Chapter 11: Investigation of pipe bombs, in: A. Beveridge (Ed.) Forensic Investigation of Explosions (2nd edition), CRC Press, Boca Raton, FL, 2012, pp. 429-491.

[35] J. Almog, A. Klein, T. Tamiri, Y. Shloosh, S. Abramovich-Bar, A field diagnostic test for the improvised explosive urea nitrate, J. Forensic Sci., 50 (2005) 582-586.

[36] J. Almog, S. Kraus, B. Glattstein, ETK-an operational explosive testing kit, J. Energ. Mater., 4 (1986) 159-167.

[37] J.P. Hutchinson, C.J. Evenhuis, C. Johns, A.A. Kazarian, M.C. Breadmore, M. Macka, E.F. Hilder, R.M. Guijt, G.W. Dicinoski, P.R. Haddad, Identification of Inorganic Improvised Explosive Devices by Analysis of Postblast Residues Using Portable Capillary Electrophoresis Instrumentation and Indirect Photometric Detection with a Light-Emitting Diode, Anal. Chem. (Washington, DC, U. S.), 79 (2007) 7005-7013.

[38] J.P. Hutchinson, C. Johns, M.C. Breadmore, E.F. Hilder, R.M. Guijt, C. Lennard, G. Dicinoski, P.R. Haddad, Identification of inorganic ions in post-blast explosive residues using portable CE instrumentation and capacitively coupled contactless conductivity detection, Electrophoresis, 29 (2008) 4593-4602.

[39] R.V. Taudte, A. Beavis, L. Wilson-Wilde, C. Roux, P. Doble, L. Blanes, A portable explosive detector based on fluorescence quenching of pyrene deposited on colored wax-printed μPADs, Lab Chip, 13 (2013) 4164-4172.

[40] M. Marshall, J.C. Oxley, Aspects of Explosives Detection, Elsevier, Boston, 2009.

[41] S. Ballou, Scientific and Technical Working Groups: An Overview. 1st February 2009; accessed 6th November 2016. Available from: http://www.forensicmag.com/article/2009/02/scientific-and-technical-working-groups-overview.

[42] TWGFEX Laboratory Explosion Group Standards & Protocols Committee. Recommended Guidelines for Forensic Identification of Intact Explosives, National Centre for Forensic Science, n.d.

[43] TWGFEX Laboratory Explosion Group Standards & Protocols Committee. Recommended Guidelines for Forensic Identification of Post-Blast Explosive Residues, National Centre for Forensic Science, 2009.

[44] S. Zitrin, T. Tamiri, Chapter 16: Analysis of explosives by infrared spectrometry, in: A. Beveridge (Ed.) Forensic Investigation of Explosions (2nd edition), CRC Press, Boca Raton, FL, 2012, pp. 671-689.

[45] E.M.A. Ali, H.G.M. Edwards, I.J. Scowen, Raman spectroscopy and security applications: the detection of explosives and precursors on clothing, J. Raman Spectrosc., 40 (2009) 2009-2014.

[46] E.M.A. Ali, H.G.M. Edwards, I.J. Scowen, In-situ detection of single particles of explosive on clothing with confocal Raman microscopy, Talanta, 78 (2009) 1201-1203.

[47] S. Almaviva, S. Botti, A. Palucci, A. Puiu, F. Schnurer, W. Schweikert, F.S. Romolo, Application of micro-Raman spectroscopy for fight against terrorism and smuggling, Opt. Eng. (Bellingham, WA, U. S.), 044113, 53 (2014) 1-7.

[48] D.K. Kuila, A. Chakrabortty, S.P. Sharma, S.C. Lahiri, Composition profile of low explosives from cases in India, Forensic Sci. Int., 159 (2006) 127-131.

[49] S.-I. Nam, On-site analysis of explosives in soil: Evaluation of thin-layer chromatography for confirmation of analyte identity (Special Report 97-21), Cold Regions Research and Engineering Laboratory, 1997, pp. 1-14.

[50] J. Yinon, S. Zitrin, The Analysis of Explosives, Chapter 2 - Chemical Methods, Pergamon Press, Oxford, 1981.

[51] R.G. Parker, M.O. Stephenson, J.M. McOwen, J.A. Cherolis, Analysis of explosives and explosive residues. Part 1: chemical tests, J Forensic Sci, 20 (1975) 133-140.

[52] R. Mu, H. Shi, Y. Yuan, A. Karnjanapiboonwong, J.G. Burken, Y. Ma, Fast Separation and Quantification Method for Nitroguanidine and 2,4-Dinitroanisole by Ultrafast Liquid Chromatography-Tandem Mass Spectrometry, Anal. Chem. (Washington, DC, U. S.), 84 (2012) 3427-3432.

[53] D. Perret, S. Marchese, A. Gentili, R. Curini, A. Terracciano, E. Bafile, F. Romolo, LC-MS-MS Determination of Stabilizers and Explosives Residues in Hand-Swabs, Chromatographia, 68 (2008) 517-524.

[54] A.M.A. Verweij, P.C.A.M. De Bruyn, C. Choufoer, P.J.L. Lipman, Liquid chromatographic, thermospray/negative ion, tandem mass spectrometric(lc/tsp/ms/ms) analysis of some explosives, Forensic Sci. Int., 60 (1993) 7-13.

[55] C. Sarazin, N. Delaunay, C. Costanza, V. Eudes, P. Gareil, Capillary electrophoresis analysis of inorganic cations in post-blast residue extracts applying a guanidinium-based electrolyte and bilayer-coated capillaries, Electrophoresis, 32 (2011) 1282-1291.

[56] J.M.F. Douse, Dynamic headspace method for the improved clean-up of gunshot residues prior to the detection of nitroglycerine by capillary column gas chromatography with thermal energy analysis detection, J. Chromatogr., 464 (1989) 178-185.

[57] K.G. Furton, J.R. Almirall, M. Bi, J. Wang, L. Wu, Application of solid-phase microextraction to the recovery of explosives and ignitable liquid residues from forensic specimens, J. Chromatogr. A, 885 (2000) 419-432.

[58] W. Fan, J. Almirall, High-efficiency headspace sampling of volatile organic compounds in explosives using capillary microextraction of volatiles (CMV) coupled to gas chromatography-mass spectrometry (GC-MS), Anal. Bioanal. Chem., 406 (2014) 2189-2195.

[59] S. Calderara, D. Gardebas, F. Martinez, Solid phase micro extraction coupled with on-column GC/ECD for the post-blast analysis of organic explosives, Forensic Sci. Int., 137 (2003) 6-12.

[60] N. Song-im, S. Benson, C. Lennard, Establishing a universal swabbing and clean-up protocol for the combined recovery of organic and inorganic explosive residues, Forensic Sci. Int., 223 (2012) 136-147.

[61] R. Borusiewicz, A review of methods of preparing samples for chromatographic analysis for the presence of organic explosive substances, Z Zagadnien Nauk Sadowych, 69 (2007) 5-29.

[62] P. White, Crime Scene to Court: The Essentials of Forensic Science, Royal Society of Chemistry, 2010.

[63] I. Corbin, B. McCord, Detection of the improvised explosives ammonium nitrate (AN) and urea nitrate (UN) using non-aqueous solvents with electrospray ionization and MS/MS detection, Talanta, 115 (2013) 533-539.

[64] N. Talaty, C.C. Mulligan, D.R. Justes, A.U. Jackson, R.J. Noll, R.G. Cooks, Fabric analysis by ambient mass spectrometry for explosives and drugs, Analyst (Cambridge, U. K.), 133 (2008) 1532-1540.

[65] SOP210: Vacuum Sampling for Traces of Explosives, Dstl Forensic Explosives Laboratory, Porton Down, Wiltshire, 2016.

[66] H. Brust, A. van Asten, M. Koeberg, A. van der Heijden, C.-J. Kuijpers, P. Schoenmakers, Pentaerythritol tetranitrate (PETN) profiling in post-explosion residues to constitute evidence of crime-scene presence, Forensic Sci. Int., 230 (2013) 37-45.

[67] V. Cavett, E.M. Waninger, J.J. Krutak, B.A. Eckenrode, Visualization and LC/MS analysis of colorless pepper sprays, J. Forensic Sci., 49 (2004) 469-476.

[68] R. Fletcher, N. Briggs, E. Ferguson, G. Gillen, Measurements of Air Jet Removal Efficiencies of Spherical Particles from Cloth and Planar Surfaces, Aerosol Sci. Technol., 42 (2008) 1052-1061.

[69] C. Hubert, X. Machuron-Mandard, J.-C. Tabet, Ambient ionization MS analysis of swabs used for explosives detection, LC-GC Eur., 8 (2013) 10-13.

[70] N. Na, C. Zhang, M. Zhao, S. Zhang, C. Yang, X. Fang, X. Zhang, Direct detection of explosives on solid surfaces by mass spectrometry with an ambient ion source based on dielectric barrier discharge, J. Mass Spectrom., 42 (2007) 1079-1085.

[71] M.N. Chaffee-Cipich, B.D. Sturtevant, S.P. Beaudoin, Adhesion of Explosives, Anal. Chem. (Washington, DC, U. S.), 85 (2013) 5358-5366.

[72] Y. Zakon, N.G. Lemcoff, A. Marmur, Y. Zeiri, Adhesion of Standard Explosive Particles to Model Surfaces, J. Phys. Chem. C, 116 (2012) 22815-22822.

[73] J. Pichtel, Distribution and fate of military explosives and propellants in soil: a review, Appl. Environ. Soil Sci., 617236 (2012) 1-33.

[74] M.E. Walsh, A.D. Hewitt, T.F. Jenkins, C.A. Ramsey, M.R. Walsh, S.R. Bigl, C.M. Collins, M.A. Chappell, Assessing sample processing and sampling uncertainty for energetic residues on military training ranges: method 8330B, ACS Symp. Ser., 1069 (2011) 91-106.

[75] A. Halasz, C. Groom, E. Zhou, L. Paquet, C. Beaulieu, S. Deschamps, A. Corriveau, S. Thiboutot, G. Ampleman, C. Dubois, J. Hawari, Detection of explosives and their degradation products in soil environments, J. Chromatogr. A, 963 (2002) 411-418.

[76] M.E. Walsh, Determination of nitroaromatic, nitramine, and nitrate ester explosives in soil by gas chromatography and an electron capture detector, Talanta, 54 (2001) 427-438.

[77] J.C. Oxley, J.L. Smith, E. Resende, E. Pearce, Quantification and aging of the post-blast residue of TNT landmines, J. Forensic Sci., 48 (2003) 742-753.

[78] C.K. Bayne, D.D. Schmoyer, R.A. Jenkins, Practical Reporting Times for Environmental Samples, Environ. Sci. Technol., 28 (1994) 1430-1436.

[79] T. Gorontzy, O. Drzyzga, M.W. Kahl, D. Bruns-Nagel, J. Breitung, E.v. Loew, K.H. Blotevogel, Microbial degradation of explosives and related compounds, Crit. Rev. Microbiol., 20 (1994) 265-284.

[80] J. Hawari, S. Beaudet, A. Halasz, S. Thiboutot, G. Ampleman, Microbial degradation of explosives: biotransformation versus mineralization, Appl. Microbiol. Biotechnol., 54 (2000) 605-618.

[81] M. Kulkarni, A. Chaudhari, Microbial remediation of nitro-aromatic compounds: an overview, J. Environ. Manag., 85 (2007) 496-512.

[82] J. Pennington, C.A. Hayes, K.F. Myers, M. Ochman, D. Gunnison, D.R. Felt, E.F. McCormick, Fate of 2,4,6-trinitrotoluene in a simulated compost system, Chemosphere, 30 (1995) 429-438.

[83] S. Sagi-Ben Moshe, O. Dahan, N. Weisbrod, A. Bernstein, E. Adar, Z. Ronen, Biodegradation of explosives mixture in soil under different water-content conditions, J. Hazard. Mater., 203-204 (2012) 333-340.

[84] J.E. Walker, D.L. Kaplan, Biological degradation of explosives and chemical agents, Biodegrad., 3 (1992) 369-385.

[85] C.A. Groom, S. Beaudet, A. Halasz, L. Paquet, J. Hawari, Detection of the cyclic nitramine explosives hexahydro-1,3,5-trinitro-1,3,5-triazine (RDX) and octahydro-1,3,5,7-tetranitro-1,3,5,7-tetrazine (HMX) and their degradation products in soil environments, J. Chromatogr. A, 909 (2001) 53-60.

[86] M.E. Walsh, T.F. Jenkins, Identification of TNT transformation products in soil, Special Report 92-16, Cold Regions Res. Eng. Lab., 1992, pp. 1-31.

[87] M.R. Walsh, M.E. Walsh, K. Gagnon, A.D. Hewitt, T.F. Jenkins, Subsampling of Soils Containing Energetics Residues, Soil Sediment Contam., 23 (2014) 452-463.

[88] S. Sagi-Ben Moshe, Z. Ronen, O. Dahan, N. Weisbrod, L. Groisman, E. Adar, R. Nativ, Sequential biodegradation of TNT, RDX and HMX in a mixture, Environ. Pollut. (Oxford, U. K.), 157 (2009) 2231-2238.

[89] N. Singh, D. Hennecke, J. Hoerner, W. Koerdel, A. Schaeffer, Degradation of trinitrotoluene in contaminated soils as affected by its initial concentrations and its binding to soil organic matter fractions, J. Environ. Sci. Health, Part A: Toxic/Hazard. Subst. Environ. Eng., 43 (2008) 348-356.

[90] G.K. Vasilyeva, V.D. Kreslavski, B.-T. Oh, P.J. Shea, Potential of activated carbon to decrease 2,4,6-trinitrotoluene toxicity and accelerate soil decontamination, Environ. Toxicol. Chem., 20 (2001) 965-971.

[91] C.L. Kitts, D.P. Cunningham, P.J. Unkefer, Isolation of three hexahydro-1,3,5-trinitro-1,3,5-triazine-degrading species of the family Enterobacteriaceae from nitramine explosive-contaminated soil, Appl. Environ. Microbiol., 60 (1994) 4608-4611.

[92] H. Yamamoto, M.C. Morley, G.E. Speitel, Jr., J. Clausen, Fate and transport of high explosives in a sandy soil: adsorption and desorption, Soil Sediment Contam., 13 (2004) 459-477.

[93] F. Monteil-Rivera, C. Groom, J. Hawari, Sorption and Degradation of Octahydro-1,3,5,7-tetranitro-1,3,5,7-tetrazocine in Soil, Environ. Sci. Technol., 37 (2003) 3878-3884.

[94] T.W. Sheremata, A. Halasz, L. Paquet, S. Thiboutot, G. Ampleman, J. Hawari, The Fate of the Cyclic Nitramine Explosive RDX in Natural Soil, Environ. Sci. Technol., 35 (2001) 1037-1040.

[95] M.P. Maskarinec, C.K. Bayne, L.H. Johnson, S.K. Holladay, R.A. Jenkins, B.A. Tomkins, Stability of explosives in environmental water and soil samples, Oak Ridge Natl. Lab., 1991, pp. 1-94.

[96] C.C. Ainsworth, S.D. Harvey, J.E. Szecsody, M.A. Simmons, V. Cullinan, Relationship between the leachability characteristics of unique energetic compounds and soil properties, Battelle Memorial Inst., 1993, pp. 1-120.

[97] H.T. Mayfield, E. Burr, M. Cantrell, Analysis of explosives in soil using solid phase microextraction and gas chromatography, Anal. Lett., 39 (2006) 1463-1474.

[98] C.L. Grant, T.F. Jenkins, K.F. Myers, E.F. McCormick, Holding-time estimates for soils containing explosives residues: comparison of fortification vs. field contamination, Environ. Toxicol. Chem., 14 (1995) 1865-1874.

[99] A.M. Jaramillo, T.A. Douglas, M.E. Walsh, T.P. Trainor, Dissolution and sorption of hexahydro-1,3,5-trinitro-1,3,5-triazine (RDX) and 2,4,6-trinitrotoluene (TNT) residues from detonated mineral surfaces, Chemosphere, 84 (2011) 1058-1065.

[100] T.A. Douglas, M.E. Walsh, C.J. McGrath, C.A. Weiss, A.M. Jaramillo, T.P. Trainor, Desorption of nitramine and nitroaromatic explosive residues from soils detonated under controlled conditions, Environ. Toxicol. Chem., 30 (2010) 345-353.

[101] T.A. Douglas, M.E. Walsh, C.J. McGrath, C.A. Weiss, Jr., Investigating the fate of nitroaromatic (TNT) and nitramine (RDX and HMX) explosives in fractured and pristine soils, J. Environ. Qual., 38 (2009) 2285-2294.

[102] K.M. Dontsova, C. Hayes, J.C. Pennington, B. Porter, Sorption of high explosives to water-dispersible clay: influence of organic carbon, aluminosilicate clay, and extractable iron, J. Environ. Qual., 38 (2009) 1458-1465.

[103] R. Batlle, C. Nerin, C. Crescenzi, H. Carlsson, Supercritical Fluid Extraction of Energetic Nitroaromatic Compounds and Their Degradation Products in Soil Samples, Anal. Chem., 77 (2005) 4241-4247.

[104] S.L. Larson, W.A. Martin, B.L. Escalon, M. Thompson, Dissolution, Sorption, and Kinetics Involved in Systems Containing Explosives, Water, and Soil, Environ. Sci. Technol., 42 (2008) 786-792.

[105] S.B. Haderlein, K.W. Weissmahr, R.P. Schwarzenbach, Specific Adsorption of Nitroaromatic Explosives and Pesticides to Clay Minerals, Environ. Sci. Technol., 30 (1996) 612-622.

[106] G. Alavi, M. Chung, J. Lichwa, M. D'Alessio, C. Ray, The fate and transport of RDX, HMX, TNT and DNT in the volcanic soils of Hawaii: A laboratory and modeling study, J. Hazard. Mater., 185 (2011) 1600-1604.

[107] T.A. Douglas, M.E. Walsh, C.A. Weiss, Jr., C.J. McGrath, T.P. Trainor, Desorption and Transformation of Nitroaromatic (TNT) and Nitramine (RDX and HMX) Explosive Residues on Detonated Pure Mineral Phases, Water, Air, Soil Pollut., 223 (2012) 2189-2200.

[108] I. Jayamani, M.P. Manzella, A.M. Cupples, RDX Degradation Potential in Soils Previously Unexposed to RDX and the Identification of RDX-Degrading Species in One Agricultural Soil Using Stable Isotope Probing, Water, Air, Soil Pollut., 224 (2013) 1-15.

[109] D. Kalderis, A.L. Juhasz, R. Boopathy, S. Comfort, Soils contaminated with explosives: environmental fate and evaluation of state-of-the-art remediation processes (IUPAC technical report), Pure Appl. Chem., 83 (2011) 1407-1484.

[110] A. Esteve-Nunez, A. Caballero, J.L. Ramos, Biological degradation of 2,4,6-trinitrotoluene, Microbiol. Mol. Biol. Rev., 65 (2001) 335-352.

[111] L. Ma, B. Xin, Y. Chen, Direct mass spectrometric detection of trace explosives in soil samples, Analyst (Cambridge, U. K.), 137 (2012) 1730-1736.

[112] A. Choodum, P. Kanatharana, W. Wongniramaikul, N. Nic Daeid, Using the iPhone as a device for a rapid quantitative analysis of trinitrotoluene in soil, Talanta, 115 (2013) 143-149.

[113] L. Capka, Z. Vecera, P. Mikuska, J. Sestak, V. Kahle, A. Bumbova, A portable device for fast analysis of explosives in the environment, J. Chromatogr. A, 1388 (2015) 167-173.

[114] B.D. Nielsen, Non-Destructive Soil Testing Using X-Ray Computed Tomography (MSc Thesis), Department of Civil Engineering, Montana State University, Bozeman, Montana, 2004.

[115] S. Peth, R. Horn, F. Beckmann, T. Donath, J. Fischer, A.J.M. Smucker, Three-dimensional quantification of intra-aggregate pore-space features using synchrotron-radiation-based microtomography, Soil Sci. Soc. Am. J., 72 (2008) 897-907.

[116] N. Nunan, K. Ritz, M. Rivers, D.S. Feeney, I.M. Young, Investigating microbial micro-habitat structure using X-ray computed tomography, Geoderma, 133 (2006) 398-407.

[117] J.A. Contreras, J.A. Murray, S.E. Tolley, J.L. Oliphant, H.D. Tolley, S.A. Lammert, E.D. Lee, D.W. Later, M.L. Lee, Hand-Portable Gas Chromatograph-Toroidal Ion Trap Mass Spectrometer (GC-TMS) for Detection of Hazardous Compounds, Journal of the American Society for Mass Spectrometry, 19 (2008) 1425-1434.

[118] C. Sadowski, T. Brande, B. Richter, D. Later, Monitoring Worker Exposure of Toxic Chemicals Using Solid Phase Microextraction (SPME) and a Portable GC-MS, LC GC North America, (2013) 26.

[119] R.R.A. Syms, S. Wright, Mems mass spectrometers: the next wave of miniaturization, 2016, pp. 023001.

[120] C. Lennard, Application of a Next-Generation Portable Gas Chromatograph-Mass Spectrometer for the On-Site Analysis of Ignitable Liquid Residues, Proceedings of ANZFSS 2014 (31st August - 5th September 2014), Adelaide, Australia.

[121] A.J. Bandodkar, A.M. O'Mahony, J. Ramirez, I.A. Samek, S.M. Anderson, J.R. Windmiller, J. Wang, Solid-state Forensic Finger sensor for integrated sampling and detection of gunshot residue and explosives: towards 'Lab-on-a-finger', Analyst, 138 (2013) 5288-5295.

[122] J.S. Caygill, S.D. Collyer, J.L. Holmes, F. Davis, S.P.J. Higson, Disposable screen-printed sensors for the electrochemical detection of TNT and DNT, Analyst, 138 (2013) 346-352.

[123] J.S. Caygill, S.D. Collyer, J.L. Holmes, F. Davis, S.P.J. Higson, Electrochemical Detection of TNT at Cobalt Phthalocyanine Mediated Screen-Printed Electrodes and Application to Detection of Airborne Vapours, Electroanalysis, 25 (2013) 2445-2452.

[124] J. Zang, C.X. Guo, F. Hu, L. Yu, C.M. Li, Electrochemical detection of ultratrace nitroaromatic explosives using ordered mesoporous carbon, Anal. Chim. Acta, 683 (2011) 187-191.

[125] M.S. Goh, M. Pumera, Graphene-based electrochemical sensor for detection of 2,4,6-trinitrotoluene (TNT) in seawater: The comparison of single-, few-, and multilayer graphene nanoribbons and graphite microparticles, Anal. Bioanal. Chem., 399 (2011) 127-131.

[126] K. Cizek, C. Prior, C. Thammakhet, M. Galik, K. Linker, R. Tsui, A. Cagan, J. Wake, J. La Belle, J. Wang, Integrated explosive preconcentrator and electrochemical detection system for 2,4,6-trinitrotoluene (TNT) vapor, Anal. Chim. Acta, 661 (2010) 117-121.

[127] J. Wang, B. Tian, E. Sahlin, Micromachined electrophoresis chips with thick-film electrochemical detectors, Anal. Chem., 71 (1999) 5436-5440.

[128] C.X. Guo, Y. Lei, C.M. Li, Porphyrin functionalized graphene for sensitive electrochemical detection of ultratrace explosives, Electroanalysis, 23 (2011) 885-893.

[129] T.H. Seah, H.L. Poh, C.K. Chua, Z. Sofer, M. Pumera, Towards Graphene Applications in Security: The Electrochemical Detection of Trinitrotoluene in Seawater on Hydrogenated Graphene, Electroanalysis, 26 (2014) 62-68.

[130] A.M. O'Mahony, J. Wang, Nanomaterial-based electrochemical detection of explosives: a review of recent developments, Anal. Methods, 5 (2013) 4296-4309.

[131] S.J. Woltman, W.R. Even, E. Sahlin, S.G. Weber, Chromatographic detection of nitroaromatic and nitramine compounds by electrochemical reduction combined with photoluminescence following electron transfer, Anal. Chem., 72 (2000) 4928-4933.

[132] R. Jimenez-Perez, M. Baron, L. Elie, J.-G. Rodriguez, Design of a virtual sensor data array for the analysis of RDX, HMX, and DMNB using metal-doped screen printed electrodes and chemometric analysis, Int. J. Electrochem. Sci., 8 (2013) 3279-3289.

[133] W. Chen, Y. Wang, C. Brueckner, C.M. Li, Y. Lei, Poly[meso-tetrakis(2-thienyl)porphyrin] for the sensitive electrochemical detection of explosives, Sens. Actuators, B, 147 (2010) 191-197.

[134] P.K. Sekhar, E.L. Brosha, R. Mukundan, K.L. Linker, C. Brusseau, F.H. Garzon, Trace detection and discrimination of explosives using electrochemical potentiometric gas sensors, J. Hazard. Mater., 190 (2011) 125-132.

[135] E. Piccin, N. Dossi, A. Cagan, E. Carrilho, J. Wang, Rapid and sensitive measurements of nitrate ester explosives using microchip electrophoresis with electrochemical detection, Analyst, 134 (2009) 528-532.

[136] P. Rabenecker, K. Pinkwart, A look behind electrochemical detection of explosives, Propellants, Explos., Pyrotech., 34 (2009) 274-279.

[137] D.S. Silvester, Recent advances in the use of ionic liquids for electrochemical sensing, Analyst (Cambridge, U. K.), 136 (2011) 4871-4882.

[138] C. Kang, J. Lee, D.S. Silvester, Electroreduction of 2,4,6-Trinitrotoluene in Room Temperature Ionic Liquids: Evidence of an EC2 Mechanism, The Journal of Physical Chemistry C, 120 (2016) 10997-11005.

[139] F.-P. Adolf, Chapter 2: The Structure of Textiles, Forensic Examination of Fibres, CRC Press, Boca Raton, 1999.

[140] S.K. David, Chapter 1: Classification of Textile Fibres, Forensic Examination of Fibres, CRC Press, Boca Raton, 1999.

[141] G. Binnig, C.F. Quate, C. Gerber, Atomic Force Microscope, Physical Review Letters, 56 (1986) 930-933.

[142] K.S. Birdi, Scanning Probe Microscopes: Applications in Science and Technology, CRC Press, Boca Raton, Fl., 2003.

[143] E. Canetta, K. Montiel, A.K. Adya, Morphological changes in textile fibers exposed to environmental stresses: Atomic force microscopic examination, Forensic Sci. Int., 191 (2009) 6-14.

[144] T. Das, T. Becker, B.N. Nair, Measurements on hydrophobic and hydrophilic surfaces using a porous gamma alumina nanoparticle aggregate mounted on Atomic Force Microscopy cantilevers, Thin Solid Films, 518 (2010) 2769-2774.

[145] A. Beveridge, Forensic Investigation of Explosions, Taylor & Francis, London, 1998.

[146] J.W. Grate, R.G. Ewing, D.A. Atkinson, Vapor-generation methods for explosives-detection research, TrAC, Trends Anal. Chem., 41 (2012) 1-14.

[147] N. Kubota, Chapter 9: Combustion of Explosives, Propellants and Explosives: Thermochemical Aspects of Combustion, Wiley-VCH Verlag GmbH & Co. KGaA, Weinheim, Germany, 2006, pp. 257-272.

[148] R. Creasey, S. Sharma, C.T. Gibson, J.E. Craig, A. Ebner, T. Becker, P. Hinterdorfer, N.H. Voelcker, Atomic force microscopy-based antibody recognition imaging of proteins in the pathological deposits in Pseudoexfoliation Syndrome, Ultramicroscopy, 111 (2011) 1055-1061.

[149] J.M. Connelly, W.C. Curby, F.T. Fox, S.F. Hallowell, Chapter 3: Detection of hidden explosives, in: A. Beveridge (Ed.) Forensic Investigation of Explosions, Taylor & Francis, London, 1998, pp. 45-73.

[150] N. Abdul-Karim, C.S. Blackman, P.P. Gill, R.M. Morgan, L. Matjacic, R. Webb, W.H. Ng, Morphological Variations of Explosive Residue Particles and Implications for Understanding Detonation Mechanisms, Anal. Chem. (Washington, DC, U. S.), 88 (2016) 3899-3908.

[151] M. Grieve, Chapter 13: Interpretation of Fibres Evidence, Forensic Examination of Fibres, CRC Press, Boca Raton, FL, 1999.

[152] D.S. Moore, R.J. Scharff, Portable Raman explosives detection, Anal. Bioanal. Chem., 393 (2009) 1571-1578.

[153] D.A. Skoog, Principles of Instrumental Analysis, Thomson, Belmont, CA, 2007.

[154] H.A. Yu, S.W. Lewis, M.S. Beardah, N. NicDaeid, Assessing a novel contact heater as a new method of recovering explosives traces from porous surfaces, Talanta, 148 (2016) 721-728.

[155] T.S. Hayes, D.W. Wardleworth, The Recovery of Explosives Residues at Trace Level, Interamerican Congress of Forensic Science (1982).

[156] I. Salt, Evaluation of the modified Contact Heater for the recovery of explosives traces (report no. Dstl/CR09231), Forensic Explosives Laboratory, Dstl, Fort Halstead, 2003.

[157] N. Song-im, Explosive Residue Analysis: Evaluation and Optimisation of Sampling, Storage and Cleanup Protocols (PhD thesis), University of Canberra, 2011.

[158] M. Bruze, B. Edman, B. Niklasson, H. Moeller, Thin layer chromatography and high pressure liquid chromatography of musk ambrette and other nitromusk compounds including photopatch studies, Photodermatology, 2 (1985) 295-302.

[159] N. Nic Daeid, H.A. Yu, M.S. Beardah, Investigating TNT loss between sample collection and analysis, Science and Justice, 57 (2017) 95-100.

[160] H. Oestmark, S. Wallin, H.G. Ang, Vapor Pressure of Explosives: A Critical Review, Propellants, Explos., Pyrotech., 37 (2012) 12-23.

[161] M.E. Walsh, C.A. Ramsey, T.F. Jenkins, The effect of particle size reduction by grinding on subsampling variance for explosives residues in soil, Chemosphere, 49 (2002) 1267-1273.

[162] H.A. Yu, D.A. DeTata, S.W. Lewis, N. Nic Daeid, The stability of TNT, RDX and PETN in simulated post-explosion soils: Implications of sample preparation for analysis, Talanta, 164 (2017) 716-726.

[163] A. Pesenti, R.V. Taudte, B. McCord, P. Doble, C. Roux, L. Blanes, Coupling Paper-Based Microfluidics and Lab on a Chip Technologies for Confirmatory Analysis of Trinitro Aromatic Explosives, Anal. Chem. (Washington, DC, U. S.), 86 (2014) 4707-4714.

[164] M.W. Townsend, P.R. Byron, P.P. DeLuca, The effects of formulation additives on the degradation of freeze-dried ribonuclease A, Pharm. Res., 7 (1990) 1086-1091.

[165] A. Kramer, J.G. Kaffezakis, T. Besser, Extension of CA[controlled atmosphere] storage by use of gases other than oxygen and carbon dioxide, Bull. Inst. Int. Froid, Annexe, 3 (1973) 121-128.

[166] S. Gschwendtner, T. Alatossava, S. Kublik, M.M. Fuka, M. Schloter, P. Munsch-Alatossava, N2 gas flushing alleviates the loss of bacterial diversity and inhibits psychrotrophic Pseudomonas during the cold storage of bovine raw milk, PLoS One, e0146015, 11 (2016) 1-17.

[167] E. Penas, C. Martinez-Villaluenga, J.M. Pihlava, J. Frias, Evaluation of refrigerated storage in nitrogen-enriched atmospheres on the microbial quality, content of bioactive compounds and antioxidant activity of sauerkrauts, LWT--Food Sci. Technol., 61 (2015) 463-470.

[168] P. Rodriguez-Alonso, J.A. Centeno, J.I. Garabal, Biochemical study of industrially produced Arzua-Ulloa semi-soft cows' milk cheese: Effects of storage under vacuum and modified atmospheres with high-nitrogen contents, Int. Dairy J., 21 (2011) 261-271.

[169] P. Munsch-Alatossava, A. Ghafar, T. Alatossava, Potential of nitrogen gas (N2) flushing to extend the shelf life of cold stored pasteurised milk, Int. J. Mol. Sci., 14 (2013) 5668-5685.

[170] P. Munsch-Alatossava, O. Gursoy, T. Alatossava, Improved storage of cold raw milk by continuous flushing of N2 gas separated from compressed air: a pilot scale study, J. Food Process. Technol., 1000101, 1 (2010) 1-4.

[171] M.A. Chappell, Solid-phase considerations for the environmental fate of TNT and RDX in soil, ACS Symp. Ser., 1069 (2011) 1-25.

[172] O. Drzyzga, D. Bruns-Nagel, T. Gorontzy, K.-H. Blotevogel, E. Von Low, Anaerobic incorporation of the radiolabeled explosive TNT and metabolites into the organic soil matrix of contaminated soil after different treatment procedures, Chemosphere, 38 (1999) 2081-2095.

[173] J. Eriksson, S. Frankki, A. Shchukarev, U. Skyllberg, Binding of 2,4,6-Trinitrotoluene, Aniline, and Nitrobenzene to Dissolved and Particulate Soil Organic Matter, Environ. Sci. Technol., 38 (2004) 3074-3080.

[174] US EPA Method 8330B, Test methods - SW-846, 2006, pp. 1-31.

[175] US EPA Method 8330A, Test methods - SW-846, 2007, pp. 1-28.

[176] C.J. Matocha, Encyclopedia of Soil Science, 2nd ed., CRC Press, 2005.

[177] K.A. Thorn, K.R. Kennedy, 15N NMR Investigation of the Covalent Binding of Reduced TNT Amines to Soil Humic Acid, Model Compounds, and Lignocellulose, Environ. Sci. Technol., 36 (2002) 3787-3796.

[178] A.Z. Li, K.A. Marx, J. Walker, D.L. Kaplan, Trinitrotoluene and Metabolites Binding to Humic Acid, Environ. Sci. Technol., 31 (1997) 584-589.

[179] J.C. Pennington, J.M. Brannon, Environmental fate of explosives, Thermochim. Acta, 384 (2002) 163-172.

[180] P. Iovieno, E. Baaaath, Effect of drying and rewetting on bacterial growth rates in soil, FEMS Microbiol. Ecol., 65 (2008) 400-407.

[181] P.S. Wong, J.M. Fukuto, Reaction of organic nitrate esters and S-nitrosothiols with reduced flavins: a possible mechanism of bioactivation, Drug metabolism and disposition: the biological fate of chemicals, 27 (1999) 502-509.

[182] H.K. Maleh, K.M. Carvalho-Knighton, D.F. Martin, RDX properties as a guide to remediation, Fla. Sci., 72 (2009) 249-265.

[183] N.P. McNamara, H.I.J. Black, N.A. Beresford, N.R. Parekh, Effects of acute gamma irradiation on chemical, physical and biological properties of soils, Applied Soil Ecology, 24 (2003) 117-132.

[184] G. Immanuel, R. Dhanusha, P. Prema, A. Palavesam, Effect of different growth parameters on endoglucanase enzyme activity by bacteria isolated from coir retting effluents of estuarine environment, Int. J. Environ. Sci. Technol., 3 (2006) 25-34.

[185] K. Rezaei, F. Temelli, E. Jenab, Effects of pressure and temperature on enzymatic reactions in supercritical fluids, Biotechnol. Adv., 25 (2007) 272-280.

[186] W.J. Braida, J.C. White, D. Zhao, F.J. Ferrandino, J.J. Pignatello, Concentration-dependent kinetics of pollutant desorption from soils, Environmental Toxicology and Chemistry, 21 (2002) 2573-2580.

[187] C. Anbeek, The dependence of dissolution rates on grain size for some fresh and weathered feldspars, Geochimica et Cosmochimica Acta, 56 (1992) 3957-3970.

[188] D.P. Chambers, P.M. Attiwill, The Ash-Bed Effect in Eucalyptus regnans Forest: Chemical, Physical and Microbiological Changes in Soil After Heating or Partial Sterilisation, Australian Journal of Botany, 42 (1994) 739-749.

[189] A. Marchuk, P. Rengasamy, A. McNeill, A. Kumar, Nature of the clay-cation bond affects soil structure as verified by X-ray computed tomography, Soil Res. (Collingwood, Aust.), 50 (2012) 638-644.

[190] A. Akbari, S. Ghoshal, Bioaccessible Porosity in Soil Aggregates and Implications for Biodegradation of High Molecular Weight Petroleum Compounds, Environmental Science & Technology, 49 (2015) 14368-14375.

[191] T. Allen, Powder Sampling and Particle Size Determination, Elsevier, Amsterdam, 2003.

[192] R. Pajor, R. Falconer, S. Hapca, W. Otten, Modelling and quantifying the effect of heterogeneity in soil physical conditions on fungal growth, Biogeosciences, 7 (2010) 3731-3740.

[193] Orica Mining Services Safety Data Sheet - Pentex D booster, 2013.

[194] Orica Mining Services Technical Data Sheet - Pentex D booster, 2013.

[195] Orica Mining Services Technical Data Sheet - Exel Millisecond Detonators, 2008.

[196] T.F. Jenkins, Ranney, T.A., Miyares, P.H., Collins, N.H., Hewitt, A.D., Use of Surface Snow Sampling to Estimate the Quantity of Explosives Residues Resulting from Land Mine Detonations (Technical Report 00-12), Cold Regions Research and Engineering Laboratory, 2000, pp. 1-9.

[197] Fluka Analytical (Sigma Aldrich), Pseudomonas: A Communicative Bacteria, Microbiology Focus, 2 (2010) 1-6.

[198] J.S. Caygill, F. Davis, S.P.J. Higson, Current trends in explosive detection techniques, Talanta, 88 (2012) 14-29.

[199] J. Wang, Electrochemical sensing of explosives, Electroanalysis, 19 (2007) 415-423.

[200] C.M.A. Brett, Electrochemistry: Principles, Methods, and Applications, Oxford University Press, Oxford, 1993.

[201] A.C. Fisher, Electrode Dynamics, Oxford University Press, Oxford, 1996.

[202] S. Singh, Sensors-An effective approach for the detection of explosives, J. Hazard. Mater., 144 (2007) 15-28.

[203] L. Yu, Y. Huang, X. Jin, A.J. Mason, X. Zeng, Ionic liquid thin layer EQCM explosives sensor, Sens. Actuators, B, 140 (2009) 363-370.

[204] A. Díaz Aguilar, E.S. Forzani, M. Leright, F. Tsow, A. Cagan, R.A. Iglesias, L.A. Nagahara, I. Amlani, R. Tsui, N.J. Tao, A Hybrid Nanosensor for TNT Vapor Detection, Nano Letters, 10 (2010) 380-384.

[205] S. Guo, D. Wen, Y. Zhai, S. Dong, E. Wang, Ionic liquid–graphene hybrid nanosheets as an enhanced material for electrochemical determination of trinitrotoluene, Biosensors and Bioelectronics, 26 (2011) 3475-3481.

[206] C. Xiao, A. Rehman, X. Zeng, Dynamics of Redox Processes in Ionic Liquids and Their Interplay for Discriminative Electrochemical Sensing, Analytical Chemistry, 84 (2012) 1416-1424.

[207] K. Bratin, P.T. Kissinger, R.C. Briner, C.S. Bruntlett, Determination of nitro aromatic, nitramine, and nitrate ester explosive compounds in explosive mixtures and gunshot residue by liquid chromatography and reductive electrochemical detection, Anal. Chim. Acta, 130 (1981) 295-311.

[208] R.B. Doppalapudi, G.A. Sorial, S.W. Maloney, Electrochemical reduction of simulated munitions wastewater in a bench-scale batch reactor, Environ. Eng. Sci., 19 (2002) 115-130.

[209] N.A. Macias-Ruvalcaba, J.P. Telo, D.H. Evans, Studies of the electrochemical reduction of some dinitroaromatics, J. Electroanal. Chem., 600 (2007) 294-302.

[210] A. Hilmi, J.H.T. Luong, A.-L. Nguyen, Development of Electrokinetic Capillary Electrophoresis Equipped with Amperometric Detection for Analysis of Explosive Compounds, Anal. Chem., 71 (1999) 873-878.

[211] S. Mamo, J. Gonzalez-Rodriguez, Development of a Molecularly Imprinted Polymer-Based Sensor for the Electrochemical Determination of Triacetone Triperoxide (TATP), Sensors, 14 (2014) 23269-23282.

[212] R.L. Marple, W.R. LaCourse, Application of Photoassisted Electrochemical Detection to Explosive-Containing Environmental Samples, Anal. Chem., 77 (2005) 6709-6714.

[213] D. Nie, D. Jiang, D. Zhang, Y. Liang, Y. Xue, T. Zhou, L. Jin, G. Shi, Two-dimensional molecular imprinting approach for the electrochemical detection of trinitrotoluene, Sensors and Actuators B: Chemical, 156 (2011) 43-49.

[214] B.K. Ong, H.L. Poh, C.K. Chua, M. Pumera, Graphenes Prepared by Hummers, Staudenmaier and Hofmann Methods for Analysis of TNT-Based Nitroaromatic Explosives in Seawater, Electroanalysis, 24 (2012) 2085-2093.

[215] H.L. Poh, M. Pumera, Nanoporous Carbon Materials for Electrochemical Sensing, Chem. - Asian J., 7 (2012) 412-416.

[216] H.G. Prabu, M.B. Talawar, T. Mukundan, S.N. Asthana, Studies on the utilization of stripping voltammetry technique in the detection of high-energy materials, Combustion, Explosion, and Shock Waves, 47 (2011) 87-95.

[217] Y. Qu, Y. Liu, T. Zhou, G. Shi, L. Jin, Electrochemical sensor prepared from molecularly imprinted polymer for recognition of 1,3-dinitrobenzene (DNB), Chin. J. Chem., 27 (2009) 2043-2048.

[218] S. Saglam, A. Uzer, Y. Tekdemir, E. Ercag, R. Apak, Electrochemical sensor for nitroaromatic type energetic materials using gold nanoparticles/poly(o-phenylenediamine-aniline) film modified glassy carbon electrode, Talanta, 139 (2015) 181-188.

[219] G. Shi, Y. Qu, Y. Zhai, Y. Liu, Z. Sun, J. Yang, L. Jin, {MSU/PDDA}n layer-by-layer assembled modified sensor for electrochemical detection of ultratrace explosive nitroaromatic compounds, Electrochem. Commun., 9 (2007) 1719-1724.

[220] L. Tang, H. Feng, J. Cheng, J. Li, Uniform and rich-wrinkled electrophoretic deposited graphene film: a robust electrochemical platform for TNT sensing, Chem. Commun. (Cambridge, U. K.), 46 (2010) 5882-5884.

[221] H.S. Toh, A. Ambrosi, M. Pumera, Electrocatalytic effect of ZnO nanoparticles on reduction of nitroaromatic compounds, Catal. Sci. Technol., 3 (2013) 123-127.

[222] A. Uzer, S. Saglam, Y. Tekdemir, B. Ustamehmetoglu, E. Sezer, E. Ercag, R. Apak, Determination of nitroaromatic and nitramine type energetic materials in synthetic and real mixtures by cyclic voltammetry, Talanta, 115 (2013) 768-778.

[223] D. Lu, A. Cagan, R.A.A. Munoz, T. Tangkuaram, J. Wang, Highly sensitive electrochemical detection of trace liquid peroxide explosives at a Prussian-blue 'artificial-peroxidase' modified electrode, Analyst (Cambridge, U. K.), 131 (2006) 1279-1281.

[224] R.A.A. Munoz, D. Lu, A. Cagan, J. Wang, 'One-step' simplified electrochemical sensing of TATP based on its acid treatment, Analyst (Cambridge, U. K.), 132 (2007) 560-565.

[225] S.A. Trammell, M. Zeinali, B.J. Melde, P.T. Charles, F.L. Velez, M.A. Dinderman, A. Kusterbeck, M.A. Markowitz, Nanoporous Organosilicas as Preconcentration Materials for the Electrochemical Detection of Trinitrotoluene, Anal. Chem. (Washington, DC, U. S.), 80 (2008) 4627-4633.

[226] Y. Wang, H. Xiong, X. Zhang, Y. Ye, S. Wang, Nitromethane biosensor based on four heme proteins modified glassy carbon electrodes, Journal of Electroanalytical Chemistry, 674 (2012) 17-22.

[227] C.K. Chua, M. Pumera, L. Rulíšek, Reduction Pathways of 2,4,6-Trinitrotoluene: An Electrochemical and Theoretical Study, The Journal of Physical Chemistry C, 116 (2012) 4243-4251.

[228] C. Lagrost, L. Preda, E. Volanschi, P. Hapiot, Heterogeneous electron-transfer kinetics of nitro compounds in room-temperature ionic liquids, J. Electroanal. Chem., 585 (2005) 1-7.

[229] D.S. Silvester, A.J. Wain, L. Aldous, C. Hardacre, R.G. Compton, Electrochemical reduction of nitrobenzene and 4-nitrophenol in the room temperature ionic liquid [C4dmim][N(Tf)2], Journal of Electroanalytical Chemistry, 596 (2006) 131-140.

[230] A. Hilmi, J.H.T. Luong, In-line coupling capillary electrochromatography with amperometric detection for analysis of explosive compounds, Electrophoresis, 21 (2000) 1395-1404.

[231] A. Hilmi, J.H.T. Luong, Micromachined Electrophoresis Chips with Electrochemical Detectors for Analysis of Explosive Compounds in Soil and Groundwater, Environ. Sci. Technol., 34 (2000) 3046-3050.

[232] M. Krausa, J. Doll, K. Schorb, W. Boke, G. Hambitzer, Fast electrochemical detection of nitro- and aminoaromates in soils and liquids, Propellants, Explos., Pyrotech., 22 (1997) 156-159.

[233] S. Huan, S. Hu, G. Shen, R. Yu, Au microelectrode based on molecularly imprinted oligomer film for rapid electrochemical sensing, Anal. Lett., 36 (2003) 2401-2416.

[234] X. Fu, R.F. Benson, J. Wang, D. Fries, Remote underwater electrochemical sensing system for detecting explosive residues in the field, Sens. Actuators, B, 106 (2005) 296-301.

[235] J. Wang, R.K. Bhada, J. Lu, D. MacDonald, Remote electrochemical sensor for monitoring TNT in natural waters, Anal. Chim. Acta, 361 (1998) 85-91.

[236] J.R.C. Junqueira, W.R. de Araujo, M.O. Salles, T.R.L.C. Paixao, Flow injection analysis of picric acid explosive using a copper electrode as electrochemical detector, Talanta, 104 (2013) 162-168.

[237] O.J.A. Schueller, S.T. Brittain, G.M. Whitesides, Fabrication of glassy carbon microstructures by soft lithography, Sens. Actuators, A, 72 (1999) 125-139.

[238] E. Fernández, L. Vidal, J. Iniesta, J.P. Metters, C.E. Banks, A. Canals, Screen-printed electrode-based electrochemical detector coupled with in-situ ionic-liquid-assisted dispersive liquid–liquid microextraction for determination of 2,4,6-trinitrotoluene, Analytical and bioanalytical chemistry, 406 (2014) 2197-2204.

[239] J. Lee, D.S. Silvester, Low-cost microarray thin-film electrodes with ionic liquid gel-polymer electrolytes for miniaturised oxygen sensing, Analyst, 141 (2016) 3705-3713.

[240] J. Lee, G. Du Plessis, D.W.M. Arrigan, D.S. Silvester, Towards improving the robustness of electrochemical gas sensors: impact of PMMA addition on the sensing of oxygen in an ionic liquid, Analytical Methods, 7 (2015) 7327-7335.

[241] H.H. Girault, Analytical and Physical Electrochemistry, Taylor and Francis, Hoboken, 2004.

[242] R.G. Compton, Understanding Voltammetry, 2nd ed., Imperial College Press, London, 2011.

[243] V. Mirceski, Square-Wave Voltammetry: Theory and Application, Springer, Berlin, Heidelberg, 2007.

[244] M. Galik, A.M. O'Mahony, J. Wang, Cyclic and Square-Wave Voltammetric Signatures of Nitro-Containing Explosives, Electroanalysis, 23 (2011) 1193-1204.

[245] E.S. Forzani, D. Lu, M.J. Leright, A.D. Aguilar, F. Tsow, R.A. Iglesias, Q. Zhang, J. Lu, J. Li, N. Tao, A hybrid electrochemical-colorimetric sensing platform for detection of explosives, J. Am. Chem. Soc., 131 (2009) 1390-1391.

[246] D.F. Laine, I.F. Cheng, Electrochemical detection of the explosive, hexamethylene triperoxide diamine (HMTD), Microchem. J., 91 (2009) 125-128.

[247] X. Ceto, A.M. O'Mahony, J. Wang, M. del Valle, Simultaneous identification and quantification of nitro-containing explosives by advanced chemometric data treatment of cyclic voltammetry at screen-printed electrodes, Talanta, 107 (2013) 270-276.

[248] D. Shoup, A. Szabo, Chronoamperometric current at finite disk electrodes, Journal of Electroanalytical Chemistry and Interfacial Electrochemistry, 140 (1982) 237-245.

[249] C.X. Guo, Z.S. Lu, Y. Lei, C.M. Li, Ionic liquid-graphene composite for ultratrace explosive trinitrotoluene detection, Electrochem. Commun., 12 (2010) 1237-1240.

[250] U. Lewin, J. Efer, W. Engewald, High-performance liquid chromatographic analysis with electrochemical detection for residues of explosives in water samples around a former ammunition plant, J. Chromatogr. A, 730 (1996) 161-167.

[251] J. Riedel, M. Berthold, U. Guth, Electrochemical determination of dissolved nitrogen-containing explosives, Electrochim. Acta, 128 (2014) 85-90.

[252] K. Malzahn, J.R. Windmiller, G. Valdes-Ramirez, M.J. Schoening, J. Wang, Wearable electrochemical sensors for in situ analysis in marine environments, Analyst (Cambridge, U. K.), 136 (2011) 2912-2917.

[253] I.S. Krull, X.D. Ding, C. Selavka, K. Bratin, G. Forcier, The trace analysis for explosives and related compounds via high performance liquid chromatography-photolysis-electrochemical detection, J. Forensic Sci., 29 (1984) 449-463.

[254] R. Wilson, C. Clavering, A. Hutchinson, Electrochemiluminescence enzyme immunoassays for TNT and pentaerthyritol tetranitrate, Anal. Chem., 75 (2003) 4244-4249.

[255] R. Blue, Z. Vobecka, P.J. Skabara, D. Uttamchandani, The development of sensors for volatile nitro-containing compounds as models for explosives detection, Sens. Actuators, B, 176 (2013) 534-542.

[256] P.K. Sekhar, E.L. Brosha, Trace detection of 2,4,6-trinitrotoluene using electrochemical gas sensor, IEEE Sens. J., 15 (2015) 1624-1629.

[257] J.B.F. Lloyd, Detection and differentiation of nitrocellulose traces of forensic science interest with reductive mode electrochemical detection at a pendent mercury drop electrode coupled with size-exclusion chromatography, Anal. Chem., 56 (1984) 1907-1912.

[258] E.J. Olson, W.C. Isley, J.E. Brennan, C.J. Cramer, P. Buhlmann, Electrochemical Reduction of 2,4-Dinitrotoluene in Aprotic and pH-Buffered Media, J. Phys. Chem. C, 119 (2015) 13088-13097.

[259] P.M.L. Bonin, D. Bejan, L. Schutt, J. Hawari, N.J. Bunce, Electrochemical Reduction of Hexahydro-1,3,5-trinitro-1,3,5-triazine in Aqueous Solutions, Environ. Sci. Technol., 38 (2004) 1595-1599.

[260] P.K. Sekhar, F. Wignes, Trace detection of research department explosive (RDX) using electrochemical gas sensor, Sens. Actuators, B, 227 (2016) 185-190.

[261] J.C. Mbah, S. Steward, N.O. Egiebor, Solid membrane electrode assembly for on board detection of peroxides based explosives, Sens. Actuators, B, 222 (2016) 693-697.

[262] S. Parajuli, W. Miao, Sensitive Determination of Triacetone Triperoxide Explosives Using Electrogenerated Chemiluminescence, Anal. Chem. (Washington, DC, U. S.), 85 (2013) 8008-8015.

[263] R. Schulte-Ladbeck, U. Karst, Liquid chromatography - post-column photochemical conversion and electrochemical detection for determination of peroxide-based explosives, Chromatographia, 57 (2003) 61-66.

[264] S. Parajuli, W. Miao, Sensitive Determination of Hexamethylene Triperoxide Diamine Explosives, Using Electrogenerated Chemiluminescence Enhanced by Silver Nitrate, Anal. Chem. (Washington, DC, U. S.), 81 (2009) 5267-5272.

[265] A.A. Saeed, B. Singh, M. Nooredeen Abbas, E. Dempsey, Evaluation of Bismuth Modified Carbon Thread Electrode for Simultaneous and Highly Sensitive Cd (II) and Pb (II) Determination, Electroanalysis, 28 (2016) 2205-2213.

[266] Z. Zhu, Y. Su, J. Li, D. Li, J. Zhang, S. Song, Y. Zhao, G. Li, C. Fan, Highly Sensitive Electrochemical Sensor for Mercury(II) Ions by Using a Mercury-Specific Oligonucleotide Probe and Gold Nanoparticle-Based Amplification, Anal. Chem. (Washington, DC, U. S.), 81 (2009) 7660-7666.

[267] A. Jang, Z. Zou, K.K. Lee, C.H. Ahn, P.L. Bishop, State-of-the-art lab chip sensors for environmental water monitoring, Meas. Sci. Technol., 032001, 22 (2011) 1-18.

[268] S. Marin, A. Merkoci, Nanomaterials Based Electrochemical Sensing Applications for Safety and Security, Electroanalysis, 24 (2012) 459-469.

[269] F. Akhgari, H. Fattahi, Y.M. Oskoei, Recent advances in nanomaterial-based sensors for detection of trace nitroaromatic explosives, Sens. Actuators, B, 221 (2015) 867-878.

[270] W. Lu, M. Xue, Z. Xu, X. Dong, F. Xue, F. Wang, Q. Wang, Z. Meng, Molecularly Imprinted Polymers for the Sensing of Explosives and Chemical Warfare Agents, Curr. Org. Chem., 19 (2015) 62-71.

[271] X. Jin, L. Yu, X. Zeng, Enhancing the sensitivity of ionic liquid sensors for methane detection with polyaniline template, Sensors and Actuators B: Chemical, 133 (2008) 526-532.

[272] A. Rehman, X. Zeng, Ionic Liquids as Green Solvents and Electrolytes for Robust Chemical Sensor Development, Acc. Chem. Res., 45 (2012) 1667-1677.

[273] M. Opallo, A. Lesniewski, A review on electrodes modified with ionic liquids, Journal of Electroanalytical Chemistry, 656 (2011) 2-16.

[274] D.S. Silvester, L. Aldous, Electrochemical Strategies in Detection Science, Chapter 10: Electrochemical Detection Using Ionic Liquids, The Royal Society of Chemistry, Cambridge, 2016.

[275] A.M. O'Mahony, D.S. Silvester, L. Aldous, C. Hardacre, R.G. Compton, Effect of Water on the Electrochemical Window and Potential Limits of Room-Temperature Ionic Liquids, J. Chem. Eng. Data, 53 (2008) 2884-2891.

[276] J. Lee, K. Murugappan, D.W.M. Arrigan, D.S. Silvester, Oxygen reduction voltammetry on platinum macrodisk and screen-printed electrodes in ionic liquids: Reaction of the electrogenerated superoxide species with compounds used in the paste of Pt screen-printed electrodes?, Electrochim. Acta, 101 (2013) 158-168.

[277] A.H. Hogt, J. Dankert, J. Feijen, Adhesion of coagulase-negative staphylococci to methacrylate polymers and copolymers, J. Biomed. Mater. Res., 20 (1986) 533-545.

[278] G.A. Crossley, S.A.M. Hesp, New class of reactive polymer modifiers for asphalt mitigation of moisture damage, Transp. Res. Rec., 1728 (2000) 52-59.

[279] J.L. Thomason, J.Z. Ali, J. Anderson, The thermo-mechanical performance of glass-fibre reinforced polyamide 66 during glycol-water hydrolysis conditioning, Composites, Part A, 41A (2010) 820-826.

[280] J.L. Thomason, G. Porteus, Swelling of glass-fiber reinforced polyamide 66 during conditioning in water, ethylene glycol, and antifreeze mixture, Polym. Compos., 32 (2011) 639-647.

[281] R. Martel, T.J. Robertson, M.Q. Doan, S. Thiboutot, G. Ampleman, A. Provatas, T. Jenkins, 2,4,6-Trinitrotoluene in soil and groundwater under a waste lagoon at the former Explosives Factory Maribyrnong (EFM), Victoria, Australia, Environmental Geology, 53 (2008) 1249-1259.

[282] E.P.H. Best, M.E. Zappi, H.L. Fredrickson, S.L. Sprecher, S.L. Larson, M. Ochman, Screening of Aquatic and Wetland Plant Species for Phytoremediation of Explosives-contaminated Groundwater from the Iowa Army Ammunition Plant, Annals of the New York Academy of Sciences, 829 (1997) 179-194.

[283] M.-C. Chuang, J.R. Windmiller, P. Santhosh, G.V. Ramirez, M. Galik, T.-Y. Chou, J. Wang, Textile-based Electrochemical Sensing: effect of Fabric Substrate and Detection of Nitroaromatic Explosives, Electroanalysis, 22 (2010) 2511-2518.

[284] M. Ueland, L. Blanes, R.V. Taudte, B.H. Stuart, N. Cole, P. Willis, C. Roux, P. Doble, Capillary-driven microfluidic paper-based analytical devices for lab on a chip screening of explosive residues in soil, J. Chromatogr. A, 1436 (2016) 28-33.

[285] R.G. Ewing, M.J. Waltman, D.A. Atkinson, J.W. Grate, P.J. Hotchkiss, The vapor pressures of explosives, TrAC, Trends Anal. Chem., 42 (2013) 35-48.

[286] Solvionic, Material Safety Data Sheet, 1-Butyl-3-Methylimidazolium bis(trifluoromethanesulfonyl)imide, available from http://en.solvionic.com/products/1-butyl-3-methylimidazolium-bistrifluoromethanesulfonylimide-99.9, accessed 21st October 2016.

[287] R.E. Del Sesto, C. Corley, A. Robertson, J.S. Wilkes, Tetraalkylphosphonium-based ionic liquids, Journal of Organometallic Chemistry, 690 (2005) 2536-2542.

[288] Sigma-Aldrich, Poly(hexyl methacrylate) data page, available at http://www.sigmaaldrich.com/catalog/product/aldrich/462373, accessed 21st October 2016.

Appendix A: Additional AFM data

Matlab code used for adhesion data extraction

```
%Program for analysis of AFM force vs. distance curves recorded with
WITec
%alpha300 and exported with Project FOUR software into individual
*.txt
%files. Export options: DO NOT include header, DO NOT include x
axis.
%Extracted data: Adhesion in nN. Output: text file with scan name
and adhesion
%value in nN.

%k = input('Enter the spring constant [N/m] of the cantilever used
for these measurements: ');
k=0.58;
[FILENAME, PATH] = uigetfile('*.txt', 'MultiSelect', 'on','Select
Files for Analysis','File path here');

for n=1:length(FILENAME)/2

    i=2*n-1;
    j=2*n;

    u=findstr(char(FILENAME(1,i)),'_T-B');
    S1=char(FILENAME(1,i));
    S2=char(FILENAME(1,j));

    if S1(1:(u-1))==S2(1:u-1)

        y=importfile_x(strcat(PATH, char(FILENAME(1,i))),1,1000);
        x=importfile_x(strcat(PATH, char(FILENAME(1,j))),1,1000);

        %Background subtraction
        y_mean=mean(y(1:200));
        y_subBG=y-y_mean;

        %Fitting 1st order polynom into retract data
        p=polyfit(x(501:540),y_subBG(501:540),1);

        %Detecting jump-off contact
        dy=diff(y_subBG(501:end))./diff(x(501:end));
        [a,b]=max(dy);

        %Calculation of adhesion force
        F_adh(n) = polyval(p,x(b+501))/p(1)*k;
        SCAN(n)= FILENAME(1,i);




    else
        display('Wrong input data')
```

```
    end

end

%Writing the results to file
[SAVENAME, SAVEPATH] = uiputfile('.txt','Save As...','File path
here');
SAVEFILE = strcat(SAVEPATH, SAVENAME);
savedat = fopen(SAVEFILE, 'w');
Results = table(SCAN',F_adh');
writetable(Results,SAVEFILE,'Delimiter','\t');
fclose(savedat);

%clear all
```

Individual graphs of explosives adhesion

TNT

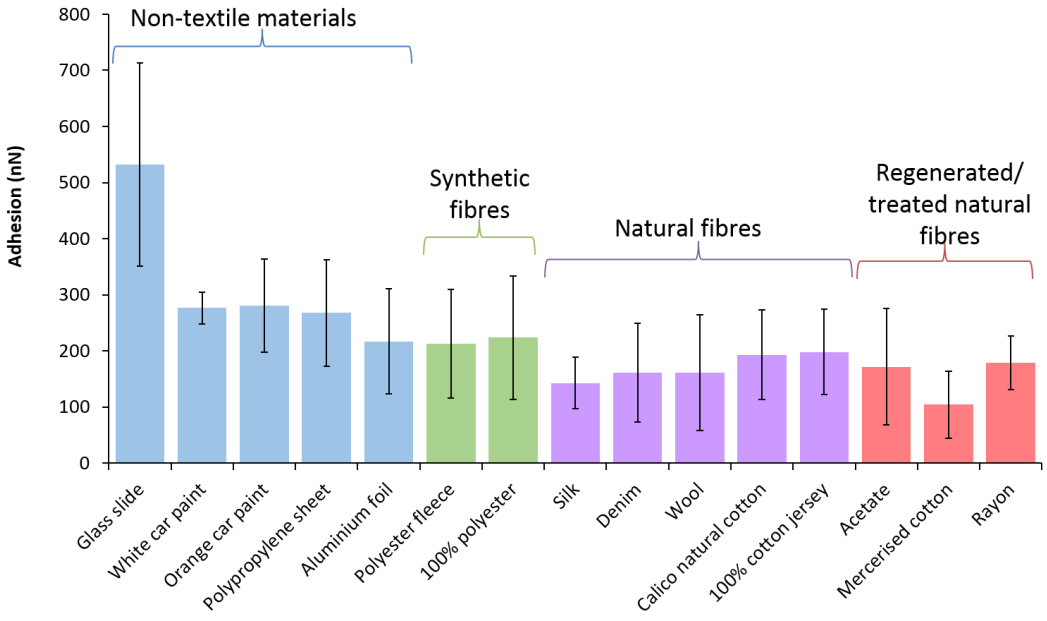

Figure A.1: Graph showing average of 118 adhesion measurements between TNT and 15 different surfaces. Error bars show standard deviations within the 118 adhesion measurements for each surface

PETN

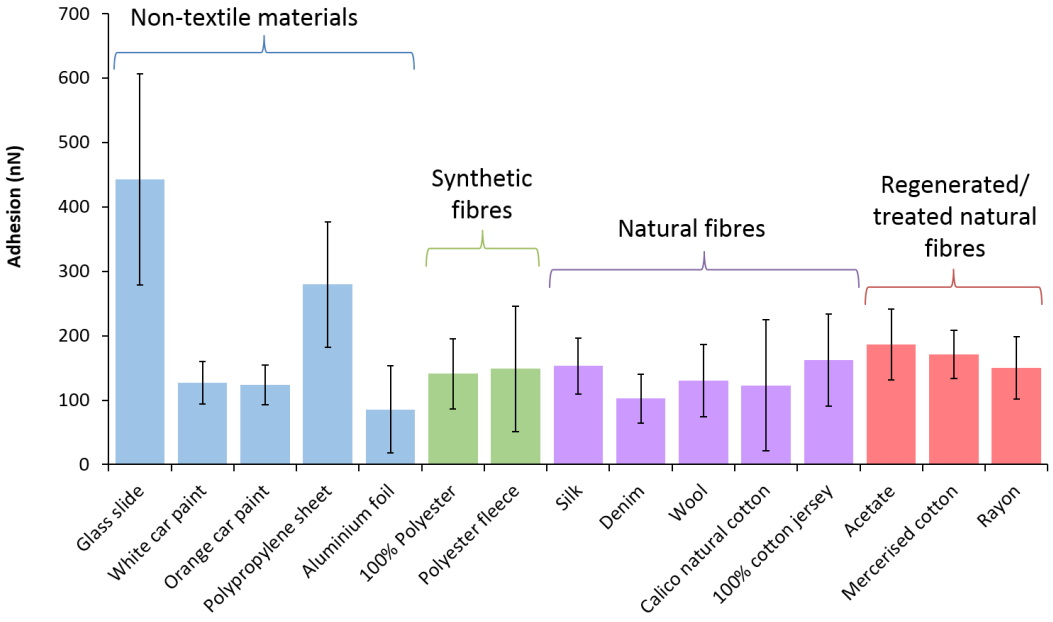

Figure A.2: Graph showing average of 118 adhesion measurements between PETN and 15 different surfaces. Error bars show standard deviations within the 118 adhesion measurements for each surface

RDX

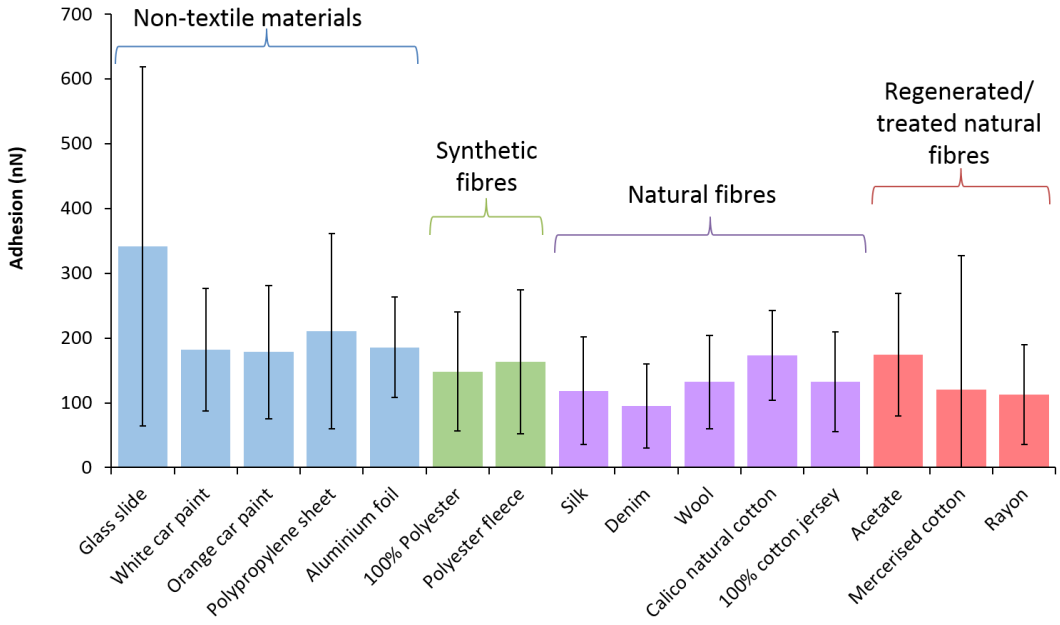

Figure A.3: Graph showing average of 118 adhesion measurements between RDX and 15 different surfaces. Error bars show standard deviations within the 118 adhesion measurements for each surface

Appendix B: HPLC-UV calibration curves

Contact heater samples: 75mm column

Calibration standards containing RDX, TNT and PETN were prepared containing 0.002, 0.004, 0.008, 0.016, 0.032 and 0.064 mg/mL of each component and Musk Tibetene at 0.01 mg/mL. The calibration standards were placed into low adsorption LC vials for analysis to minimise any possible adsorption of the analytes prior to, or during, analysis. Each calibration standard was injected in triplicate and the results averaged. For Musk Tibetene quantification, the (larger) peak area from the 212 nm detector was used. TNT, PETN, RDX and Musk Tibetene peak areas were used for quantification purposes. All calibration curves had R2 values of at least 0.999. Calibration curves for TNT, PETN and RDX obtained using these conditions are displayed in Figure B.1.

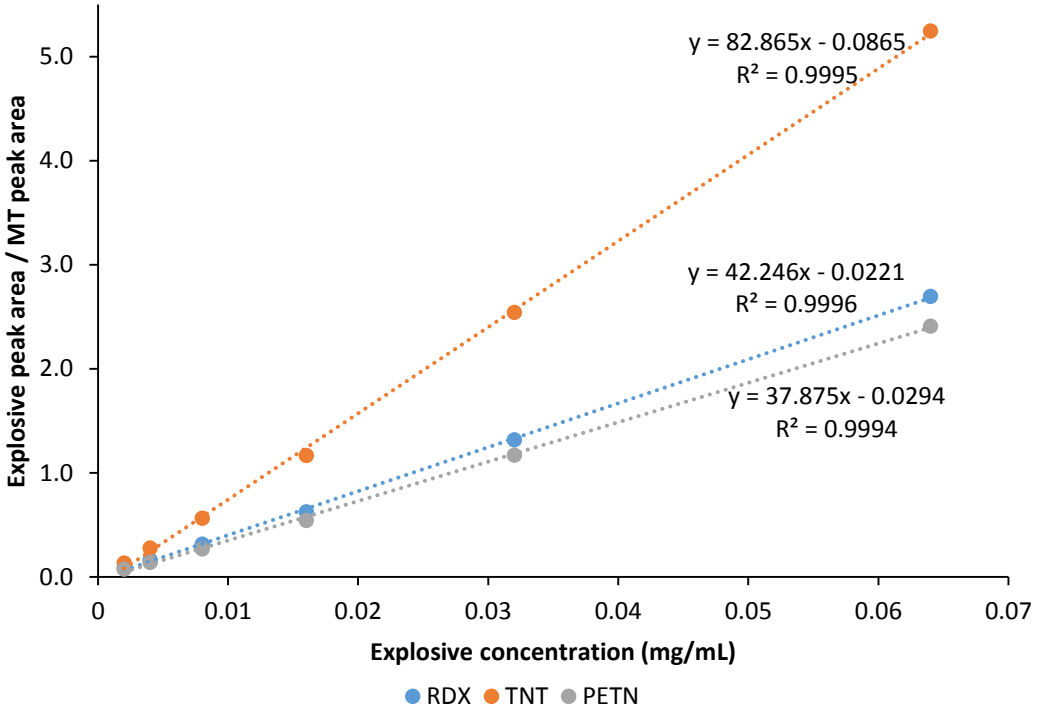

Figure B.1: Calibration curves for TNT, PETN and RDX obtained on a 75 mm YMC-UltraHT Pro C18 column

Contact heater samples: 50mm column

A number of sample analyses were performed on a slightly shorter HPLC column. The final conditions employed for this 50 mm column are detailed in Section 3.2.5. A new set of calibration standards were prepared for explosive quantification on this column. Standards were prepared at concentrations of 0.001, 0.002, 0.004, 0.008, 0.016 and 0.032 mg/mL in TNT, PETN and RDX, to give calibration curves with R2 values of greater than 0.999. These calibration curves are displayed in Figure B.2.

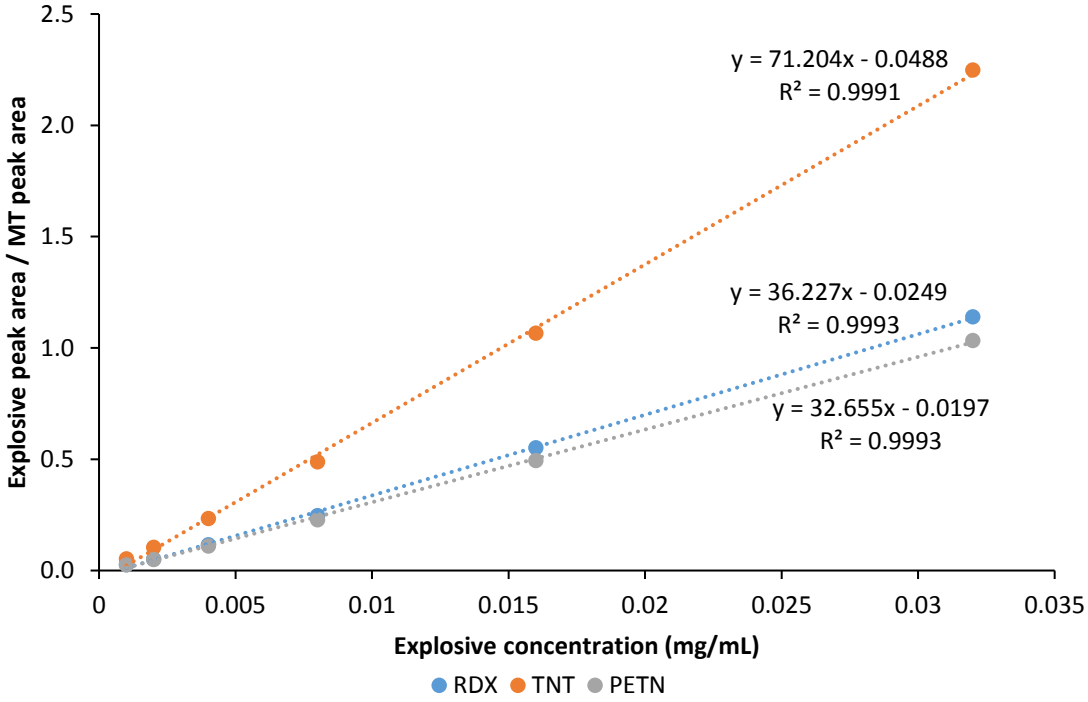

Figure B.2: Calibration curves for TNT, PETN and RDX on a 50 mm YMC-UltraHT Pro C18 column

Vacuum samples

Due to column availability, samples obtained following vacuum sampling were analysed on an alternative column to those used for the contact heater samples. Details of the HPLC-UV conditions used for analysis of the vacuum samples are provided in Section 3.2.5. Calibration standards were prepared at concentrations of 0.001, 0.002, 0.004, 0.008, 0.016 and 0.032 mg/mL in TNT, PETN and RDX, to give calibration curves with R2 values of greater than 0.999. These calibration curves are displayed in Figure B.3.

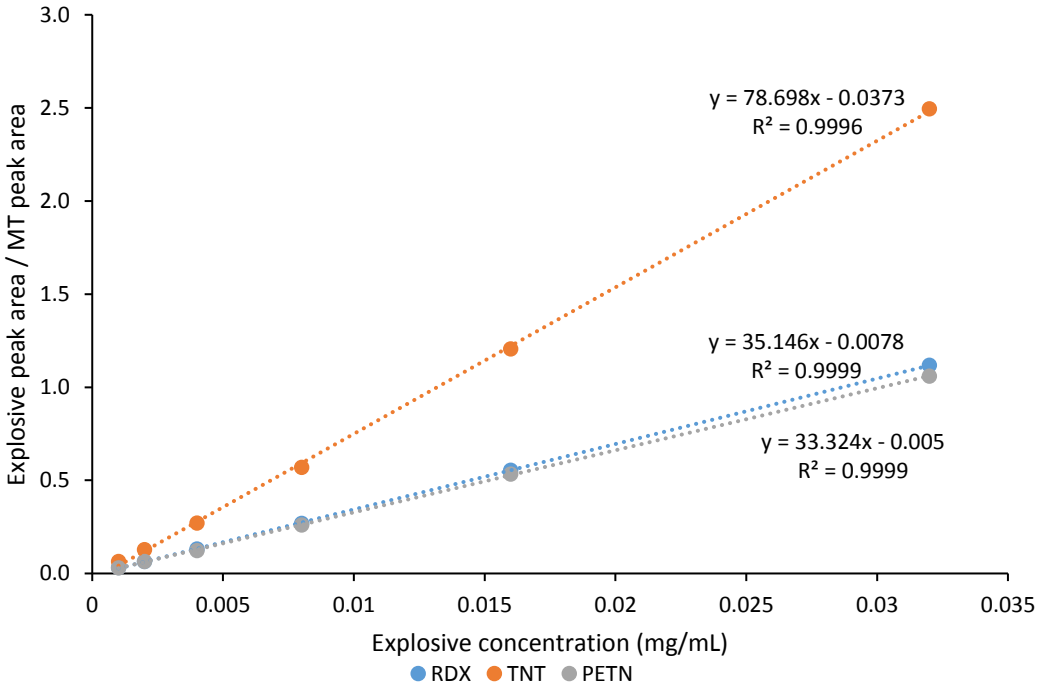

Figure B.3: Calibration curves for TNT, PETN and RDX on a 100 mm Agilent Pursuit Diphenyl column

Appendix C: PHMA characterisation and gel polymer mixing ratios

PHMA size exclusion chromatogram

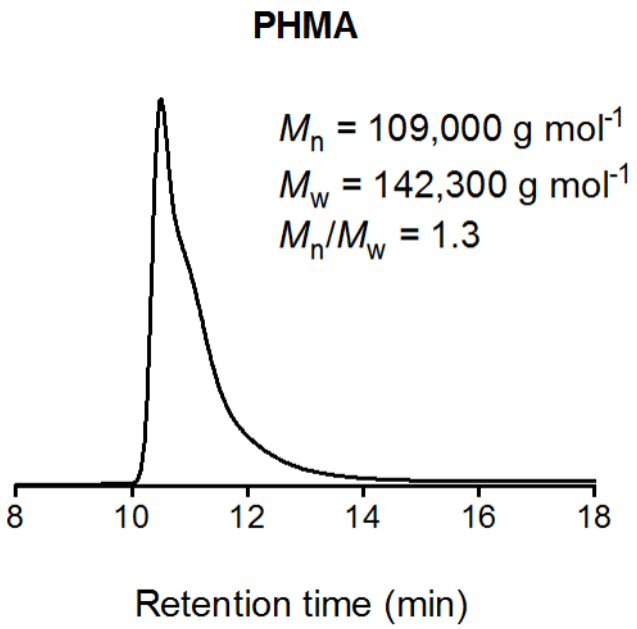

Figure C.1: Size exclusion chromatogram for poly(hexyl methacrylate)

Quantities of RTIL and polymer used to make up the gel polymer mixing ratios assessed in this work

Table C.1: Densities of RTILs and polymers used in Chapter 6

Compound	Density (g/mL)
$[C_4mim][NTf_2]$	1.43 [286]
$[P_{14,6,6,6}][NTf_2]$	1.08 [287]
PMMA	1.18 [240]
PHMA	0.863 [288]

Table C.2: Quantities of $[C_4mim][NTf_2]$ used in conjunction with PMMA

PMMA doping mass (%)	Mass PMMA (mg)	Volume RTIL (µL)	Mass RTIL (mg)	Volume acetone added to dissolve for dropping (µL)
10	49	308.0	441	0
20	88	246.0	352	0
30	115	188.0	269	14.3
40	106	112.0	159	20.2
50	108	75.6	108	33.4

Table C.3: Quantities of $[P_{14,6,6,6}][NTf_2]$ used in conjunction with PMMA

PMMA doping mass (%)	Mass PMMA (mg)	Volume RTIL (µL)	Mass RTIL (mg)	Volume acetone added to dissolve for dropping (µL)
10	11	91.8	99.1	14.4
20	22.7	84.2	90.9	15.6
30	33.8	73.1	78.9	16.8
40	45.6	63.3	68.4	18
50	58.8	54.4	58.8	19.2

Table C.4: Quantities of $[P_{14,6,6,6}][NTf_2]$ used in conjunction with PHMA

PHMA doping mass (%)	Volume PHMA solution (45.1 mg/mL in acetone) (µL)	Mass PHMA (mg)	Volume RTIL (mL)	Mass RTIL (mg)	Volume acetone added to dissolve for dropping (µL)
10	55.4	2.5	20.8	22.5	5
20	104.2	4.7	17.5	18.9	8
30	146.3	6.6	14.4	15.5	12
40	208.4	9.4	13.1	14.2	16
50	250.6	11.3	10.5	11.3	24